SYNTHESIS, CHARACTERIZATION AND BIOLOGICAL STUDIES OF 3d-METAL COMPLEXES OF SCHIFF BASES OF AMINOGLYCOSIDES AND β-LACTAM ANTIBIOTICS

A THESIS SUBMITTED TO THE

CENTRAL DEPARTMENT OF CHEMISTRY

INSTITUTE OF SCIENCE AND TECHNOLOGY

TRIBHUVAN UNIVERSITY

NEPAL

FOR THE AWARD OF

DOCTOR OF PHILOSOPHY

IN CHEMISTRY

BY

NARENDRA KUMAR CHAUDHARY

JULY, 2018

SYNTHESIS, CHARACTERIZATION AND BIOLOGICAL STUDIES OF 3d-METAL COMPLEXES OF SCHIFF BASES OF AMINOGLYCOSIDES AND β-LACTAM ANTIBIOTICS

A THESIS SUBMITTED TO THE

CENTRAL DEPARTMENT OF CHEMISTRY

INSTITUTE OF SCIENCE AND TECHNOLOGY

TRIBHUVAN UNIVERSITY

NEPAL

FOR THE AWARD OF

DOCTOR OF PHILOSOPHY

IN CHEMISTRY

BY

NARENDRA KUMAR CHAUDHARY

JULY, 2018

DECLARATION

Thesis entitled **"SYNTHESIS, CHARACTERIZATION AND BIOLOGICAL STUDIES OF 3d-METAL COMPLEXES OF SCHIFF BASES OF AMINOGLYCOSIDES AND β-LACTAM ANTIBIOTICS",** which is being submitted to Central Department of Chemistry, Institute of Science and Technology (IOST), Tribhuvan University, Nepal for the award of the degree of Doctor of Philosophy (Ph. D.), is a research work carried out by me under the supervision of Professor Dr. Parashuram Mishra, Department of Chemistry, Mahendra Morang Adarsh Multiple Campus, Biratnagar, Tribhuvan University, Nepal.

This research is original and has not been submitted earlier in part or full in this or any other form to any University or Institute, here or elsewhere, for the award of any degree.

Narendra Kumar Chaudhary

RECOMMENDATION

This is to recommend that **Mr. Narendra Kumar Chaudhary** has carried out research entitled **"SYNTHESIS, CHARACTERIZATION AND BIOLOGICAL STUDIES OF 3d-METAL COMPLEXES OF SCHIFF BASES OF AMINOGLYCOSIDES AND β-LACTAM ANTIBIOTICS"** for the award of Doctor of Philosophy (Ph. D.) in **Chemistry** under my supervision. To my knowledge, this work has not been submitted for any other degree.

He has fulfilled all the requirements laid down by the Institute of Science and Technology (IOST), Tribhuvan University, Kirtipur for the submission of the thesis for the award of Ph. D. degree.

Professor Dr. Parashuram Mishra
Supervisor
Department of Chemistry,
Mahendra Morang Adarsh Multiple Campus, Biratnagar
Tribhuvan University, Nepal

July 2018

CERTIFICATE OF APPROVAL

Date: 25/07/2018

On the recommendation of Professor Dr. Parashuram Mishra, this Ph. D. thesis submitted by Narendra Kumar Chaudhary, entitled **"SYNTHESIS, CHARACTERIZATION AND BIOLOGICAL STUDIES OF 3d-METAL COMPLEXES OF SCHIFF BASES OF AMINOGLYCOSIDES AND β-LACTAM ANTIBIOTICS"** is forwarded by Central Department Research Committee (CDRC) to the Dean, IOST, T. U.

_____

Dr. Ram Chandra Basnyat
Professor,
Head,
Central Department of Chemistry,
Tribhuvan University
Kirtipur, Kathmandu,
Nepal

ACKNOWLEDGEMENTS

The text free of errors is difficult in a rapidly changing field, where today's knowledge is soon replaced by tomorrow's. At this moment of accomplishment, first of all I pay my deep sense of gratitude to all, who provided help and support to me in the journey of my research work. I am extremely thankful to Professor Dr. Parashuram Mishra, who offered me the chance to do research in the field of coordination chemistry under his supervision. His constant guidance, invaluable discussions, and perpetual inspiration always acted as motivating factors to my research work.

It's my fortune to gratefully acknowledge Professor Mahendra Narayan Yadav, Campus Chief, and Mr. Sitaram Gupta, Head, Department of Chemistry, Mahendra Morang Adarsh Multiple Campus Biratnagar, for their encouragement and necessary facilities provided for pursuing the research work. Words may fail to express gratitude to my research colleagues Professor Dr. Nagendra Prasad Sah, Professor Dr. Devendra Adhikari, Professor Dr. Damodar Thapa, Dr. Raju Ram Thapa, Dr. Ajaya Bhattarai, and Dr. Ram Prasad Koirala, who so willingly gave their time and expertise for successful completion of the research work

I would like to express my deepest gratitude to Professor Dr. Megh Raj Pokhrel, former Head, Central Department of Chemistry, Kirtipur for extending his warm hand for me to achieve the goal of research. I am very much indebted to Professor Dr. Vinay Kumar Jha, Professor Dr. Paras Nath Yadav, and Professor Dr. Amar Prasad Yadav of Central Department of Chemistry, for his invaluable suggestions and guidance at every moment of my research journey.

I also express my gratitude to Dr. Shiv Narayan Yadav, Former Head, Department of Microbiology and Mr. Tara Nand Yadav, Head, Department of Botany for their immense help during the various stages of my research. I am very much thankful to all nonteaching staffs of the Departments for all their help and support.

I am indebted to Nepal Academy of Science and Technology (NAST), Nepal for providing me Ph. D. fellowship. I am happy to acknowledge the services of SAIF,

STIC Cochin, SAIF, CDRI Lucknow, SAIF, IIT, Mumbai and IIT, Delhi, India for their help in sample analyses. I also extend my great honor to the entire team of Solid State and Structural Unit, Indian Institute of Science, Bangalore, India for their cooperation in recording the spectra of some compounds.

Last but not least, I would like to pay high regards to my lovable wife Mrs. Kalpana Chaudhary, my daughter Nabina and son Rahul whose moral support and encouragement energized me to pursue the research work. Above all, I would like to thank God, The Almighty, for having made everything possible by giving me strength and courage to do this work.

Narendra Kumar Chaudhary
July, 2018

ABSTRACT

The menace of drug resistance has been haunting the human world in the recent years and there is an urgent need to discover new chemotherapeutic agents with novel bioactivities and functionalities to address the severe challenges of multidrug resistance. Over a few decades of intensive research on metal-based drugs, Schiff base metal complexes have been considered as the active field of research in the coordination chemistry. The present research work evaluates the bio-functional activities of some aminoglycosides and β-lactam antibiotics in their derived form. Their structural modification by the formation of Schiff base and metal complexes, and their correlation with bio-functional activities has been a subject of much interest in the medicinal chemistry research. In view of this, three novel Schiff base ligands (KMAXC, AXCPC3, and AXCPC2) have been prepared and complexed with four transition metal ions viz. Co^{+2}, Ni^{+2}, Cu^{+2} and Zn^{+2}. The ligands and complexes were fully characterized with various physicochemical and spectroscopic techniques, like CHNS analysis, conductivity measurement, melting point measurement, FT-IR, ^{1}H NMR, ^{13}C NMR, electronic absorption, mass spectrometry, magnetic susceptibility and EPR studies.

Thermal stability and kinetic properties of the complexes were analyzed by thermogravimetric and differential thermal analysis (TGA/DTA) technique. The Coats-Redfern method was applied to extract thermodynamic parameters to explain the kinetic behavior of the complexes. Thermal data revealed high thermal stability and non-spontaneous nature of the various decomposition steps in most of the complexes.

The crystalline nature of the complexes was checked by powder X-ray diffraction study. XRPD data were analyzed in X'pert high score software and the diffractograms were carefully analyzed to extract the information about the nature of complexes. Some complexes were found crystalline and some were amorphous. The cell parameters and space group of the complexes were investigated by computing data in CHECKCELL and CRYSFIRE program package software. The surface morphology of the ligands and complexes were evaluated by scanning electron microscopy (SEM)

study and revealed their varying surface structures. The evaluated geometry of the complexes by spectroscopic techniques has been further supported by the information gathered from the molecular modeling study. The structure optimization by MM force field calculation was achieved by running the proposed molecular structures in CsChem3D Ultra-11 and ArgusLab 4.0.1 software program.

The biological potency of the synthesized compounds was investigated by antibacterial activity study, which was done by modified Kirby-Bauer paper disc diffusion technique. For this purpose, clinical strains of both gram-positive and gram-negative bacteria have been isolated and cultured in the laboratory. They have been interacted with synthesized compounds at variable concentrations in a solution prepared in DMSO. In most of the study, metal complexes of the prepared Schiff base ligands were found biologically active with enhanced potency, compared to the free ligand and starting compounds.

LIST OF ABBREVIATIONS

AM1	Austin model 1
Amk	Amikacin
Amx	Amoxicillin
AXCPC2	Amoxicillin-pyridine-2-carbaldehyde
AXCPC3	Amoxicillin-pyridine-3-carbaldehyde
B. subtilis	*Bacillus subtilis*
BHPP	1,4-bis[(2-hydroxybenzaldehyde)propyl]piperazine
BM	Bohr magneton
Co-AXCPC2	Cobalt complex of amoxicillin-pyridine-2-carbaldehyde ligand
Co-AXCPC3	Cobalt complex of amoxicillin-pyridine-3-carbaldehyde ligand
Co-KMAXC	Cobalt complex of kanamycin-amoxicillin ligand
Cu-AXCPC2	Copper complex of amoxicillin-pyridine-2-carbaldehyde ligand
Cu-AXCPC3	Copper complex of amoxicillin-pyridine-3-carbaldehyde ligand
Cu-KMAXC	Copper complex of kanamycin-amoxicillin ligand
DMF	Dimethyl formamide
DMSO	Dimethyl sulphoxide
DTA	Differential thermal analysis
DTG	Differential thermogravimetric
E. coli	*Escherichia coli*
EAS	Electronic absorption spectroscopy
EPR	Electron paramagnetic resonance
ESI-MS	Electrospray ionization mass spectrometry
ESP	Electrostatic potential
ESR	Electron spin resonance
FT-IR	Fourier transform – infra red
FWHM	Full width half maximum
ILCT	Intra ligand charge transfer
IR	Infra red
K. pneumoniae	*Klebsiella pneumoniae*
KMAXC	Kanamycin-amoxicillin

LMCT	Ligand-Metal charge transfer
M. P.	Melting point
MM2	Molecular mechanics 2
MS	Mass spectrum
Ni-AXCPC2	Nickel complex of amoxicillin-pyridine-2-carbaldehyde ligand
Ni-AXCPC3	Nickel complex of amoxicillin-pyridine-3-carbaldehyde ligand
nm	Nanometer
NMR	Nuclear magnetic resonance
P. vulgaris	*Proteus vulgaris*
ppm	Parts per million
RMS	Root mean square
S. aureus	*Staphylococcus aureus*
SCF	Self-consistent field
SEM	Scanning electron microscopy
TOF	Time of flight
TG	Thermogravimetric
TGA	Thermogravimetric analysis
UFF	Universal force field
UV/Visible	Ultraviolet/ Visible
XRPD	X-ray powder diffraction
Zn-AXCPC2	Zinc complex of amoxicillin-pyridine-2-carbaldehyde ligand
Zn-AXCPC3	Zinc complex of amoxicillin-pyridine-3-carbaldehyde ligand
Zn-KMAXC	Zinc complex of kanamycin-amoxicillin ligand

LIST OF SYMBOLS

A	Absorbance
$Å$	Angstrom
A	Arrhenius pre-exponential factor
a	Crystallite size
c	Concentration of solution in mole/L
d	Interplanar distance
E*	Activation energy
G	Exchange coupling interaction parameter
g	Lande's splitting factor
$g_{\parallel}$	g tensor in the z-axis
$g_{\perp}$	g tensor in x and y-axis
h	Plank's constant
I	Intensity of transmitted light
I_0	Intensity of incident light
k_B	Boltzmann constant
r	Correlation coefficient
R	Gas constant
T	Absolute temperature
T	Transmittance
x	Order of reaction
α	fraction decomposed
β	Conversion constant called Bohr magneton
β	Full width half maximum
β	linear heating rate
ΔG^*	Free energy of activation
ΔH^*	Enthalpy of activation
ΔS^*	Entropy of activation
ε	Molar absorptivity
θ	Scattering angle

λ	Wavelength
Λ_M	Molar conductivity
ν	Frequency of absorption
μ	Micro
µg/µl	Microgram per microliter
µS cm^{-1}	Micro Siemens per centimeter

LIST OF TABLES

LIST OF FIGURES

LIST OF SCHEMES

APPENDIX

TABLE OF CONTENTS

CHAPTER 2

CHAPTER 3

CHAPTER 1

INTRODUCTION

1.1 General Perspective

Coordination chemistry of transition metal complexes is gaining much popularity in the recent years due to their versatile applications in the various fields of chemical and medical sciences and comprises a large body of bio-inorganic chemistry research. It has inspired the chemical researchers to design and fabricate novel metal complexes, all over the world. Metal ions make bridge between the drug substances and pathogenic organisms and thus the field of metal drug interaction chemistry is growing rapidly in the medical and chemical sciences. Microbial interaction with a variety of metal ions at various oxidation states is sometimes beneficial or detrimental that depends on the physical and chemical nature of the metal ions (Abdallah *et al.*, 2009). Treatment of diseases by pure herbal medicines from nature's chest has been a quest of mankind since ancient times. Currently, there is a substantial decline in the use of pure herbal medicines because of complexity in their chemical extraction and slow interaction with diseases (Dias *et al.*, 2012). Pharmaceutical research has expanded after the Second World War to include a massive screening of microorganisms for new antibiotics because of the discovery of penicillin. With the successful record of synthetic medicinal chemistry, the identification of new metabolite from living organisms would be the core pharmaceutical discovery efforts. However, the menace of drug resistance is haunting the medical science and the discovery of synthetic drugs is today's therapeutic desire of pharmaceutical research. Still, many natural product based drugs are in the clinical practices that need extensive research (Bérdy, 2012; Li & Vederas, 2009).

The first metal based drug that emerged in the late 19^{th} century was cisplatin whose serendipitous discovery as a potent anticancer drug opened the gate of unexplored world of metal-based chemotherapeutic agents. It was the most effective anticancer

drug in the market (Chakraborty *et al.*, 2010; Gibson, 2016). The resounding therapeutic success of cisplatin and its analogs has triggered tremendous effort in search of alternative metal-based chemotherapeutic agents in the past few decades. Since then the metal-drug interaction in the field of coordination chemistry has been focused well and considered as an active field of research (Romero-Canelón & Sadler, 2013). There is a great battle between antibiotic research and increased antibacterial resistance in the medical science which provides ample scope for the generation of a new class of antibiotics with high-grade biological activities. There is an urgency to discover and characterize new drugs with enhanced activity, selectivity, bioavailability and fewer side effects than conventional drugs to treat current diseases.

The compounds of interest for the present research work are the Schiff bases of biologically active aminoglycosides and β-lactam antibiotics and their fabrication with some selected 3d-metal ions. Incorporation of metallo-elements in the cage of novel Schiff base ligand containing various donor atoms change the physiological and biological profiles of such molecules (Vardhan *et al.*, 2015). In our study, the azomethine linkage of Schiff base is a key part of its structure that provides multifunctional activities in the various fields of sciences. The ligands not only control the reactivity of metal of the complexes but also play a critical role in determining the nature of interactions involved in recognition of biological target sites. There are many biologically active and naturally derived compounds whose structures are very similar to Schiff bases that possess various bio-functional activities, as an antibiotic, anti-microbial, anti-tumor, analgesic, anti-inflammatory and several others (Chaturvedi & Kamboj, 2016). The potential interest in the research of Schiff base metal complexes is also due to its linkage with a number of interdisciplinary research areas that include material science, catalysis, magnetochemistry, and electronics. The application in electronics is widely expanding in the recent years.

1.2 Schiff Bases and Their Chemistry

Schiff bases comprise one of the most widely used families of organic compounds, formed as the condensation product of the chemical reaction of the active carbonyl group and a primary amine. Their discovery and chemistry are the results of great

pioneer work of a German chemist Hugo Schiff in the year 1864. This has revolutionized the chemical research in the field of coordination chemistry in the late 19th century (Brodowska & Łodyga-Chruscinska, 2014; Jia & Li, 2013). In doing research in aniline chemistry, he studied the reactions of aniline with many other aldehydes and finally reached to the discovery of the imine-based organic compound called Schiff base. They are also called anils, imines or azomethines. This class of compounds is mainly recognized by the presence of an active imine (-CH=N-) group that carry potential binding site for the metal ions through nonbonding electrons of the nitrogen atom (Da Silva *et al.*, 2011). In the present research work, the structural unit of Schiff bases also possesses many other hetero-elements like oxygen and sulphur as main component elements for chelate formation with metals. The nature of donor atoms that act as coordination site, their electronegativity and steric factors largely determine the bonding ability of the ligands. By virtue of the presence of lone pair electrons on N-atom, electron donating character of the double bond and low electronegativity of nitrogen, N-atom of the azomethine group (>C=N) acts as a very good donor site and Schiff bases are considered as active ligands (Kostova & Saso, 2013).

Recently, Schiff bases occupy a leading position in metal coordination chemistry and provide a significant attraction in creating novel lead due to their simplicity in preparation, variation in properties, biomedical, biochemical and industrial applications (Jayaseelan *et al.*, 2016). There are several amines and carbonyl compounds in the library of organic chemistry that enable the synthesis of Schiff bases with diverse structural features. For the synthesis of Schiff bases, the basic carbonyl group may be aldehydes (aromatic or aliphatic) or a ketone. The stability of imine group is controlled by the presence of substituent groups attached to (>C=N) linkage. The general reaction for the formation of Schiff base is illustrated in the Scheme 1.

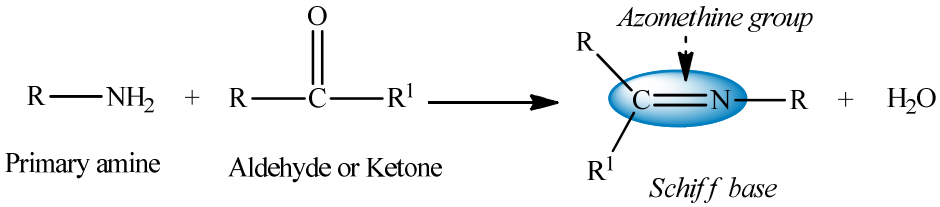

Scheme 1: Reaction scheme for Schiff base formation

Where R represents an alkyl, aryl, cycloalkyl or heterocyclic groups which may be variably substituted and R^1 may be an alkyl, aryl group or H atom. The formation of Schiff base is a reversible process and generally takes place by refluxing the mixture under the neutral condition or in the presence of acid or base catalysts. The formation is generally driven to the completion by the separation of product or removal of water.

1.3 Schiff Base Transition Metal Complexes

Many research papers have been published during the last few decades on the synthesis and pharmacology of Schiff base metal complexes. Schiff bases are versatile pharmacophores that cave in metal ions within their structural unit due to the presence of various donor atoms (Kajal *et al.*, 2013; Kostova & Saso, 2013). Transition metal complexes of Schiff bases are generally formed by the chelation of Schiff base ligands with metal ions at variable oxidation states. The vacant d-orbitals of metal ions make available space for the easy coordination of nonbonding electrons of donor atoms of ligand and even sometimes this ligation takes place by deprotonation process. There is a general rule of coordination chemistry that chelation makes the complex compounds more stable due to electron circulation inside the ring and changes the physiological profile of the complexes (Ceyhan *et al.*, 2011; Sumrra *et al.*, 2014). In fact, their stability increases when the chelate ring is five or six member. The aryl group bonded to the nitrogen or to the carbon of the azomethine group prevents them from rapid decomposition and polymerization.

A lone pair electron in sp^2 hybrid orbital of azomethine nitrogen is of considerable chemical and biological importance since it makes easy coordination with metals. Variation in the denticity of Schiff bases makes control over the stereochemistry of metal complexes which affects in their physiological profiles. These complexes carry

a wide range of applications in catalytic chemistry, analytical, clinical and biochemical fields and in addition, they also possess considerable physiological activities (Abou-Hussein & Linert, 2014; Cozzi, 2004; Shebl, 2014). Multifunctional activities of such metal complexes are the prime sources of metal-based research in the chemical science. Many drug substances have the metal ion that plays a key for the better success of biological activities (Barnham & Bush, 2014). Several research papers describe the enhanced activities of metal complexes compared to the free ligand. Recently a large volume of research reports on Schiff bases highlights them as a type of potential antibiotic which by chelation with metals further enhance their potency. Chelation causes a drastic change in the biological properties of the ligands and the metal moiety (Majumder *et al.*, 2003). It has been reported that chelation is the cause and cure of many diseases including cancer. The present study of the research focuses the formation of several Schiff base ligands from different precursor compounds and their metal complexes with 3d-metal ions. These chelated complexes of Schiff bases are easily absorbed in the human intestinal cells and increase their antibacterial strength.

1.4 Biological Applications of Schiff Bases and Their Metal Complexes

Recent advances in coordination chemistry reveal Schiff base as a privileged ligand since most of the bio-molecules in the living system are structurally similar to this class of compound. The biofunctional activity of metal-based complexes in medicine and chemotherapy has spurred the growth of interest in the scientific world in the past few decades, after the successful clinical application of Cisplatin as a potential anticancer drug. So, metal drug interaction in medical science is becoming a subject of great research interest (Farrell, 2002; Hannon, 2007; Reedijk, 2008). Transition metal chemistry of Schiff bases has gained momentum in the late 19^{th} century and since then metal-based drugs of Schiff bases drew the significant interest of researchers in the medical science for their immense biological activities. Most of the metals being unnatural to the human body, because of having no effective mechanism for their rejection and toxic behavior (Murtaza *et al.*, 2012), there has been a rapid expansion in research and development of novel metal-based drugs with improved pharmacological properties. Several medical problems that arise due to free metal ions toxicity may be ameliorated by their chelation with ligands.

Schiff base metal complexes have important biological applications as antibacterial, antifungal, antitumor, analgesic, anti-inflammatory and antimicrobial agents. It has found, that some drugs have greater activity when administered as metal complexes than as free organic compound (Leelavathy & Arulantony, 2013; Shoaib *et al.*, 2013). The discussion in this report is limited to the comparable antibacterial study of Schiff base ligands and their metal complexes. The potential biological activity of Schiff base metal complexes is related to the presence of lone pair electrons that participate in anchoring of bio-molecules in the living body.

1.5 Other Applications of Schiff Bases and Their Metal Complexes

Besides the bio-medical applications, Schiff base metal complexes also bear various important applications in chemical, industrial and electronic fields. In the material science, they are found to have good corrosion inhibitory activity (Madkour & Elroby, 2015). This phenomenon is the spontaneous formation of a monolayer on the surface to be protected. A large number of Schiff base metal complexes are identified by an excellent catalytic activity in a variety of synthetic chemical reactions at high temperature (> 100 °C) and in the presence of moisture. Many research reports display their use in homogeneous and heterogeneous catalysis. In many biological systems, Schiff bases and metal complexes show active participation in the synthesis of some life molecules like enzymes and biopolymers (Hameed *et al.*, 2017). Numerous scientific publication reports, appearing annually in the recent years, highlight the keen interest of researchers in metal complexes in which Schiff bases play a critical role as ligands. Due to excellent selectivity, sensitivity and stability of Schiff bases for specific metal ions, a large number of Schiff base ligands have been used as cation carriers in potentiometric sensors.

In modern technology fields, Schiff bases and metal complexes deliver important applications because of their photo- and thermochromic properties (Rawat et al., 2015). They have applications in optical computers, to measure and control the intensity of radiation, in imaging systems, as well as in the molecular memory storage devices. Due to photochromic properties, they function as photo stabilizer, dyes for solar collectors and solar filters. Schiff bases can also be used as stationary phase in

gas chromatography, due to their thermal stability (Brodowska & Łodyga-Chruscinska, 2014).

1.6 Aminoglycoside under Investigation

The antibiotic therapy to prevail over the disease in the treatment process is the principal concept of modern medical science. The basic problem we are facing with antibiotic therapy is that after a new antibiotic is introduced, resistance to it will, sooner or later, arise. Thus there is a continuing race between the discovery and development of new antibiotics (Aminov, 2010; Walsh & Wencewicz, 2013). Out of the several classes of antibiotics, the one of our interest is aminoglycosides. The aminoglycosides are a valuable class of antibiotics that exhibit versatility in their biological activities. The naturally occurring aminoglycosides have also recently been investigated as antifungal agents (Fosso *et al.*, 2015). These are highly potent, broad-spectrum antibiotics with many desirable properties for the treatment of life-threatening infections. Chemically, they are amino modified sugars with ring units linked by glycosidic linkage and are considered as the first important therapeutic agents produced by bacterial fermentation. Streptomycin was the first aminoglycosidic antibiotic emerged in 1944 and thereafter, a series of milestone compounds like kanamycin, gentamicin, and tobramycin has been introduced which established the usefulness of this class of antibiotics for the treatment of gram-negative bacterial infections. In the recent years, many semi-synthetic and modified aminoglycosides have been introduced in the medical library, with improved antibacterial sensitivity. Almost all of the aminoglycosides have essentially the same mode of antibacterial action; they inhibit bacterial protein synthesis by binding to specific sites on the 30S subunit of the 70S prokaryotic ribosome (Wilson, 2014). In addition to their potential antibacterial efficacy, all aminoglycosides can cause toxic effects to the kidneys and inner ear. This nephrotoxicity is reversible, while the ototoxicity is the permanent effect of the ear. The toxic effects of aminoglycosides were initially discovered in the first clinical trials of streptomycin. Within the internal ear, streptomycin preferably damages the vestibular organ and in some cases, also damage cochlea that results in permanent hearing loss or tinnitus (Kalkandelen *et al.*, 2002). The other aminoglycosides like kanamycin, and amikacin are cochleotoxic (Mingeot-Leclercq *et al.*, 1999). In the present research work, kanamycin is

undertaken for the generation of novel Schiff base, in combination with other compounds.

Kanamycin

Kanamycin, in complex form, has three component units; kanamycin A (major component), B, and C. The disulphate of kanamycin A at its low concentration is a broad spectrum antibiotic, very actively used to treat the infections caused by many gram-positive bacteria. In unmodified form, kanamycin has shown severe toxic effects like nephro- and ototoxicity which results in kidney failure and irreversible hearing loss respectively (Schweitzer *et al.*, 1984). The four amine groups in kanamycin A, in combination with seven hydroxyl groups, serve it as a better substrate to obtain semi-synthetic and improved antibiotics. Amine groups in sugar rings of kanamycin A, not only provide anchoring sites for the metal ions but also serve as the reactive site for the formation of Schiff base by the condensation with active carbonyl groups. The structure of kanamycin is presented in the Figure 1.

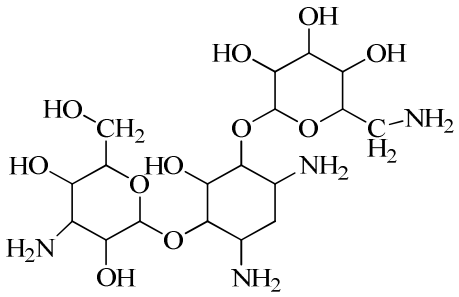

Figure 1: Structure of Kanamycin

1.7 β-Lactam under Investigation

β-Lactams are the most successful class of antibiotic developed so far and the pace of their discovery is illuminating these days (Lewis, 2013). Despite the high level of clinical success, a serious mechanism of resistance had emerged which could render the penicillin inactive by the production of β-lactamase (Geddes *et al.*, 2007). Several attempts have made to overcome the effect of β-lactamase and we have reached to the discovery of fourth generation semi-synthetic β-lactam. The first clinically available

β-lactam antibiotic, benzyl penicillin was identified and developed in the year 1920s and came into clinical use during Second World War. Despite its narrow range of antibacterial activity and unsuitability for oral administration, several efforts were made to generate new penicillin based therapeutic agents (Ligon, 2004). This enabled research into the effects of adding various side chains and the generation of semi-synthetic penicillin has emerged. A research finding in the year 1940s, the β-lactamase enzyme produced by *Staphylococcus aureus* strain that inactivated the penicillin available at that time, broke the rapid and widespread clinical use of penicillin. Thus the research endeavor was directed at developing penicillin that overcomes the effect of β-lactamase enzyme. Further penicillin research in the year 1961, led to the important discovery of ampicillin, the first orally available broad-spectrum β-lactam antibiotic with upgraded activity against various gram-negative organisms. In continuation of the penicillin research, a single change to the side chain of ampicillin resulted in developing amoxicillin, in the year 1972. Amoxicillin had the same potent broad spectrum antibiotic activity as ampicillin, but with much better oral absorption and showed more rapid bactericidal activity against certain bacterial pathogens.

Amoxicillin Trihydrate

Amoxicillin trihydrate (Figure 2) is a bacteriolytic β-lactam antibiotic drug of class penicillin, structurally similar to ampicillin and is used against a similar variety of infections. It is the 4-hydroxy analog of ampicillin. The bio-functional activity of Amoxicillin is related to lactam ring that inhibits bacterial growth by proteolysis mechanism (Chaudhary & Mishra, 2014; Iqbal *et al.*, 2005). The presence of the amine group in this compound is suggested it a better starting compound for the synthesis of new Schiff base. Being unstable in the acidic medium in our stomach, Amoxicillin requires stability for better antibacterial functions which is achieved by complexation with metal ions in the form of Schiff base, containing potential donor atoms like N, O, and S (Chaudhary, 2013).

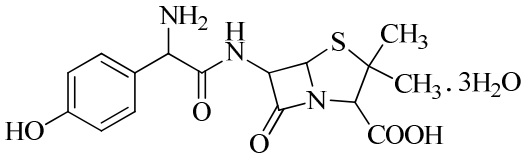

Figure 2: Structure of Amoxicillin Trihydrate

1.8 Pyridine Derivatives Used for the Preparation of Schiff Bases

Heterocyclic compounds are widely distributed in nature and play an essential role in various biochemical processes. Pyridine belongs to heterocyclic aromatic compound with distinctive fishy odor. It deserves its position in the various fields of chemistry due to its intensive application. A large number of pyridine-based heterocyclic compounds are associated with diverse pharmacological properties such as antimicrobial, anticancer, antiviral, anti-HIV, antifungal and several other activities (Altaf *et al.*, 2015). Many drug chemicals like isoniazid and nicotine (anti-tuberculosis drug) and vitamin B compounds like niacin and pyridoxal have pyridine ring as a structural component (Chaudhary & Mishra, 2017). Thus insight into the aldehyde derivatives of pyridine has been considered for the research. In the present investigation, pyridine-2-carbaldehyde and pyridine-3-carbaldehyde were used for the generation of novel Schiff base ligands with amoxicillin trihydrate. The presence of aldehyde group is the best precursor for the Schiff base condensation reaction with $–NH_2$ group of amoxicillin. The chemical structures of these compounds are shown in the Figure 3.

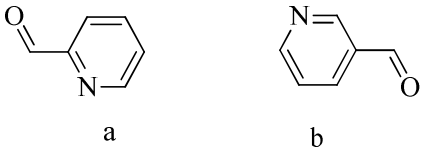

Figure 3: Structures of (a) Pyridine-2-carbadehyde (b) Pyridine-3-carbadehyde

1.9 Amoxicillin Derived Schiff Bases

Schiff Base Ligands:

Multidrug therapy is considered as a new evolving technique to prevail over the bacterial infections. Many of the previous antibiotics are under the bacterial resistance which causes the substantial burden to the human population. In the days of penicillin, this was only the drug to treat bacterial infections but in the coming days, as the report says; many antibiotics have lost their effectiveness against common bacterial infections (Hecht, 2004; Ventola, 2015). In the present investigation, we have worked for the synthesis of amoxicillin derived Schiff bases by the interaction with kanamycin, pyridine-2-carbaldehyde, and pyridine-3-carbaldehyde compounds. This is aimed to enrich the medical library with a new class of antibiotics with better activities. Schiff base ligands have attracted significant and increasing interest for the researchers due to complex formation behavior with metals. They possess various donor sites that facilitate coordination properties. The presence of aldehydes and amino groups in such compounds are the basic formulation to consider for the preparation of Schiff base ligands. Further, the various pharmaceutical importances of Schiff base ligands forced us to do research work in this field. The structure of Schiff base ligands is given in the Figures 4 - 6.

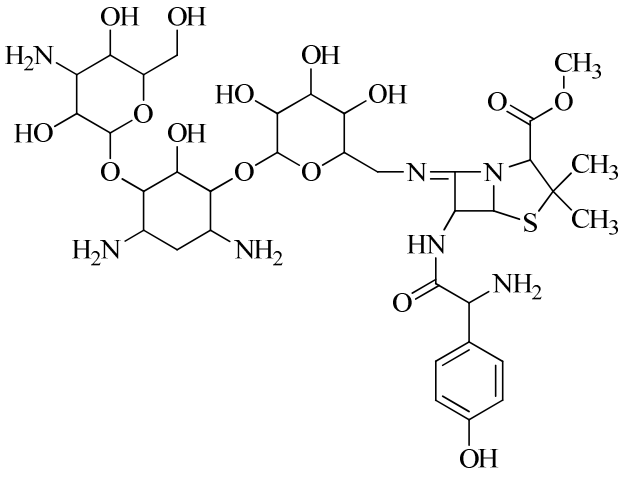

Figure 4: Structure of KMAXC Schiff base Ligand

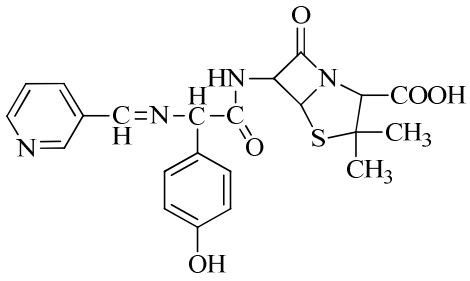

Figure 5: Structure of AXCPC3 Schiff base Ligand

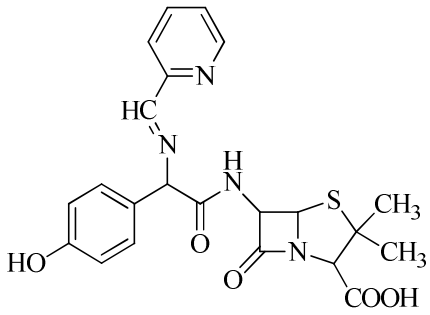

Figure 6: Structure of AXCPC2 Schiff base Ligand

1.10 Choice of Metallo-Elements under Investigation

Many life-critical processes require metal ions and their role varies across structural to catalytic. Transition metal ions have a rich chemistry due to close lying energy bands made up of partly filled d-orbitals, and thus serve as unique agents in a variety of biological processes. The ability to recognize, to understand at the molecular level, and to treat diseases caused by insufficient metal-ion function constitutes an important aspect of medicinal bioinorganic chemistry. Normal metabolic functions and immune systems in the livings essentially require some metals in trace and ultra trace amounts whose presence significantly change the physiological profile of the bio-molecules and work at the molecular level in the cells (Prashanth *et al.*, 2015). Such metals play important structural, electrochemical and catalytic functions in the body. There is a long history of the use of metals in medicines but metal-based drugs now become a pioneer research work in the medical science. These metals at high and low concentrations poison living bodies and give birth of many kinds of diseases. Transition metals have special ability to coordinate with ligands and form stable complexes in the biological systems (Abu-Dief & Mohamed, 2015). Many biological

pieces of evidence in the living system display the fact that increased concentration of some metal ions block the transport site for others and cause depletion of some other metal ions. Besides the various drug substances, many human food ingredients containing bio-molecules are essentially the bio-stimulators and bio-ligands which are capable of coordinating some of the metallo-elements and thus alter their homeostasis behavior (Holm *et al.*, 1996). In the present research work, four 3d-metals, viz. Co(II), Ni(II), Cu(II) & Zn(II) have been considered for the formation of stable complexes. These metals have partly filled d-orbitals which offer a significant role in the coordination behavior with ligands.

1.10.1 Cobalt

Cobalt belongs to first-row transition metal series and displays three oxidation states, +1, +2 and +3. Its +3 oxidation state is extremely unstable but nevertheless is important in biology. +2 oxidation state of the cobalt is the most stable and bears significant importance in the biological system. It is an essential element for life in a very trace amount and constitutes a central component of the vitamin B_{12} (cyanocobalamin), which is essential in protein formation and DNA regulation. Cobalt is used to treat anemia in pregnant women because it stimulates the production of red blood cells (RBC). However, its high concentration may damage human health (Sinha, 2014). Several literatures reveal important bio-functions of cobalt complexes as having antibacterial, anti-tumor and others.

1.10.2 Nickel

Nickel is the earth's 7^{th} most abundant transition metal, which exists mostly in +2 oxidation state in its complexes. Its role in the material science is unforgettable. The alloying behavior of nickel with various other metals and nonmetals is a very interesting field of research in material science. Ni^{+2} may have a variety of coordination numbers and geometries in the complex. Nickel complexes mostly configure octahedral, tetrahedral and square planar geometries. The enzyme chemistry in the bio-medical science highlights nickel as an essential component of large numbers of enzymes in the human body, without which the normal metabolic functions are inconceivable (Boer *et al.*, 2013). Literatures report the multifunctional

bio-activities of nickel complexes of Schiff bases and hence nickel has considered for the research.

1.10.3 Copper

Copper belongs to 3d-transition metal series and its coordination chemistry is limited to its two accessible oxidation states, +1 and +2. It is an essential element due to its bio-essential activity, oxidative nature and its involvement in complex formation in many biological processes (Lakshmipraba & Arunachalam, 2010). It was first to be an essential biological element in the 1920s when anemia was found to result from copper deficient diets in animals and the addition of copper salts corrected this adversity (Matak *et al.*, 2013). It serves as a catalytic component in many enzymes. Copper in trace quantity is required by all living organisms to maintain proper cellular functions. Excessive copper concentration, however, is extremely toxic due to its chemical reactivity. Wilson's disease and Menkes kinky hair disease are the two lethal hereditary disorders caused due to malfunctioning in copper absorption (Bandmann *et al.*, 2015). Its +1 oxidation state has a diamagnetic d^{10} electronic configuration and forms complexes without any crystal field stabilization energy. Its complexes are biologically relevant due to its reductive activation towards molecular oxygen. Its +2 oxidation state exists as a d^9 electronic configuration which favors coordination with various ligands that assume square planar to distorted octahedral geometries. Crystal field stabilization energy of its complexes makes it less labile towards ligand exchange phenomenon and is regarded as the best candidate for incorporation into pharmaceutical industries. However, its +3 oxidation state is relatively rare.

1.10.4 Zinc

Zinc offers +2 oxidation states in most of its coordination compounds because of its complete d-shell electronic configuration. The d^{10} electronic configuration of Zn(II) ion affords no crystal field stabilization energy and there is no evidence that it is oxidized or reduced in biological reactions. Generally, Zn(II) complexes favor four coordinated tetrahedral structure but in its various complexes, six coordinated octahedral geometry has also observed. It is significantly one of the most important essential metallo-element, necessary to all forms of life. Its d^{10} electronic

configuration tends to form stable complexes with proteins and enzymes. Its role in the biological system is supposed to be due to the involvement in the maintenance of vitamin A level in blood by releasing it from liver (Cabral *et al.*, 2005). Zinc is believed to participate in the synthesis and storage of insulin in β-cells. It is an essential cofactor in many metabolic enzymes and regulatory proteins. Many enzymes show their functions only in the presence of zinc. Besides its role in biological systems, it has also antiseptic properties which are widely used in cosmetics. Several research findings in the field of bioinorganic chemistry reveal zinc complexes as potential drug candidates in clinical practices. However excess zinc in the human body is toxic and interfere with the normal functions of the metalloproteins (Jabali & Abu Ali, 2016).

1.11 Objectives of the Present Study

1.11.1 General Objective

The world is running out of antibiotics. The emergence of superbugs is at the heart of the gradual demise of the antibiotic era. There is no discovery of new potent antibiotics in the past few decades. The antibiotic era is likely to fade away, sooner rather that later. So, growing interest in metal drug complexes has become a potential field of research in coordination chemistry and medical science. The search for more efficient and safer antibiotics generates the ideas to design and modify the existing drug libraries. The current research publications of drug substances reveal that the drug resistance has become a great problem in the recent years (Raman *et al.*, 2007), for the treatment of many infectious diseases caused by bacterial pathogens and other causative agents. Schiff base complexes are found to have immense application in various fields of sciences. Although a number of chemotherapeutic agents are available in the market there is a global threat in the medical science because the pathogenic organisms are developing resistance to these agents. So, it is important to search more effective and safer chemotherapeutic agents.

The present research work was attempted with a view to synthesizing novel Schiff base ligands of aminoglycosides and β-lactam antibiotics and encapsulation of some 3-d transition metals inside their cage. The related literature search has revealed that

there was no extensive study done for the generation of Schiff bases from the antibiotics of these types. Due to the large sized molecular structure of these antibiotics, much precautions and reaction conditions have been applied to get the ultimate results.

1.11.2 Specific Objective

The present research work has been undertaken with the following specific objectives:

- To synthesize novel Schiff base ligands and analyze their structures by spectroscopic techniques such as IR, ^{1}H & ^{13}C NMR, MS, UV-visible (EAS), ESR, TGA/DTA, magnetometry, X-ray powder diffraction and elemental analysis.
- To synthesize metal complexes of prepared ligands taking Co(II), Ni(II), Cu(II) and Zn(II) salts and their structural analysis by spectroscopic techniques such as IR, ^{1}H & ^{13}C NMR, MS, UV-visible (EAS), ESR, TGA/DTA, magnetometry, X-ray powder diffraction and elemental analysis.
- To investigate the physical parameters of synthesized compounds such as pH, melting point, and conductivity.
- To familiarize the surface topography of ligands and metal complexes by scanning electron microscopy (SEM) study.
- To screen the antibacterial activities of synthesized ligands and metal complexes.

1.12 Justification of the Study

Active participation of drug substances for the therapeutic success is a matter of great concern for the researchers in the pharmaceutical industries. There is a challenging demand in medical science for the better search for potentially active drugs that are used for the treatment of diseases. Increased antibacterial resistance terrorizes human health that requires myopic thinking in the scientific world and so insight into modifications of previous drugs has to be visioned well. Metallo-elements in trace and ultra-trace amounts are also very essential for the normal physiological function of the human body. No research works related to Schiff bases of aminoglycosides

(kanamycin) and β-lactam antibiotics (amoxicillin) are in the literature search. With this expectation, metal complexes of novel Schiff bases derived from aminoglycosides and β-lactam antibiotics will be the new hope for better drug substances in the clinical practices.

CHAPTER 2

LITERATURE REVIEW

2.1 General Overview

This chapter explores the research works related to Schiff base metal complexes that had been carried in the past. Due to their versatile applications in various fields of sciences, there is a vast dimension of research and the field is expanding enormously. Almost one hundred and fifty years of study, in the field of Schiff bases and their transition metal complexes, forecasts the research interest of the scientists and this field is growing enormously in the recent years. It is not worth to say that the research of this type plays a key role in the advancement of coordination chemistry. In the recent decades, a large volume of research works in chemistry has been dedicated to the synthesis, characterization and biological applications of metal complexes of Schiff bases. Schiff base is the most familiar discovery of Hugo Schiff, who has called one of the founders of modern chemistry. The work of Professor Wohler excluded the concept of *vis-vitalis* theory, demonstrating that there is no metaphysical difference between organic and inorganic substances. The great pioneer work of Berzelius, Wohler and Hugo Schiff changed the vision of thinking about the organic chemical substances. Professor Schiff memorized himself by the word: "Remember that you descend from Berzelius because Berzelius taught chemistry to the old Wohler and the old Wohler taught me". Professor Schiff, the native of Germany, has continued his research work in Italy and introduced himself as an Italian chemist (Qin *et al.*, 2013; Rani *et al.*, 2015). After the novel work of Schiff in 1864, many researchers were involved in this research field and got success in synthesis and structural design of this class of compounds.

For the continuation of Schiff base research, Kaban and Fidaner (1990) synthesized a novel Schiff base ligand by the condensation of hetarylcarboxaldehydes with p-phenetidine and characterized by spectral techniques. Four octahedral Mn(II), Co(II),

Ni(II) and Cu(II) complexes and one tetrahedral Zn(II) complex of new Schiff base ligand 1,2-bis(2'-pyridylmethyleneimino)benzene derived from 2-pyridinecarboxaldehyde and 1,2-phenylenediamine were prepared by Kasselouri et al. (1993). They have been characterized by various physical and spectral techniques. Maclachlan *et al.* (1996) have reported the synthesis of Cu(II) and $V^{IV}O$ complexes of an open chain (1:2) Schiff-base ligand (H_2L1), derived by the template condensation of diaminomaleonitrile (DMN) and salicylaldehyde, and dicopper(II) complexes of (2:2) macrocyclic Schiff-base ligands derived by template condensation of diformylphenols and diaminomaleonitrile and also investigated their crystalline structure by X-ray diffraction study. The work has been expanded enormously in the early 21^{st} century after the successful applications of Schiff bases and metal complexes in various disciplinary sciences.

Recent investigations in coordination chemistry regard Schiff base organic compounds as one of the most employed classes of ligands. The research area encompassing the coordination compounds with the azomethine group as the main character is widely expansive due to their potential interest aroused in various interdisciplinary fields. Metal coordination to organic ligands brings a dramatic change in physiological and pharmacological profiles of chelated compounds (Haas & Franz, 2009). Chelation also provides stability of the compounds. Schiff bases are generally the drug substances which are used in medical science as chemotherapeutic agents. Chemotherapy, in general, refers to the treatment of disease with chemicals. When used in reference to infectious diseases, the term is antimicrobial chemotherapy. Besides their chemotherapeutic applications, they have played major roles in other fields also. Simple preparative method and easy structural design further popularize Schiff base and its metal complexes in the research field. This literature review highlights some areas of interest to Schiff bases and metal complexes based on their applications.

2.2 Pharmaceutical and Biomedical Applications

There are numerous publications covering the potential use of Schiff bases in therapeutic and biological fields either as potential drug candidates or diagnostic probes and analytical tools. Moreover, Schiff bases are present in various natural,

semi-synthetic and synthetic compounds and have been demonstrated to be essential for their biological activities. The review article of Abu-Dief & Mohamed (2015); Prakash & Adhikari (2011); Da Silva *et al.*, (2011) and Anand *et al.*, (2012) have summarized the important applications of Schiff bases and their metal complexes. A huge number of Schiff base metal complexes are of potential biological interest because of their remarkable biomedical applications, being used as successful models of biological compounds. They have important applications as anticancer (Chakraborty *et al.*, 2010; Sahu *et al.*, 2012), antibacterial (Al-Sha'alan, 2007; Keypour *et al.*, 2014), antiviral (Shebl, 2014), antifungal (Jarrahpour *et al.*, 2004; Sherif & Abdel-Kader, 2014), analgesics (Osowole & Balogun, 2012), anti-inflammatory and several others.

Salicylaldehyde is a very important drug component found in many drugs that contain its cyclic system. Some piperazine derivatives are also known to possess antimalarial activities. Therefore to widen the applications of these class of compounds, El-Sherif *et al.* (2012) have synthesized Schiff base ligand 1,4-bis[(2-hydroxybenzaldehyde)propyl]piperazine (BHPP) from salicylaldehyde and 1,4-bis(3-aminopropyl)piperazine. They further metalize the ligand with three divalent metal ions (Co^{+2}, Ni^{+2}, and Cu^{+2}) and investigated their structure and biological activity. The hexadentate Schiff base ligand (BHPP) was found to possess better antibacterial activity against both gram-positive and gram-negative bacteria. Three complexes also exhibited moderate activity against the fungal strains when compared with standard Amphotericin. The structure of BHPP ligand is presented in the Figure 7.

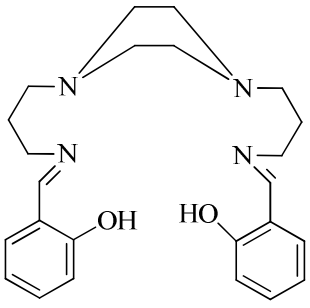

Figure 7: Chemical structure of (BHPP)

The Schiff base compound, Salicylidene Anthranilic Acid (SAA) derived from Salicylaldehyde and 2-substituted aniline and its three metal complexes with Cu(II), Ni(II) & Co(II) have found to possess good anti-inflammatory and anti-ulcer activity. However, the copper complex of this compound showed increased antiulcer activity.

A binuclear tetradentate Schiff base ligand was prepared from 3,3',4,4'-tetraminobiphenyl and 2-aminobenzaldehyde (Figure 8) and its three transition metal complexes with Cu^{+2}, Ni^{+2} and VO^{+2} have been synthesized (Mahalakshmi & Rajavel, 2010). The structure of the ligand and its metal complexes was established by spectral, analytical and electrochemical studies. The antibacterial evaluation of ligand and its metal complexes showed the higher antibacterial activity of the complexes compared to the free ligand.

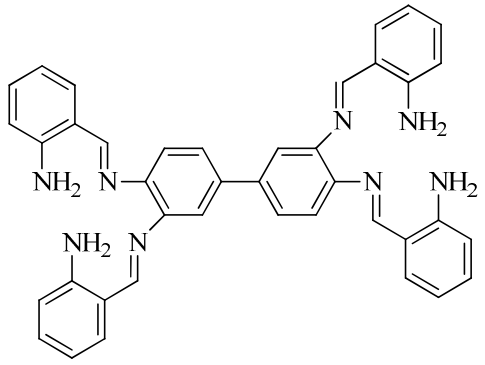

Figure 8: Structure of binucleated tetra dentate Schiff base ligand

Urease has the detrimental effect on human health by causing peptic ulcers, stomach cancer etc. Transition metal complexes of some Schiff bases are also found to have potential urease inhibitors. Chen *et al.* (2010) prepared four Schiff base ligands HL^{1-4} by the reaction of 3,5-dibromosalicylaldehyde with 2-chlorobenzylamine (L^1), benzylamine (L^2), cyclohexylamine (L^3) and N,N'-dimethylethylenediamine (L^4). These were complexed with four transition metals (Cu, Co, Ni, and Zn). Their evaluation for the inhibitory activity on jack bean urease suggested stronger effect and greater urease inhibitory power. The proposed structure of copper the complex of HL^1 is shown in Figure 9.

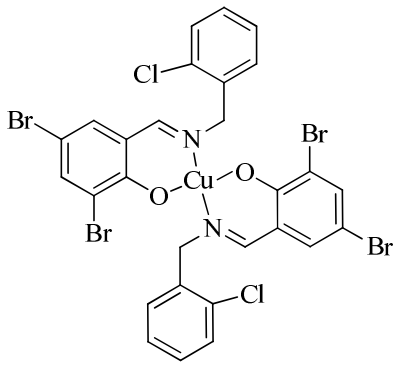

Figure 9: Proposed structure of Cu complex with HL

Many of the Schiff bases and their metal complexes are reported to have anti-cancer properties. Benzamide and its derivatives possess medicinal values as antibacterial, antifungal, analgesic, antihelmintic, anti-inflammatory, antimalarial, antitumor and antiallergic activities and also employed in the preparation of aromatic ligand. Similarly, the role of thiophene derivatives in the medicinal chemistry is very well known for their therapeutic applications. Ni(II) and Zn(II) complexes of general composition $M(L)X_2$ and $M(L)_2X_2$ ($X = Cl^{-1}$, OAc^{-1}) of Schiff base (Figure 10) obtained by the condensation of 2-aminobenzamide with Thiophene-2-carbaldehyde are reported to have better anti-proliferation effect on human breast cancer cell line (MCF-7) and human hepatocellular liver carcinoma cell line (HepG2) compared to the of free ligand (Tyagi *et al.*, 2015).

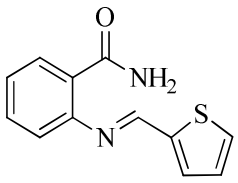

Figure 10: Structure of Schiff base ligand

Samanta *et al.* (2007) reported the synthesis of tetradentate Schiff base ligands L^1, L^2 and L^3 from 2-acetyl pyridine with 1,3-diaminopropane and N,N-dimethyl-1,3-diaminopropane for L^1 and L^2, and Pyridine-2-carbaldehyde with 1,4-diaminobutane for L^3 ligands. Anti-microbial activities of these Schiff base ligands and their metal complexes against Candida tropicalis and Bacillus megaterium have shown to possess interesting biochemical functions.

Reiss *et al.* (2014) have synthesized four metal complexes of the type $[ML_2(H_2O)_2]$ (M = Co(II), Ni(II), Cu(II) and Zn(II)) with Schiff base ligand of cefotaxime and salicylaldehyde. Cefotaxime is a β-lactam antibiotic under the class cephalosporin and possesses increased antibacterial activity. In the present work, they have tried to enhance antibacterial activity by the formation of Schiff base ligand and metal complexes. All the compounds were tested for *in vitro* antibacterial activity against pathogenic bacterial strains. The results revealed the superior antibacterial activity of the metal complexes than the Schiff base.

Three new transition metal complexes of the type $ML_2.2H_2O$ [M = Co(II), Ni(II) and Cu(II)] have been synthesized with Schiff base derived from 3-substituted-4-amino-5-mercapto-1,2,4-triazole and 4-chloro-3-coumarinaldehyde. Their structures have been proposed from physical measurements and spectral techniques. The *in vitro* antibacterial and antifungal studies revealed higher antimicrobial activities of metal complexes than the free ligand (Patil *et al.*, 2011).

A series of three metal (Co^{II}, Ni^{II}, and Cu^{II}) complexes have been synthesized with the Schiff base derived from 4-aminoantipyrine and 8-formyl-7-hydroxy-4-methylcoumarin/5-formyl-6-hydroxycoumarin and they have coordinated to metal ions through ONO donor sites (Manjunath *et al.*, 2016). The compounds have been investigated for antibacterial, antifungal and DNA cleavage studies. The results showed promising antibacterial and antifungal properties of the complexes. The Co^{II} and Ni^{II} complexes also showed interesting anthelmintic activities.

Abdel-Rahman *et al.* (2016) have reported the synthesis of three tridentate Schiff bases amino acids by the direct condensation of 3-methoxysalicylaldehyde or 4-diethylaminosalicylaldehyde with various α-amino acids. They were further metallized with copper and produced Cu(II) complexes. The experimental results suggested the octahedral geometry of Cu(II) complexes of Schiff bases amino acids. The *in vitro* antimicrobial study of Schiff bases amino acids and their Cu(II) complexes with pathogenic bacterial and fungal strains revealed stronger antibacterial and antifungal efficiency compared to their corresponding ligands.

Ghosh *et al.* (2016) have investigated the antibacterial and catecholase activities of Co(III) and Ni(II) Schiff base complexes. In the research study, the Schiff base ligand was prepared by four-hour reflux of salicylaldehyde with 2-(pyridine-2-ylthio)ethanmine by the following reaction scheme 2.

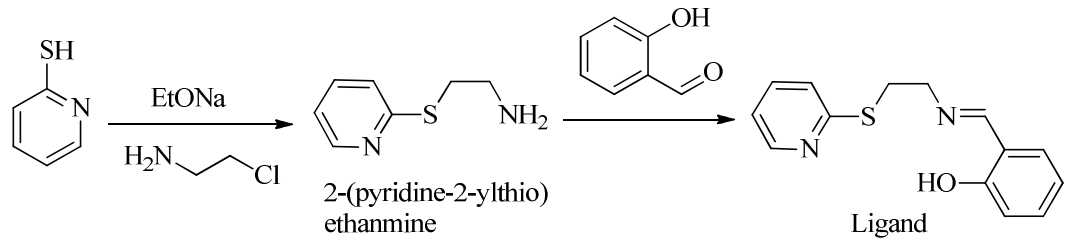

Scheme 2: Preparation of ligand from salicyladehyde and 2-(pyridine-2-ylthio)ethanmine

The fair analysis of antibacterial activities of both the compounds revealed that Ni(II) complex showed better activity against *B. subtilis* than *E. coli* whereas Co(II) complex showed fair activity against *B. subtilis* and was inactive against *E. coli*.

Purine and triazole based organic compounds and their derivatives are reported to have relevant biological functions and many of them are naturally occurring compounds. Amer *et al.* (2013) have prepared a series of Cu(II) complexes of Schiff bases derived from 7H-2,6-diaminopurine and 4H-3,5-diamino-1,2,4-triazole with 2-pyridinecarbaldehyde, salicylaldehyde, 2,4-dihydroxybenzaldehyde, and 2-hydroxy-1-naphthaldehyde. The tetradentate ligands were coordinated to the metal center through the N-atom of azomethine group and the nearest N-atom of it or O-atom of OH group. The *in vitro* antibacterial and antifungal results showed moderate activity against *E. coli* and *S. aureus*. Similarly, the *in vitro* antitumor activity of the complex showed a moderate activity against the studied cell lines.

The metal-based antibiotics are reported to have better pharmacological properties. To derive additional knowledge about antibiotic action, Anacona *et al.* (2015) have reported the isolation and characterization of metal(II) complexes containing a Schiff base ligand derived from the condensation of cephalothin and sulfadiazine. The antibacterial study revealed the higher bactericidal activity of Cu(II) and Zn(II) complexes than the uncomplexed cephalothin and the sulfadiazine against the bacteria

strains. The Mn(II), Co(II) and Ni(II) complexes showed to be less toxic than the two referenced drugs and the Schiff base ligand.

Cao *et al.* (2016) have synthesized and investigated the *in vitro* anticancer activities of four new amino acid Schiff base oxovanadium(IV) complexes. X-ray structural analysis showed that the V(IV) atoms in all four complexes are six-coordinated in a distorted octahedral environment. The anticancer study revealed moderate activities toward human lung carcinoma and human hepatoma cell lines.

Ceyhan *et al.* (2013) have reported the synthesis of three new Schiff base ligands derived from benzaldehyde derivatives and trans-1,4-cyclohexanediamine and also investigated electrochemical, photoluminescence, thermal and anticancer activity properties. These were screened for their cytotoxicity against HeLa and Vero and C6 cancer cell lines. The results showed that all of the compounds have cell selective activity against all the cell lines. Moreover the Schiff base compound IGA 3 has been found to show the highest antiproliferative activity against HeLa cell line.

Anticancer property of copper complexes is conjectured to be less toxic and more potent. Copper is a biologically relevant metal as it is associated with various biomolecules related to essential physiological activities. In a research work of Chakraborty *et al.* (2010), the anticancer activities of a family of Schiff base copper complexes of general formula [Cu(Pyimpy)Cl_2] were tested. The results indicated prominent anticancer properties *in vitro* as well as in vivo.

2.3 Catalytic Aapplications

Transition metal complexes are powerful catalysts for various organic transformations. They play important roles in oxidative processes employed in laboratory synthesis and chemical industries. In the recent years, Schiff bases and their metal complexes have been extensively investigated due to their wide range of applications as valuable catalysts. The Schiff base compounds have the ability to stabilize many metals in various oxidation states and control the performance of metals in several catalytic transformations.

The Schiff bases and their transition metal derivatives are known to possess catalytic activity for the oxidation of alcohols and alkenes in several synthetic organic reactions because of their cheap, easy synthesis, their thermal and chemical stability. Abdel-Rahman *et al.* (2016) have synthesized a new series of hexa-coordinated Cu(II) complexes of tri and tetradentate Schiff base ligands. The ligands were prepared by the condensation of 2-hydroxy-1-naphthaldehyde with 2-aminopyridine for npap ligand, 4-nitro-o-phenylenediamine with isatin and 5-bromosalicylaldehyde for bsisnph and 4-nitro-o-phenylenediamine with isatin and 2-hydroxy-1-naphthaldehyde for npisnph ligands. These ligands were derivatized for copper (II) complexes. The resulted compounds were tested for catalytic oxidation of benzyl alcohols to corresponding aldehydes and ketones. The detailed investigation showed that copper complex of bsisnph Schiff base ligand possess excellent catalytic activity than other compounds.

Various lanthanide and ruthenium compounds are also known to possess excellent catalytic activity in several organic synthetic chemical reactions and deserve themselves as a very good catalyst. In the similar work of Bhowon *et al.* (2004), some ruthenium and lanthanide Schiff base complexes derived from pyrrole-2-carboxaldehyde and 3,4-diaminotoluene, 1,2-diaminocyclohexane, 1,8-diaminonaphthalin, 1,3-diaminopropane, 1,2-phenylenediamine, 1,2- diaminoethane and aminophenol were prepared and characterized. They have been investigated as catalysts for the oxidation of primary alcohols in the presence of N-methylmorpholine-N-oxide as an oxidant. The catalytic activity results revealed that the synthesized metal complexes of Schiff bases were found to be better catalysts than other ruthenium and lanthanide catalysts.

A number of transition metal complexes are known to catalyze transfer hydrogenation of ketones (Venkatachalam & Ramesh, 2006). In this cited paper, The catalytic transfer hydrogenation of imines to amines was performed by one of the synthesized ruthenium(III) bis-bidentate Schiff base complexes $[RuCl(PPh_3)(L1)_2]$ in the presence of isopropanol/KOH. The catalytic results were found to be accessible and even better than other normal catalysts which otherwise difficult to achieve or even impossible.

Rhodium and Iridium complexes are mostly catalysts that have potential industrial applications to lead very efficient chemical processes. Biswas *et al.* (2015) have synthesized novel Rhodium(III)-triphenylphosphine complex, $[Rh(PPh_3)(L)Cl_2](PF_6)$ with thioether containing NNS donor ligand 2-(methylthio)-N-((pyridine-2-yl)methylene)benzenamine and investigated its catalytic activity. The results showed that the complex effectively catalyzed the transfer hydrogenation reaction of ketones with high yield in 2-propanol.

In the recent years, the interest in the vanadium complexes in coordination chemistry has grown enormously due to their multifaceted activities. Tahmasebi *et al.* (2016) have carried out the synthesis, characterization and crystal structure determination of oxovanadium Schiff base complexes. Additionally, they have studied and observed the catalytic activity of synthesized vanadium complexes in the epoxidation of alkenes. The results of this study showed that the epoxidation of alkenes takes place more efficiently even in a small concentration of oxovanadium catalyst.

2.4 Applications in Modern Technology

The metal-containing organic polymers incorporating Schiff base complexes offer considerable interest in the recent years because of their novel electronic, magnetic and catalytic properties. The coordinating ability of metals within the polymer backbone permits them to act as good sensors and also building blocks for supramolecular structure. Besides of biological interest of Schiff base metal complexes, they have been extended for their use in the advancement of modern technology. Over exploitation of fossil fuels and increasing air pollution problems can be overcome by the use of organic polymers that trap the solar energy more efficiently providing zero emissions of both air pollutants and greenhouse gases. In the present review of the literature, it has attempted to summarize some of such importance of Schiff base metal complexes in the field of modern science. The recent research popularizes Schiff base metal complexes as a class of valuable chemicals that are used in optical computers, to measure and control the intensity of the radiation, in imaging systems, as well as in the molecular memory storage, as organic materials in reversible optical memories and photodetectors in biological systems.

Several research investigations suggested that the polymers of Schiff base metal complexes have applications as organic photovoltaic materials with good stability, electroactivity and electrical conductivity (Jeevadason *et al.*, 2014). The π-electron conjugated system provides space for the electron delocalization along the polymer chain and to the possibility of high charge carrier mobility. The substituted Schiff base polymers in organic solar cells have their increased performance.

Kaya and Kamacı (2012) have synthesized novel low band gap and thermally stable poly(azomethine-urethane)s (PAMUs) to investigate aliphatic and aromatic group effects on some physical properties such as thermal stability, optical and electrochemical properties. The PU-VANDAP has a lesser electrochemical band gap than the PU-VANDAH, which suggests that the aromatic group is more suitable for the photovoltaic purpose than aliphatic groups. The investigation thus showed that Schiff bases with aromatic groups could be more reliable in photovoltaic applications, than their aliphatic groups.

Kaya *et al.* (2015), in their another paper have measured the electrochemical and optical band gaps of a series of polymeric Schiff bases containing methyl and carboxyl groups in the structure by cyclovoltametry and UV-visible techniques. They have carried out the synthesis of Schiff bases (CBAA4MP, CBAA5MP, and CBAA3MP) which differ from each other based on the position of methyl group. The derived monomers were changed into their polymer kind (P-CBAA4MP, P-CBAA5MP, and P-CBAA3MP) by oxidative polycondensation in the aqueous alkaline medium using NaOCl as the oxidant. The electrochemical and optical band gap studies revealed that the P-CBAA5MP possesses increased conductivity and suggested to be used as semi-conductive polymer in electronics, optoelectronic and photovoltaic cells.

Photochromism is the phenomenon of reversible and dramatic change in the photochemical behavior of chemical species when irradiated by electromagnetic radiation in the ultraviolet or visible region. The chemical species differ from one to another form in their frequency of absorption of light. The absorption of radiation leads to a photochemically stable but thermodynamically metastable state, with the different colour from that of original state (Rawat *et al.*, 2015). One of the important

applications of photochromism is the colour changing lenses for sunglasses used as eyeglasses. Schiff bases are the model compounds that present photochromism. Due to photochromic properties, Schiff base compounds behave as photostabilizers dyes for solar collectors and solar filters. They are also used in optical sound recording technology. In the research work of Tanaka *et al.* (2010), the photochromic properties of novel calixsalen type chiral Schiff base macrocycles (Figure 11) have been studied and found colour change from yellow to orange-red upon photoirradiation on enantiomerically pure crystals of (S,S,S,S,S,S)-1 compound. The orange-red crystals returned to their initial yellow state after storage for 1 h in the dark.

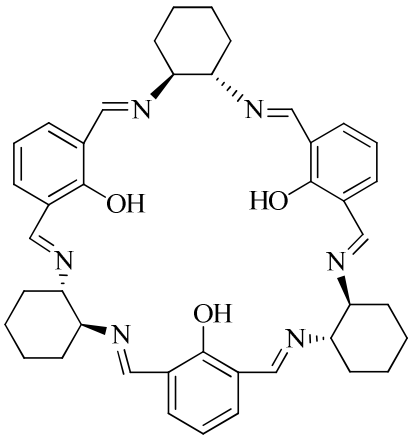

Figure 11: Calexsalen type chiral Schiff base macrocycle

In the similar work of Liang *et al.* (2007), the photochemical properties of novel Schiff bases based on calyx[4]arene were studied in CH_3CN by UV-visible and fluorescence spectral techniques. The study revealed the important applications of these Schiff bases in supramolecular devices through combining the photochromic behavior with non-linear optical or charge transfer properties.

Zhu *et al.* (2016) have synthesized a series of three o-hydroxynaphthaldehydehydrazone derived Schiff bases and studied their thermochromism and photochromism behavior. The photochromism of the compounds was investigated by IR and UV-visible spectrophotometry which is time variable under irradiation of 254 nm UV light. Their study suggested the probable mechanism of photochromism and thermochromism behavior of the compounds which may be due to keto-amine and enol-imine tautomerism.

2.5 Surfactant and Corrosion Inhibition Applications

Iron and its alloys (steel) are the important materials used in various industrial and engineering applications. However, their regular use in the industrial process requires cleaning of the metal surface and for this purpose, acid solutions are used to remove undesirable scale and corrosion products. This corrosion can cause serious damage to the metal and degrade its properties. To prevent from this acidic corrosion, some organic inhibitors possessing donor atoms are required which prevent the metal surface from acidic attack. Some Schiff base compounds containing imine group and donor atoms like nitrogen, oxygen, and sulfur are effective to prevent corrosion of metal surface in acidic medium.

Aouniti *et al.* (2016) have synthesized Schiff base (E)-2-methyl-N-(thiophen-2-ylmethylidene) aniline from 2-acetyl thiophene and studied corrosion inhibition behavior on steel/1.0 M HCl interface by using gravimetric and electrochemical methods at 308 K. Their study revealed that the corrosion inhibition might take place through its adsorption at the metal/solution interface. The synthesized Schiff base demonstrated good inhibitive properties for mild steel corrosion and its efficiency increases with increasing concentration of the inhibitor.

Some Schiff base like (E)-2-(3-nitrobenzylidene) hydrazine carbothioamide and (E)-2-(4-(dimethylamino) benzylidene) hydrazine carbothioamide are the efficient corrosion inhibitor for mild steel in industrial water. Their inhibition efficiency increases with the increase of Schiff base concentration and decreases with rising temperature. The inhibition performance and adsorption behavior have been investigated by gravimetric, potentiodynamic polarization and electrochemical impedance spectroscopy technique (Shivakumar & Mohana, 2013).

Singh and Quraishi (2012) have investigated the corrosion inhibitory efficiency of some Isatin based bidentate Schiff bases for mild steel in 1.0 M HCl solution. The study revealed excellent inhibition effect for the corrosion. They have explained the high inhibition efficiencies of Schiff bases which are attributed to the adherent adsorption of the inhibitor molecules on the mild steel surface.

El-Baradie *et al.* (2014) have synthesized Co(II), Ni(II) and Cu(II) complexes of L-histidine Schiff base derived from 2,4-dihydroxybenzaldehyde and 2-hydroxynaphthaldehyde and studied their corrosion inhibition effect on Aluminium in 2M H_2SO_4 by weight loss method. The obtained data indicated these compounds as efficient corrosion inhibitors with increased inhibition efficiency on increasing the inhibitor concentration and temperature which is suggestive of a chemical adsorption process.

The sulphur as a donor atom in the Schiff bases bears a strong affinity on transition metal surfaces. A Schiff base of such type, namely N-(2-hydroxybenzylidene) thiosemicarbazide (HBTC) was investigated as a corrosion inhibitor for carbon steel in saline water by using various electrochemical measurements. The investigation has suggested the Schiff base compound, a good corrosion inhibitor of carbon steel in diluted acidic medium (Samide & Tutunaru, 2011).

Oxazepine compounds have potential medicinal and pharmaceutical applications. Several research studies put the information that the heterocyclic residues containing Schiff bases possess excellent biological activities. Hamak and Eissa (2013) have synthesized a series of Schiff base by the condensation of 1,4-Bis(3-aminopropyl)-piperazine and various aromatic aldehydes in ethanol in the presence of the acetic acid catalyst. Their oxazepine derivatives have been prepared by the treatment of Schiff base with phthalic anhydride. The corrosion inhibiting action of these compounds has been investigated on steel in 1M H_2SO_4 by electrochemical techniques. The study revealed the effective corrosion inhibiting activities of all the synthesized compounds.

Corrosion in metallic surfaces is much concerned with the material loss in the technological activities. Saline media is one of the leading agents that cause corrosion. The formation water produced during petroleum production in the deep oil wells contains a variety of dissolved organic and inorganic compounds. These compounds have aggressive properties to corrode the material substances and for this purpose, inhibitors are commonly used. Corrosion inhibitors block the active sites and enhance the adsorption process and thus decrease the corrosion rate to extend the life of equipment. Nitrogen-based organic surfactants have been used successfully as the corrosion inhibitor in the oil and gas fields even without an understanding of the

inhibition mechanism. Migahed *et al.* (2011) have synthesized a new family of Schiff base nonionic surfactants and evaluated their corrosion inhibition effect on X-65 type tubing steel in deep oil wells formation water. The results showed good inhibition properties for the corrosion. This is attributed to the strong adsorption ability of surfactant molecules on the metal surface.

Negm *et al.* (2011) have synthesized a new series of cationic Schiff bases and evaluated the corrosion inhibitory effect on carbon steel in acidic medium (2N HCl) at 25 °C using the weight loss technique. The results showed the decreasing corrosion rate by increasing the doses of Schiff base surfactants.

CHAPTER 3

MATERIALS AND METHODS

This chapter delineates the chemicals/reagents used for the synthesis of novel Schiff base ligands and the metal complexes. The various physical, analytical and spectral techniques employed for the characterization will be discussed here and the details of the antibacterial activity study will also be addressed. Procedural details regarding the synthesis of Schiff base ligands and their metal complexes will be discussed. The X-ray powder diffraction study will be reported at the appropriate subchapter that will provide the information regarding the crystallinity of the compounds. The technique for the detailed antibacterial activity study will also be presented here.

3.1 Materials / Reagents

All the chemicals and the reagents used for the investigation were of analytical grade and used without further purification. The drug chemicals were procured from various international standard companies and also from pharmaceutical companies through the local dealers of the market. The distilled methanol was used as the solvent for the synthesis. The distillation of methanol was done by standard techniques before use. Four metal chloride salts ($MCl_2.xH_2O$, M = Co(II), Ni(II), Cu(II) and Zn(II)) were used for the synthesis of metal complexes. Due to lower solubility of Kanamycin in alcohol, 90% methanol was used for this purpose. The clinical strains of human pathogenic bacterial organisms needed for the antibacterial sensitivity study were collected from the microbiology laboratory of Nobel Medical College Teaching Hospital and Suraksha Hospital, Biratnagar. List of chemicals and reagents used for the synthesis of Schiff bases and metal complexes are summarized in the Table A1. The instruments and glass apparatus used in the experiment are listed in the Table A2.

3.2 Synthesis of Schiff Base Ligands

Out of several synthetic methods of Schiff base formation, solvent free synthesis by microwave irradiation technique is considered as the recent and fast method with no chemical pollution that supports green chemistry but has limitations in its use (Jain & Mishra, 2012; Panda *et al.*, 2013). However, synthesis by reflux method is considered as a traditional method but used widely in the research. Three series of Schiff base ligands were prepared by the chemical reactions of drug substances in their stochiometric ratios.

3.2.1 KMAXC Schiff Base Ligand

Initially, amoxicillin trihydrate (4 mmol, 1.678 g) was dissolved in 30 mL hot methanol and was refluxed at 25 °C for 4 hours under constant stirring condition. The pH of the solution was maintained to 4.5 by adding few drops of sulphuric acid. In the next operation of this synthetic process, kanamycin sulphate (4 mmol, 2.33 g) was dissolved in 30 mL (90%) hot methanol and homogeneously stirred for few hours under hot condition. These two were mixed and the final mixture was refluxed for 15 hours at 35 °C. During its preparation, the pH of the mixture was adjusted to neutral by adding few drops of 0.1N NaOH solution (Chaudhary & Mishra, 2015). The light yellow solid was obtained after volume reduction. It was recrystallized and dried under vacuum over anhydrous calcium chloride. The solid product was stored in an airtight vial, till its further use.

3.2.2 AXCPC2 Schiff Base Ligand

The novel Schiff base ligand (AXCPC2) ((E)-6-(2-(4-hydroxyphenyl)-2-(pyridine-2-methyleneamino)acetamido)-3,3-dimethyl-7-oxo-4-thia-1-aza—bicyclo[3.2.0] heptanes-2-carboxylic acid) was prepared by refluxing the equimolar mixture (1:1) of amoxicillin trihydrate and Pyridine-2-carbaldehyde in methanol solvent medium. For this purpose, 5 mmol (2.0975 g) amoxicillin trihydrate in 30 mL methanol was stirred under hot condition over the magnetic stirrer for several hours and 5 mmol (0.471 mL) pyridine-2-carbaldehyde was added. The pH of the mixture was checked and maintained neutral by adding 0.1N NaOH solution. The mixture was refluxed for 4

hours till it became clear yellow color (Chaudhary & Mishra, 2018). The solution was left undisturbed for better crystal formation and bright yellow solid was separated after volume reduction. The solid was recrystallized from hot methanol and dried in the desiccator using anhydrous $CaCl_2$. The ligand was stored in the airtight vial in the refrigerator till its further use.

3.2.3 AXCPC3 Schiff Base Ligand

The novel Schiff base ligand AXCPC3 was prepared as follows: 5 mmol (2.0975 g) amoxicillin trihydrate in 30 mL methanol was carefully stirred under magnetic stirrer at the hot condition. Solubility in Methanol was marked at the temperature elevation state. Meanwhile, the pH of the amoxicillin was adjusted to 7 to make a neutral solution by adding 0.1N NaOH solution. 5 mmol (0.471 mL) pyridine-3-carboxaldehyde (nicotinaldehyde) was added dropwise to the hot amoxicillin solution under constant stirring condition (Chaudhary & Mishra, 2017). Finally, the solution was refluxed for 4 hours and bright yellow solid was separated after volume reduction (Yang & Sun, 2006). The solid was filtered and recrystallized from hot methanol and dried in the desiccator using anhydrous $CaCl_2$. The ligand was stored in the air tight vial in the refrigerator till its further use.

3.3 Synthesis of Metal Complexes

The synthesis of metal complexes was attempted by the standard procedure reported in the literature (Khan *et al.*, 2013; Naeimi *et al.*, 2013; Jain & Mishra, 2012; Singh & Singh, 2014). In our investigation, the mixture of ligand and appropriate metal chloride salts in the calculated volume of methanol was refluxed under the constant stirring condition by using magnetic stirring beads. The crystalline product was dried in the desiccator and kept in the airtight vial in the refrigerator till its further use.

3.3.1 Metal Complexes of KMAXC Schiff Base Ligand

To the hot and homogeneously stirred 50 mL aqueous methanolic solution of KMAXC (2 mmol, 1.662 g), was added 5 mL methanolic solution of metal chloride (2 mmol) salts. The mixture was then refluxed under the stirring condition at 45 °C

for 15 hours. On cooling, the precipitates of metal complexes of different color were obtained, filtered and washed with methanol. The complexes were re-crystallized and stored in the airtight vial in refrigerator till their further use.

3.3.1.1 Synthesis of Co-KMAXC

General procedure for the synthesis of metal complexes is depicted in the sub unit 3.3.1. For the preparation of Co-KMAXC complex, 5 mL methanolic solution of $CoCl_2.6H_2O$ (2 mmol, 0.4758 g) salt was used. The purple colored solid was precipitated after the volume reduction of the solution. The solid product was filtered and washed with methanol. It was stored in the airtight vial in refrigerator, till its further use.

3.3.1.2 Synthesis of Cu-KMAXC

General procedure for the synthesis of metal complexes is depicted in the sub unit 3.3.1. For the preparation of Cu-KMAXC complex, 5 mL methanolic solution of $CuCl_2.2H_2O$ (2 mmol, 0.3409 g) salt was used. Light blue colored solid was precipitated after the volume reduction of the refluxed solution. The solid product was filtered and washed with methanol. It was stored in the air tight vial in refrigerator, till its further use.

3.3.1.3 Synthesis of Zn-KMAXC

General procedure for the synthesis of metal complexes is depicted in the sub unit 3.3.1. For the preparation of Zn-KMAXC complex, 5 mL methanolic solution of $ZnCl_2$ (2 mmol, 0.2725 g) salt was used. The yellow colored solid was precipitated after the volume reduction of the solution. The solid product was filtered and washed with methanol. It was stored in the airtight vial in refrigerator, till its further use.

3.3.2 Metal Complexes of AXCPC2

The Schiff base ligand under this category was prepared by the procedure reported in the section 3.2.2. Co(II), Ni(II), Cu(II) and Zn(II) salts were used for the preparation

of respective complexes. To the hot and homogeneously stirred solution of ligand (1 mmol, 0.454 g) in 20 mL methanol, was added hot solution of metal salts dissolved in methanol and refluxed for several hours using Liebig water condenser. The physical change observed in the solution was the simple indication for the complex formation. The specific reaction conditions applied during the complex formation is described in the following subsequent units.

3.3.2.1 Synthesis of Co-AXCPC2

To the hot and homogeneously stirred solution of ligand (1 mmol, 0.454 g) in 20 mL methanol, was added hot solution of $CoCl_2.6H_2O$ (0.5 mmol, 0.1189 g) in 10 mL methanol. The mixture solution was refluxed for 3 hours under hot water bath with constant stirring. The stirring is done to homogenize the molecules and to facilitate bonding of the ligand with metal ions. The coffee colored Co-AXCPC2 complex was obtained by volume reduction of the solution. The solid was separated, washed with methanol and dried in the desiccator. The complex was stored in the airtight vial in the refrigerator, till its further use.

3.3.2.2 Synthesis of Ni-AXCPC2

General procedure for the synthesis of metal complexes is depicted in the sub unit 3.3.2. For Ni-AXCPC2 complex, 10 mL methanolic solution of $NiCl_2.6H_2O$ (0.5 mmol, 0.1188 g) salt was used. Beaver colored solid was separated after the volume reduction of the solution. The solid product was filtered and washed with methanol. It was stored in the airtight vial in the refrigerator, till its further use.

3.3.2.3 Synthesis of Cu-AXCPC2

General procedure for the synthesis of metal complexes is depicted in the sub unit 3.3.2. For Cu-AXCPC2 complex, 10 mL methanolic solution of $CuCl_2.2H_2O$ (0.5 mmol, 0.085 g) salt was used. Rifle green colored solid product was separated after the volume reduction of the solution. The solid product was filtered and washed with methanol. It was stored in the airtight vial in the refrigerator, till its further use.

3.3.2.4 Synthesis of Zn-AXCPC2

General procedure for the synthesis of metal complexes is depicted in the sub unit 3.3.2. For Zn-AXCPC2 complex, 10 mL methanolic solution of $ZnCl_2$ (0.5 mmol, 0.0681 g) salt was used. Ruddy brown colored solid was separated after the volume reduction of solution. The solid product was filtered and washed with methanol. It was stored in the airtight vial in the refrigerator, till its further use.

3.3.3 Metal Complexes of AXCPC3

Four metal chloride salts have been selected for the synthesis of metal complexes under this category of Schiff base ligand. They were Co(II), Ni(II), Cu(II) and Zn(II) complexes of AXCPC3 Schiff base.

3.3.3.1 Synthesis of Co-AXCPC3

The novel ligand was prepared by the procedure described in 3.2.3. The Co-AXCPC3 complex was prepared by adding hot solution of $CoCl_2.6H_2O$ (0.5 mmol, 0.1189 g) in 10 mL methanol to the hot solution (approx. 60 °C) of the AXCPC3 Schiff base (1 mmol, 0.454 g) in the same solvent (20 mL methanol). The mixture was stirred over magnetic stirrer under hot condition. The resulting mixture was refluxed for 2 hours for the complex formation. Alternate stirring of the mixture was also done to facilitate the bonding of ligand with the metal ion. The blue colored Co-AXCPC3 complex was obtained by slow cooling of the solution at room temperature. The solid was filtered, washed with methanol and dried in the desiccator using anhydrous calcium chloride. The complex was stored in the airtight vial in the refrigerator, till its further use.

3.3.3.2 Synthesis of Ni-AXCPC3

The similar experimental procedure was applied as in 3.3.3.1 for the synthesis of the Ni-AXCPC3 complex of AXCPC3 Schiff base ligand. $NiCl_2.6H_2O$ (0.5 mmol, 0.1188 g) in 10 mL methanol solution was used for the preparation of Ni-AXCPC3 complex. Green colored solid product was collected by filtration process and washed with hot

methanol. It was dried in the desiccators using anhydrous calcium chloride and was stored in the airtight vial in the refrigerator, till its further use.

3.3.3.3 Synthesis of Cu-AXCPC3

The similar experimental procedure was applied as in 3.3.3.1 for the synthesis of the Cu-AXCPC3 complex of AXCPC3 Schiff base ligand. $CuCl_2.2H_2O$ (0.5 mmol, 0.0852 g) in 10 mL methanol was used for the preparation of Cu-AXCPC3 complex. Green colored solid product was collected by filtration process and washed with hot methanol. It was dried in the desiccator using anhydrous calcium chloride and was stored in the airtight vial in the refrigerator, till its further use.

3.3.3.4 Synthesis of Zn-AXCPC3

The experimental procedure was similar to that described in the earlier sections. $ZnCl_2$ (0.5 mmol, 0.0681 g) in 10 mL methanol was used for the preparation of Zn-AXCPC3 complex. The light yellow colored solid product was collected by filtration process and washed with hot methanol. It was dried in the desiccator using anhydrous calcium chloride and was stored in the airtight vial in the refrigerator till its further use.

3.4 Characterization Techniques

The physical and spectral characterization of the synthesized compounds furnishes the important information which is essential for structure elucidation and stereochemistry. The characterization techniques employed for the present research are elemental microanalysis, pH measurement, conductivity measurement, FT-IR, Electronic absorption spectral study, ^{1}H & ^{13}C NMR, ESI-MS, EPR, XRPD study, SEM and TGA/DTA analysis. They will be discussed below at the appropriate subchapters.

3.4.1 Elemental Microanalysis

Elemental (CHN) microanalysis supports in the structure determination by providing percentage composition of the elements which are applicable to discover the

molecular formula. Its information is also accessible to ascertain the structure and purity of the synthesized compounds.

3.4.2 pH Measurement

The legational behavior of Schiff base ligands for the formation of metal complexes is generally driven by deprotonation reaction and the variation in pH value is considered as an important evidence of chemical reactions in synthetic chemistry. The formation of metal complex can be predicted by the decrease in pH value in general case. Therefore the pH values of the synthesized compounds were determined in suitable solvents. For the present research, this measurement was carried by dissolving the compounds in DMSO and/or methanol solvents. In our work, the pH measurement was done in Elico-16 pH meter in Bio-inorganic and Materials Chemistry Research Laboratory of Mahendra Morang Adarsh Multiple Campus, Biratnagar.

3.4.3 Conductivity Measurement

Conductivity measurement is an important physical technique to gain supportive information about the metal complex formation in coordination chemistry. The molar conductance values of the complexes were measured in M/1000 solution of synthesized compounds in either of DMSO or methanol solvents. The change in conductance values from ligand to complex formation is a necessary clue for the chelation of ligands with metal ions. The conductivity measurement was done in Labtronics auto digital conductivity meter (Model LT-16) in Bio-inorganic and Materials Chemistry Research Laboratory of Mahendra Morang Adarsh Multiple Campus, Biratnagar.

3.4.4 Electronic Absorption Spectra (EAS) and Magnetic Moment Study

Electronic absorption spectroscopy (also called UV-visible spectroscopy) is an important instrumental tool for the coordination chemists to draw the important information about the structural aspects of the complexes. For the present research work, the electronic absorption spectral study was achieved in M/1000 solution of the synthesized compounds in DMSO and/or methanol solvents. The study was

conducted in Labtronics UV-visible spectrophotometer in Surface Chemistry Laboratory of Mahendra Morang Adarsh Multiple Campus, Biratnagar. The magnetic moment of the metal complexes was analysed in Lakeshore VSM 7410 model instrument and the data were collected from SAIF IIT Madras, India.

3.4.5 FT-IR Spectral Study

The IR spectral study is another important instrumental tool for the characterization of the ligands and complexes. Basically, it gives information regarding the presence of functional groups, other structural components and the metal ligand bonding parameters. The instrument uses infrared radiations of the electromagnetic spectrum for the vibrations of the bonds in the compounds, from which wealth of information can be achieved. The data of the IR bands can be processed to derive the presence of structural components of the molecules. The bands due to metal-ligand coordination are mainly observed in the far IR region around 500 cm^{-1}. The IR spectra were recorded as KBr pellets on a Perkin Elmer 783 FT-IR spectrophotometer in the range of 4000-400 cm^{-1}.

3.4.6 ^{1}H & ^{13}C NMR Spectral Study

The ^{1}H & ^{13}C NMR spectral data provide valuable information regarding the structure of Schiff base ligands and metal complexes. NMR spectroscopy is such a modern instrumental tool without which a chemical researcher cannot think for the design of the proper structure of unknown compounds. The binding mode of the ligand with metal centers in diamagnetic complexes can be well achieved by their ^{1}H & ^{13}C NMR spectral comparison. For the present research work, the ^{1}H & ^{13}C NMR spectra were recorded on Bruker Avance III, 400 MHz spectrometer, using DMSO-d6 as solvent and TMS as the internal reference chemical.

3.4.7 ESI-MS Spectral Study

Mass spectrometry is also an important instrumental tool for the determination of molecular mass of the synthesized compounds. The correlation of molecular mass with microanalytical data provides the information about the molecular formula of the

compounds. Recently mass spectrometry uses electrospray ionization technique and it is also called ESI-MS. This is advantageous for the formation of molecular ion peaks because this is soft ionization technique and little fragmentation occurs in the compounds. It is also suitable for the determination of molecular mass of metal complexes, since, in LC-MS, the metal ions may corrode the column. For the present investigation, ESI-MS spectra were recorded in positive mode on Agilent Q-TOF mass spectrometer equipped with an electron spray ionization source in the mass range of 200 to 1100 at SAIF-CDRI Lucknow, India. In another investigation, MS spectra were carried out TOF-MS on water KC-455 model instrument at IIT Delhi, India.

3.4.8 TGA/DTA Study

For the present investigation, thermal events (TGA/DTA) of the compounds were recorded on Perkin-Elmer thermal analyzer with a linear heating rate of 10 °C min^{-1} and 20 °C min^{-1} in the range of 40-730 °C at SAIF, STIC Cochin, India. In another case, TGA/DTA studies were carried on Shimadzu TGA-50H thermal analyzer scanning at a linear heating rate of 10 °C min^{-1} at University of Delhi, India and their decomposition profiles were noticed at different stages of temperature ranges. The thermogram of the complexes reveals the change in curve area corresponding to their decomposition at various temperatures.

3.4.9 EPR Study

Electron paramagnetic resonance (EPR) spectroscopy is a very powerful instrumental tool that provides valuable structural and geometrical information about a wide variety of complexes with unpaired electrons. Also for the biochemists and biological researchers, EPR technique holds successful applications to solve several pertinent biological problems (Sahu *et al.*, 2013). It requires the presence of an unpaired electron spin and thus the paramagnetic substances only afford this behavior. The room temperature X-band ESR-JEOL spectra of the complexes were recorded on JES-FA200 ESR spectrometer at SAIF, IIT Bombay, India. The standard lines that are used in the EPR model are of Mn, which has been omitted in the graph.

3.4.10 X-ray Powder Diffraction Study

The powder diffraction is a scientific instrumental technique that uses X-ray as electromagnetic radiation that strikes on powder or microcrystalline samples for the structural characterization of material substances. The instrument dedicated for this study is called X-ray powder diffractometer.

In our research, single crystal growth was unsuccessful so the structure and crystallinity of the compounds were checked by powder diffraction technique. Several crystalline parameters can be achieved by the observation of diffractograms of the compounds. The XRD powder pattern was recorded on a vertical type Philips 1130/00 X-ray diffractometer operated at 40 kV and 50 Ma generators using the monochromitized CuKα line at the wavelength 1.54056 Å as the radiation source and this was done at Delhi University, India. In another experiment, this event was accomplished using Bruker AXS D8 Advance X-ray diffractometer with the monochromatised Cu-Kα line at wavelength 1.5406 Å as the radiation source and the measurements were taken over the range of 2θ (10 to 70°). The diffractogram of the compounds was obtained by solving the raw data in X'pert Highscore Plus software program. Further crystallographic information was obtained by CRYSFIRE and CHECKCELL software program.

3.4.11 Surface Morphology Analysis

The scanning electron microscope (SEM) uses a focused beam of high energy electrons that scan the surface of solid materials and generate a surface image. The high energy electronic interaction with atoms in the molecules produces various signals that contain information about the surface topography, chemical composition and crystalline structure (Kareem *et al.*, 2016). This interaction on the sample surface dissipates secondary electrons and backscattered electrons which are used for imaging samples. The secondary electrons originate from within a few nm from the surface and provide topographic information. The backscattered electrons originate from much deeper within the sample and interact much strongly (Hafner, 2007). In our study, this analysis was performed in JEOL JSM-6390 LV scanning electron microscope.

3.5 Molecular Modeling Study

Molecular modeling is a computer simulation technique to design the molecular graphics and optimize the molecular geometry of the proposed structures. In our investigation, 3D molecular modeling of the proposed structure of the Schiff base ligands and metal complexes was achieved by ChemDraw 3D Ultra program package and ArgusLab 4.0.1 version software program package (Singh *et al.*, 2014; Souza *et al.*, 2008). ChemDraw is molecular modeling software to sketch the chemical structures of the molecules. It is supported by various tools to design the molecules in 2D and 3D forms. ArgusLab is a program to build graphic representations of molecular models. The various tools of this software enable to optimize geometry, calculate energy, build surfaces and perform Gaussian calculations to customize the molecular model. It assists in visualizing molecular orbitals, electron densities, electrostatic potentials and spin densities on the surface of molecules. Electrostatic potential mapped electron density on the surface of molecules can also be visualized. This is also supported by various molecular properties calculations like single point energy calculation and geometry optimization calculation to draw the stable molecular geometry of the proposed molecules.

3.6 Antibacterial Sensitivity Study

Recent antibacterial resistance data of the popular antibiotics are terrorizing the medical science. Antibiotics are one of the core drugs for the treatment of several kinds of diseases and are said to be the miracle drug of the modern medicine (Bérdy, 2012; Li & Vederas, 2009; Walsh & Wencewicz, 2013). Medical practitioners prescribe antibiotics in every prescription. The high dose use of antibiotics is the main cause for cell toxicity in the human body and many adverse effects can be seen, that sometimes may cause death. Improper use of antibiotics is also the cause for the failure of this drug (Anacona & Lopez, 2012; Garcia-Migura *et al.*, 2011; Reiss *et al.*, 2014). Hence it is essential to revive them either by modified drug design or by their complexation with various transition metals. Literature review search described in chapter 2 reveals the potential use of Schiff bases and their transition metal complexes as valuable antibiotics. They bear potential pharmacological properties and thus, this

class of compounds is considered as the valuable pharmacophore in the pharmaceutical science.

In the present investigation, the antibacterial study has been carried to show the biological potency of synthesized Schiff bases and their transition metal complexes. This has been executed by modified Kirby-Bauer paper disc diffusion technique.

3.6.1 Sterilization of Equipments

Sterilization is a process to kill all the types of micro-organisms from the objects. This can be achieved by various techniques like exposure to heat, chemical treatment, high pressure or sensitive membrane filtration process. In the present investigation, all the essential equipment were first thoroughly washed with detergents and distilled water and then sterilized by exposure to dry heat in a hot air oven at 200 °C for 2 hours. They were kept in laminar flow till their further use.

3.6.2 Procedure for the Preparation of Media

For most of the antibacterial study, nutrient agar medium was used for better growth because it contains sufficient nutrients required for the growth of micro-organisms. The nutrient agar suspension was prepared by the provided guidelines of the manufacturing company. The petri dish, agar suspension, and other glass accessories were autoclaved at 120 °C for 15 minutes. The autoclaved suspension was cooled for few minutes and then carefully poured into each plate. The plates were kept in UV laminar flow to create a sterile zone and to prevent bacterial contamination. The plates were left on the sterile zone until the agar has solidified.

3.6.3 Preparation of Culture

Both gram-positive and gram-negative pathogenic bacteria have been examined for the antibacterial investigation. They were *E. coli, P. vulgaris, K. pneumonia, B. subtilis and S. aureus.* A fresh culture of such clinical bacterial strains was collected from the microbiological laboratory of Nobel Medical College and Teaching Hospital, Biratnagar and also from Suraksha Hospital Pvt. Ltd, Biratnagar, Nepal.

3.6.4 Organism Information

Escherichia coli

It is a type of gram-negative and nonsporulating bacterium, typically of rod-shaped and about 2µm long. The morphological evidence suggests that the diameter of the bacterial cell ranges from 0.25-1 µm, with cell volume 0.6-0.7 μm^3. It belongs to *Enterobacteriaceae* family. Its cell wall is composed of a thin peptidoglycan layer and an outer membrane. This outer membrane provides a barrier to antibacterial agents and thus most of the antibiotics are under resistant to this organism.

About hundred strains of *E. coli* bacteria have been isolated and known so far, that inhabit the large intestine of many mammals, including human. Most of the strains are harmless to us that help in digestion of food and keep harmful bacteria under control. Some of the strains help in the metabolism of vitamin K and B complex formation. However, some strains of *E. coli* cause severe food poisoning leading to enterohemorrhagic diarrhea. This bacterial strain destroys the cells lining the wall of the large intestine and damages the blood vessels, causing internal bleeding. Such condition is dangerous for small children and causes risk for death (Hien *et al.*, 2008). People with weak immune systems, such as young children or elderly are more vulnerable to this bacterial strain. In the present investigation, the antibiotic study has been conducted with clinical strains of human pathogenic *E. coli*.

Proteus vulgaris

Morphologically, *Proteus vulgaris* is a rod shaped gram-negative bacillus, belongs to the bacterial family of Enterobacteriaceae. It is a common inhabitant of the human intestinal tract as a part of normal human intestinal flora along with *E. coli* and *Klebsiella* species and a urinary tract pathogen. In humans, it can cause many different types of infections including urinary tract infection and wound infection. It is a common cause of sinus and respiratory infection, especially in South East Asia. *Proteus vulgaris* can be deadly in the respiratory infection if left untreated or if treated with antibiotics that have only an intermediate effect on the pathogen. The course of

treatment is very long for the respiratory infection, even if treated by sensitive antibiotics.

Proteus vulgaris is a type of motile bacterium whose mobility is due to peritrichous flagella. The bacterial cell possesses extracytoplasmic outer membrane which in the environment share with other gram-negative bacteria. *P. vulgaris* has the ability to produce urease and to alkalinize the urine by hydrolyzing urea to ammonia and this environment is favorable for its survival. Urease production, together with the presence of bacterial motility and fimbriae may also favor the upper urinary tract infection. It also causes sepsis neonatorum and bactemia with fever and neutropenia.

Klebsiella pneumoniae

Klebsiella pneumoniae is a gram-negative, nonmotile and rod-shaped bacterium of Enterobacteriaceae family. German microbiologist, Edwin Klebs, in 19th century studied this organism and hence named *Klebsiella*. This organism normally lives inside human intestine, where it does not cause disease. Clinically it is considered as the human pathogenic organism that specifically causes destructive changes in lungs. The most common disease caused by this organism is bronchitis (also called bronchopneumonia) which in acute form can cause the fatal death of people. In addition, *Klebsiella* can also cause infections in the urinary tract, lower biliary tract, bloodstream and surgical wound sites. Mostly the middle-aged and older people are more vulnerable to this disease. Healthy people usually do not get Klebsiella infections. The patients who require external devices like ventilators or intravenous catheters and the patients who are taking long courses of certain antibiotics are most at risk for this infection. There is no evidence of bacterial spread through the atmospheric air; however, it spreads through person to person contact or less commonly by the contaminated environment. Recent research report suggests the high risk of resistance to antibiotics in the course of treatment of this organism.

Bacillus subtilis

Bacillus subtilis is rod-shaped gram-positive strained bacterium which belongs to the family *Bacillaceae*. The bacterial cell is externally covered by a rigid cell wall which

is composed of the polymers of sugars and amino acids called peptidoglycan. They form tough and protective endospore to survive and tolerate extreme environmental conditions of temperature. Endospores can stay dormant for a long period of time and reactivates under the favorable condition. Generally, they are found in soil and also inhabit the gastrointestinal tract of humans. It grows well in the oxygenated environment but can adapt in low to no oxygen condition. The mobility of bacteria is due to the presence of flagella found around its body. Except for few species, the majority of Bacillus species is non-pathogenic and has never been associated with disease in human. The clinical spectrum of infections caused by Bacillus species includes food poisoning, localized infections related to trauma, deep-seated soft tissue infections and other infections (e.g. meningitis, endocarditis, osteomyelitis, and bacteremia).

B. subtilis is not a frank human pathogen but has on several occasions been isolated from human infections. Infections attributed to *B. subtilis* include bacteremia, endocarditis, pneumonia, and septicemia. However, these infections were found in patients in decreased immune states. There also have been several reports of food poisoning attributed to large numbers of *B. subtilis* contaminated food. Unlike several other species, *B. subtilis* is not considered toxigenic. It does produce the extracellular enzyme subtilisin that has been reported to cause allergic or hypersensitivity reactions in individuals repeatedly exposed to it. Overall, *B. subtilis* has a low degree of virulence.

Staphylococcus aureus

Staphylococcus aureus was discovered by the surgeon Sir Alexander Ogston of Scotland in 1880 in the pus from surgical abscesses. It is a Gram-positive coccal bacterium that belongs to the bacterial family of *Staphylococcaceae*. It can grow very well on all culture media. It is a facultative anaerobic organism which can grow even in the absence of oxygen. The commonest infections caused by this organism are those of skin and superficial tissues of the body. It can also cause respiratory infections such as sinusitis and food poisoning. In medical literature, this bacterium is often referred to as *S. aureus* and in a group, it appears as grape-like clusters. *S.*

aureus is morphologically small round shaped and non-motile cocci. Transmission of this pathogenic organism occurs through air droplets. When an infected person coughs or sneezes, the bacterial suspension of small droplets of saliva or mucous spreads in the air and then transmits to others. Another common method of transmission is through direct contact with bacterially contaminated objects. Approximately 30% of healthy individuals carry this organism in their noses, pharynx and on their skin.

Besides the commonest skin infection, it can cause other infections like pneumonia, meningitis, osteomyelitis, and endocarditis. The blood infection by pathogenic *S. aureus* organism results in the symptoms like fever, chills, and hypotension. In skin infections, it results in the pus-filled abscesses with drainage of pus. In food poisoning, this bacterium releases a toxin into the foods and the people taking this contaminated food can suffer from severe nausea and vomiting. In the recent years the antibacterial resistance to *S. aureus* strains of the bacterium has been increasing and the ability of this organisms to spread in both hospital and community settings has increased (Naber, 2009).

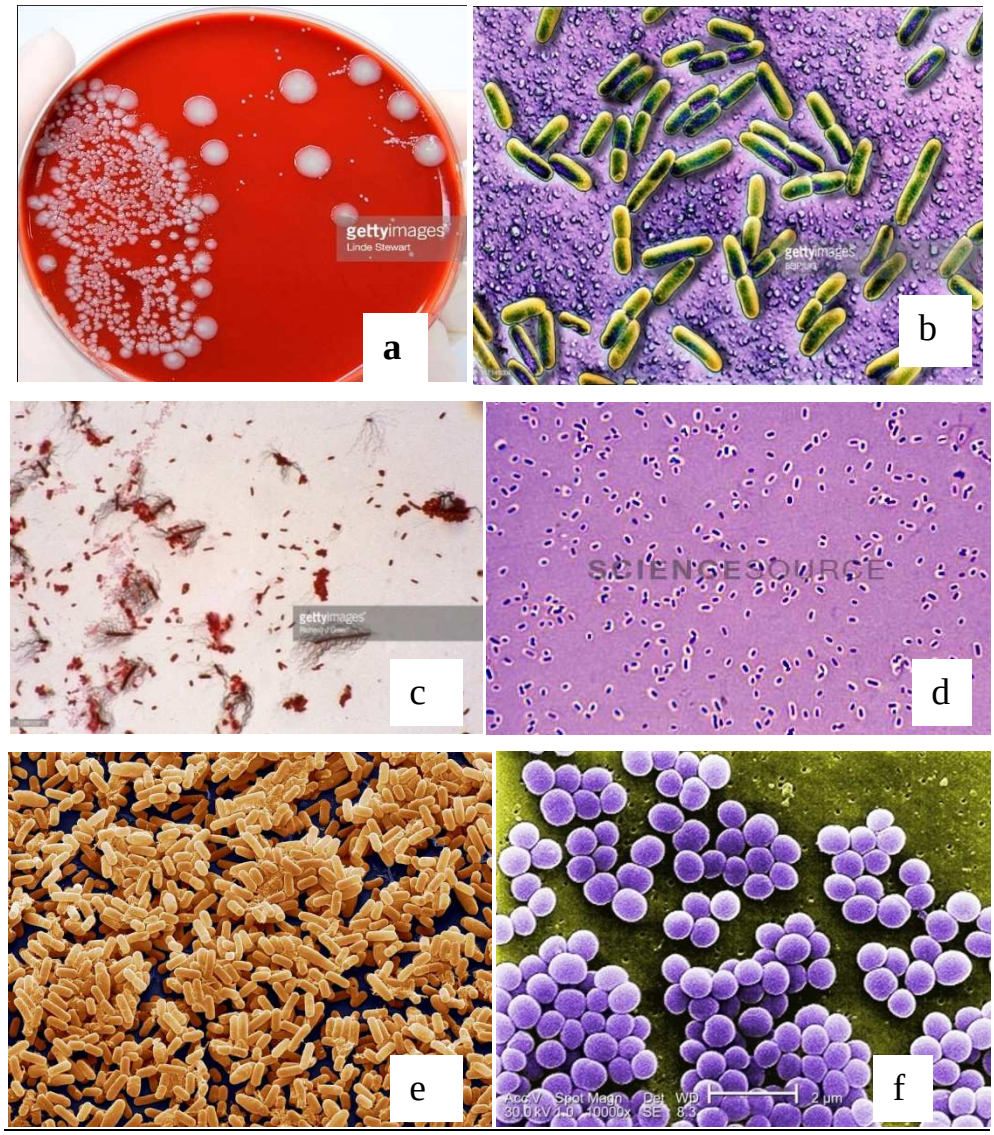

Figure 12: *E. coli* (a&b), *P. vulgaris* (c), *K. pneumonia* (d), *B. subtiis* (e), *S.aureus* (f)

(*Source: Internet*)

3.6.5 Preparation of Paper Disc

Whatman filter paper no. 1 was used for the preparation of paper disc. The filter paper was cut by paper punching machine to the size of 5 and 6 mm. The paper disc was heated to remove the moisture and to activate absorption capacity. The disc was sterilized before loading of the synthesized compounds.

3.6.6 Loading of Chemicals

The different concentrations of synthesized chemicals were prepared in DMSO solvent and the paper disc was loaded with chemicals with the help of a capillary tube. The loaded paper was dried by blowing hot air through hair drier machine and the maximum amount of solution was absorbed.

3.6.7 Inoculation of Organism and Measurement of Growth Inhibition Zone

Few colonies of organisms were suspended in tryptone soya broth to make homogenous suspension and kept for two hours at 37 °C for uniform growth. The bacterial culture was then swabbed on agar media with the help of sterile stick swab. The loaded paper discs were stuck on the swabbed media and the plates were incubated at 37 °C for 24 – 36 hours in the incubator. The discs of both negative and positive control drugs were also stuck on the media for comparison of the inhibition zone. The diameter of the zone of inhibition was examined and measured with the help of antibiogram zone measuring scale.

CHAPTER 4

RESULTS AND DISCUSSION

4.1 Physical Measurements

The better understanding of the behavior of metal complexes can be well accomplished by the study of their physical properties, which includes colour, solubility, melting point, pH and conductivity measurements. These are essential to gain supportive information, regarding the ligand and complex formation during the chemical processes. The different chemicals have their unique physical properties and their detailed study helps in designing the mechanism of the reaction and also helps in predicting the nature of the compounds.

4.1.1 Colour

The interaction of electron cloud of the ligand with degenerate d-orbitals of metal ions split them into different energy levels, corresponding to the geometry of the complexes. Exposure of electromagnetic radiation to such complexes leads to characteristic absorption of energy and electronic transition from lower to higher energy level takes place. If the complex absorbs electromagnetic radiation in the visible region of the spectrum, then it emits energy complementary to absorbed radiation and produces colour of the chemicals. Change in the colour of the complexes is due to the different range of electronic absorption, either by π bonding or nonbonding or by free electrons. Generally, the chromophores in presence of auxochromes show electronic absorption in UV-visible region and provide the characteristic colour of the substances. Conjugation further enhances the intensity of colour. The free electrons of metals in their complexes exhibit electronic absorption and furnish various colours of the metal complexes. The different colours of the synthesized compounds have been referenced in the Table 2-4.

4.1.2 Solubility and Melting Points

The solubility and melting points are the characteristic physical properties of the chemicals. The solubility of the ligands and metal complexes was examined in water and various organic solvents. Their solubility data are reported in the Table A3. The observation of solubility data revealed that the ligands and metal complexes were insoluble in water but soluble in organic solvents. The ligands were soluble in methanol, DMSO, and DMF whereas metal complexes were soluble in DMSO and DMF. The melting points were determined by filling finely powdered sample in a glass capillary and heating in GallenKamp melting point apparatus.

4.1.3 Conductivity Measurement

Conductivity data evaluates the nature of the complexes as electrolytes or non-electrolytes. In the present investigation, the conductivities of the complexes at the concentration of M/1000 were measured at room temperature and their data are presented in the Table 1. The observation of data revealed the non-electrolyte type of the metal complexes which is indicated by their conductivity values below 100 µS cm^{-1}.

4.1.4 pH Measurement

The complexation in coordination chemistry is often accompanied by deprotonation of ligand which is the true cause of the variation of pH in the solution phase. In the general case, there is drop down in pH values of the solution in moving from ligand to metal complexes. The variation in pH values is committed to being the indication of the complex formation during the reaction. The pH values of ligands and their metal complexes are reported in the Table 1. The data shows the variation of pH values from 3.98 to 6.3. Moreover, the ligands have higher pH values than the metal complexes.

Table 1: Molar conductivity (Λ_M) and pH data

S.N.	Compounds	Geometry	Λ_M in μS/cm (Ω^{-1} $mol^{-1}cm^2$)	pH
1	KMAXC	-	-	6.23
2	AXCPC3	-	-	5.58
3	AXCPC2	-	-	5.60
4	Co-KMAXC	Octahedral	20.1	4.32
5	Cu-KMAXC	Square Planar	18.9	4.28
6	Zn-KMAXC)	Tetrahedral	5.1	5.69
7	Co-AXCPC3	Octahedral	21.8	4.56
8	Ni-AXCPC3	Square Planar	19.9	4.35
9	Cu-AXCPC3	Tetrahedral	35.2	4.23
10	Zn-AXCPC3	Tetrahedral	5.6	5.12
11	Co-AXCPC2	Octahedral	25.6	3.98
12	Ni-AXCPC2	Square Planar	20.9	4.25
13	Cu-AXCPC2	Tetrahedral	31.1	4.11
14	Zn-AXCPC2	Octahedral	8.7	5.10

4.2 Microanalytical Results

Elemental analysis is an analytical technique for the rapid determination of carbon, hydrogen, nitrogen, and sulphur in the organic matrices and other types of materials either qualitatively or quantitatively. CHNS analysis is a cost-effective technique that can provide crucial information on the purity and composition of chemical substances. The instrument used for this purpose is called elemental analyzer. In our research work, the microanalytical results of the Schiff base ligands and their metal complexes are reported in the Table 2-4. The microanalytical results are in good consistent with the proposed stoichiometry of the compounds.

Table 2: Physical properties and microanalytical data of KMAXC Schiff base ligand and metal complexes

Complex	Empirical Formula	Formula Weight	Color	Yield %	Calculated (Found) (%)				
					C	H	N	O	S
KMAXC	$C_{35}H_{55}N_7O_{15}S$	845.92	Light yellow	71	49.72 (49.12)	6.48 (6.38)	11.64 (11.75)	28.40 (28.9)	3.75 (3.91)
Co-KMAXC	$C_{35}H_{55}CoN_7O_{16}S$	920.85	Purple	65	45.70 (44.99)	6.10 (6.20)	10.62 (10.78)	27.85 (27.89)	3.53 (3.55)
Cu-KMAXC	$C_{35}H_{55}CuN_7O_{16}S$	925.46	Light blue	68	45.38 (45.48)	5.89 (5.92)	10.64 (10.66)	27.71 (27.75)	3.45 (3.48)
Zn-KMAXC)	$C_{35}H_{55}N_7O_{16}SZn$	927.30	yellow	56	45.39 (45.35)	5.95 (5.88)	1052 (10.75)	27.55 (27.68)	7.15 (7.21)

Table 3: Physical properties and microanalytical data of AXCPC3 Schiff base ligand and metal complexes

Complex	Empirical Formula	Formula Weight	Color	M.P. (°C)	Calculated (Found) (%)				
					C	H	N	O	S
AXCPC3	$C_{22}H_{22}N_4O_5S$ (L)	454.13	Bright yellow	140	58.14 (58.21)	4.88 (4. 81)	12.33 (12.25)	17.60 (17.57)	7.06 (6.95)
Co-AXCPC3	$C_{44}H_{46}CoN_8O_{12}S_2$ ($CoL_2.2H_2O$)	1001.2	Blue	285	52.74 (52. 69)	4.63 (4.69)	11.18 (11.26)	19.16 (19.20)	6.40 (6.64)
Ni-AXCPC3	$C_{44}H_{42}N_8NiO_{10}S_2$	964.18	Green	270	54.73 (54.55)	4.38 (4. 59)	11.60 (11.59)	16.57 (16.45)	6.64 (6.44)
Cu-AXCPC3	$C_{44}H_{42}CuN_8O_{10}S_2$	969.18	Green	160	54.45 (54.52)	4.36 (4.49)	11.55 (11. 63)	16.49 (16.55)	6.61 (6.73)
Zn-AXCPC3	$C_{44}H_{42}N_8O_{10}S_2Zn$	970.18	Light yellow	250	54.35 (54.41)	4.35 (4.43)	11.52 (11.57)	16.45 (16.49)	6.60 (6. 57)

Table 4: Physical properties and microanalytical data of AXCPC2 Schiff base ligand and metal complexes

Complex	Empirical Formula	Formula Weight	Color	Calculated (Found) (%)				
				C	H	N	O	S
AXCPC2	$C_{22}H_{22}N_4O_5S$ (L)	454.13	Cocoa Brown	58.14 (58.18)	4.88 (4.82)	12.33 (12.29)	17.60 (17.62)	7.06 (7.01)
Co-AXCPC2	$C_{44}H_{42}CoN_8O_{10}S_2$	965.18	Coffee	54.71 (54.69)	4.38 (4.40)	11.60 (11.58)	16.56 (16.51)	6.64 (6.67)
Ni-AXCPC2	$C_{44}H_{42}N_8NiO_{10}S_2$	964.18	Beaver	54.73 (54.69)	4.38 (4.37)	11.60 (11.55)	16.57 (16.55)	6.64 (6.60)
Cu-AXCPC2	$C_{44}H_{42}CuN_8O_{10}S_2$	969.18	Rifle green	54.45 (54.39)	4.36 (4.41)	11.55 (11.48)	16.49 (16.52)	6.61 (6.56)
Zn-AXCPC2	$C_{44}H_{46}N_8O_{12}S_2Zn$ ($ZnL_2.2H_2O$)	1006.2	Ruddy brown	52.41 (52.42)	4.60 (4.63)	11.11 (11.15)	19.04 (19.12)	6.36 (6.32)

4.3 Spectroscopic Results and Discussion

4.3.1 FT-IR Spectral Study

4.3.1.1 FT-IR Spectra of KMAXC and Metal Complexes

The FTIR spectral comparison of Schiff base ligand and metal complexes provide crucial information about the metal-ligand interaction and coordination mode of the ligand to the metal ions (Aziz *et al.*, 2012). In our work, the pentadentate KMAXC ligand displayed various IR spectral bands characteristic of the groups present in it, which have been shifted and even diminished in some cases after coordination with the metal ions. The broad absorption bands in the IR spectra at 3442 cm^{-1} (KMAXC), 3419 cm^{-1} (Co-KMAXC), 3425 cm^{-1} (Cu-KMAXC) and 3432 cm^{-1} (Zn-KMAXC) complexes are attributed to the coalesce of ν(O-H / N-H) stretching bands (Rahaman & Mruthyunjayaswamy, 2014). The symmetric and asymmetric ν(C-H) stretching frequencies of the CH_3 group in the spectra of KMAXC ligand and metal complexes are noticed around 3000 cm^{-1} (Coates, 2000). The significant differences in the absorption frequencies are observed in the region between 1775 and 1200 cm^{-1} and at lower frequencies below 600 cm^{-1}. The intense band due to azomethine ν(C=N) stretch is perceived at 1644 cm^{-1} for the KMAXC (Krishnapriya *et al.*, 2008) and it

has shifted to lower wave numbers in the spectra of metal complexes (Nair *et al.*, 2012). The IR spectra of metal complexes display absorption bands in the region of 1635-1641 cm^{-1} characteristic to ν(C=N) stretching frequencies. The IR spectral bands for ν(C=N) stretch of Co-KMAXC, Cu-KMAXC, and Zn-KMAXC complexes were observed at 1641, 1637, and 1635 cm^{-1} respectively. In fact, in all the complexes, the absorption band for ν(C=N) stretch has shifted to lower wave numbers, indicating their participation in the coordination with metal ions. The IR absorption frequency at 1675 cm^{-1} due to amide ν(C=O) stretch in ligand has undergone negative shift at 1668 cm^{-1}, 1660 cm^{-1} and 1663 cm^{-1} corresponding for Co-KMAXC, Cu-KMAXC and Zn-KMAXC complexes (Liou *et al.*, 2005). This confirms the participation of amide (C=O) group for ligation with metal ions. The ν(C-N) stretching frequency for amide and amine groups at 1442 cm^{-1} in IR spectrum of KMAXC has shifted to 1434 cm^{-1} for Co-KMAXC complex, 1428 cm^{-1} for Cu-KMAXC complex and 1424 cm^{-1} for Zn-KMAXC complex respectively and these nicely support the participation of such groups in the coordination process with metal ions. The metal-ligand bonding has further substantiated by the appearance of absorption band in the region of 420-435 cm^{-1} and a medium intensity band in the region of 500-530 cm^{-1} assignable for ν(M-N) and ν(M-O) stretching vibrations, which were absent in the spectrum of free KMAXC ligand (Abdallah *et al.*, 2010; Osowole & Daramola, 2011) These overall data suggest the ligand metal interaction through azomethine-N, amide-N, amine-2 N of Kanamycin moiety, heterocyclic-O and amide-O of the ligand. The FT-IR data are summarized in the Table 5 and the corresponding spectra are displayed in the Figures 13 - 16.

Table 5: FTIR spectral data of KMAXC Schiff base ligand and metal complexes

Complex	ν(NH, OH)	ν (C=N) azomethine	ν (C=O) amide	ν(C-N) amide/amine	ν(M-N)	ν(M-O)
KMAXC	3442	1644	1675	1442	-	-
Co-KMAXC	3419	1641	1668	1434	429	502
Cu-KMAXC	3425	1637	1660	1428	425	528
Zn-KMAXC	3432	1635	1663	1424	433	520

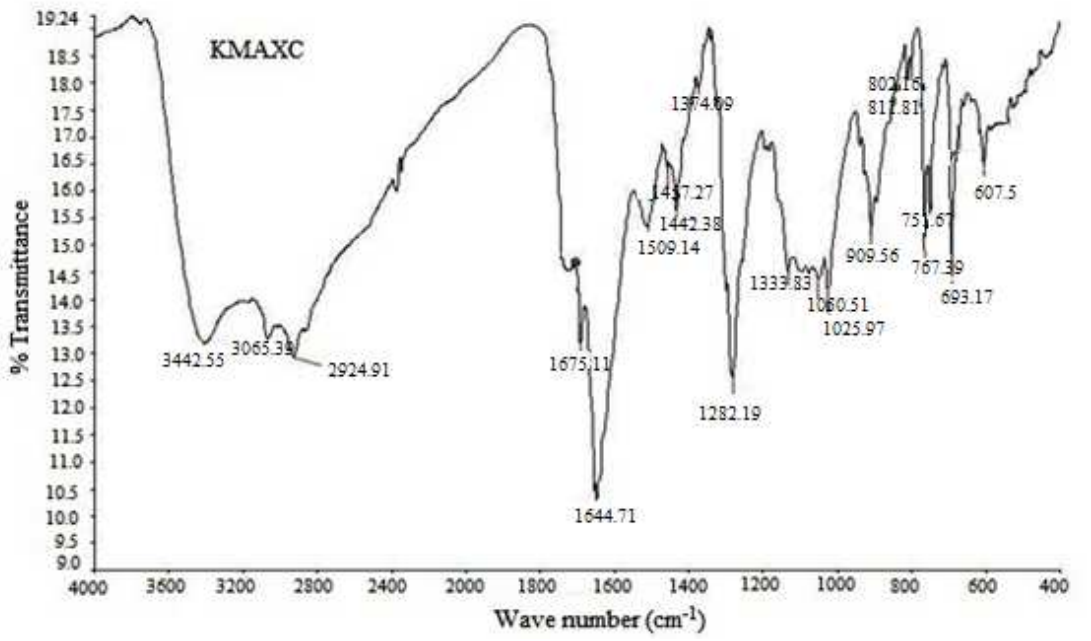

Figure 13: FTIR spectrum of KMAXC ligand

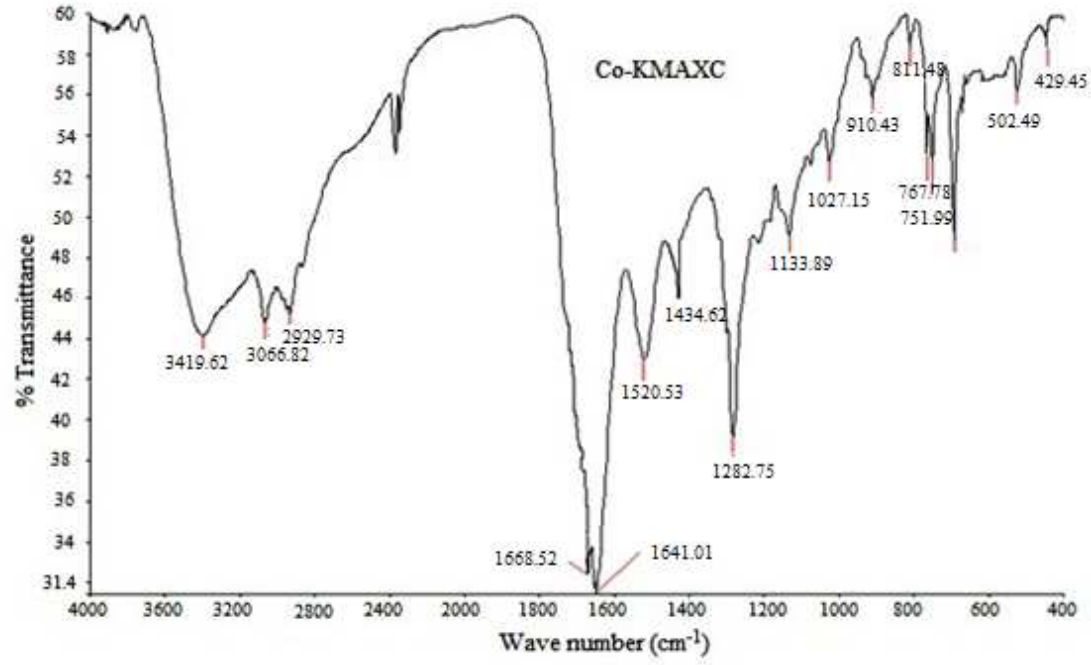

Figure 14: FTIR spectrum of Co-KMAXC

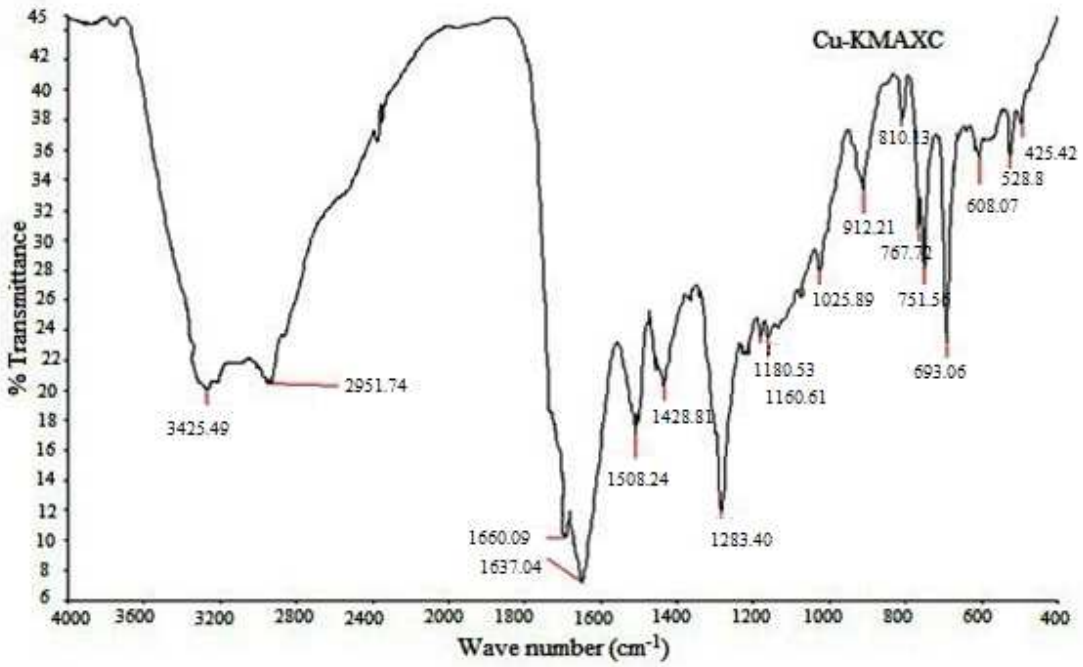

Figure 15: FTIR spectrum of Cu-KMAXC

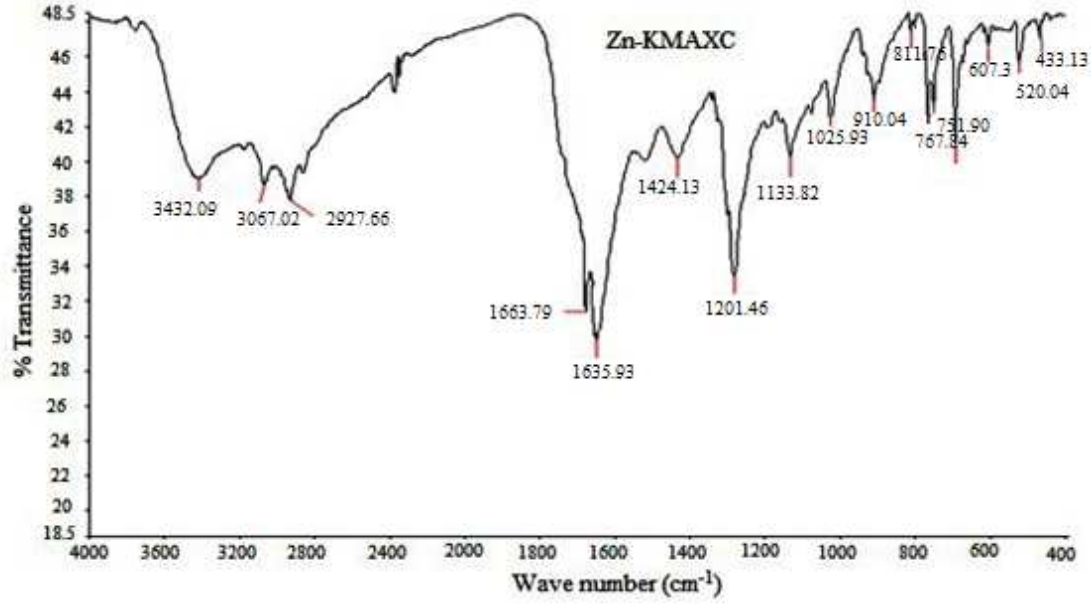

Figure 16: FTIR spectrum of Zn-KMAXC

4.3.1.2 FT-IR Spectra of AXCPC3 and Metal Complexes

The most significant IR spectral bands are presented in the Table 6. The IR spectrum of free ligand (AXCPC3) and all the metal complexes (Co-AXCPC3, Ni-AXCPC3, Cu-AXCPC3, and Zn-AXCPC3) reveal characteristic broad absorption bands in the region between 3100 and 3500 cm^{-1}, corresponding ν(N-H) and ν(O-H) phenolic stretch. The azomethine ν(C=N) stretching vibration band for AXCPC3 is noticed at 1640 cm^{-1} which has shifted to 1633, 1625, 1636 and 1629 cm^{-1} for Co-AXCPC3, Ni-AXCPC3, Cu-AXCPC3 and Zn-AXCPC3 complexes respectively, implying its coordination to the metal center through azomethine nitrogen (Imani *et al.*, 2015; Rama & Selvameena, 2015). The IR absorption bands for AXCPC3 and metal complexes in the region of 1510-1513 cm^{-1} and 1433-1437 cm^{-1} are attributed to asymmetric and symmetric stretching vibrations of COOH groups respectively (Anacona *et al.*, 2013). These absorption bands in the free ligand (AXCPC3) and its metal complexes are almost in the same region, indicating its non-coordination with metal ions. The well-resolved bands at 3417 cm^{-1} for Co-AXCPC3 complex corresponds to the ν(O-H) stretching vibrations (Figure 18) (Pahontu *et al.*, 2013). The less intense band at 606 cm^{-1} is assignable to bending vibration of two lattice water molecules of the outer sphere region. The metal-ligand bonding in Co-AXCPC3 is evidenced by the observation of new bands in the lower frequency regions at 425 and 526 cm^{-1} characteristic to ν(Co-N) and ν(Co-O) stretching vibrations, that are not seen in the IR spectrum of AXCPC3. The Ni-AXCPC3 complex attributes specific bands at 1625 cm^{-1} ν(C=N) azomethine, 3337 cm^{-1} ν(O-H), 429 cm^{-1} ν(Ni-N) and 687 cm^{-1} for outer sphere lattice water molecules. The Cu-AXCPC3 complex executes a strong azomethine band at 1636 cm^{-1} which has undergone a negative shift by 4 cm^{-1} relative to that of the free ligand. The other significant FTIR bands are observed at 3379 cm^{-1} ν(O-H), 444 cm^{-1} ν(Cu-N) and 686 cm^{-1} for outer sphere lattice water molecules. The formation of the Zn-AXCPC3 complex is evidenced by strong azomethine band at 1629 cm^{-1} ν(C=N) which has shifted by 11 cm^{-1} towards a lower wave number relative to the free ligand AXCPC3, indicating metal coordination with azomethine nitrogen. The metal nitrogen coordination is further evidenced by a sharp peak at 415 cm^{-1} corresponding to ν(Zn-N) stretch (Joshi & Habib, 2014). The bending vibration of lattice water molecules is confirmed by the less intense peak at 657 cm^{-1}. FT-IR spectrum in combination with other spectral studies also reveals the

coordination of metal with the nitrogen of amide group. The spectra of metal complexes are shown in the Figures 17 – 21.

Table 6: FTIR spectral data of AXCPC3 Schiff base ligand and metal complexes

Complex	ν(NH) & ν(OH)	ν(C=N) (imine)	ν_{asym} COOH)	ν_{sym}(COOH)	ρ_w H_2O	ν(M-N)	ν(M-O)
AXCPC3	3303	1640	1510	1433	-	-	-
Co-AXCPC3	3417 (b)	1633	1510	1433	606	425	526
Ni-AXCPC3	3337	1625	1513	1435	687	429	-
Cu-AXCPC3	3379	1636	1512	1436	686	444	-
Zn-AXCPC3	3340	1629	1512	1437	657	415	-

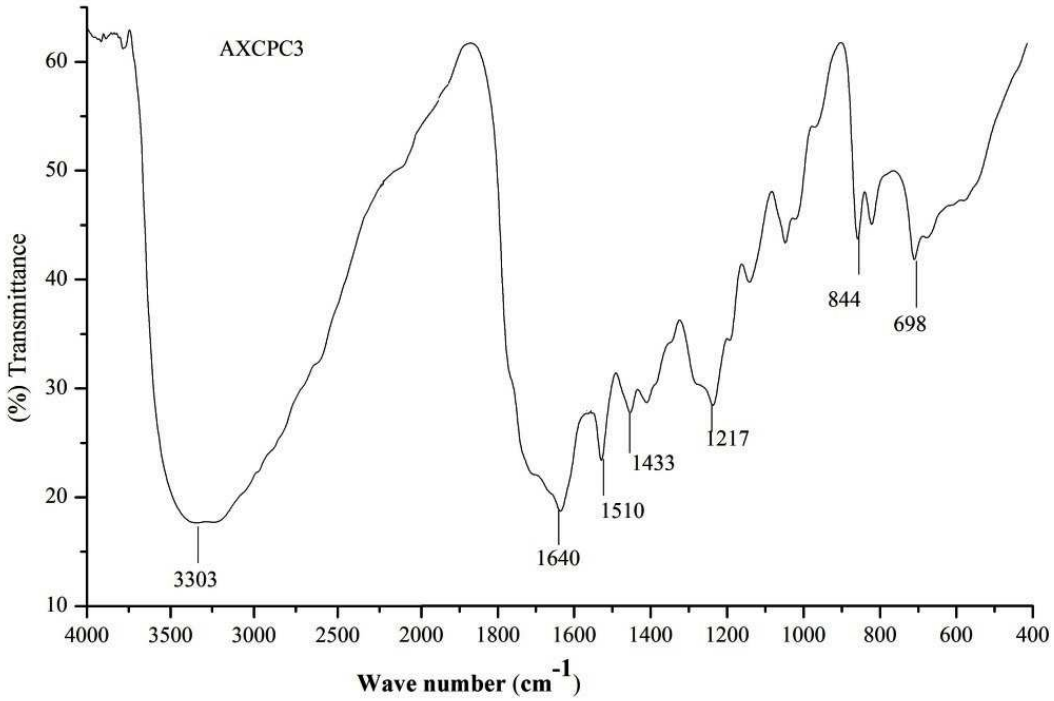

Figure 17: FTIR spectrum of AXCPC3 ligand

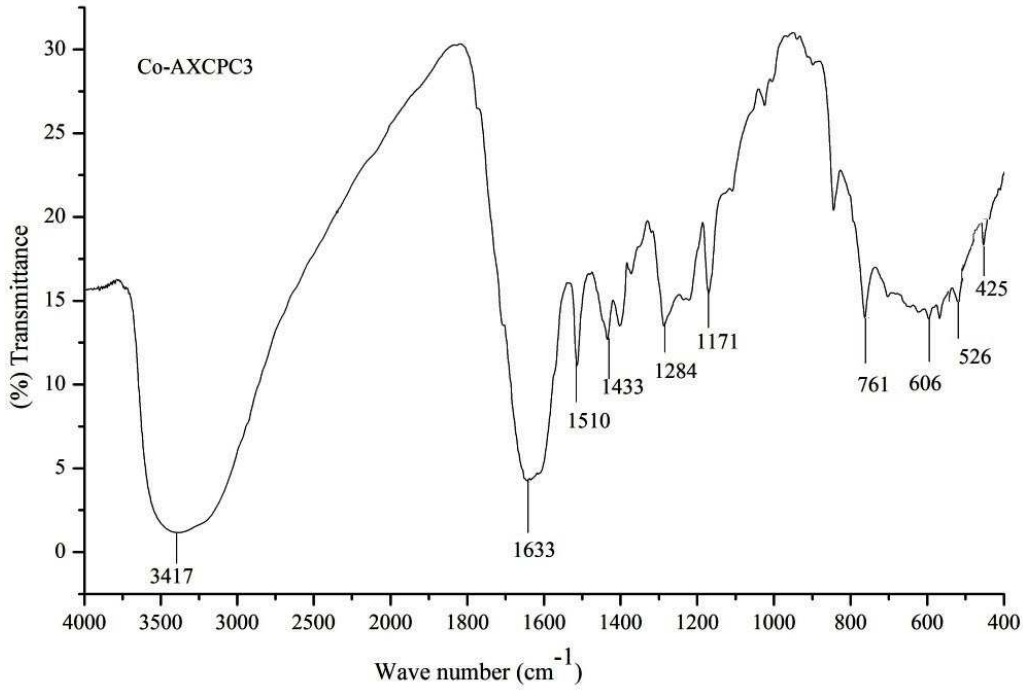

Figure 18: FTIR spectrum of Co-AXCPC3

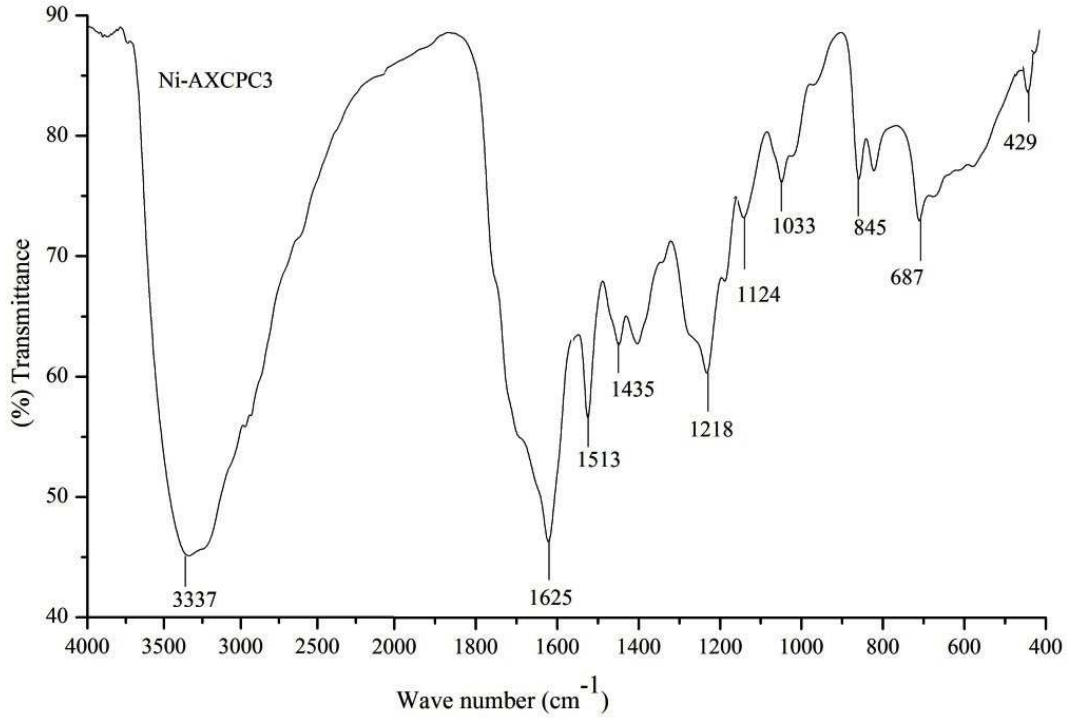

Figure 19: FTIR spectrum of Ni-AXCPC3

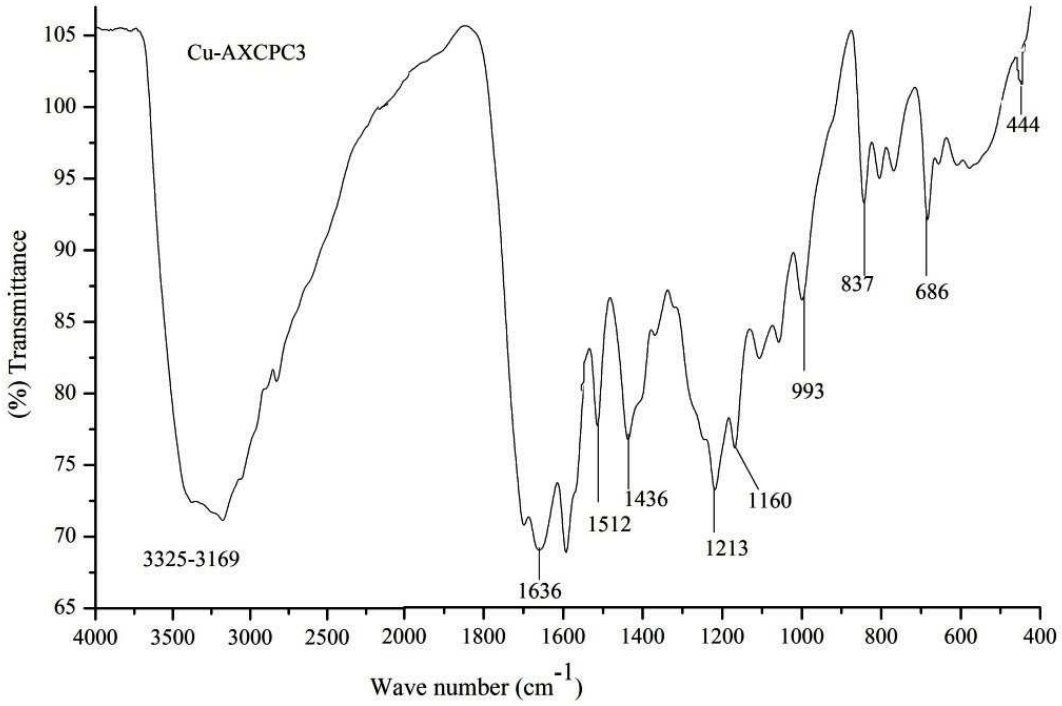

Figure 20: FTIR spectrum of Cu-AXCPC3

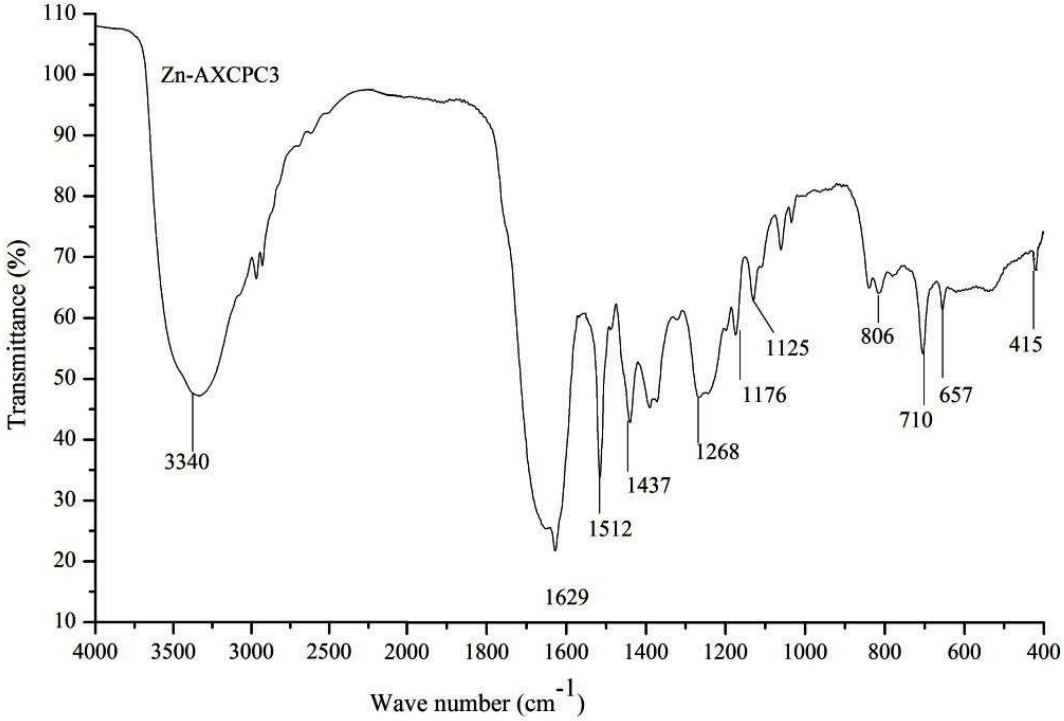

Figure 21: FTIR spectrum of Zn-AXCPC3

4.3.1.3 FT-IR Spectra of AXCPC2 and Metal Complexes

The FT-IR spectra of ligand and metal complexes are shown in the Figures 22 - 26. The IR spectrum of AXCPC2 ligand exhibits broad absorption band in the region between 3600 and 2800 cm^{-1} with a peak at 3336 cm^{-1} and two shoulder peaks at 2963 and 2928 cm^{-1} corresponding to ν(N-H), ν(O-H) and ν(C-H) overlapping stretching vibrations. The shoulder peaks associated with this broad absorption band are attributed to methyl ν(C-H) symmetric and asymmetric stretch. The metal complexes also exhibit broad absorption band corresponding to ν(N-H), ν(O-H) and ν(C-H) overlapping stretching vibrations in the similar regions, with highest peak intensity at 3397, 3391, 3395 and 3308 cm^{-1} for respective Co-AXCPC2, Ni-AXCPC2, Cu-AXCPC2 and Zn-AXCPC2 complexes. The ν(C=N) stretch attributed to azomethine bond for AXCPC2 at 1657 cm^{-1} has observed to experience a downward shift of 7 to 13 cm^{-1} upon complexation with metal ions (Anis *et al.*, 2013; Reiss *et al.*, 2014). The related ν(C=N) stretch peak for Co-AXCPC2, Ni-AXCPC2, Cu-AXCPC2 and Zn-AXCPC2 complexes are observed at 1650, 1644, 1647 and 1651 cm^{-1} respectively. The IR spectrum of AXCPC2 exhibits ν(COOH) symmetric and asymmetric stretching vibration bands at 1439 and 1514.8 cm^{-1} and no appreciable change of this value is observed in the IR spectra of metal complexes. The carboxylic ν(C=O) stretch for the ligand is observed at 1737 cm^{-1} and this value has shifted to 1710, 1740, 1725 and 1740 cm^{-1} for Co-AXCPC2, Ni-AXCPC2, Cu-AXCPC2 and Zn-AXCPC2 complexes. This shift in positions may be attributed to change in electronic environment after complexation (Živec *et al.*, 2012). Most of the IR absorption bands of the complexes in the fingerprint region are similar, providing their identity. Metal-nitrogen bonding in the complexes is ascribed by the appearance of less intense peaks in the region of 418 to 463 cm^{-1} (Table 7). The Co-AXCPC2 and Zn-AXCPC2 complexes also exhibit less intense IR absorption peaks at 568 and 525 cm^{-1}, which correspond to metal-oxygen bonding.

Table 7: FTIR spectral data of AXCPC2 Schiff base ligand and metal complexes

Complex	ν(NH) & ν(OH)	ν(C-H) methyl	ν(C=N) (imine)	ν_{asym} (COOH)	ν_{sym} (COOH)	ν(C=O) carboxylic	ν(M-N)	ν(M-O)
AXCPC2	3336	2963, 2928	1657	1514.8	1439	1737	-	-
Co-AXCPC2	3397 (b)	2959, 2927	1650	1514.42	1440	1710	463.47	567.92
Ni-AXCPC2	3391		1644	1514.49	1440.96	1740	422	-
Cu-AXCPC2	3395	2957,	1647	1513.52	1440.24	1725	418	-
Zn-AXCPC2	3308	2960, 2926	1651	1514.35	1438	1740	418.32	525.21

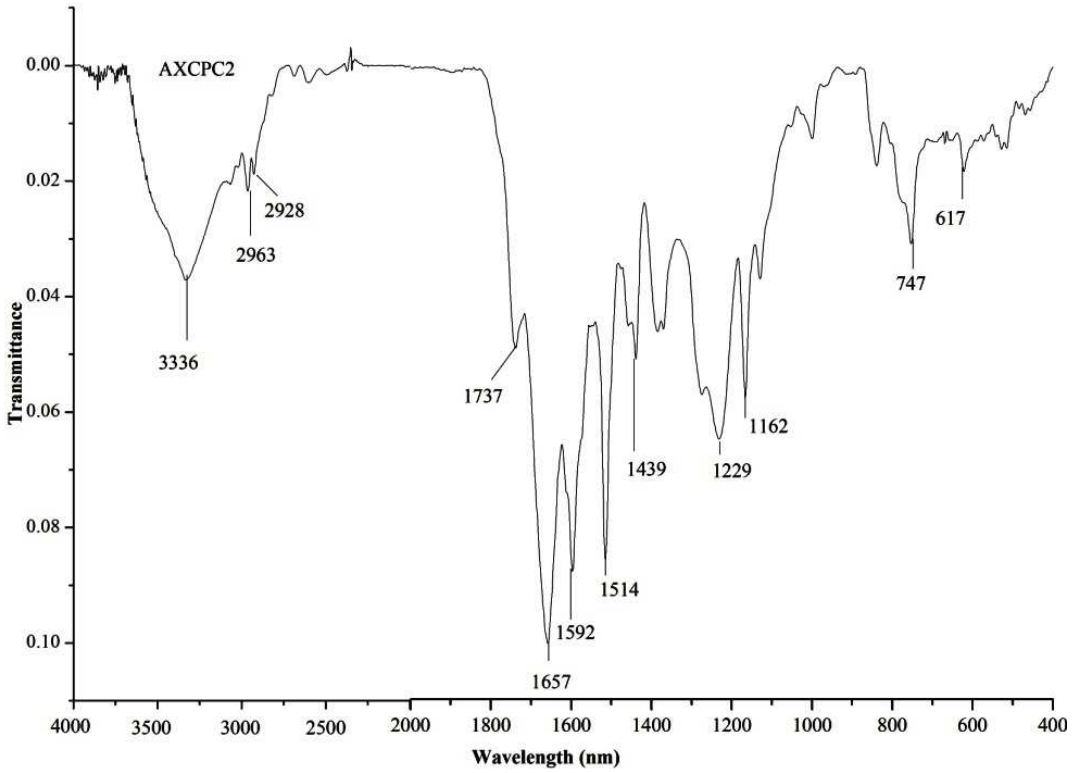

Figure 22: FTIR spectrum of AXCPC2 ligand

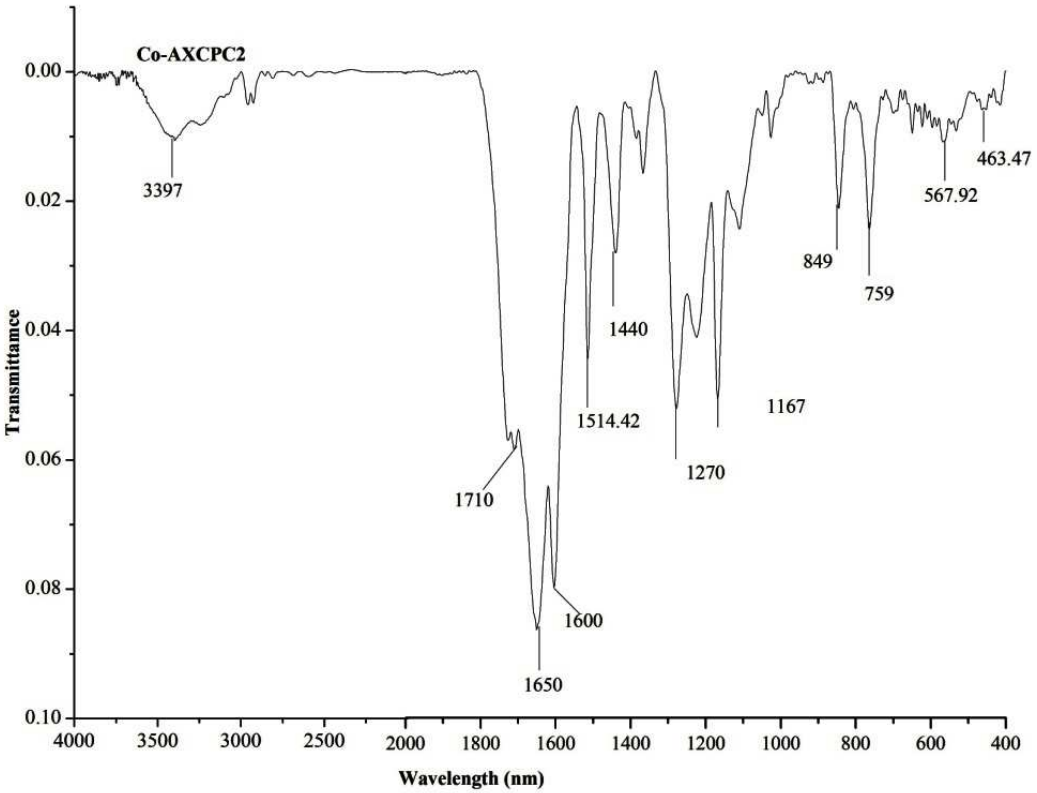

Figure 23: FTIR spectrum of Co-AXCPC2

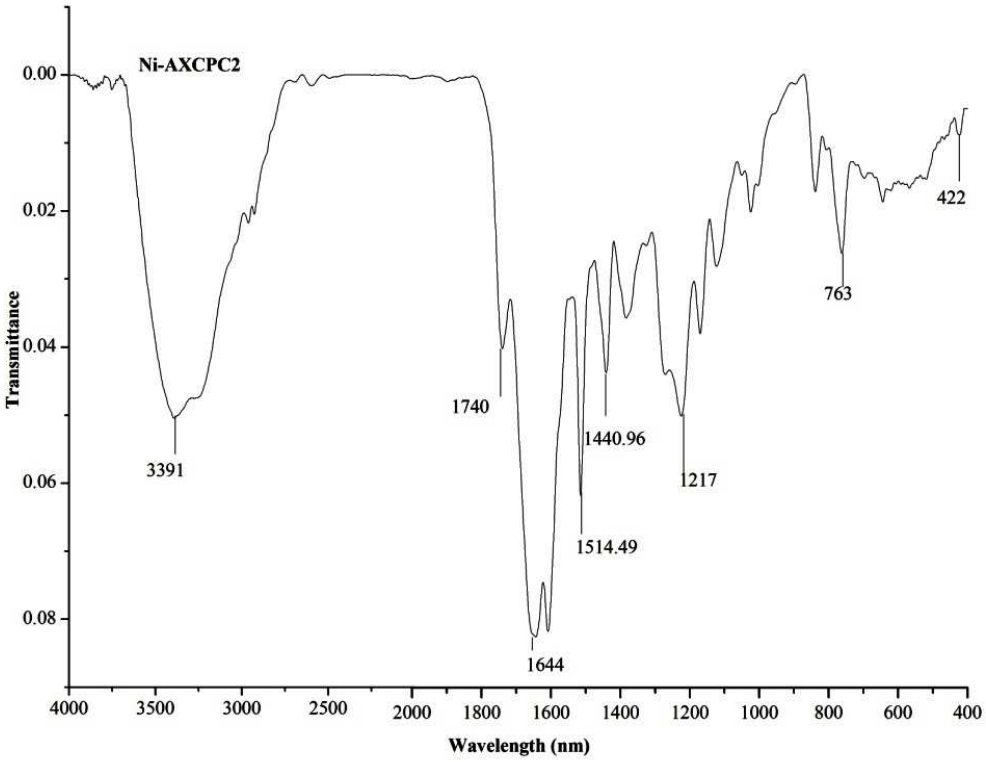

Figure 24: FTIR spectrum of Ni-AXCPC2

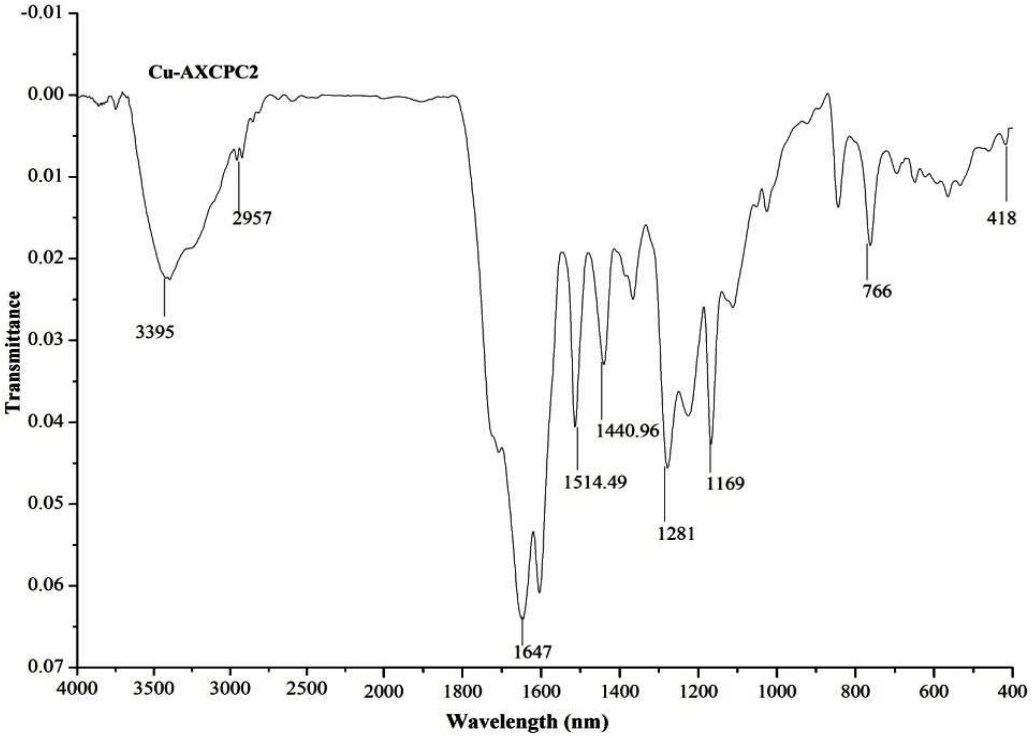

Figure 25: FTIR spectrum of Cu-AXCPC2

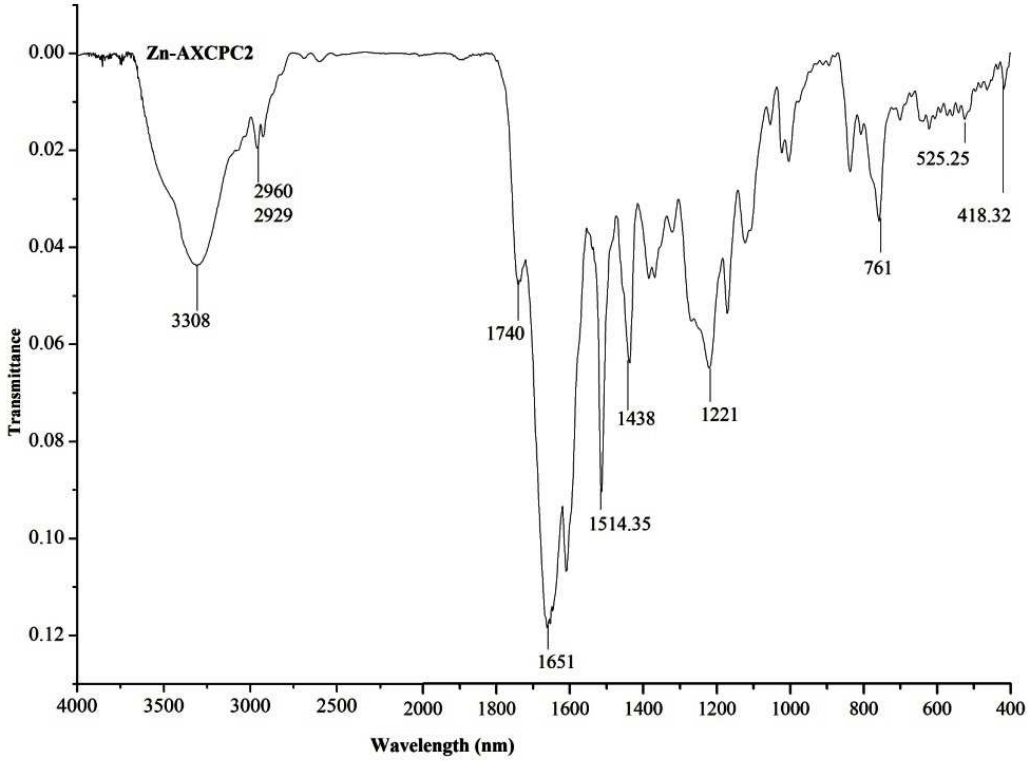

Figure 26: FTIR spectrum of Zn-AXCPC2

4.3.2 ^{1}H & ^{13}C NMR Spectral Study

NMR spectroscopy is used to identify the carbon-hydrogen framework of the organic ligand and metal complexes. Due to the different electronic environment of protons in the molecules, they show the resonance peaks at different regions of the spectrum, depending on their extent of shielding and deshielding effects. The shielded protons deliver NMR signal towards low chemical shift value and deshielded protons deliver the signal at high chemical shift value region (Field, *et al.*, 2007; Silverstein, *et al.*, 2005). Furthermore, the splitting of signals into multiplets furnishes important information regarding the types of protons present in the molecule. Sometimes the loss of signal in the NMR spectrum of metal complexes relative to ligand also executes important information about the point of attachment of ligand with metal center (Claridge, 1999).

4.3.2.1 ^{1}H NMR Spectra of KMAXC Schiff Base and Zn-KMAXC Complex

The formation of Schiff base (KMAXC) ligand and its diamagnetic Zn-KMAXC complex is supported by the ^{1}H NMR spectral study. The spectral comparison delivers the idea about the binding nature of ligand to metal ions. The integral intensities of each signal in the ^{1}H NMR spectra of KMAXC and Zn-KMAXC complex are found to agree with the number of different types of protons present. In our study, the ^{1}H NMR spectrum of KMAXC ligand displays the resonance signals at 1.79, 3.65, and 11.5 ppm assigned to CH_3, $COOCH_3$, and Ar-OH protons respectively. No change in the positions of these signals has observed in the ^{1}H NMR spectrum of Zn-KMAXC complex, indicating non-involvement of these groups in the coordination process. The spectrum of KMAXC ligand exhibits a multiplet in 6.6-7.8 ppm region which may be assigned to Ar-H protons. Doublet peaks at 4.75 and 5.45 ppm are assigned to N-CH and N=C-CH protons of the β-lactam ring and at 9.05 ppm are assignable to NH proton lying between amide carbonyl and the β-lactam ring of the ligand. However, the resonance signal assigned to NH proton in free ligand disappeared in the ^{1}H NMR spectrum of Zn-KMAXC complex, indicating deprotonation of this group and the involvement in chelation process. Side chain methylene proton of kanamycin moiety linked to azomethine nitrogen exhibits doublet peaks at 2.09 ppm. No appreciable shift in ^{1}H NMR peak positions has

observed in the spectrum of Zn-KMAXC complex that has been assigned to kanamycin moiety except the decrease in intensity of NH_2 peak. The change in peak position of NH_2 protons in Zn-KMAXC complex is also an indication of its participation in coordination. The intense single peak at 3.2 and 4.07 ppm may be attributed to NH_2 and OH protons of Kanamycin. The ^{1}H NMR spectra of KMAXC and Zn-KMAXC are respectively shown in the Figures 27 and 28.

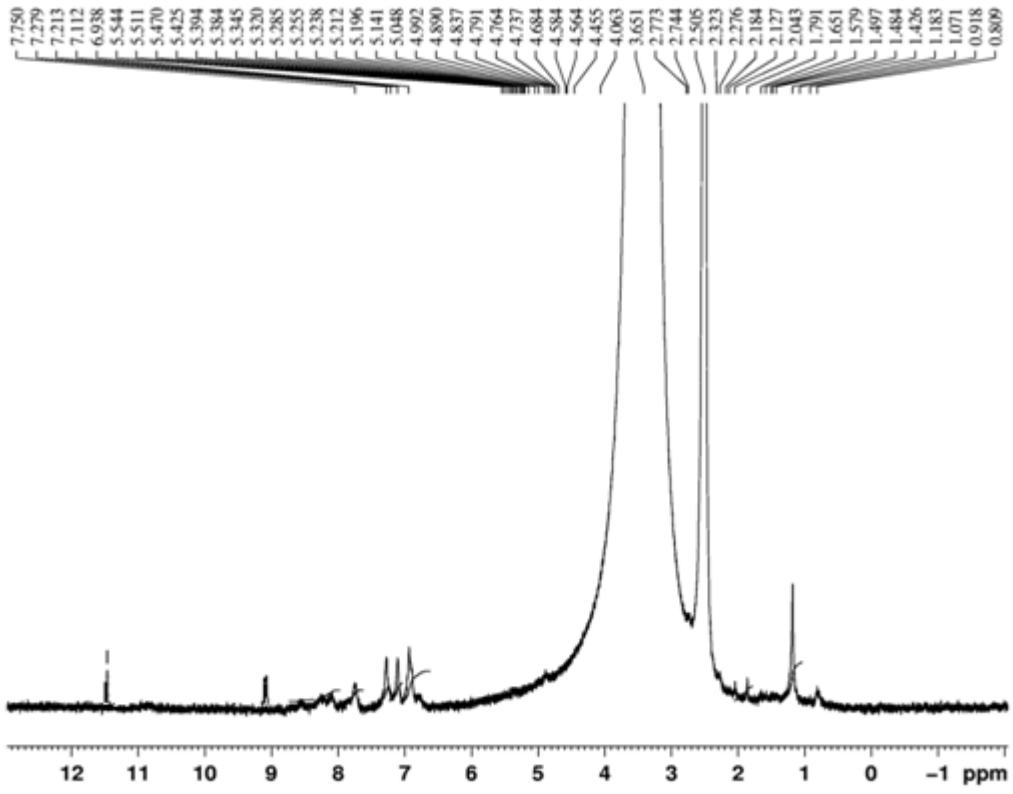

Figure 27: ^{1}H NMR spectrum of KMAXC

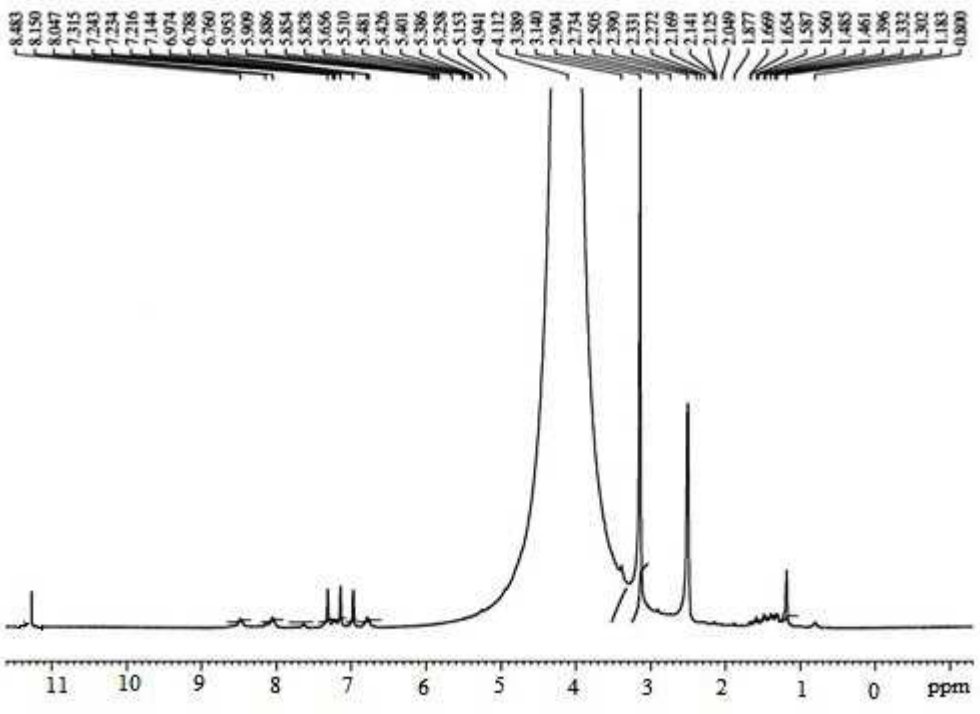

Figure 28: ^{1}H NMR spectrum of Zn-KMAXC

4.3.2.2 ^{1}H NMR Spectra of AXCPC3 Schiff Base and Zn-AXCPC3 Complex

The ^{1}H NMR spectra of the AXCPC3 ligand and its diamagnetic Zn-AXCPC3 complex were recorded in the DMSO-d_6 solvent and their spectral comparison was made to confirm the binding mode of ligand to the metal centers. The ^{1}H NMR spectral data of the mentioned compounds are computed in the Table 8 and the spectra are shown in the Figures 29 and 30. In the spectrum of AXCPC3, the signal for carboxylic proton appears at δ 10.122 ppm, which is still present in the spectrum of Zn-AXCPC3. The signal for a phenolic OH proton in both AXCPC3 and Zn-AXCPC3 appears at δ 9.425 ppm as a broad peak. The pyridine ring protons execute multiple peaks in the range of δ 8.535 - 8.864 ppm for AXCPC3 and this peak range is still present in the spectrum of Zn-AXCPC3, with slight variations (Carreño *et al.*, 2015). The azomethine proton in AXCPC3 executes ^{1}H NMR signal at δ 9.094 ppm which has shifted downfield at δ 9.295 ppm, suggesting its coordination with zinc ion of Zn-AXCPC3 (Asadi *et al.*, 2014). Two doublets observed at δ 6.718 - 7.625 for AXCPC3 and δ 6.72-7.66 ppm for the complex are attributed to aromatic ring protons. The methyl protons of amoxicillin moiety in both AXCPC3 and Zn-AXCPC3

appear as a singlet peak in the region of δ 1.118-1.562 ppm. Amide NH proton for AXCPC3 executes signal at 8.241-8.271 ppm, which is absent in the spectrum of Zn-AXCPC3, and this confirms the coordination of amide N-atom with metal center via deprotonation (Naglah *et al.*, 2015).

Table 8: ^{1}H NMR spectral data of AXCPC ligand and Zn-complex

Comp.	Chemical shift (δ) ppm		Assignment
Ligand	AXCPC3	AXCPC2	
	10.122 (s)	10.122 (s)	Carboxylic proton
	9.425 broad	9.723 broad	Phenolic OH proton (May be due to H-bond)
	9.094 (s)	9.225 (s)	Azomethine proton
	8.535 -8.864 (m)	8.197-8.443	Pyridine ring protons
	8.241 - 8.271 (s)	8.008-8.130	Amide NH proton
	6.718 - 7.625 two (d)	6.691-7.767	Ar-H protons
	1.118 - 1.562	1.146 - 1.495	Methyl protons
Zn-complex	Zn-AXCPC3	Zn-AXCPC2	
	10.123 (S)	10.123 (S)	Carboxylic proton
	9.425 broad	9.75 broad	Phenolic OH proton (May be due to H-bond)
	9.295 (s)	9.440 (s)	Azomethine proton
	8.534 -8.865 (m)	8.187-8.594	Pyridine ring protons
	6.720 - 7.660 two (d)	6.713-7.784	Ar-H protons
	1.118 - 1.571	1.229 - 1.521	Methyl protons

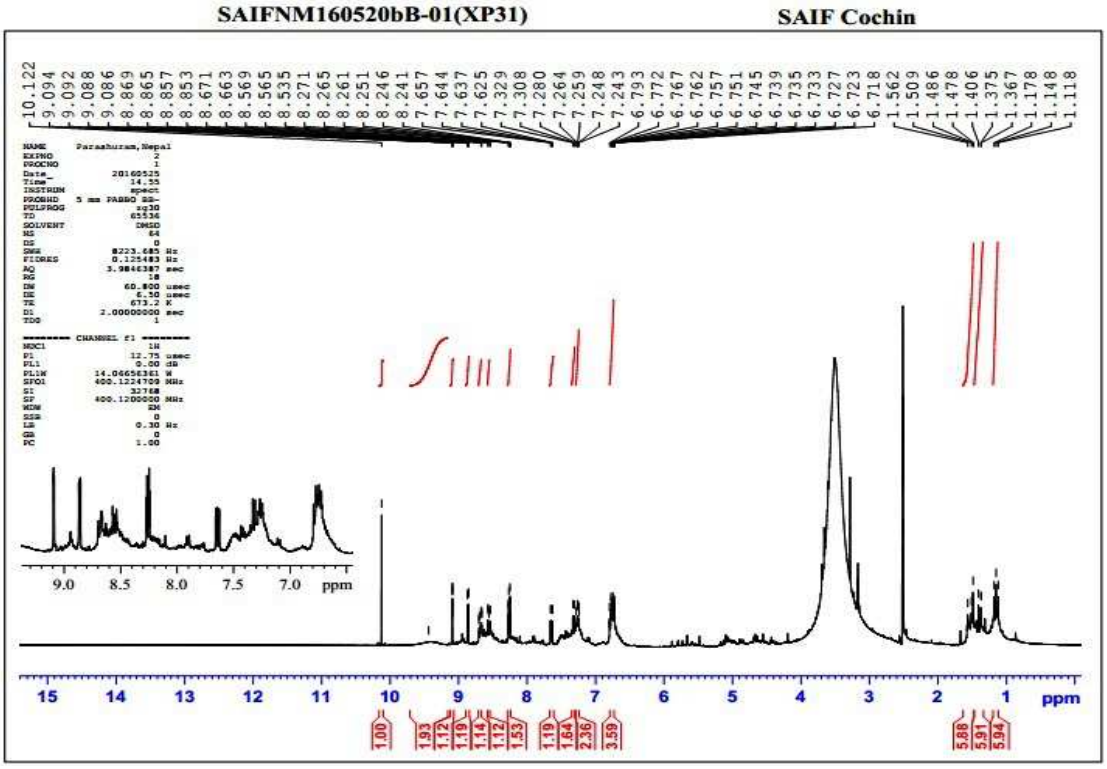

Figure 29: ^{1}H NMR spectrum of AXCPC3 ligand

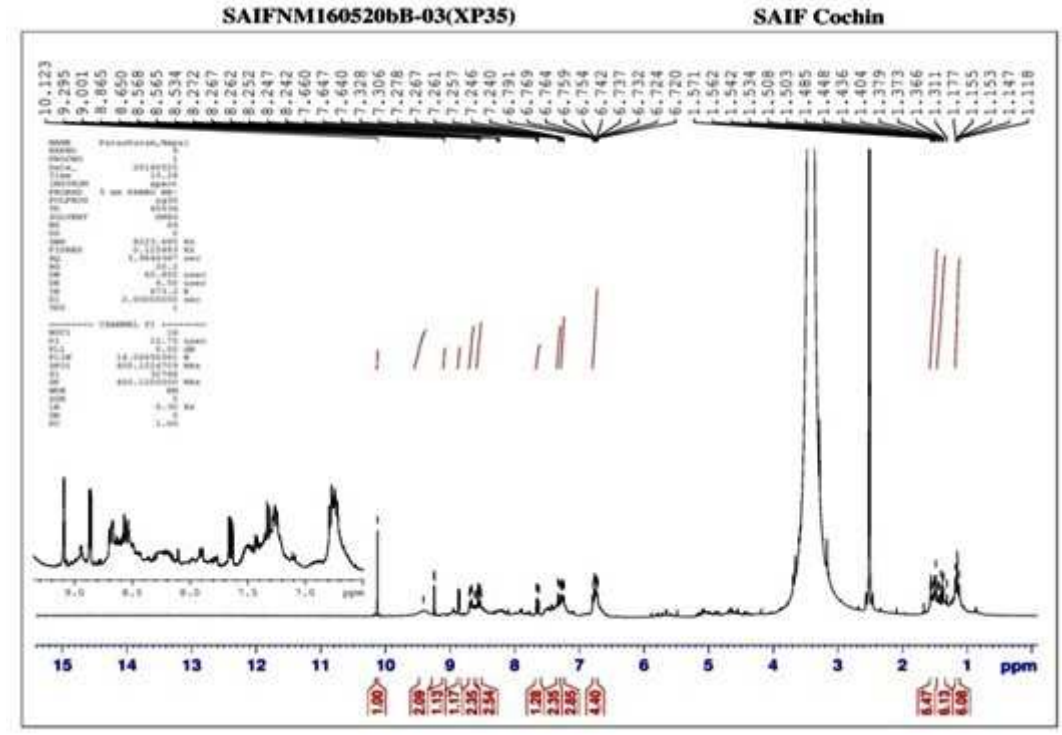

Figure 30: ^{1}H NMR spectrum of Zn-AXCPC3

4.3.2.3 ^{1}H NMR Spectra of AXCPC2 Schiff Base and Zn-AXCPC2 Complex

The ^{1}H NMR spectra of AXCPC2 ligand and diamagnetic Zn-AXCPC2 complex are presented in the Figures 31 & 32 and their chemical shift data are documented in the Table 8. The structure of the ligand and Zn-AXCPC2 complex under this category is almost similar to AXCPC3 and therefore the spectral explanation is similar to the above section.

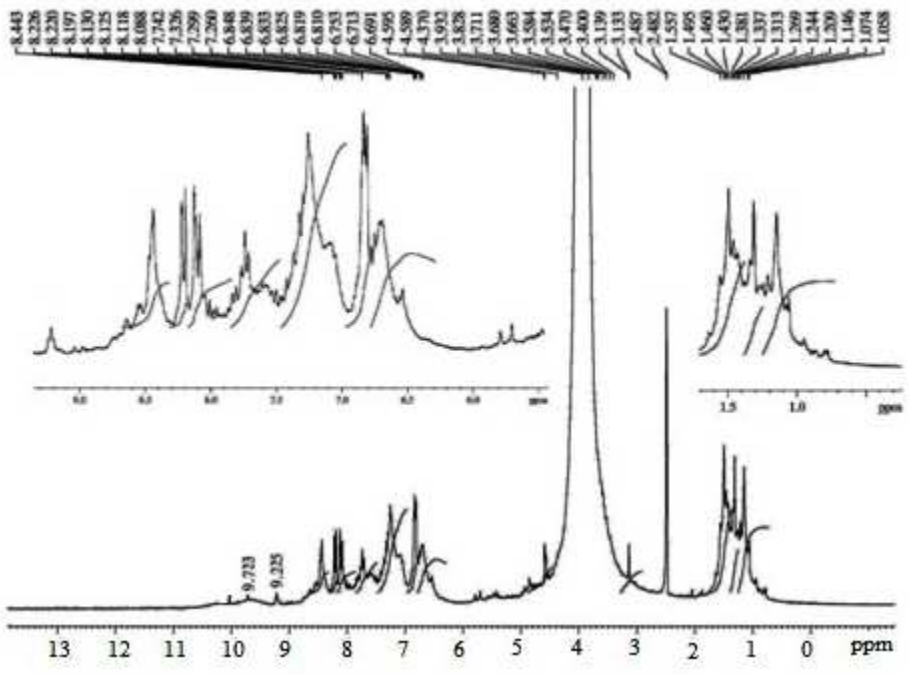

Figure 31: ^{1}H NMR spectrum of AXCPC2 ligand

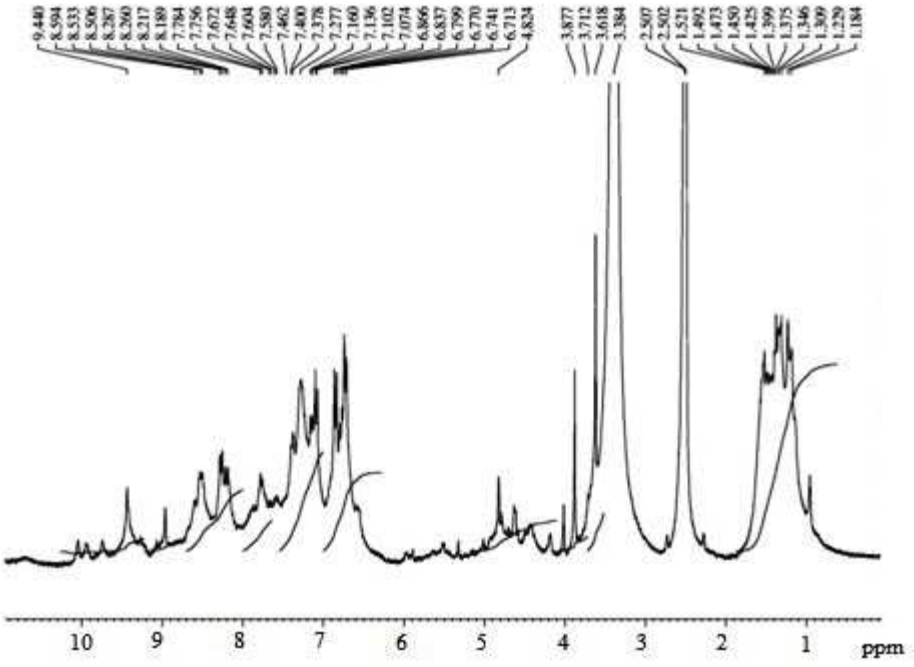

Figure 32: ^{1}H NMR spectrum of Zn-AXCPC2

4.3.2.4 ^{13}C NMR Spectra of AXCPC2 Schiff Base

^{13}C NMR spectral study furnishes idea about the different kinds of carbon atoms and their electronic environment in the molecules. The ^{13}C NMR spectrum of AXCPC2 Schiff base ligand delivers a signal for carboxylic carbon at 174.05 ppm. The signal for azomethine carbon appears at 152.279 ppm. The signal at 171.043 ppm is attributed to lactam carbonyl carbon and the signal for other carbons of lactam and thiazole ring appear in the range of 40.229 to 55.177 ppm. The aromatic ring carbons deliver the signal in the range of 115.622 to 131.259 ppm and the signals in the range of 137.492 to 149.636 are attributed to pyridine ring carbons. The methyl carbons show the signal at 29.450 ppm. The recorded spectrum of AXCPC2 ligand is given in the Figure 33 and the spectral data are reported in the Table 9.

Table 9: ^{13}C NMR spectral data (δ ppm) of AXCPC2 ligand

AXCPC2 Ligand	Assignment	Chemical Shift δ ppm
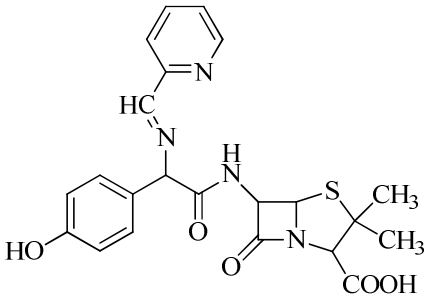	COOH	174.05
	C=O	171.043
	CH=N	152.279
	Pyridine ring carbon	149.636, 149.027, 137.492
	Aromatic ring carbon	131.259, 128.283, 123.083, 122.526, 115.622
	Lactam & thiazole ring carbon	55.177, 40.785, 40.507, 40.229,
	DMSO	39.951, 39.673, 39.396, 39.118
	CH_3	29.450

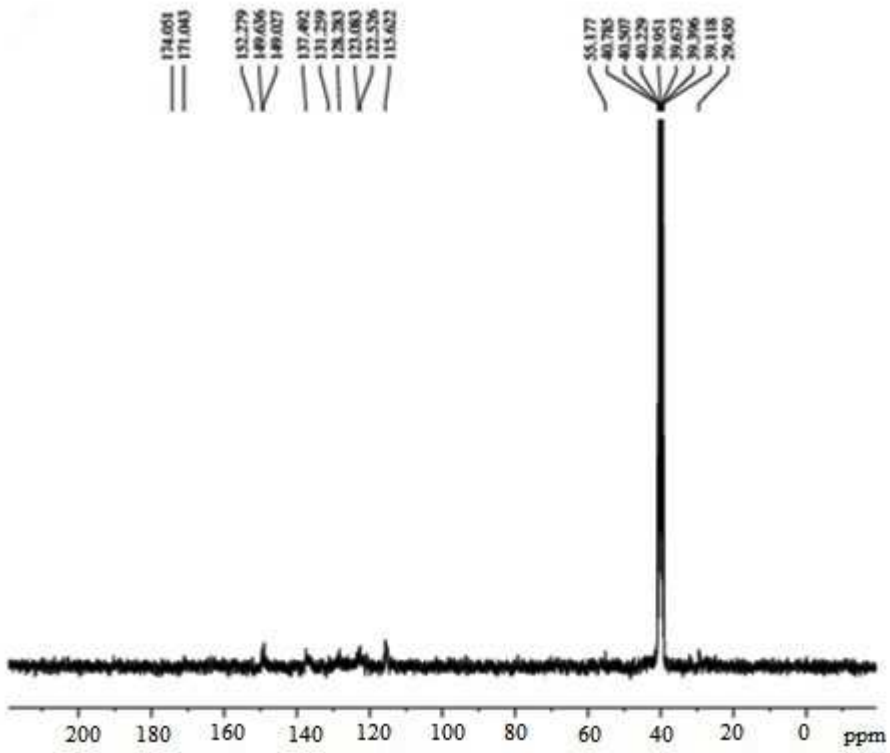

Figure 33: ^{13}C NMR spectrum of AXCPC2 Schiff base ligand

4.3.3 Mass Spectral Study

4.3.3.1 Mass Spectra of KMAXC and Metal Complexes

The mass spectra of KMAXC ligand and its metal complexes were recorded and are used to compare their stoichiometric composition. The mass spectrum of KMAXC ligand shows a molecular ion peak at m/z 845, which corresponds to formula weight of the compound. In addition, other peaks for the ligand are observed at m/z 683, 506, 414, 373, 341 and 266 with significant intensity and they correspond to fragment ion peaks. The molecular ion $(MH)^{\cdot+}$ peaks for metal complexes appear at m/z 921, 925 & 927 for Co-KMAXC, Cu-KMAXC and Zn-KMAXC complexes respectively and confirmed their formula weights. For Co-KMAXC complex, the various peaks at m/z 740, 712, 684, 657, 629, 464, 396, 363 and 342 correlate fragment ion peaks. Likewise for the Cu-KMAXC complex, the fragment ion peaks are observed at m/z 869, 711, 681, 655, 628, 362, and 341. The Zn-KMAXC complex delivers fragment ion peaks at m/z 785, 657, 483, 466, 359 and 305. The mass spectra of ligand and metal complexes are presented in the Figures 34 – 37.

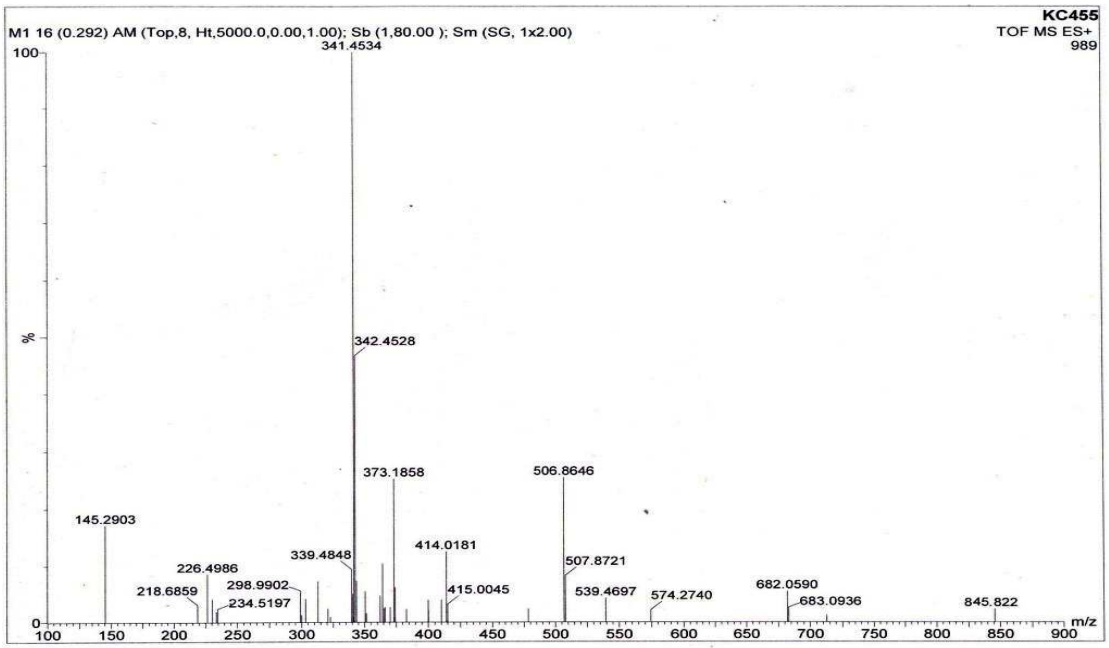

Figure 34: Mass spectrum of KMAXC ligand

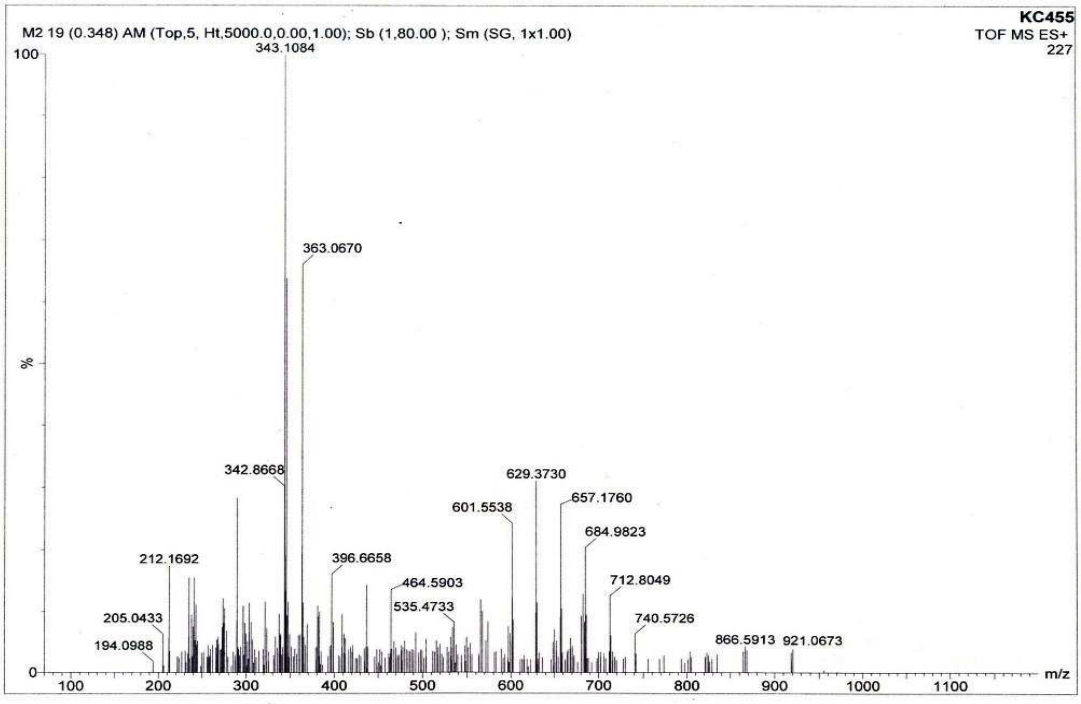

Figure 35: Mass spectrum of Co- KMAXC

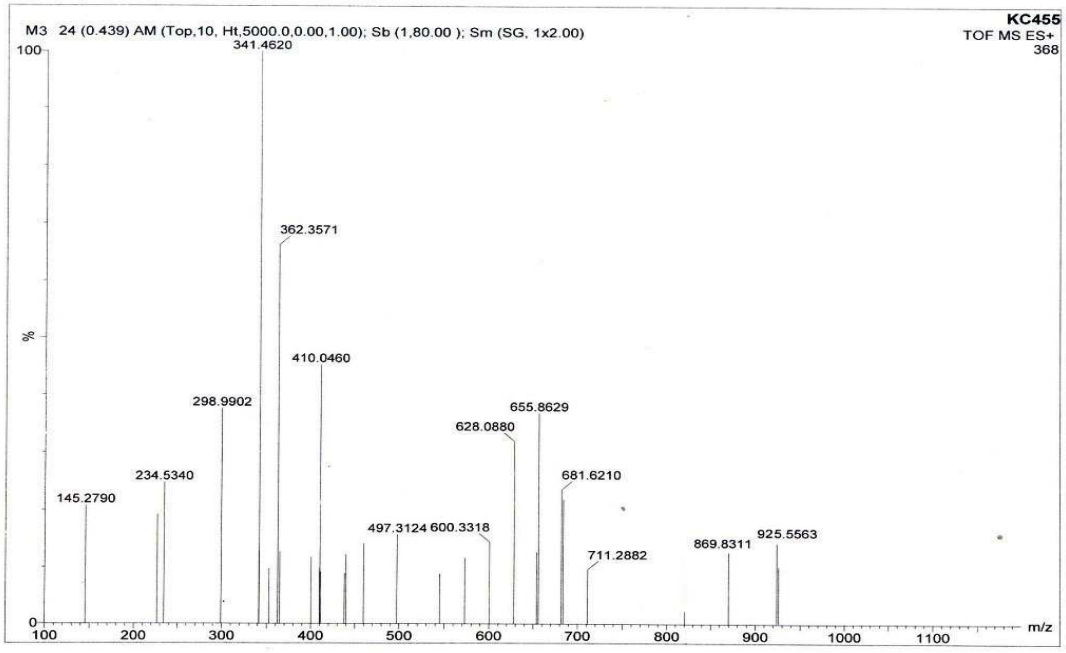

Figure 36: Mass spectrum of Cu- KMAXC

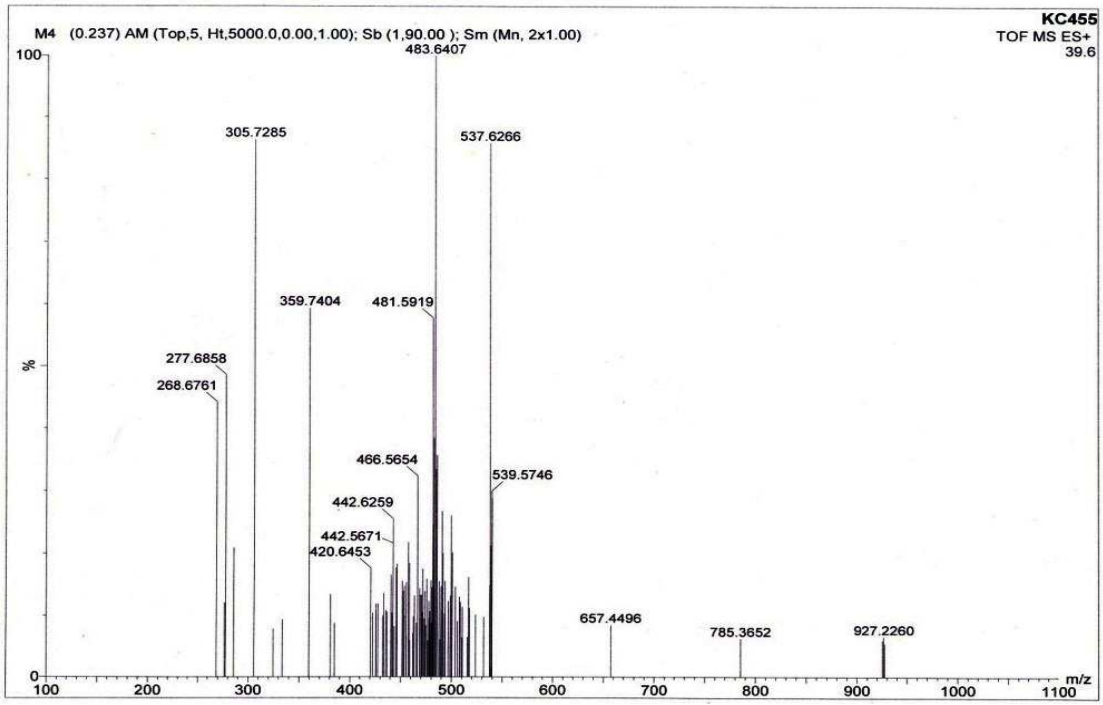

Figure 37: Mass spectrum of Zn- KMAXC

4.3.3.2 Mass Spectra of AXCPC3 and Metal Complexes

The TOF mass spectrum of the synthesized compounds was carried in ES positive mode which revealed molecular ion peak $[M+H]^{\cdot+}$ at m/z 455 for the free ligand AXCPC3 and this corresponds proposed molecular formula weight of the ligand. Besides this, some additional peaks at m/z 414, 382, 352, 250 and 172 are due to the fragment peaks produced by fragmentation of molecular ion. The molecular ion peak for metal complexes such as Co-AXCPC3, Ni-AXCPC3, Cu-AXCPC3, and Zn-AXCPC3 appear at m/z 1001.2, 964, 969 and 970 respectively, which are consistent with their proposed molecular formula (Table 3). The Co-AXCPC3 delivers fragment ion peaks at m/z 734, 553, 531, 473, 431, 385 and 204 with considerable intensity. The fragment ion peaks for Ni-AXCPC3 are observed at m/z 882, 854, 726, 685, 641, 507 and 434. Likewise the Cu-AXCPC3 delivers fragment ion peaks at m/z 813, 682, 668, 628, 419, 369, 327 and 307. The Zn-AXCPC3 delivers this type of peaks at m/z 726, 685, 619, 507, 456, 412 and 384. The mass spectra of AXCPC3 and metal complexes are presented in the Figures 38 - 42.

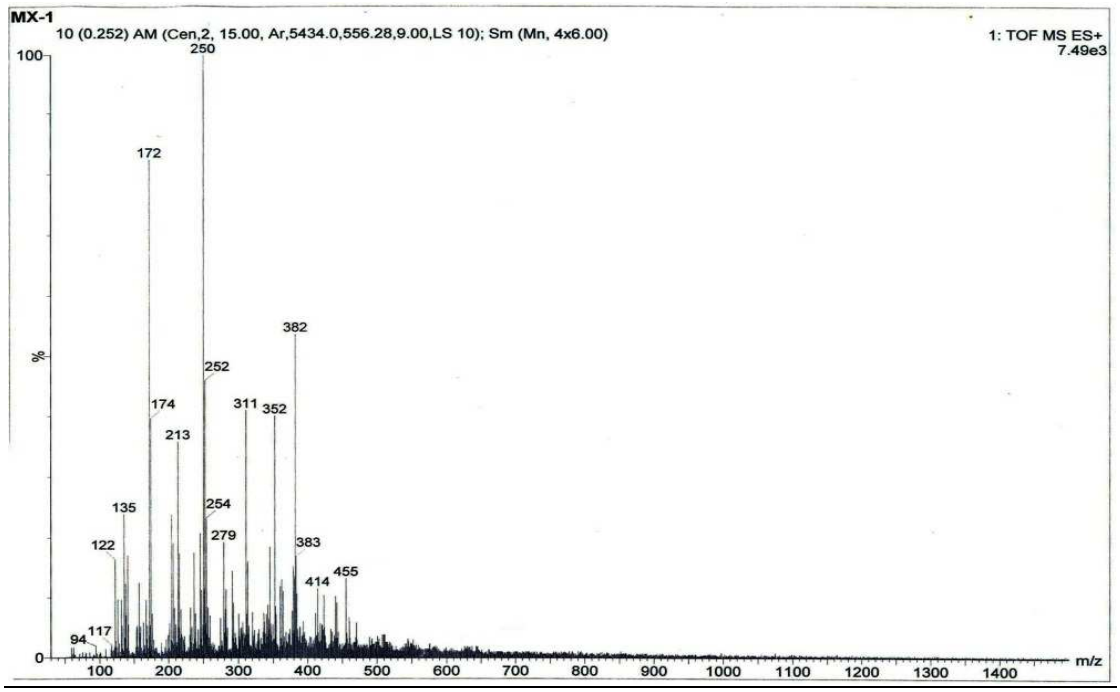

Figure 38: Mass spectrum of AXCPC3 ligand

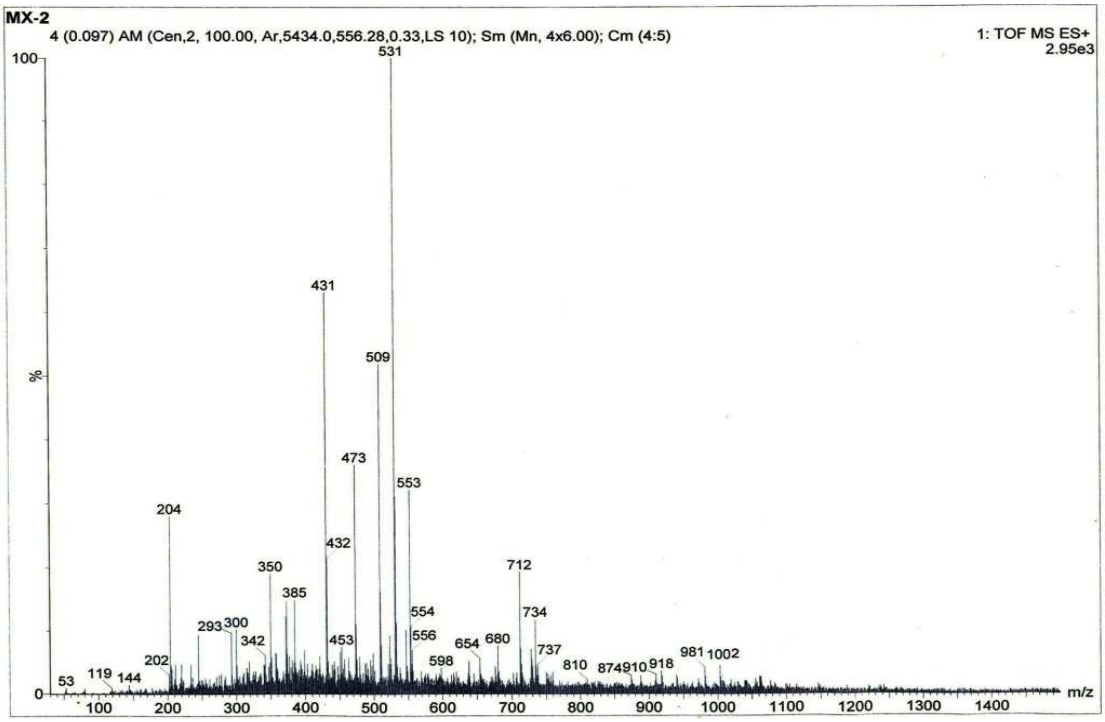

Figure 39: Mass spectrum of Co-AXCPC3

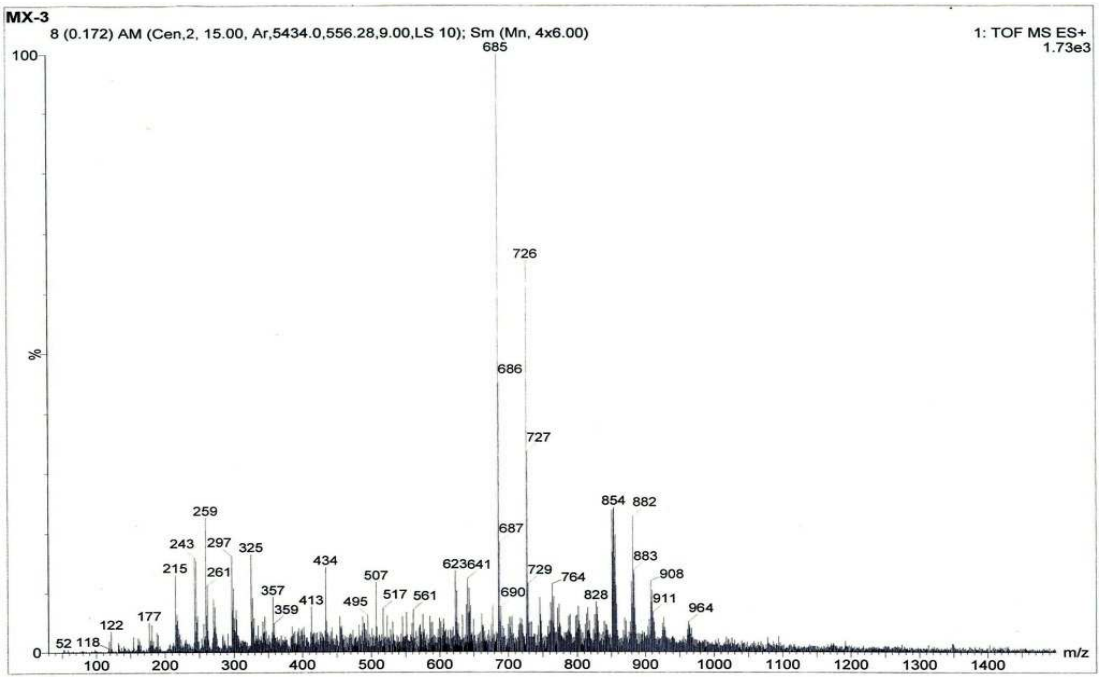

Figure 40: Mass spectrum of Ni- AXCPC3

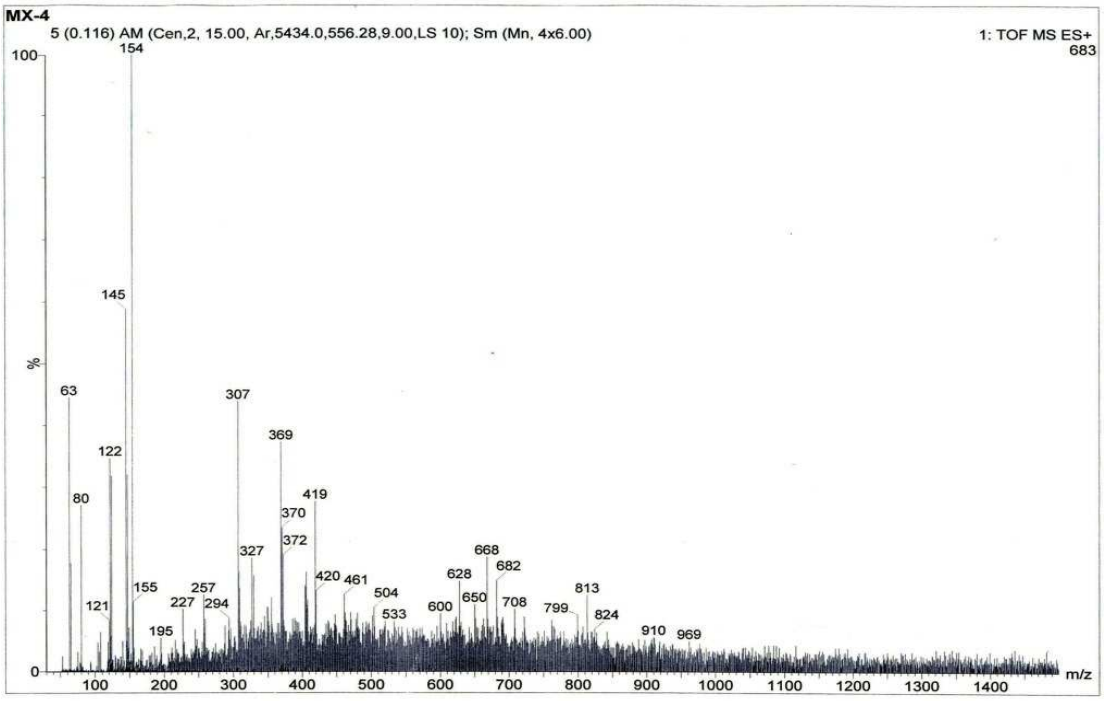

Figure 41: Mass spectrum of Cu- AXCPC3

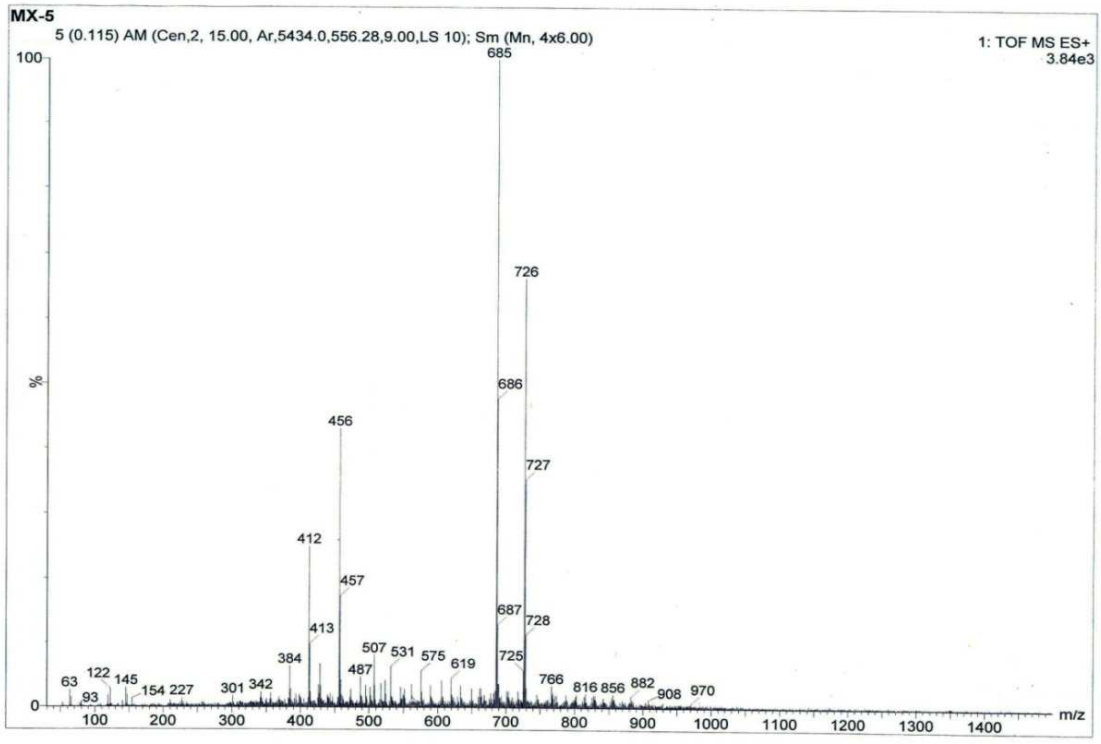

Figure 42: Mass spectrum of Zn- AXCPC3

4.3.3.3 Mass Spectra of AXCPC2 and Metal Complexes

The mass spectra of AXCPC2 ligand and its four metal complexes are presented in the Figures 43 - 47. The peak at m/z 456 in the Figure 43 signifies molecular ion peak $[M+H]^{\cdot+}$ for AXCPC2 ligand. The Figure 43 also delivers medium to high intensity peaks at m/z 413, 390, 316, 284, 210 and 196. These peaks are associated to fragmentation of the molecular ion peak of the ligand. The metal complexes viz. Co-AXCPC2, Ni-AXCPC2, Cu-AXCPC2 and Zn-AXCPC2 deliver respective molecular ion peaks at m/z 966, 965, 970 and 1006.2, which strongly support proposed molecular formula of the complexes. In addition, Co-AXCPC2 complex delivers fragment ion peaks at m/z 643, 574, 499, 396, 364, 349, 241 and 214. Likewise the Ni-AXCPC2 complex delivers similar peaks at m/z 575, 483, 411, 381, 379, 363, 292, 270 and 240 that are due to fragmentation of the molecular ion. The fragment ion peaks for Cu-AXCPC2 complex are observed at m/z 643, 482, 396, 364 and 182. For Zn-AXCPC2 complex, the peaks at m/z 807, 711, 579, 495, 385, 320 and 210 report various fragments of the molecular ion. All these data of the molecular ions and fragment ions nicely correlate the proposed molecular geometry of the compounds.

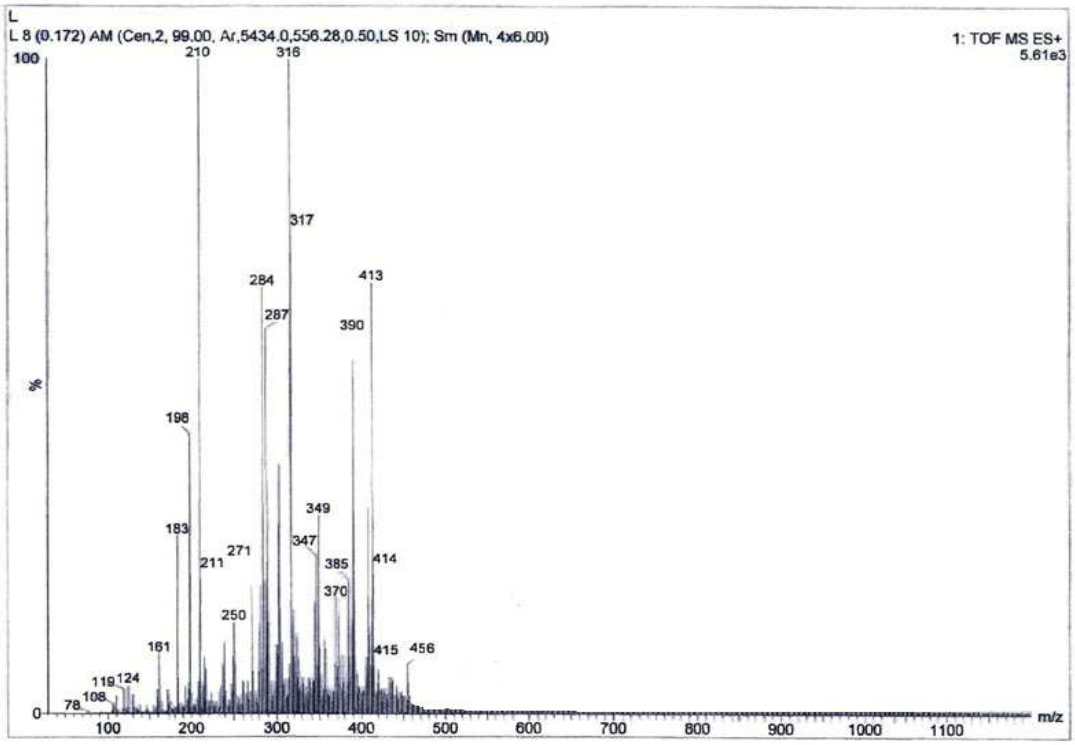

Figure 43: Mass spectrum of AXCPC2 ligand

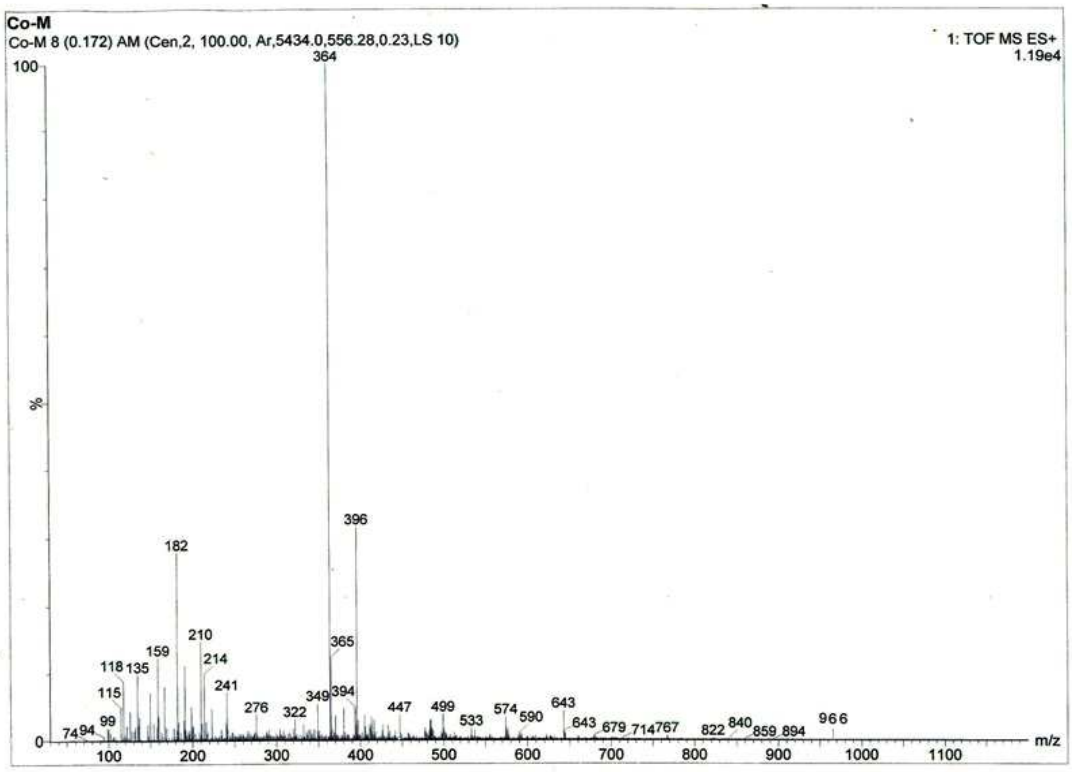

Figure 44: Mass spectrum of Co-AXCPC2

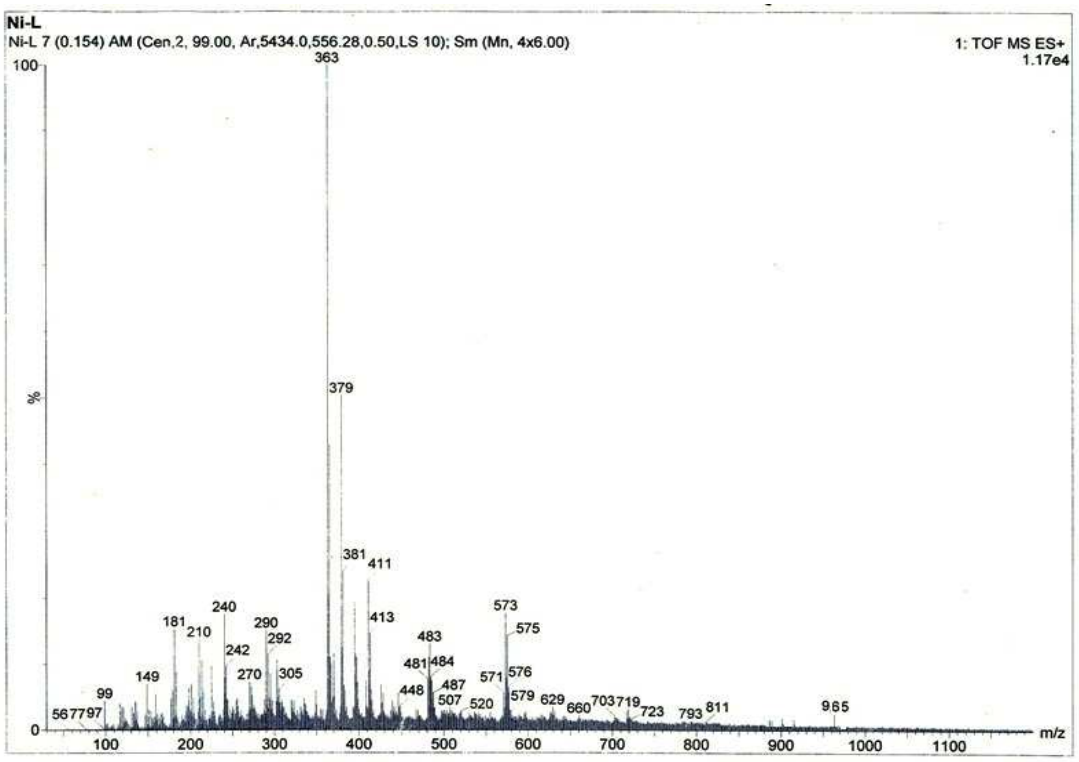

Figure 45: Mass spectrum of Ni-AXCPC2

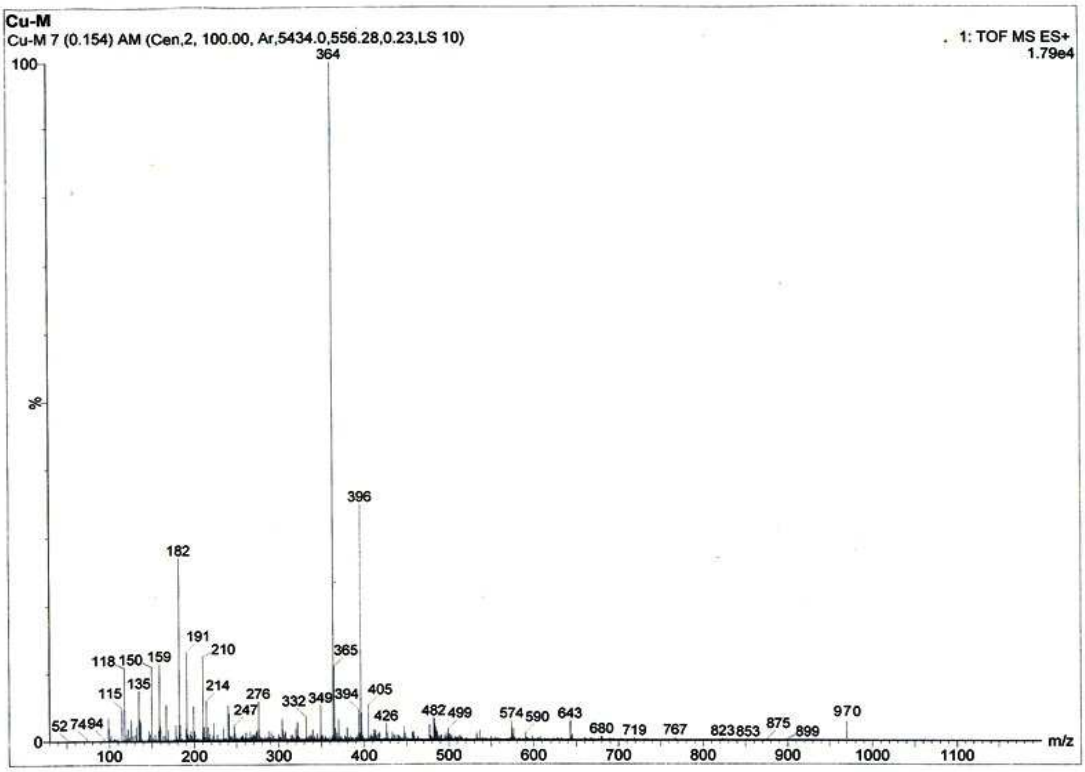

Figure 46: Mass spectrum of Cu-AXCPC2

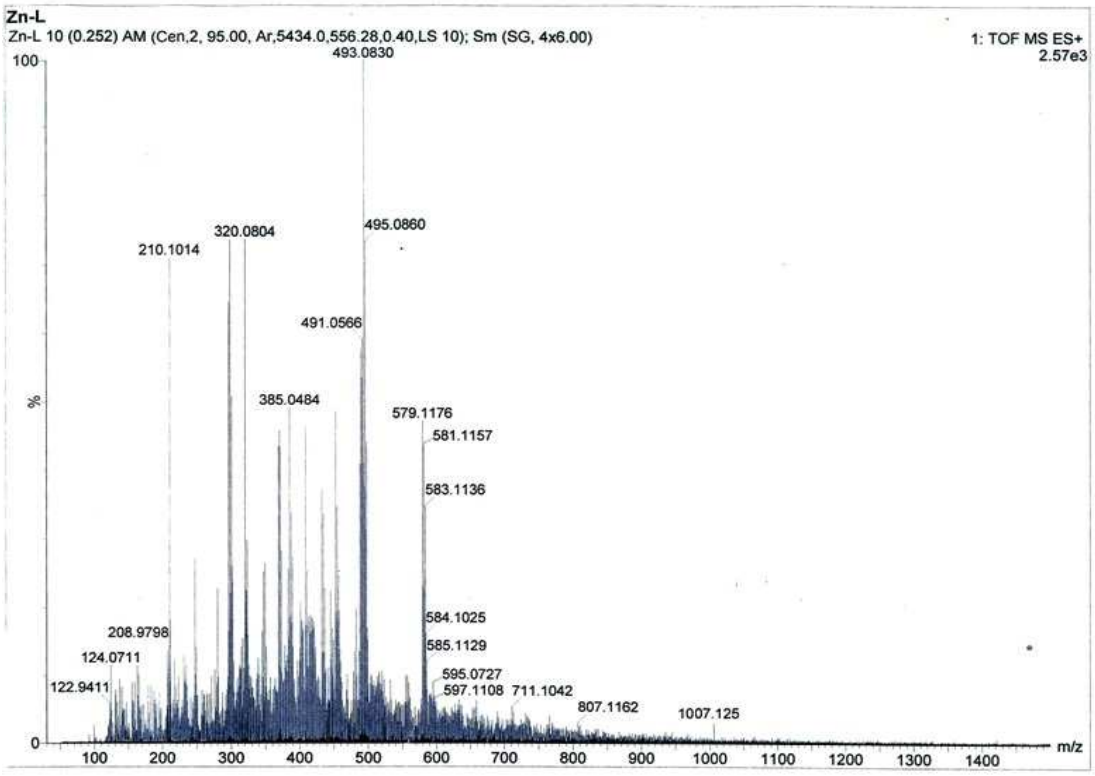

Figure 47: Mass spectrum of Zn-AXCPC2

4.3.4 Electronic Absorption Spectra (EAS) and Magnetic Moments Analysis

4.3.4.1 EAS of KMAXC and Metal Complexes

Besides of the high energy $\pi \rightarrow \pi^*$ transition bands, attributed to aromatic ring of amoxicillin moiety, the appearance of additional absorption band at 356 nm corresponds to $n \rightarrow \pi^*$ intra ligand charge transfer band with the involvement of C=N group of the ligand. The electronic absorption spectrum of Co-KMAXC complex displays $n \rightarrow \pi^*$ transition band at 324 nm. The ligand-metal charge transfer band (LMCT) for this complex is deduced by the absorption band observed at 364 nm. The additional d-d transition band at 615 nm corresponds to $^4T_{1g}(F) \rightarrow {}^4T_{1g}(P)$ transition and represents the octahedral geometry of this complex (El-Sherif *et al.*, 2012). For Cu-KMAXC complex, the appearance of three closely spaced absorption bands at 322, 325 and 350 nm may be due to $n \rightarrow \pi^*$ transition. The electronic absorption band at 660 nm may be assigned to $^2A_{1g}(F) \rightarrow {}^2B_{1g}(P)$ transition and corresponds to the square planar geometry of this complex. This is further supported by d-d transition band displayed at 670 nm. The electronic absorption spectrum of Zn-KMAXC complex

displays a high-intensity absorption band at 365 nm, which has been assigned to ligand-metal charge transfer band and reveals its tetrahedral geometry. The concern geometry of these complexes is also supported by their observed magnetic moment values. The Co-KMAXC and Cu-KMAXC complexes, with observed magnetic moment values 3.12 and 1.81 BM suggest their paramagnetic nature and execute 2 and 1 unpaired electrons respectively. The zinc complex was found diamagnetic. The electronic absorption data for KMAXC ligand and its metal complexes are reported in the Table 10.

Table 10: Electronic absorption spectral data of KMAXC and its metal complexes

No.	Compound	Peak positions (nm)	Assignment
1	KMAXC	356, 430	$n\rightarrow\pi^*$ Intra ligand CT band
2	Co-KMAXC	324, 364	$n\rightarrow\pi^*$ LMCT band
		615	$^4T_{1g}(F)\rightarrow{}^4T_{1g}(P)$
3	Cu-KMAXC	322, 350	$n\rightarrow\pi^*$ LMCT band
		660, 670	$^2A_{1g}(F)\rightarrow{}^2B_{1g}(P)$, d-d transition
4	Zn-KMAXC	365	$n\rightarrow\pi^*$ LMCT band

4.3.4.2 EAS of AXCPC3 and Metal Complexes

The electronic absorption spectrum of AXCPC3 ligand displays $n\rightarrow\pi^*$ intra ligand charge transfer band at 356 nm which may be due to the involvement of C=N group of the ligand moiety (Dey *et al.*, 2014). Moreover, the additional bands in the higher wavelength region are observed in the complexes that signify metal-ligand coordination. The Co-AXCPC3 complex exhibits two distinct bands in the high wavelength region of the spectrum at 457-488 nm and 549 nm. The former band is assignable to $^4T_{1g(F)}\rightarrow{}^4T_{1g}(P)$ and latter band indicates $^4T_{1g(F)}\rightarrow{}^4T_{2g}(F)$ transition, confirming its octahedral geometry (Sherif & Abdel-Kader, 2015). The magnetic moment value (4.75 BM) executes high spin state of cobalt with 3 unpaired electrons and this further supports this geometry. The high energy bands for this complex are observed at the range of 346-371 nm, assignable to $n\rightarrow\pi^*$ ligand metal charge transfer (LMCT) transition. The electronic absorption spectrum of Ni-AXCPC3 complex displays d-d transition band at 460 nm assignable to $^1A_{1g}\rightarrow{}^1B_{1g}$ transition along with

the bands in the low wavelength region at 346 nm (Rudbari *et al.*, 2016; Kundu *et al.*, 2016). Diamagnetic nature of this complex is suggestive of complete distortion of octahedral geometry and confirms its square planar geometry. The magnetic moment value (1.82 BM) for Cu-AXCPC3 executes 1 unpaired electron and the electronic absorption spectrum of paramagnetic Cu-AXCPC3 complex exhibit absorption band in the high wavelength region at 485 nm, attributed to $^2T_2 \rightarrow {}^2E$ transition which is suggestive of tetrahedral geometry (Jana *et al.*, 2012). Other high energy bands for this complex are observed at 337 and 344 nm which corresponds to $n \rightarrow \pi^*$ ligand metal charge transfer (LMCT) transition. The Zn-AXCPC3 complex displays an absorption band at 346 nm assignable to the LMCT transition, compatible with tetrahedral geometry and this is further supported by its diamagnetic nature and absence of a d-d band, due to its complete d^{10} electronic configuration. The data are summarized in the Table 11.

Table 11: Electronic absorption spectral data of AXCPC3 and its metal complexes

No.	Comp.	Peak positions (nm)	Assignment
1	AXCPC3	356	$n \rightarrow \pi^*$ intra ligand CT band
2	Co-AXCPC3	346-371	$n \rightarrow \pi^*$ LMCT band
		457-488	$^4T_{1g}(F) \rightarrow {}^4T_{1g}(P)$
		549	$^4T_{1g}(F) \rightarrow {}^4T_{2g}(F)$
3	Ni-AXCPC3	346	$n \rightarrow \pi^*$ LMCT band
		460	$^1A_{1g} \rightarrow {}^1B_{1g}$
4	Cu-AXCPC3	337, 344	$n \rightarrow \pi^*$ LMCT band
		485	$^2T_2 \rightarrow {}^2E$
5	Zn-AXCPC3	346	$n \rightarrow \pi^*$ LMCT band

4.3.4.3 EAS of AXCPC2 and Metal Complexes

The electronic absorption spectral data for AXCPC2 ligand and its corresponding metal(II) complexes are presented in the Table 12. The electronic absorption spectrum of AXCPC2 ligand shows a peak at 301 nm, which is assignable to $n \rightarrow \pi^*$ transition. The intra ligand charge transfer band for the ligand appears at 361 nm. The $n \rightarrow \pi^*$ transitions in metal complexes appear at the similar wavelength regions with minor variations in the data and this may be due to the change in electron density around the

target group. Besides these absorption peaks, metal complexes deliver peaks in the high wavelength regions and this probably describes the geometry around metal ions. The octahedral Co-AXCPC2 complex displays three absorption peaks at 465, 590 and 853 nm, assignable to $^4T_{1g(F)} \rightarrow {}^4T_{1g}(P)$, $^4T_{1g}(F) \rightarrow {}^4A_{2g(F)}$, and $^4T_{1g(F)} \rightarrow {}^4T_{2g(F)}$ transitions respectively. The ligand metal charge transfer band (LMCT) is attributed by the absorption peak at 409 nm. The observed magnetic moment value (5.32 BM) executes high spin state of cobalt with 3 unpaired electrons and further confirms octahedral geometry of this complex (El-Sherif *et al.*, 2012; Singh *et al.*, 2013; Zhang *et al.*, 2012). The Ni-AXCPC2 complex exhibits two absorption bands at high wavelength region at 516 and 690 nm, which may be due to $^1A_{1g} \rightarrow {}^1B_{1g}$ and $^1A_{1g} \rightarrow {}^1B_{2g}$ transitions respectively and these assign square planar geometry of the complex. The tetrahedral geometry for the Cu-AXCPC2 complex has been proved by $^2T_2 \rightarrow {}^2E$ transition with corresponding absorption band appeared at 508 and 625 nm. This is further supported by observed magnetic moment value (1.75 BM), with one unpaired electron. The diamagnetic Zn-AXCPC2 complex delivers high energy bands at 308 and 402 nm, which correspond to $n \rightarrow \pi^*$ and ligand metal charge transfer band. Due to the complete d^{10} electronic configuration, d-d transition band was not observed. Association of two H_2O molecules in the zinc complex has been suggested by thermal analysis study and coordination number six has favored around Zn^{+2} ion in the complex. Based on the experimental evidence, microanalytical, spectral and thermal studies, an outer orbital octahedral geometry has assigned for zinc complex (Iqbal *et al.*, 2005).

Table 12: Electronic absorption spectral data of AXCPC2 and its metal complexes

No.	Comp.	Peak positions (nm)	Assignment
1	AXCPC2	304, 361	$n \rightarrow \pi^*$, intra ligand CT band
2	Co-AXCPC2	309, 410,	$n \rightarrow \pi^*$, LMCT band
		465,	$^4T_{1g}(F) \rightarrow {}^4T_{1g}(P)$
		590,	$^4T_{1g}(F) \rightarrow {}^4A_{2g}(F)$
		853	$^4T_{1g}(F) \rightarrow {}^4T_{2g}(F)$
3	Ni-AXCPC2	307, 420,	$n \rightarrow \pi^*$, LMCT band
		516,	$^1A_{1g} \rightarrow {}^1B_{1g}$
		690	$^1A_{1g} \rightarrow {}^1B_{2g}$
4	Cu-AXCPC2	310, 396,	$n \rightarrow \pi^*$, LMCT band
		508, 625	$^2T_2 \rightarrow {}^2E$
5	Zn-AXCPC2	308, 402	$n \rightarrow \pi^*$, LMCT band

4.3.5 EPR Spectral Analysis

Electron paramagnetic resonance (EPR) spectroscopy is a very powerful tool that can provide valuable structural and dynamic information of the molecules. It requires the presence of an unpaired electron spin in the molecules. The unpaired electrons have a small magnetic field, which in the presence of spectrometer's magnet, either will align (m_s = -1/2) or oppose (m_s = +1/2) the direction of the magnetic field. The separation of energy states depicts the mathematical relationship, $\Delta E = h\nu = g\beta H$, where g is Lande's splitting factor and β is conversion constant called Bohr magneton (Murphy, 2009).

In EPR spectroscopy, the transition of electron states between the Zeeman levels occurs upon the absorption of a quantum of radiation in the microwave region. For a free electron, the value of g is 2.0023192778 and any deviation from this value is due to orbital contribution to the magnetism in the complexes. The EPR spectrum provides valuable information regarding the g tensor values ($g_\parallel$, $g_\perp$, and g_{av}) and exchange coupling interaction parameter (G). The value of G is calculated by Hathaway expression;

$$G = \frac{g_\parallel - 2}{g_\perp - 2}$$

The g_{av} value averaged over all directions is calculated by the expression;

$$g_{av} = \frac{1}{3}\ [g_{\parallel} + 2g_{\perp}]$$

Here $g_{\parallel}$ denotes g tensor in the z-axis (g_z) and $g_{\perp}$ denotes g tensor in x and y-axis (g_x and g_y). The data of g tensor and G values are used to know the electronic environment and the possible geometry of the complexes. According to Hathaway, if the value of G is greater than 4.0, the exchange coupling interaction is negligible and if G is lesser than 4.0, a considerable exchange coupling is present in the complex (Bharti *et al.*, 2010; Mahmoud *et al.*, 2016; Mishra *et al.*, 2013; Rajasekar *et al.*, 2010). Kivelson and Nieman have reported that for an ionic environment $g_{\parallel}$ is 2.3 or larger, but for a covalent environment, $g_{\parallel}$ is less than 2.3 (Abdel Aziz *et al.*, 2012; Ahmed & Khaled, 2015; Aziz *et al.*, 2012).

4.3.5.1 EPR of Cu- AXCPC3

The solid state X-band EPR spectrum of the Cu- AXCPC3 complex (Figure 48) was recorded at room temperature under the frequency 9447.606 MHz with no marker lines used and the center line at 316.213 mT, as seen in the graph. The standard lines that are used in EPR model are of Mn which has been omitted in the graph. The EPR spectrum of the metal complex provides useful information about the metal ion environment within the complex. The highly symmetrical EPR spectrum of the Cu-AXCPC3 complex (Figure 47) exhibits a single isotropic signal with $g_{\parallel}$ value 2.18 and $g_{\perp}$ value 2.08 (El-Gammal *et al.*, 2015). The absence of the poorly resolved hyperfine signal may be attributed to the considerable exchange coupling interaction between Cu(II) ions in the complex. The order of splitting factors $g_{\parallel} > g_{\perp} > 2.0023$ clearly indicates that the unpaired electron is localized in the d orbital of Cu(II) ion and is characteristic of axial symmetry (Bagihalli *et al.*, 2008; Patil *et al.*, 2011). The calculated g_{av} value is 2.11 whose deviation from the free electron (2.003) is due to the covalent character of the metal-ligand bond. This fact is further supported by $g_{\parallel}$ value less than 2.3. The value of exchange coupling interaction parameter 'G' is 2.25 which indicates considerable exchange interaction in the complex (Abdel Aziz *et al.*,

2012). All these parameters are inconsistent with the tetrahedral geometry of Cu-AXCPC3 complex.

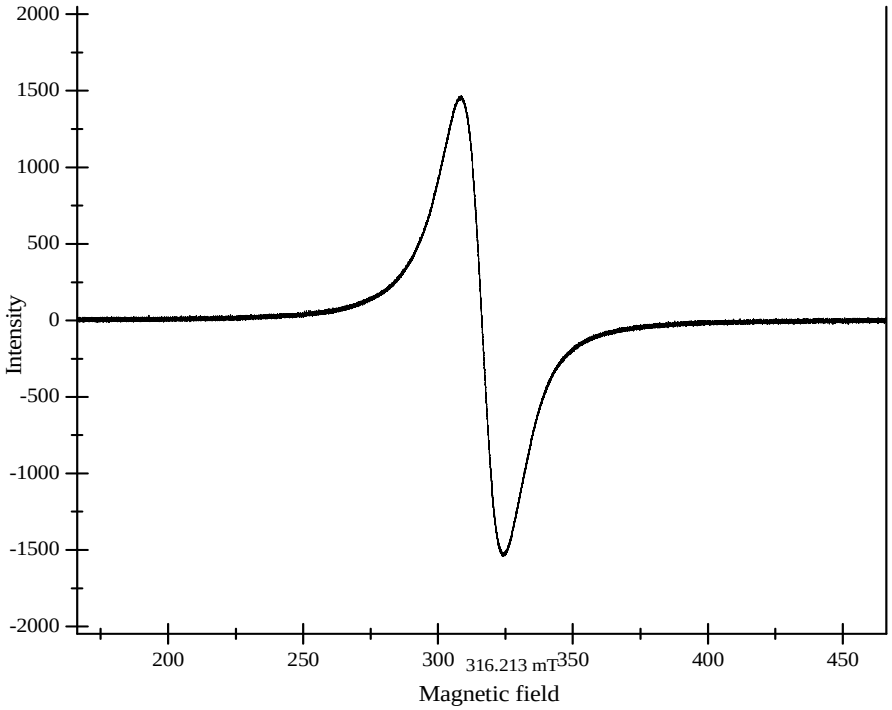

Figure 48: EPR spectrum of Cu- AXCPC3 Schiff base ligand

Table 13: g tensor data of Copper Complexes

Compound	g tensor values			
	$g_{\parallel}$	$g_{\perp}$	g_{av}	G
Cu-AXCPC3	2.18	2.08	2.11	2.25
Cu-AXCPC2	2.149	2.04	2.076	3.72

4.3.5.2 EPR of Cu- AXCPC2

The solid state X-band EPR spectrum of the Cu-AXCPC2 complex is presented in the Figure 49. The EPR spectrum was recorded at room temperature under the frequency of 9445.144 MHz with center line at 314.187 mT. The g tensor data for this complex, reported in the Table 13 shows $g_{\parallel}$ value 2.149 and $g_{\perp}$ value 2.04. The order of splitting factor $g_{\parallel} > g_{\perp} > g_e$ (2.0023) is complementary to EPR spectrum of Cu-AXCPC3 complex and is characteristic of axial symmetry. The calculated g_{av} value is 2.076 and exchange coupling interaction parameter value (G) is 3.72. The $G < 4$ indicates considerable exchange interaction in the complex.

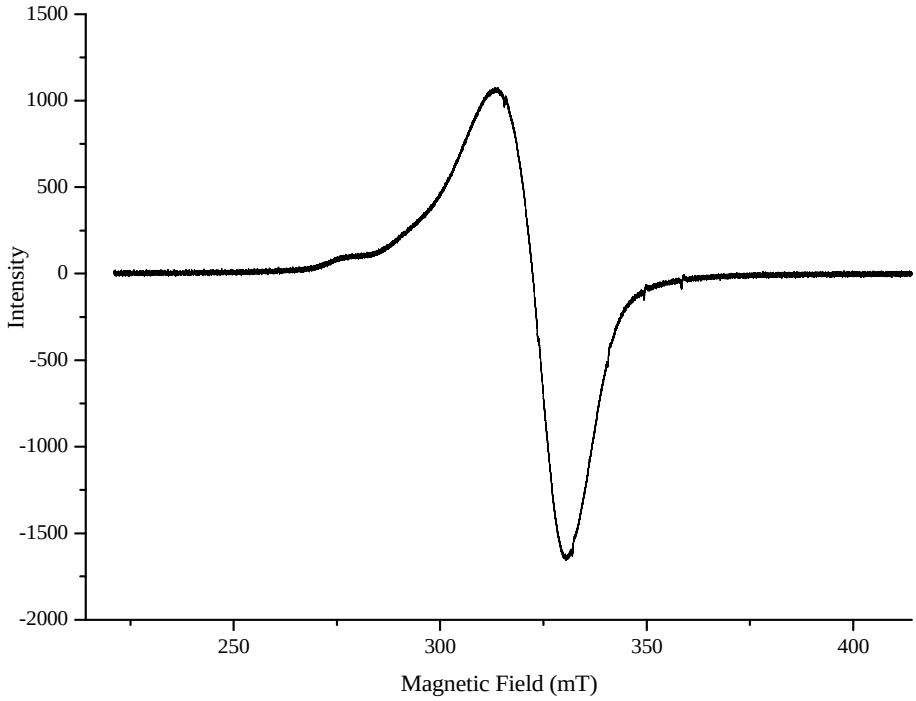

Figure 49: EPR spectrum of Cu- AXCPC2 Schiff base ligand

4.4 Thermal Analysis

Heat sensitive physical and chemical properties of the complexes are well studied by thermal analysis techniques and have found wide applications in the recent years in characterizing the chemicals by measuring changes of properties at elevated temperatures as a function of increasing temperature. Measurements are used primarily to determine the composition of substances and also to predict their thermal stability. The thermogravimetric analysis (TGA) measures the changes in weight of substance as a function of temperature (Al-Resayes, 2010; Ebrahimi-Kahrizsangi & Abbasi, 2008; Sharaby, 2007). The instrument used to measure thermal events of the chemicals is called thermal analyzer. The sample under investigation is heated at a controlled rate in an atmosphere of nitrogen and the mass loss of the substances is recorded as a function of temperature. The results from thermogravimetric run may be presented by (i) weight versus temperature curve, referred to as thermogravimetric (TG) curve, or (ii) rate of the weight loss versus temperature curve, referred to as the differential thermogravimetric (DTG) curve. The weight of the substances in the thermogram may be scaled as true weight scale or as a percentage of total weight. The

differential thermogravimetric (DTG) curve measures the rate of weight loss and its correlation with TG curve affords the way of analyzing physico-chemical properties of the substances. The peak of DTG curve corresponds to the curved portion of TG curve, whereas the peak maximum in DTG curve is identical with the point of maximum slope of TG curve. The height of curve above the line of (dw/dt = 0) affords a measure of the stability of the intermediates. Any change in the rate of weight loss can be seen as a trough in the DTG curve, indicating two consecutive thermal reactions, or as a shoulder to a peak, indicating two overlapping reactions. The thermal events in TG curve are sometimes not clearly resolved, but in DTG curve, these are more clearly seen.

Thermogravimetric data can be used to evaluate kinetic parameters of thermal reactions involving weight loss or gain. It is convenient and advantageous over conventional isothermal studies in determining kinetic parameters. Using a single sample and with considerably less thermal data, almost all the kinetic parameters can be evaluated.

Coats & Redfern (1963) used different integrating approximation and developed a popular equation to solve the kinetic parameters from thermal data. The Coats-Redfern equation is as follows:

$$ln\left[-\frac{ln(1-\alpha)}{T^2}\right] = ln\left[\frac{AR}{\beta E^*}\right] - \frac{E^*}{RT}$$

Where, α represents fraction decomposed ($\alpha = \frac{W_i - W_t}{W_i - W_f}$, where W_i = initial weight of sample, W_t = weight of the sample at T K, W_f = final weight of the sample) at temperature T K, β denotes linear heating rate, (dT/dt). E^* and A are the activation energy and Arrhenius pre-exponential factor respectively. R represents a general gas constant. Molding the equation for straight line (y = mx + c), a linear plot of left side $ln\left[-\frac{ln(1-\alpha)}{T^2}\right]$ versus $1000/T$ of Coats-Redfern equation gives a straight line, whose slope (E^*/R) furnishes activation energy parameter and the pre-exponential factor (A) can be determined from the intercept (Abdel-Rahman *et al.*, 2016; Abdel Aziz *et al.*, 2012; Doğan *et al.*, 2009; Singh & Singh, 2012). In the present work, several kinetic

parameters were calculated by using Coats-Redfern equation. The other thermodynamic parameters such as entropy of activation (*ΔS**), enthalpy of activation (*ΔH**) and free energy of activation (*ΔG**) have been calculated by using the following formula:

$$\Delta S^* = Rln\left[\frac{Ah}{k_B T}\right]$$

$$\Delta H^* = E^* - RT$$

$$\Delta G^* = \Delta H^* - T\Delta S^*$$

In the equation, k_B represents Boltzmann constant and *h* represents Plank's constant.

4.4.1 TGA/DTA Study of Metal Complexes of AXCPC3

The TGA/DTA studies of the metal complexes of AXCPC3 were carried out within the temperature range from room temperature to 750 °C with the linear heating rate of 20 °C/ minute in the nitrogen atmosphere. The computed thermal decomposition data in the Table 14 are in good agreement with the suggested microanalytical data in Table 3. The following findings have been achieved in our research analysis.

The thermogram of the Co-AXCPC3 complex (Figure 50) showed four decomposition steps in the temperature range of 50 to 380 °C. The first decomposition step in the range of 50 to 110 °C with % mass loss of 4.826% (0.226 g) is assignable to loss of two lattice water molecules in the outer sphere region. The DTG temperature for this step is 80.85 °C and corresponding DTA temperature is 103.68 °C and reveals endothermal effect. The second and third decomposition steps with % mass loss of 25.923% and 33.837% in the temperature range of 241 - 273 °C and 279-300 °C respectively are considered to be due to loss of organic ligand moiety. The last decomposition step represents complete loss of ligand from the complex in the temperature range of 338 - 380 °C, leaving nearly 7.49% cobalt oxides as end residue. The corresponding DTG temperatures for the consecutive second, third and fourth steps are 268.38 °C, 284.05 °C, and 357.21 °C respectively. The Ni-AXCPC3 complex exhibited the decomposition in two steps (Figure 51). The first

decomposition step in the temperature range of 44 to 113 °C with % mass loss of 5.6% (0.153 g) is assignable to loss of lattice water molecules in the outer sphere region, with DTG temperature 85.91 °C. The DTA temperature (105.33 °C) of this step reveals endothermal effect. The second step involves % mass loss of 30.861 % (0.484 g) in the temperature range of 232 to 403 °C with corresponding DTG and DTA temperature 278.16 °C and 382.91 °C respectively. This step attributes the loss of ligand moiety. The DTA data suggests exothermal effect of this step. The Cu-AXCPC3 complex decomposed in four steps (Figure 52) and the results are complementary to Co-AXCPC3 complex. For this complex, the first decomposition occurred in the temperature range of 49 to 105 °C with % mass loss of 2.699% (0.1 g) and DTG temperature 76.79 °C. The second decomposition step corresponds to % mass loss of 8.814 % in the temperature range of 148 to 163 °C with DTG temperature 159.86 °C. The third and fourth decomposition steps correspond to % mass loss of 21.635% and 42.395% respectively. They decomposed in the temperature range of 187 to 246 °C and 293 to 390 °C respectively. The DTG temperatures for third and fourth steps are 237.13 °C and 326.01 °C respectively. The DTA peak at 385.92 °C for the fourth step infers exothermal effect. The Zn-AXCPC3 complex exhibited decomposition in three steps (Figure 53) and are also complementary with the Co-AXCPC3 complex. The first step involves % mass loss of 3.047% in the temperature range of 46 to 107 °C with DTG temperature 75.46 °C and DTA peak temperature at 115.75 °C, which correspond endothermal effect. The next step involves 18.233 % mass loss in the temperature range of 230 to 287 °C with DTG temperature 260.99 °C. The third step involves % mass loss of 36.441% in the temperature range 310 to 410 °C, with corresponding DTG temperature 330.41 °C. Nearly 8.5% mass remains as stable end residue of zinc oxide. For this step, the DTA peak temperature is 365.88 °C and this executes exothermal effect. The calculated thermal data of all the metal complexes nicely describe and support their composition and geometry.

Kinetic Parameter

The calculated data of thermodynamic parameters for the various decomposition steps of the metal complexes are listed in Table 15. The high and increasing values of activation energy in the subsequent steps for the metal complexes reveal high thermal

stability which may be due to the covalent bond character. The positive *ΔG** values justify the non-spontaneous nature of the decomposition steps. The variation in *ΔS** values for the complexes (both negative and positive) are attributed to more ordered activated state than the reactants in some steps. The positive *ΔH** values reveal the endothermic nature of the various decomposition steps (Kianfar *et al.*, 2015; Mahmoud *et al.*, 2014).

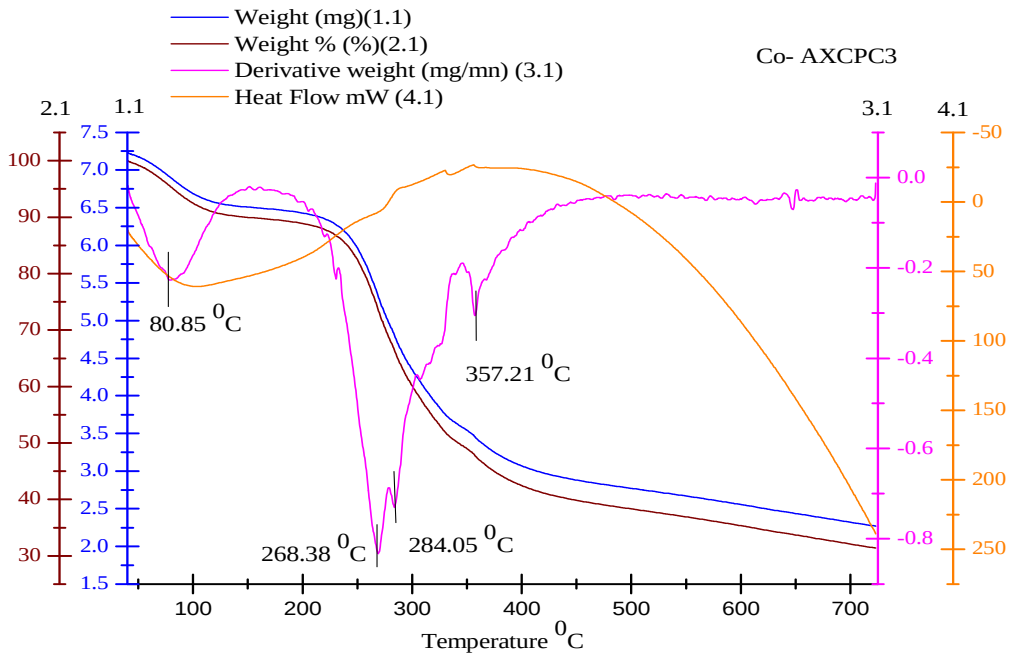

Figure 50: Thermogram of Co-AXCPC3

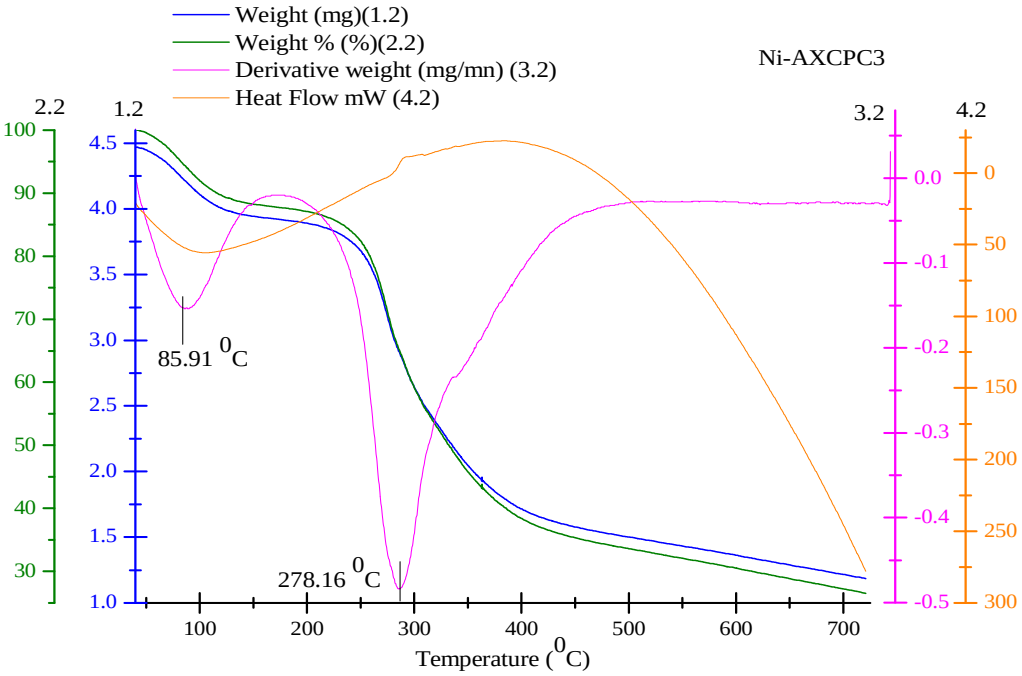

Figure 51: Thermogram of Ni-AXCPC3

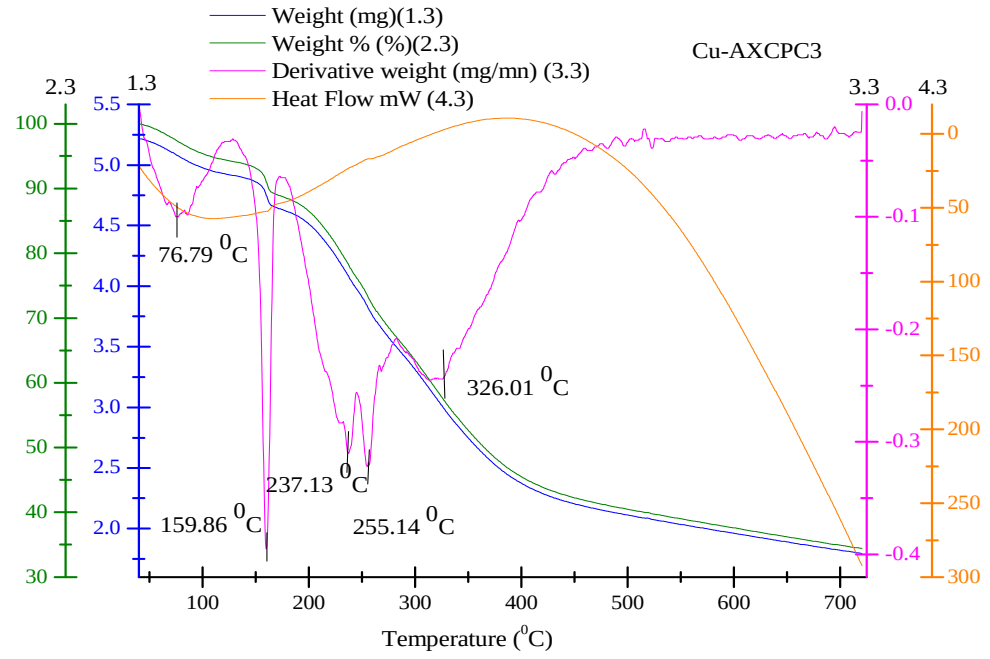

Figure 52: Thermogram of Cu-AXCPC3

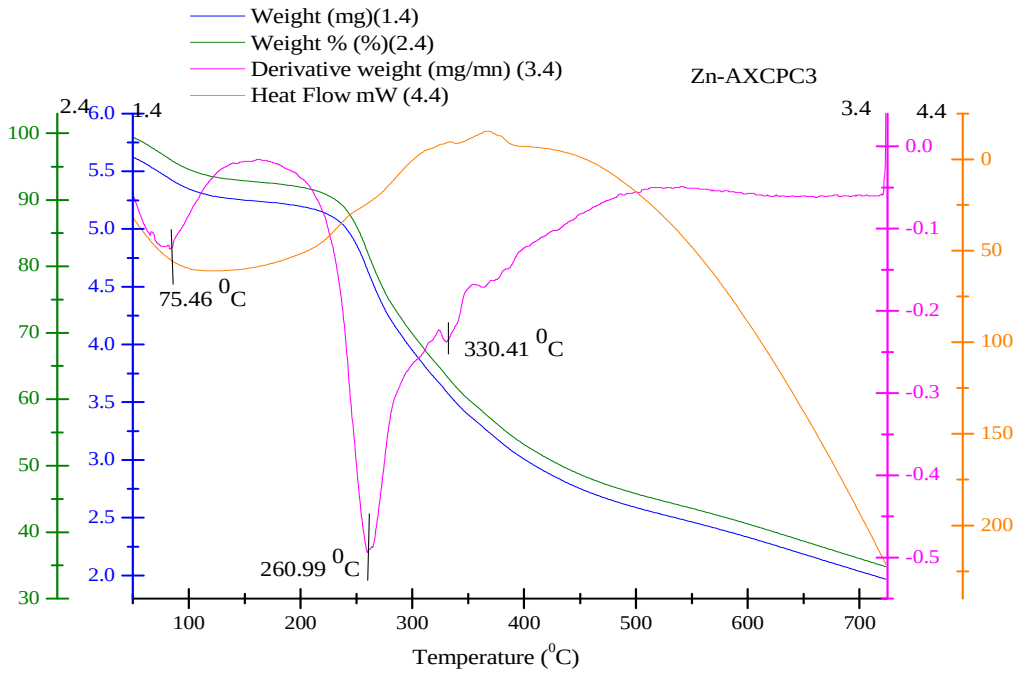

Figure 53: Thermogram of Zn-AXCPC3

Table 14: Thermal decomposition data of metal complexes of AXCPC3 ligand

Comp.	Step	TG range (°C)					DTA	
		$\Delta_{m\%}$ *found*	T_i	T_f	T_{DTG}	Mass loss	T_{dta}	Peak
Co-AXCPC3	1	4.826	50	110.2	80.85	-0.226	103.68	endo
	2	25.923	241.63	276.73	268.38	-0.829	-	-
	3	33.837	279	300	284.05	-0.729	-	-
	4	52.247	338	380	357.21	-0.306	334.9	endo
Ni-AXCPC3	1	5.601	44	113	85.91	-0.153	105.33	endo
	2	30.861	232	403	278.16	-0.484	382.91	exo
Cu-AXCPC3	1	2.699	49	115	76.79	-0.100	111.23	endo
	2	8.814	148	163	159.86	-0.395	-	-
	3	21.635	187	246	237.13	-0.310	-	-
	4	42.395	293	390	326.01	-0.244	385.92	exo
Zn-AXCPC3	1	3.047	46	107	75.46	-0.121	-	-
	2	18.233	230	287	260.99	-0.491	-	-
	3	36.441	310	410	330.41	-0.238	365.88	exo

Table 15: Kinetic and thermodynamic parameters of metal complexes of AXCPC3 ligand

Comp.	Step	*r*	*A* (s^{-1})	T_{max} (K)	*E** (kJ/mol)	*ΔS** (J/K.mol)	*ΔH**(kJ/mol)	*ΔG**(kJ/mol)
Co-AXCPC3	1	-0.98495	5.62×10^{6}	353.85	58.36	-117.92	55.4719	97.19789
	2	-0.99209	5.06×10^{19}	541.38	229.22	126.559	224.718	156.202
	3	-0.99052	1.19×10^{36}	557.05	403.95	18.3647	399.319	389.089
	4	-0.99343	1.14×10^{22}	630.21	288.1474	170.339	282.907	175.525
Ni-AXCPC3	1	-0.99453	7.054×10^{6}	358.91	59.62	-40.236	56.634	71.075
	2	-0.9887	1.35×10^{13}	551.16	160.7139	35.4267	160.288	140.762
Cu-AXCPC3	1	-0.99401	4.064×10^{7}	349.79	63.4725	-110.3698	60.564	64.191
	2	-0.99698	10.06×10^{51}	432.86	447.68	765.803	444.080	112.594
	3	-0.99643	5.98×10^{11}	510.13	129.453	-24.716	125.2115	137.819
	4	-0.99604	6.55×10^{5}	599.01	93.1345	-140.1638	92.6438	176.603
Zn-AXCPC3	1	-0.99448	5.89×10^{6}	348.46	57.8981	-117.3976	55.00	95.908
	2	-0.99491	2.92×10^{15}	533.99	176.7582	45.523	172.318	148.00
	3	-0.99118	7.64×10^{5}	603.41	96.5845	-103.320	91.567	153.911

4.4.2 TGA/DTA Study of Metal Complexes of AXCPC2

The TGA/DTA of the AXCPC2 ligand and its metal complexes were carried within the temperature range from room temperature to 750 °C with the linear heating rate of 10 °C/ minute in the nitrogen atmosphere. The thermal data have been extracted from the intimate analysis of their thermograms and the data are presented in the Table 16. The following findings have been achieved in our research analysis.

The thermogram of AXCPC2 Schiff base ligand showed continuous decomposition from 54 to 619.73 °C with major four decomposition steps and after this temperature, the ligand leaves no residue. The decomposition step in the temperature range of 53.89 to 101.43 °C with the small mass loss of 0.162 mg (2.849%) is associated with loss of moisture and makes no sense for the thermal stability. The second decomposition step in the temperature range of 172.94 to 232.11 °C with mass loss of 0.954 mg (16.842%) may be attributed to the loss of ligand moiety. Two small shoulder peaks are associated with second decomposition step. The mass loss of 2.46 mg (43.529%) is associated with third decomposition step with the temperature range of 276.47 to 298.54 °C (T_{DTG} = 284.35 °C). This decomposition step is also attributed to the loss of ligand moiety. T_{DTA} peak at 296.5 °C for this step concludes endothermal effect. The last decomposition step represents complete loss of ligand molecule in the temperature range of 528.17 to 619.73 °C with T_{DTG} = 574.22 °C. T_{DTA} peak at 551 °C for this step shows exothermal effect.

The Co-AXCPC2 complex exhibits decomposition in two steps. The first decomposition step with mass loss of 0.571 mg (16.525%) occurred in the temperature range of 194.91 to 309.61 °C and this is assigned to the loss of organic moiety of the ligand. The second decomposition step involves the mass loss of 2.406 mg (69.647%) in the temperature range of 527.36 to 585.06 °C with T_{DTG} peak at 547.88 °C and this may be attributed to the complete loss of ligand part. The thermogram after this temperature gave horizontal platue and nearly 8% mass residue represents cobalt oxide as end product. The associated T_{DTA} peak at 510 °C shows exothermal effect. The thermogram of Ni-AXCPC2 complex exhibits decomposition in two steps, very much similar to Co-AXCPC2 complex. The first step involves the decomposition in the temperature range of 191.4 to 267.04 °C with T_{DTG} peak at

211.37 °C. The second step involves the decomposition in the temperature range of 489.65 to 551.22 °C with T_{DTG} peak at 513.88 °C and T_{DTA} peak at 511.16 °C. This step shows exothermal effect. After the second decomposition step, the thermogram shows horizontal platue with approximately 7.75% nickel oxide as stable residue. The thermogram of Cu-AXCPC2 complex showed decomposition in three major steps. The first step involves the mass loss of 2.062 mg (23.733%) in the temperature range of 175.76 to 244.81 °C and this may be attributed to the loss of ligand moiety. The second step involves the mass loss of 3.927 mg (44.964%) in the temperature range of 271.37 to 299.93 °C with T_{DTG} peak at 281.73 °C. The third step involves major mass loss of the substance with 6.056 mg (69.336%) in the temperature range of 441.02 to 502.57 °C and after this the thermogram became horizontal, indicating complete loss of organic moiety and leaves nearly 8.2% copper oxide as stable residue. The T_{DTA} peak associated with this step is 458 °C and shows exothermal effect. The thermogram of the Zn-AXCPC2 complex also exhibits major three decomposition steps as like Co-AXCPC2 complex but with several shoulder peaks. Nearly 3.5% weight loss at T_{DTG} = 86.01 °C is associated to loss of two molecules of lattice water in the thermogram of the Zn-AXCPC2 complex. The first decomposition step involves the mass loss of 0.865 mg (12.557%) in the temperature range of 189.04 to 226.83 °C with T_{DTG} = 209.54 °C. This may be attributed to the loss of organic parts of the ligand. The second decomposition step involves the mass loss of 1.922 mg (27.928%) in the temperature range of 262.92 to 284.46 °C. This step is associated with one shoulder peak at T_{DTG} = 307.37 °C. This step of the thermogram involves the loss of ligand moiety. The third and final step in the temperature range of 582.67 to 672.77 °C with T_{DTG} = 618.27 °C is associated with the complete loss of ligand moiety and leaves nerly 8% zinc oxide as stable residue. This can be concluded by the horizontal portion of thermogram after 672.77 °C. The T_{DTA} peak for this step at 619 °C concludes exothermal effect. The thermograms of Schiff base ligand and its metal complexes are presented in the Figures 54 – 58.

Kinetic Parameter

The thermodynamic and kinetic parameters of the ligand and metal complexes have been extracted from thermogravimetric (TG) and differential thermal analysis (DTA) curves and the computed values are presented in the Table 17. These parameters were

evaluated graphically by employing the Coats-Redfern method. Following remarks can be pointed out:

(1) The activation energy (*E**) values of the subsequent steps are increasing on going from one to another decomposition steps and this reveals the decreasing rate of decomposition of complexes. The rate of decomposition of ligand parts from the complex is becoming slow and this reflects the greater stability of the complex (Gaber *et al.*, 2015).

(2) The negative entropy of activation, *ΔS**, values in the most of the decomposition steps reveals slow reaction process with more ordered activated complex. Moreover, positive values of *ΔS** are also seen in some decomposition steps and this reflects spontaneous decomposition process (Montazerozohori *et al.*, 2014).

(3) The positive value of enthalpy, *ΔH**, in all the decomposition steps means that the decomposition processes are endothermic (Mahmoud *et al.*, 2014).

(4) The endothermic decomposition processes of various decomposition steps are further supported by positive values of *ΔG** in most of the steps and justify non-spontaneous nature (Kianfar *et al.*, 2015).

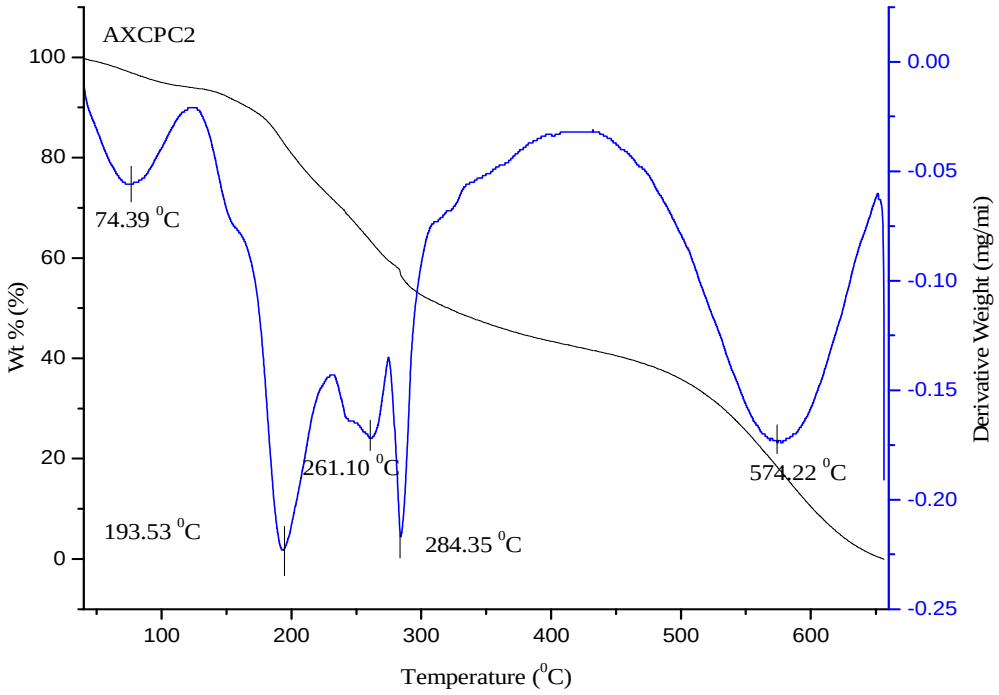

Figure 54: Thermogram of AXCPC2 Schiff base ligand

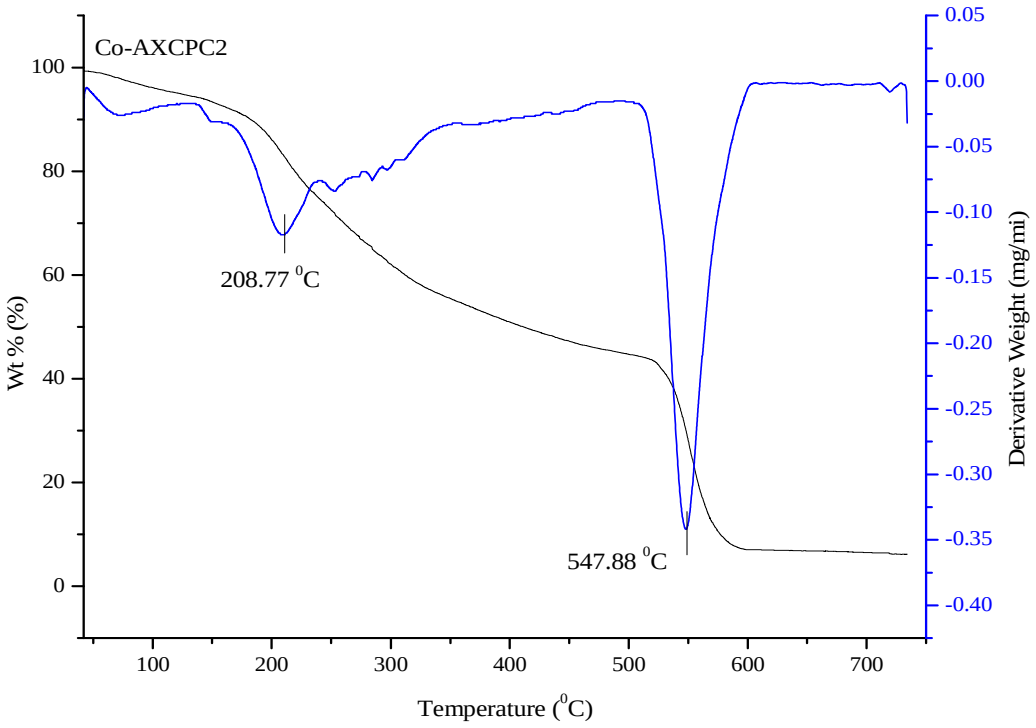

Figure 55: Thermogram of Co- AXCPC2

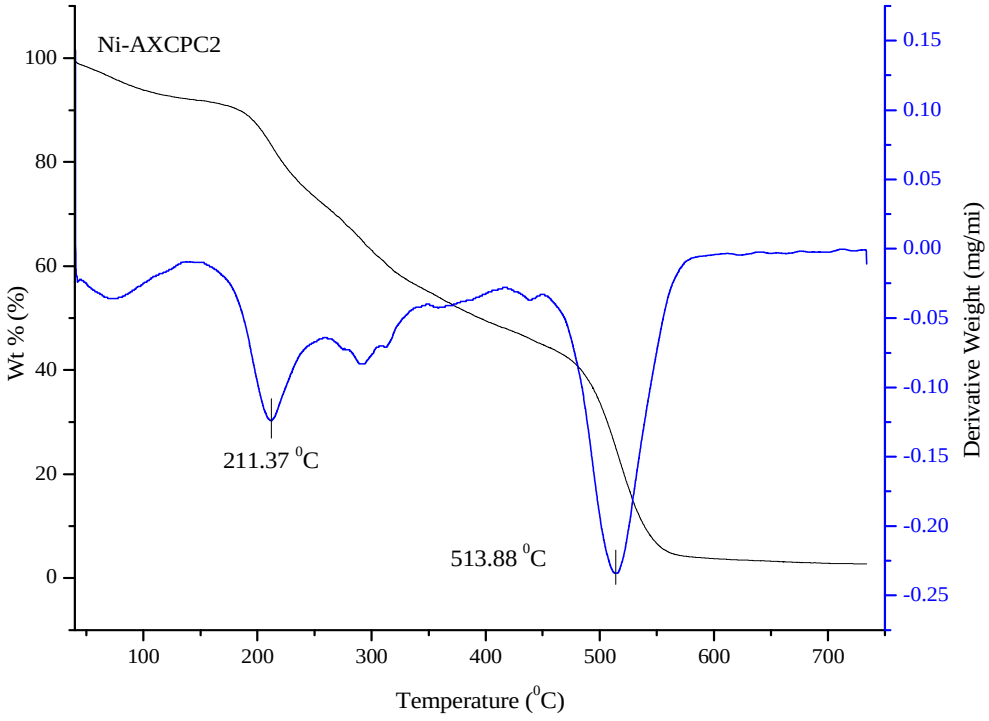

Figure 56: Thermogram of Ni- AXCPC2

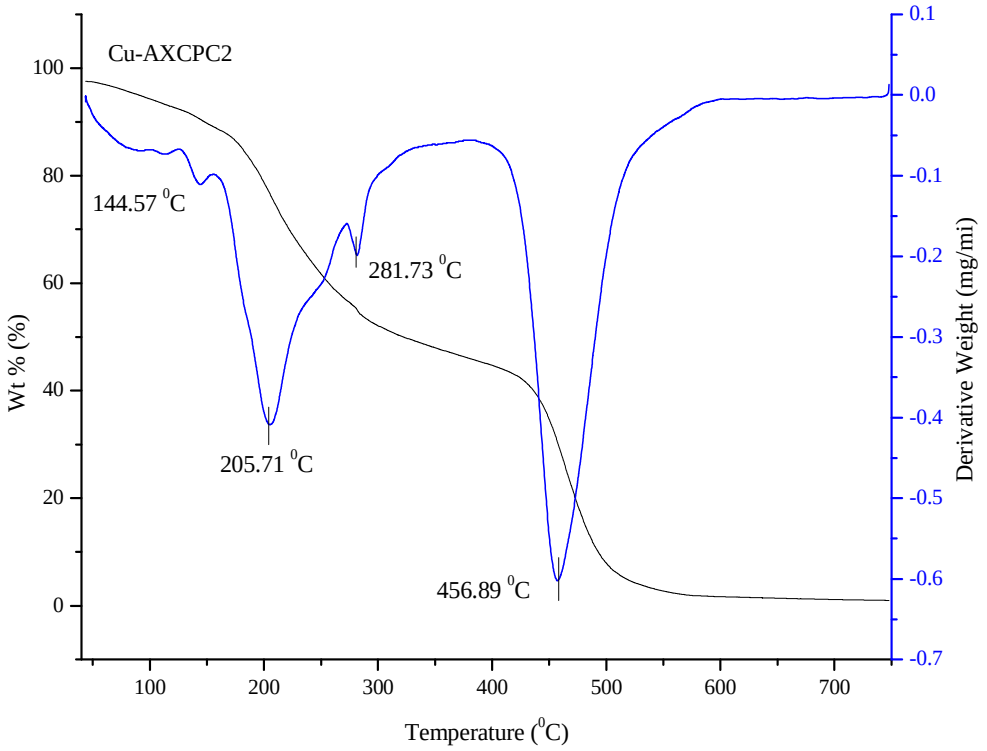

Figure 57: Thermogram of Cu- AXCPC2

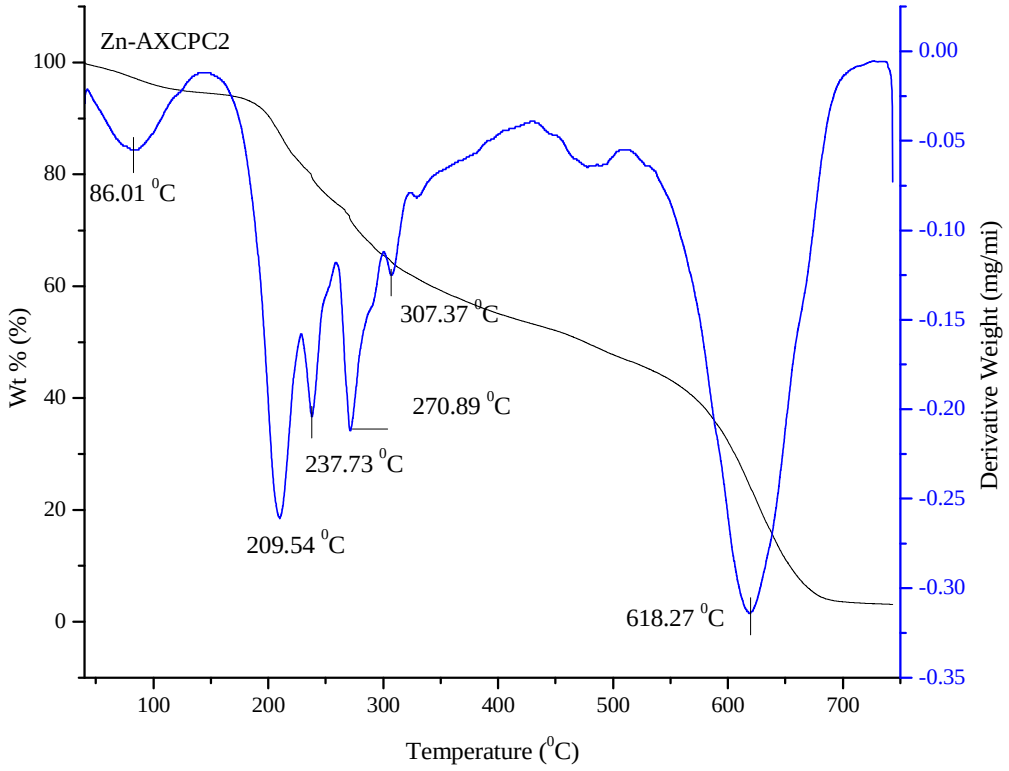

Figure 58: Thermogram of Zn- AXCPC2

Table 16: Thermal decomposition data of metal complexes of AXCPC2 ligand

Complex	Step	TG range (°C)					Mass loss	DTA	
		$\Delta_{m\%}$ *found (Cal.)*		T_i	T_f	T_{DTG}		T_{DTA}	Peak
AXCPC2	1	2.849		53.89	101.43	74.39	0.162	-	-
	2	16.842		172.94	232.11	193.53	0.954	-	-
	3	43.529		276. 47	298.54	284.35	2.46	296.5	Endo
	4	81.667		528.17	619.73	574.22	4.631	551	exo
Co-AXCPC2	1	16.525		194.91	309.61	208.77	0.571	-	-
	2	69.647		527.36	585.06	547.88	2.406	510	exo
Ni-AXCPC2	1	16.454		191.4	267.04	211.37	0.564	-	-
	2	74.754		489.65	551.22	513.88	2.566	511.16	exo
Cu-AXCPC2	1	23.733		175.76	244.81	205.71	2.062	-	-
	2	44.964		271.37	2992.93	281.73	3.927	-	-
	3	69.336		441.02	502.57	456.89	6.056	458	exo
Zn-AXCPC2	1	12.557		189.04	226.83	209.54	0.865	-	-
	2	27.928		262.92	284.46	270.89	1.922	-	-
	3	75.299		582.67	672.77	618.27	5.189	619	exo

Table 17: Kinetic and thermodynamic parameters of metal complexes of AXCPC2 ligand

Comp.	Step	*r*	*A* (s^{-1})	T_{max} (K)	*E** (kJ/mol)	*ΔS** (J/K.mol)	*ΔH**(kJ/mol)	*ΔG**(kJ/mol)
AXCPC2	1	-0.98242	3.94×10^{8}	347.39	71.9763	-82.425	69.087	28.702
	2	-0.98265	2.93×10^{10}	466.53	108.96	-49.05	105.081	22.988
	3	-0.99165	1.897×10^{30}	557.35	332.7696	328.75	328.135	-182.9
	4	-0.98539	1.56×10^{11}	847.22	221.028	-40.106	213.983	34.19
Co-AXCPC2	1	-0.98253	9.2×10^{2}	481.77	51.091	-192.96	47.086	93.009
	2	-0.98148	2.23×10^{24}	820.88	419.258	212.009	412.43	-173.6
Ni-AXCPC2	1	-0.98108	1.16×10^{6}	484.37	80.665	-133.64	76.63	64.8
	2	-0.98349	1.86×10^{19}	786.88	325.358	115.128	318.81	-90.27
Cu-AXCPC2	1	-0.981	3.13×10^{8}	478.71	99.86	-87.005	95.88	41.74
	2	-0.98863	4.66×10^{36}	554.73	408.458	451.134	403.84	-249.8
	3	-0.98164	$1,5 \times 10^{17}$	729.89	275.889	75.675	269.82	-54.9
Zn-AXCPC2	1	-0.98843	1.3×10^{21}	482.54	213.025	154.5	209.01	-74.34
	2	0.98989	2.089×10^{27}	543.89	305.09	272.32	300.57	-147.8
	3	0.98545	5.93×10^{13}	891.27	277.84	8.864	270.43	-7.629

4.5 X-ray Powder Diffraction (XRPD) Study

X-ray powder diffraction study of the substances has become a valuable tool for the characterization of complexes in the field of coordination chemistry. Crystal structure determination from powder diffraction data is much more difficult and complicated than from single crystal data. This is because; there is the collapse of the three dimensions of crystallographic information onto the single dimension of a powder diffraction pattern. Although the single crystal approach is much more suitable and straightforward than the powder diffraction technique for structure determination, the formation of single crystal for all the chemical complexes is not accessible.

4.5.1 XRPD Study of Metal Complexes of KMAXC

Single crystal growth of the complexes was unsuccessful, so X-ray powder diffraction technique was carried to get useful crystal information data to deduce accurate cell parameters, crystal system, and the cell volume. Powder diffraction patterns of KMAXC ligand and its metal complexes were recorded over the range (2 theta = 15° - 80°) and crystallographic data are listed in Table 18. The indexing procedures were performed using Crysfire program package software. The diffractogram of Cu-KMAXC and Zn-KMAXC complexes are presented in the Figures 59 & 60. The diffraction pattern reveals well-defined crystalline peaks indicating crystalline nature of the ligand and its complexes and the data confirms the triclinic crystal systems for KMAXC, Co-KMAXC and Cu-KMAXC complexes with space group P1. Zn-KMAXC complex exhibits orthorhombic crystal system with space group Pmmm. The cell dimensions for the ligand and metal complexes presented in the Table 18 are in good agreement with the refined crystal systems. The average particle size in the range of 45-66 nm suggests nanocrystalline nature of the compounds.

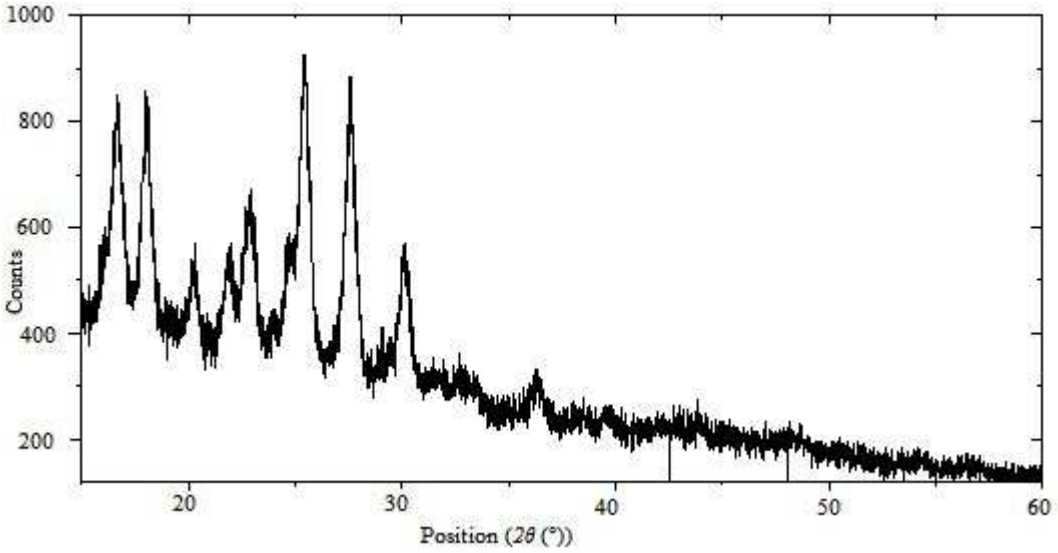

Figure 59: Diffractogram of Cu-KMAXC

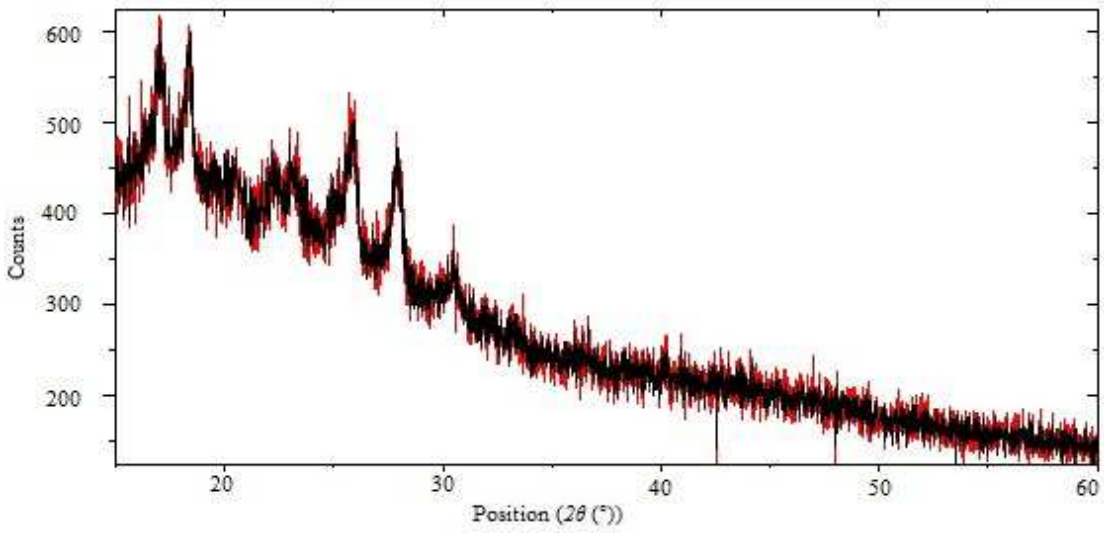

Figure 60: Diffractogram of Zn-KMAXC

Table 18: Crystal lattice parameters of kanamycin-amoxicillin Schiff base ligand and Metal Complexes

Compounds	KMAXC	Co-KMAXC	Cu-KMAXC	Zn-KMAXC)
Formula	$C_{34}H_{55}N_7O_{15}S$	$C_{34}H_{55}CoN_7O_{16}S$	$C_{34}H_{55}CuN_7O_{16}S$	$C_{34}H_{55}N_7O_{16}SZn$
FW	845.92	920.85	925.46	927.30
Temp (K)	298	298	298	298
Wavelength	1.54056	1.54056	1.54056	1.54056
Crystal System	Triclinic	Triclinic	Triclinic	Orthorhombic
Space group	P1	P1	P1	Pmmm
Unit cell dimension				
a(Å)	7.3029	5.7771	3.6035	23.2423
b(Å)	6.9291	11.4059	10.4736	9.6121
c(Å)	10.6422	19.394	23.4791	8.0821
α^o	70.4605	77.569	46.473	90
β^o	123.7612	101.502	69.481	90
γ^o	120.2416	51.169	61.6011	90
Volume (A^3)	385.66	832.62	564.84	1805.6
θ range (°)	15 - 80	15 - 80	15 - 80	15 - 80
	$-4 \le h \le 3$	$-2 \le h \le 0$	$-1 \le h \le 0$	$0 \le h \le 2$
	$-4 \le k \le 3$	$-3 \le k \le 0$	$-3 \le k \le 4$	$0 \le k \le 1$
Limiting indices	$0 \le l \le 7$	$0 \le l \le 8$	$0 \le l \le 11$	$0 \le l \le 3$
Particle size(nm)	47.35	51.23	58.29	65.45
Density	1.32	1.45	1.23	1.35
Z	1	1	1	2

4.5.2 XRPD Study of Metal Complexes of AXCPC3

Single crystal growth of the synthesized compounds was unsuccessful, so their crystallinity was assured by X-ray powder diffraction study. X-ray diffractogram of compounds AXCPC3, Co-AXCPC3, Ni-AXCPC3, and Zn-AXCPC3 were of relatively very poor quality and suggested their amorphous nature. The crystal structure of compound Cu-AXCPC3 was ascertained by its well resolved crystalline peaks (Figure 61) which crystallize in triclinic crystal system with space group P121. The diffractogram of Cu-AXCPC3 registered 22 reflection peaks in the range of (2θ) 0 to 50° with maxima at 15.974° corresponding to d spacing value of 5.584 Å. The cell dimensions *a(6.2282 Å). b(109390 Å),c(20.3388 Å), α(63.1585°), β(113.5723°)* and *γ(64.269°)* are in good agreement with refined triclinic crystal system. The unit cell volume for this compound was calculated to be 747.4131 $Å^3$ with FOM 31. The details of crystallographic data are summarized in Table 19. The crystallite size was calculated from Scherrer's formula $a = 0.9\lambda/\beta Cos\theta$, where λ is the wavelength, β is the full-width half maximum of the characteristic peak and θ is the diffraction angle for the hkl plane (Grivani *et al.*, 2014; Mahapatra *et al.*, 2013). The calculated average value of crystallite size 69.34 nm suggests its nanocrystalline nature.

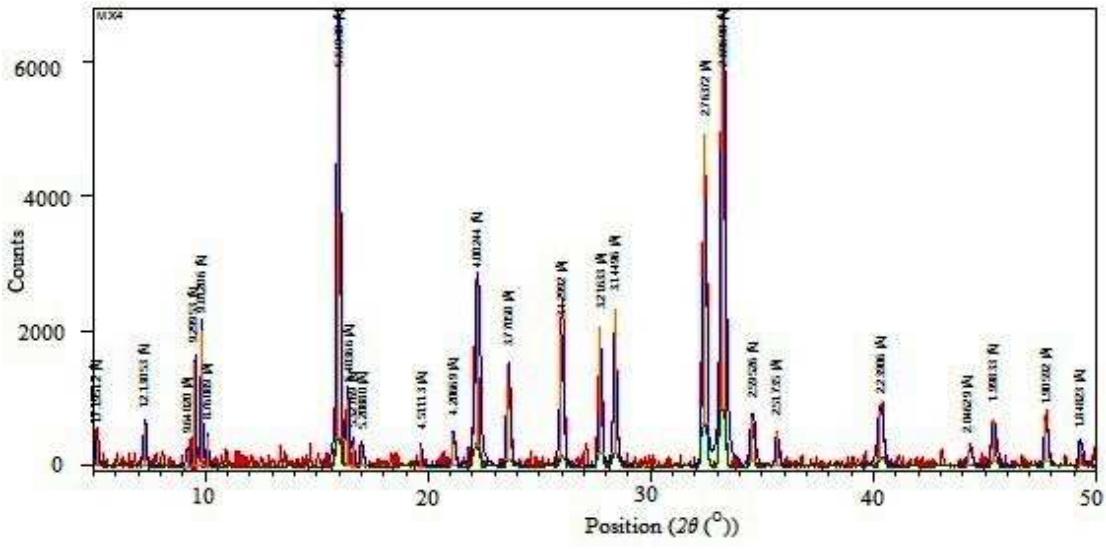

Figure 61: Diffractogram of Cu-AXCPC3

Table 19: Diffraction data of Cu-AXCPC3

Peak no.	2θ	θ	$Sin\theta$	$Sin^2\theta$	$h^2+k^2+l^2$	*hkl*	*d*	*FWHM*	*% Int.*	*a* in nm
1	7.2685	3.63425	0.06338	0.004017	1	0 0 1	12.16238	0.2244	16.00	61. 22
2	13.7483	6.87415	0.11968	0.014323	1	0 1 0	6.44119	0.6731	21.90	20.37
3	15.9738	7.9869	0.13894	0.019304	2	1 1 0	5.54843	0.0935	100.00	146.64
4	16.3780	8.189	0.14243	0.020286	10	1 0 -3	5.41242	0.1496	42.23	91.65
5	21.1607	10.58035	0.18361	0.033712	9	1 2 2	4.19868	0.2244	6.47	61.102
6	22.2011	11.10055	0.19253	0.03706	11	1 -1 -3	4.00421	0.2244	33. 02	61.102
7	23.5966	11.7983	0.20446	0.041803	1	1 0 0	3.77046	0.1870	28.72	73.323
8	26.0686	13.0343	0.22553	0.050863	6	1 1 2	3.41826	0.1309	44.73	104.747
9	27.7288	13.8644	0.23962	0.057417	4	0 2 0	3.21726	0.1496	38.35	91.654
10	28.4032	14.2016	0.24533	0.060186	10	1 3 0	3.14240	0.1496	42.24	91.654
11	32.3941	16.19705	0.27894	0.077807	20	2 0 -4	2.76379	0.1122	70.54	122.205
12	33.2184	16.6092	0.28584	0.081704	40	2 0 -6	2.69707	0.2057	91.73	66.657
13	34.5584	17.2792	0.29702	0.088220	13	2 0 -3	2.59550	0.2244	13.44	61.103
14	35.6718	17.8359	0.30629	0.093813	2	1 -1 0	2.51700	0.2244	8.91	61.103
15	37.2666	18.6333	0.31951	0.102086	20	2 4 0	2.41287	0.3739	7.05	36.671
16	40.3520	20.176	0.34490	0.11895	80	0 4 8	2.23521	0.2617	23.89	52.394
17	43.0415	21.52075	0.36683	0.13456	9	1 -2 -2	2.10157	0.4487	11.08	30.5585
18	44.3550	22.1775	0.37747	0.14248	30	2 5 1	2.04234	0.2244	11.90	61.103
19	45.3976	22.6988	0.38588	0.14890	69	2 1 -8	1.99783	0.2244	15.90	61.103
20	47.7559	23.87795	0.40478	0.16384	25	3 4 0	1.90454	0.1870	16.97	73.324
21	48.6714	24.3357	0.41211	0.16983	58	3 0 -7	1.87083	0.2991	5.79	45.843
22	49.3094	24.6547	0.41714	0.174	18	3 3 0	1.84658	0.2736	7.79	50.116
							Average crystallite size			69.3474

4.5.3 XRPD Study of Metal Complexes of AXCPC2

The single crystal growth of metal complexes of the AXCPC2 ligand was not successful and the crystallinity was studied by powder X-ray diffraction technique. The diffractogram of Co-AXCPC2 (Figure 62) displays 12 reflection peaks with a most intense peak at 15.992° corresponding to d spacing value of 5.54217 Å. The cell dimensions $\alpha = b = 8.29$ Å, $c = 16.71$ Å, $\alpha = \beta = \gamma = 90°$, represents tetragonal crystal system with p3 space group. The calculated unit cell volume for this complex is 1147.36 $Å^3$. The average crystallite size of 51.02825 nm executes nanocrystalline nature of this complex. The details of crystallographic data are summarized in the Table 20. The diffractogram of the Ni-AXCPC2 complex (Figure 63) registered 24 well-resolved reflection peaks with peak maxima at 18.5777° corresponding to interplanar d spacing value of 4.7762 Å. The cell dimensions $a = b = 12.333$ Å, $c = 20.713$ Å, $\alpha = \beta = \gamma = 90°$, represents tetragonal system and the space group is P42BC. The calculated unit cell volume is 3150.7 $Å^3$ and the average crystallite size has measured 46.5554 nm and this represents nanocrystalline nature of the complex. The crystallographic data for this complex is presented in the Table 21. Thirty reflection peaks have been registered in the diffractogram of the Cu-AXCPC2 complex. The diffractogram for the Cu-AXCPC2 complex has shown in the Figure 64. The most intense peak with 100% intensity has recorded at 16.2628° with interplanar d spacing value 5.4505 Å. The unit cell dimensions $a = 13.179$ Å, $b = 16.931$ Å, $c = 7.274$ Å, $\alpha = \gamma = 90°$, $\beta = 102°$, suggest monoclinic crystal system with space group p21. The calculated unit cell volume of this complex is 1581 $Å^3$. The average crystallite size 57.3205 nm suggests nanocrystalline nature of this complex. The crystallographic data of this complex is presented in the Table 22. The diffractograms of AXCPC2 and Zn-AXCPC2 revealed their amorphous nature.

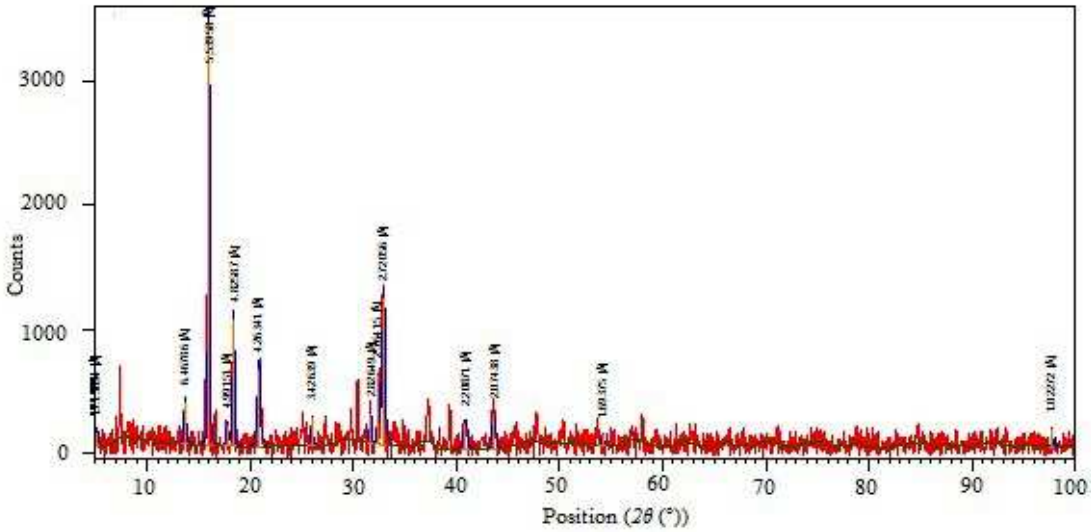

Figure 62: Diffractogram of Co-AXCPC2

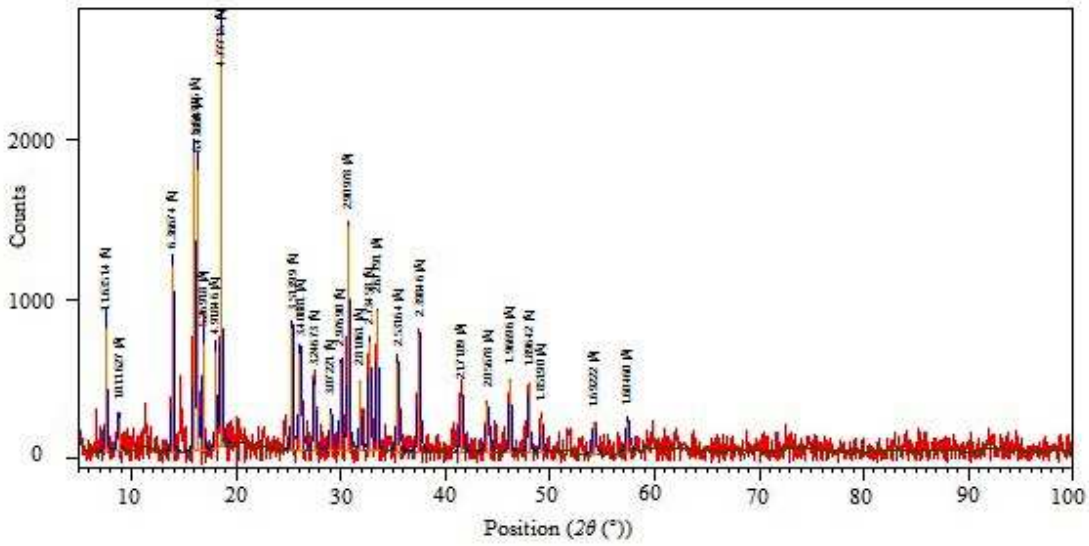

Figure 63: Diffractogram of Ni-AXCPC2

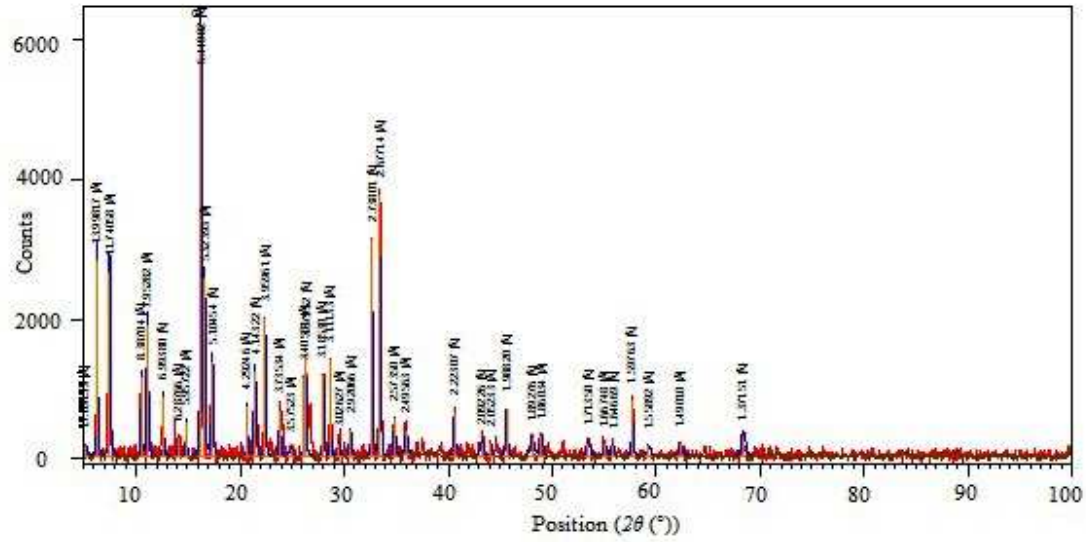

Figure 64: Diffractogram of Cu-AXCPC2

Table 20: Diffraction data of Co-AXCPC2

Peak No.	*Pos. [°2Th.]*	*Height [cts]*	*FWHM [°2Th.]*	*d-spacing [Å]*	*Rel. Int. [%]*	*a in mm*
1	7.4154	725.19	0.1122	11.92174	20.22	74.03
2	13.6477	314.71	0.2244	6.48842	8.77	37.06
3	15.9920	3587.09	0.0935	5.54217	100.00	89
4	18.3661	1148.50	0.0935	4.83075	32.02	89.07
5	20.9198	810.49	0.3365	4.24647	22.59	24.77
6	30.4417	565.72	0.1122	2.93645	15.77	74.64
7	32.3858	740.94	0.1122	2.76449	20.66	74.72
8	32.8751	1421.90	0.2617	2.72444	39.64	32.05
9	37.2894	532.92	0.2244	2.41145	14.86	37.489
10	39.3005	310.67	0.2244	2.29256	8.66	37.54
11	40.7898	206.85	0.4487	2.21223	5.77	18.8
12	43.5793	433.21	0.3648	2.07516	12.08	23.17
Average crystallite size						51.02825

$\alpha = b = 8.29$ Å, $c = 16.71$ Å, $\alpha = \beta = \gamma = 90°$, $V = 1147.36$ Å^3 Crystal system = Tetragonal, Space group = P3

Table 21: Diffraction data of Ni-AXCPC2

Peak No.	*Pos. [°2Th.]*	*Height [cts]*	*FWHM [°2Th.]*	*d-spacing [Å]*	*Rel. Int. [%]*	*a in mm*
1	5.0900	196.14	0.1496	17.36177	7.14	55.5
2	7.5926	766.86	0.1496	11.64385	27.92	55.52
3	8.7166	158.37	0.1870	10.14478	5.76	44.42
4	13.8981	1181.56	0.1122	6.37208	43.01	74.12
5	15.9848	1950.63	0.1122	5.54465	71.01	74.17
6	16.2928	1842.52	0.1122	5.44052	67.07	74.17
7	16.8352	737.55	0.1496	5.26642	26.85	55.64
8	18.0546	579.13	0.1496	4.91341	21.08	55.66
9	18.5777	2747.05	0.1683	4.77620	100.00	49.489
10	25.3372	778.31	0.1496	3.51526	28.33	55.83
11	26.1422	584.74	0.2244	3.40881	21.29	37.24
12	27.4645	366.11	0.2617	3.24762	13.33	31.95
13	30.0245	529.20	0.2244	2.97630	19.26	37.31
14	30.7166	1405.73	0.1870	2.91079	51.17	44.79
15	31.8454	379.78	0.1870	2.81015	13.83	44.82
16	32.7564	653.46	0.1870	2.73405	23.79	44.85
17	33.4709	838.90	0.1309	2.67730	30.54	64.1
18	35.4419	569.25	0.2617	2.53280	20.72	32.1
19	37.4912	670.38	0.2991	2.39893	24.40	28.13
20	41.5184	374.71	0.2617	2.17508	13.64	32.25
21	44.0104	206.99	0.4487	2.05753	7.53	18.85
22	46.1410	378.70	0.1870	1.96736	13.79	45.31
23	47.9809	380.82	0.2244	1.89613	13.86	37.82
24	49.1731	183.60	0.3648	1.85138	6.68	23.29
Average crystallite size						46.5554

$a = b = 12.333$ Å, $c = 20.713$ Å, $\alpha = \beta = \gamma = 90°$, $V = 3150.7$ Å^3, Crystal system = Tetragonal, Space group = P42BC,

Table 22: Diffraction data of Cu-AXCPC2

Peak No.	*Pos. [°2Th.]*	*Height [cts]*	*FWHM [°2Th.]*	*d-spacing [Å]*	*Rel. Int. [%]*	*a in mm*
1	5.2647	36.73	0.3739	16.78629	0.59	22.21
2	6.3082	2822.61	0.1309	14.01161	45.36	63.44
3	7.5178	2718.12	0.1309	11.75954	43.68	63.45
4	10.5455	1021.70	0.1122	8.38912	16.42	74.07
5	11.1337	1914.99	0.1309	7.94720	30.77	63.489
6	12.6512	850.62	0.1122	6.99718	13.67	74.1
7	14.8775	428.11	0.1496	5.95472	6.88	55.61
8	16.2628	6222.57	0.1309	5.45050	100.00	63.58
9	16.6517	2577.96	0.1122	5.32405	41.43	74.17
10	17.3634	1322.77	0.1496	5.10740	21.26	55.65
11	20.6922	746.13	0.1309	4.29267	11.99	63.68
12	21.4376	1235.69	0.1309	4.14507	19.86	63.7
13	22.4437	1922.63	0.1309	3.96148	30.90	63.72
14	23.8721	757.74	0.1496	3.72758	12.18	55.79
15	24.9273	62.62	0.3739	3.57213	1.01	22.33
16	26.3830	1532.36	0.1122	3.37824	24.63	74.48
17	28.0151	1084.08	0.1309	3.18503	17.42	63.89
18	28.7013	1388.37	0.1122	3.11042	22.31	74.57
19	29.5545	240.10	0.1870	3.02255	3.86	44.76
20	31.8202	152.02	0.0935	2.81231	2.44	89.65
21	32.7118	3177.93	0.1122	2.73768	51.07	74.75
22	33.4831	3898.48	0.0935	2.67635	62.65	89.74
23	34.8491	522.94	0.2617	2.57451	8.40	32.089
24	35.9416	390.12	0.1496	2.49872	6.27	56.179
25	40.6242	628.59	0.1870	2.22086	10.10	45.1
26	44.4599	72.38	0.7478	2.03777	1.16	10.74
27	45.6453	646.92	0.2244	1.98757	10.40	37.739
28	48.9512	261.18	0.2617	1.86079	4.20	32.46
29	57.7173	776.70	0.1122	1.59730	12.48	76.39
30	68.3228	233.99	0.2280	1.37179	3.76	38.089
Average crystallite size						57.3205

a = 13.179 Å, b = 16.931 Å, c = 7.274 Å, $\alpha = \gamma = 90°$, $\beta = 102°$, $V = 1581Å^3$, Crystal system = monoclinic, Space group = P21

4.6 Scanning Electron Microscopy Study

4.6.1 SEM Study of AXCPC3 and Metal Complexes

The metal coordination to the ligand significantly changes the surface morphology of the complexes and this was investigated by SEM analysis. The SEM micrograph of AXCPC3 ligand and its metal complexes are shown in Figure 65. It is seen the differences in surface morphology of the metal complexes due to change in the metal ions (Modi et al., 2015; Shakir *et al.*, 2015). The SEM micrograph of AXCPC3 ligand demonstrates non-uniform platelets structure of variable lateral dimensions. Moreover, the inhomogeneous matrix with broken ice like structure has observed in the SEM micrograph of the Ni-AXCPC3 complex. The micrograph of Cu-AXCPC3 complex displays agglomerated morphology with small sized grains scattered in the homogeneous matrix and give the appearance of coral like structure. In the SEM micrograph of Zn-AXCPC3 complex, small sized particles crumbled together to give rock like structure with somewhere cotton like appearance (Justin Dhanaraj & Johnson, 2014; Leelavathy & Arulantony, 2013).

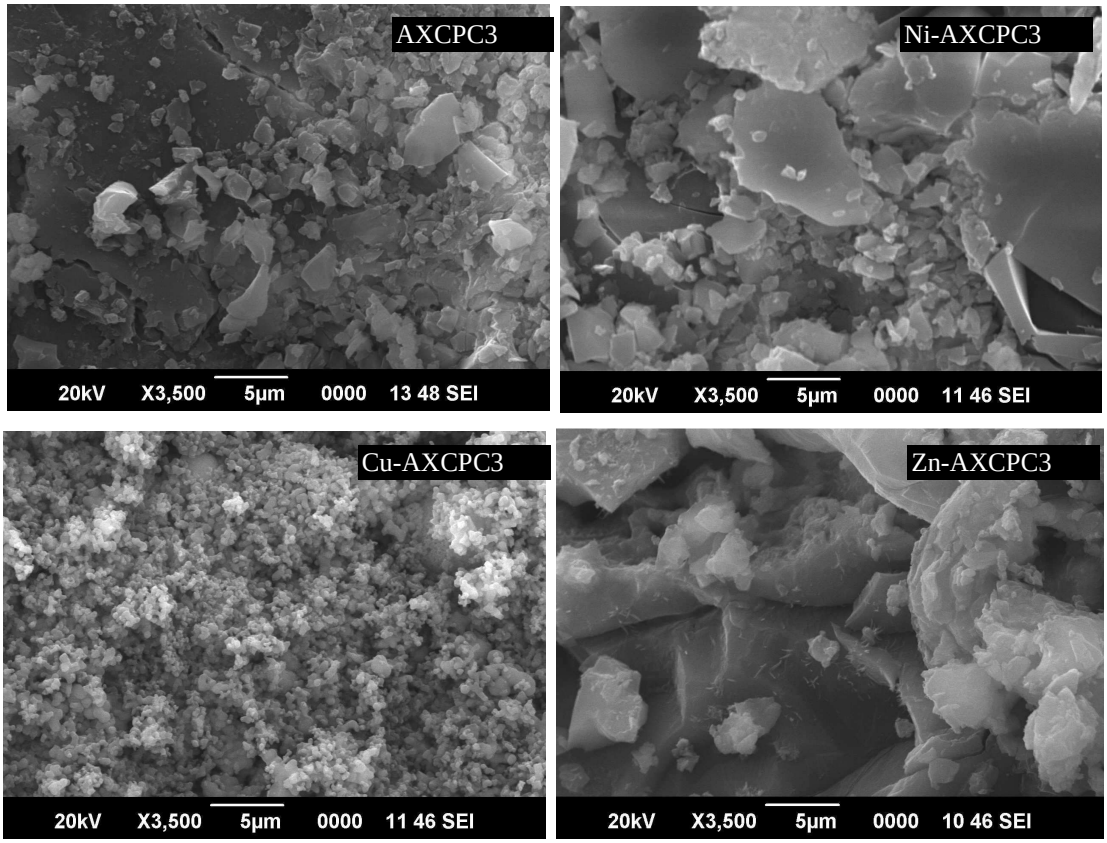

Figure 65: SEM micrograph images of metal complexes of AXCPC3

4.6.2 SEM Study of AXCPC2 and Metal Complexes

An intimate observation of SEM micrographs of AXCPC2 ligand and metal complexes reveals the fact that there is a significant difference in their images, which may be attributed to change in the metal ions. The SEM images of AXCPC2 ligand and metal complexes are shown in the Figure 66. The SEM micrograph of AXCPC2 ligand displays non-uniform sized and irregularly shaped crystalline structure. However, Co-AXCPC2 complex shows sharp edged needle like crystal. The Ni-AXCPC2 complex reveals ice like crystalline structure and agglomerated morphology is seen for the Cu-AXCPC2 complex. The broken rock like structure with layered morphology has observed in the SEM micrograph of the Zn-AXCPC2 complex (Shakir *et al.*, 2015).

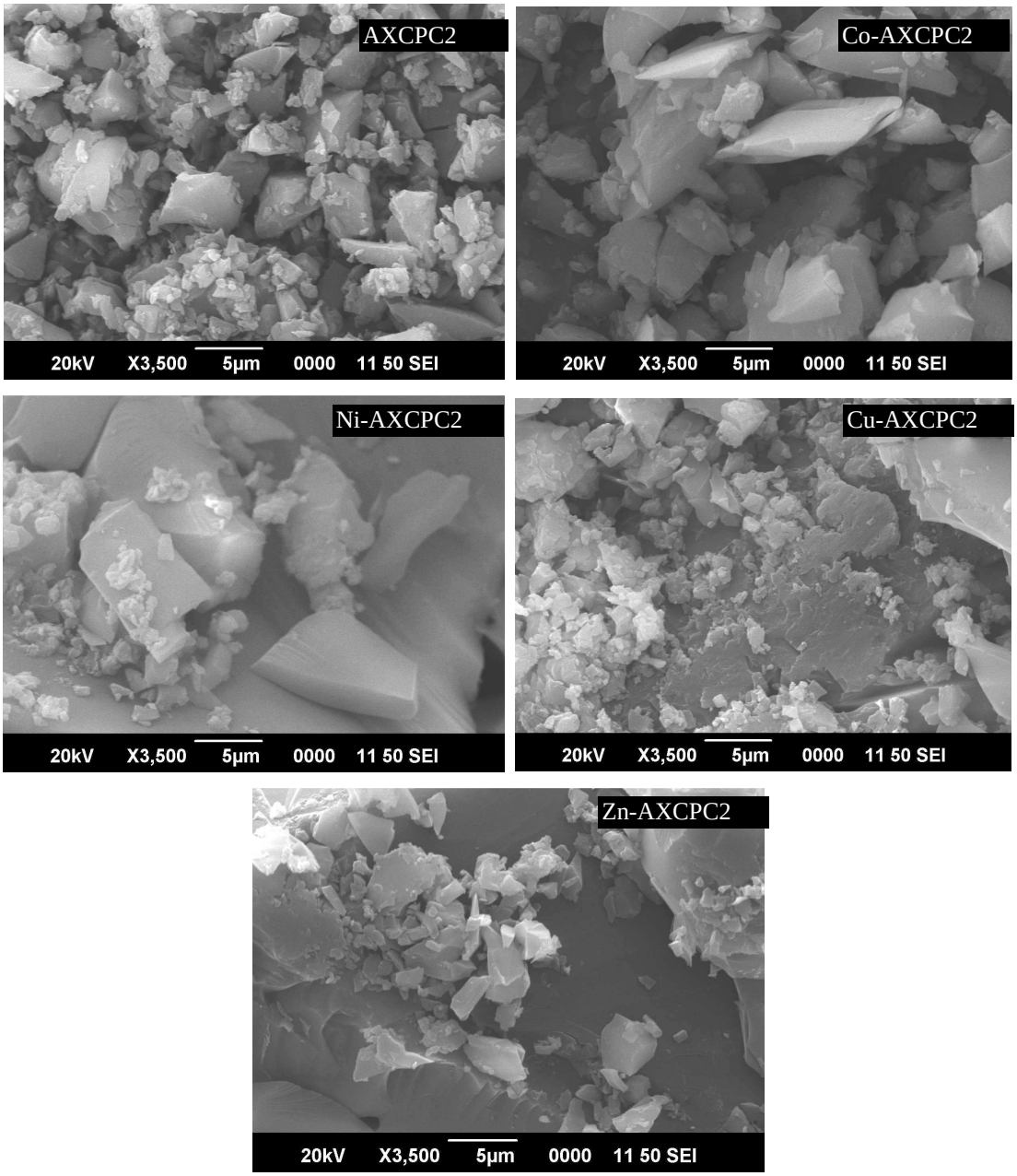

Figure 66: SEM micrograph images of AXCPC2 Schiff base ligand and its metal complexes

4.7 Proposed Molecular Structures and Geometry

A very intimate study of the analytical, magnetic and spectroscopic results and the application of computational software are led to propose the molecular geometry of the complexes. A set of principles and database are incorporated in the computer software to design the structure of the complexes. Various bonding parameters like bond lengths, bond energies and bond angles around the metal center can be exercised

by the overlook of proposed molecular structures. In the present study, the computational software for designing the molecular architecture of the ligand and complexes are ChemDraw and ArgusLab program package. The possible structures of the complexes under investigation, on the basis of experimental evidence are presented in the Figures 67 - 77.

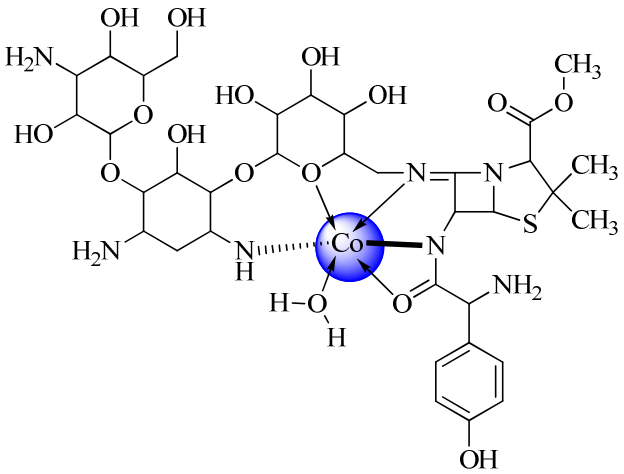

Figure 67: Proposed structure of Co-KMAXC ligand

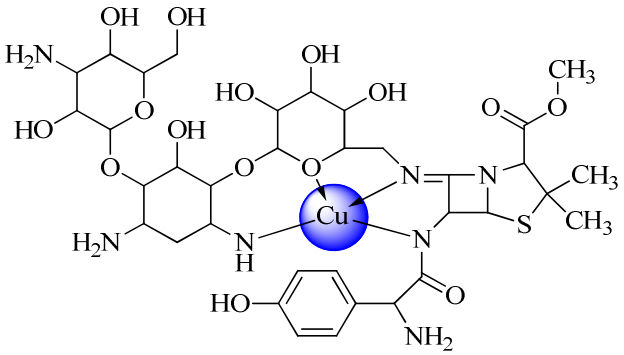

Figure 68: Proposed structure of Cu-KMAXC ligand

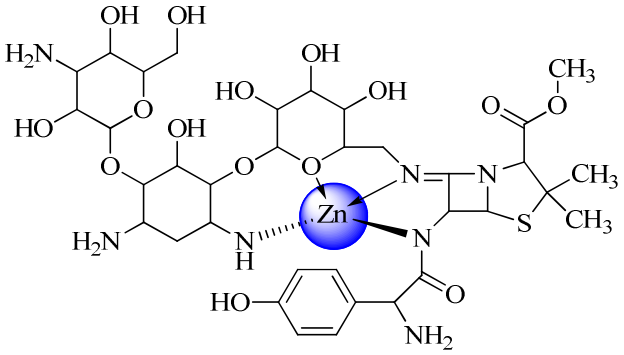

Figure 69: Proposed structure of Zn-KMAXC ligand

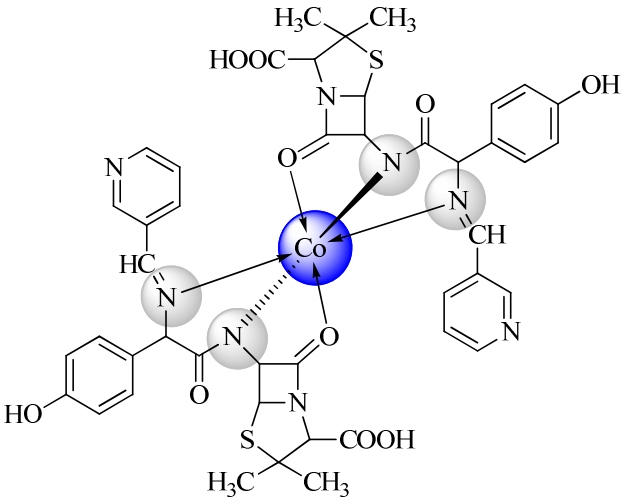

Figure 70: Proposed structure of Co-AXCPC3 ligand

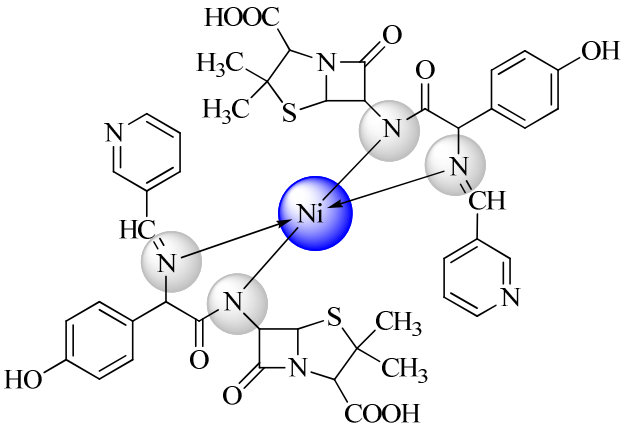

Figure 71: Proposed structure of Ni-AXCPC3 ligand

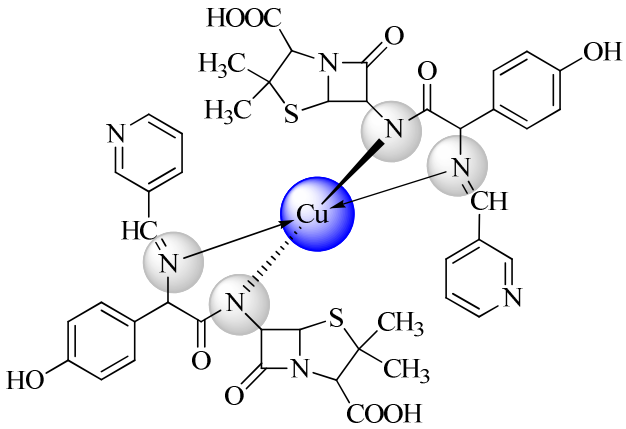

Figure 72: Proposed structure of Cu-AXCPC3 ligand

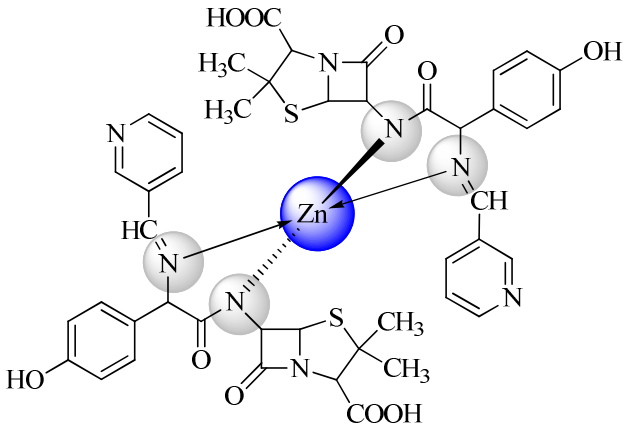

Figure 73: Proposed structure of Zn-AXCPC3 ligand

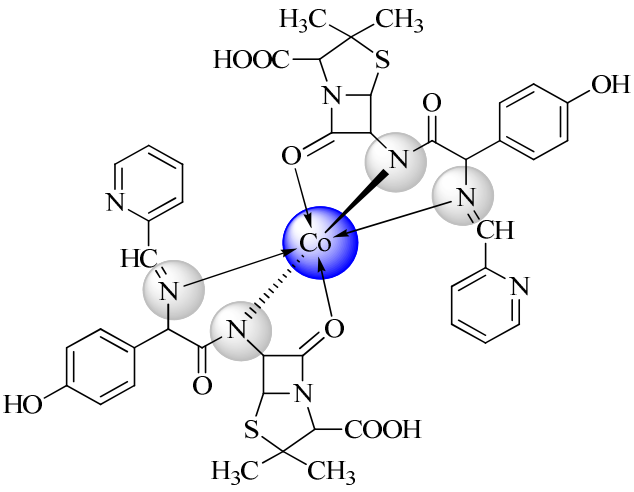

Figure 74: Proposed structure of Co-AXCPC2 ligand

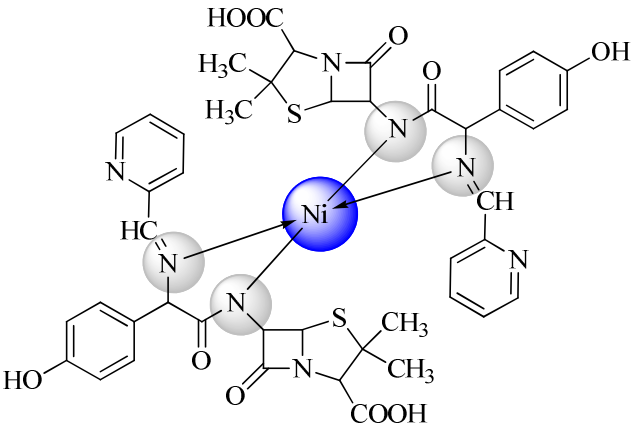

Figure 75: Proposed structure of Ni-AXCPC2 ligand

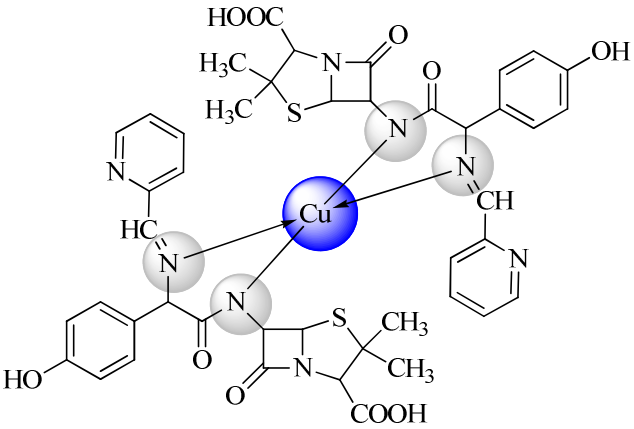

Figure 76: Proposed structure of Cu-AXCPC2 ligand

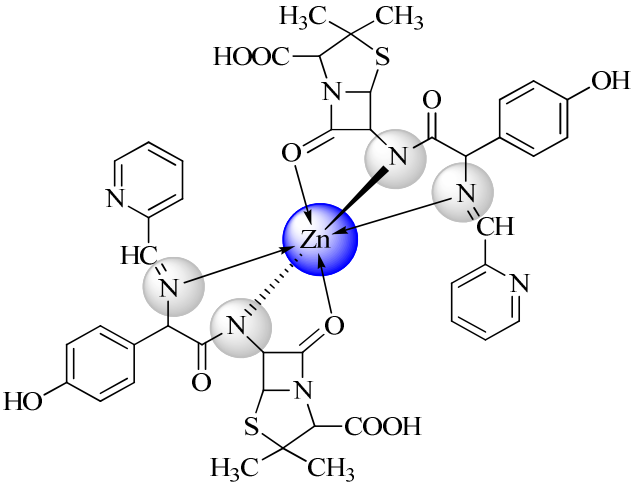

Figure 77: Proposed structure of Zn-AXCPC2 ligand

4.8 Molecular Modeling Study

Molecular modeling is a computational tool to give a much more accurate assessment of theoretical predictions regarding the structure of the molecules. Various physical and chemical information of the molecules can be best achieved by molecular modeling software program package (Pirhadi *et al.*, 2016). Theoretical predictions like electron density and electrostatic potential maps provide a clear picture of the behavior of the molecules. In our investigation, the correct stereochemistry of the complexes has been assured through, manipulation and modification of the molecular coordinates to obtain reasonable and low energy molecular geometries. Energy minimization has repeated several times to find the minimum (Padmaja *et al.*, 2011). The change in bond length values of metal-nitrogen in the complexes compared with ligand further suggests their coordination. The most stable conformer was fully optimized with molecular orbital functions PM3 supported in ArgusLab molecular modeling software (El-Sherif *et al.*, 2012). The minimum geometrical energy of the complexes, optimized by MM2 calculation in CsChem 3D Ultra software was similar to the calculations made in ArgusLab software.

4.8.1 Molecular modeling study of metal complexes of KMAXC

The details of the bond lengths and bond angles as per 3D structure of the metal complexes optimized by MM2 calculations are given in Table 23 and the optimized structures of the metal complexes are shown in the Figures 78 - 80. 3D molecular modeling of the proposed structure of the metal complexes was studied by CsChem 3D Ultra program package and optimized structures revealed octahedral geometry for Co-KMAXC, square planar geometry for Cu-KMAXC and tetrahedral geometry for Zn-KMAXC complexes. This investigated geometry of the complexes is also supported by several spectral techniques. The energy minimization values for the metal complexes suggested their maximum stability. The change in bond length values of metal-nitrogen and metal-oxygen in the complexes compared with ligand further suggests their coordination.

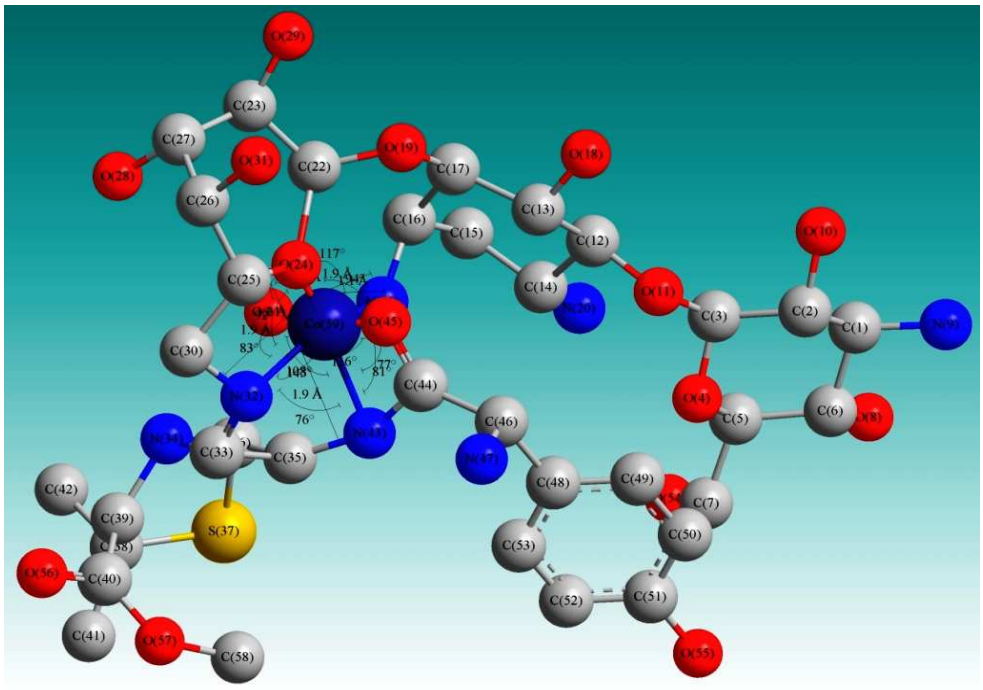

Figure 78: Optimized structure of Co-KMAXC

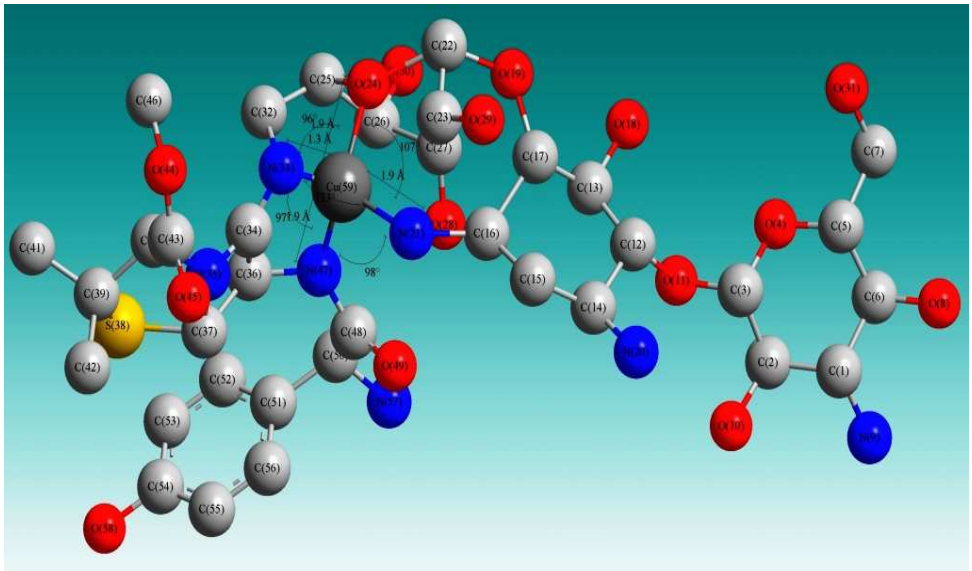

Figure 79: Optimized structure of Cu-KMAXC

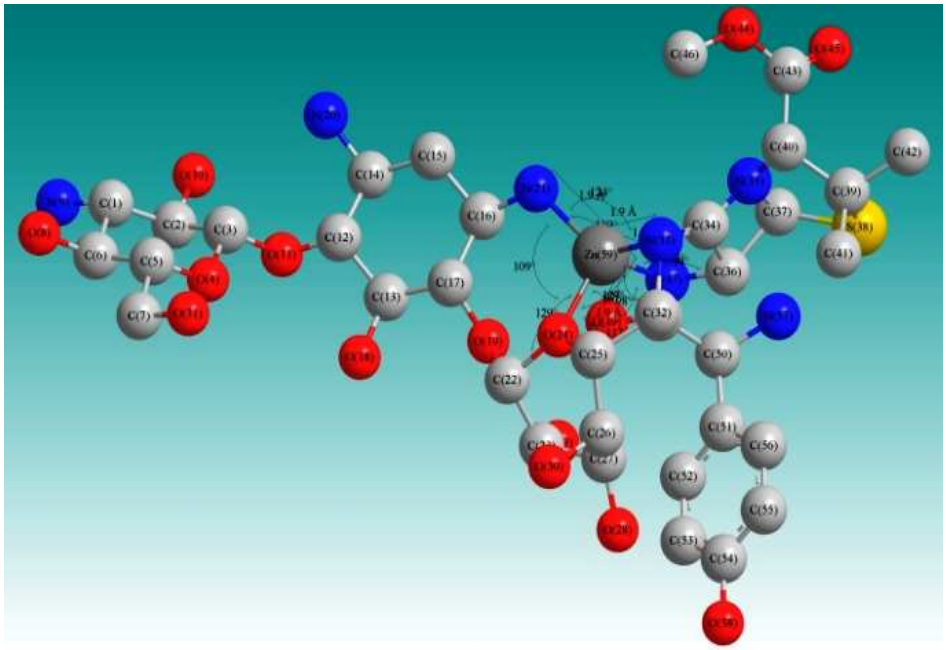

Figure 80: Optimized structure of Zn-KMAXC

Table 23: Selected bond lengths and bond angles of metal complexes of KMAXC Schiff base ligand

Co-KMAXC		Cu-KMAXC		Zn-KMAXC	
Bond lengths (Å)		Bond lengths (Å)		Bond lengths (Å)	
O(58)-Co(59)	1.059	N(25)-Cu(59)	1.369	N(25)-Zn(59)	1.938
O(60)-Co(59)	1.215	O(60)-Cu(59)	1.858	O(60)-Zn(59)	1.926
O(15)-Co(59)	1.197	Cu(59)-O(58)	1.834	Zn(59)-O(58)	1.911
N(25)-Co(59)	1.854	O(15)-Cu(59)	1.866	O(15)-Zn(59)	1.941
N(26)-Co(59)	1.860	N(26)-Cu(59)	1.860	N(26)-Zn(59)	1.930
N(42)-Co(59)	1.824	N(42)-Cu(59)	1.879	N(42)-Zn(59)	1.951
Bond angles (°)		Bond angles (°)		Bond angles (°)	
O(58)-Co(59)-O(60)	98.308	N(25)-Cu(59)-O(60)	91.570	N(25)-Zn(59)-O(60)	95.362
O(58)-Co(59)-O(15)	117.640	N(25)-Cu(59)-O(58)	109.978	N(25)-Zn(59)-O(58)	131.455
O(58)-Co(59)-N(25)	157.046	N(25)-Cu(59)-O(15)	94.527	N(25)-Zn(59)-O(15)	78.095
O(58)-Co(59)-N(26)	88.509	N(25)-Cu(59)-N(26)	164.131	N(25)-Zn(59)-N(26)	127.588
O(58)-Co(59)-N(42)	84.499	N(25)-Cu(59)-N(42)	91.908	N(25)-Zn(59)-N(42)	72.477
O(60)-Co(59)-O(15)	105.039	O(60)-Cu(59)-O(58)	156.406	O(60)-Zn(59)-O(58)	76.493
O(60)-Co(59)-N(25)	90.790	O(60)-Cu(59)-O(15)	83.091	O(60)-Zn(59)-O(15)	91.984
O(60)-Co(59)-N(26)	163.160	O(60)-Cu(59)-N(26)	82.572	O(60)-Zn(59)-N(26)	135.402
O(60)-Co(59)-N(42)	85.927	O(60)-Cu(59)-N(42)	128.450	O(60)-Zn(59)-N(42)	86.165
O(15)-Co(59)-N(25)	79.650	O(58)-Cu(59)-O(15)	85.650	O(58)-Zn(59)-O(15)	148.519
O(15)-Co(59)-N(26)	85.026	O(58)-Cu(59)-N(26)	78.885	O(58)-Zn(59)-N(26)	81.859
O(15)-Co(59)-N(42)	152.633	O(58)-Cu(59)-N(42)	62.399	O(58)-Zn(59)-N(42)	59.392
N(25)-Co(59)-N(26)	77.576	O(15)-Cu(59)-N(26)	99.361	O(15)-Zn(59)-N(26)	86.610
N(25)-Co(59)-N(42)	75.129	O(15)-Cu(59)-N(42)	147.628	O(15)-Zn(59)-N(42)	150.187
N(26)-Co(59)-N(42)	79.386	N(26)-Cu(59)-N(42)	80.454	N(26)-Zn(59)-N(42)	115.163
Co(59)-O(58)-C(41)	108.810	Cu(59)-O(58)-C(41)	107.965	Zn(59)-O(58)-C(41)	108.006
Co(59)-N(42)-C(43)	135.675	Cu(59)-N(42)-C(43)	110.956	Zn(59)-N(26)-C(11)	120.989
Co(59)-N(42)-C(41)	70.740	Cu(59)-N(42)-C(41)	96.622	Zn(59)-N(25)-C(44)	119.075
Co(59)-N(26)-C(11)	116.164	Cu(59)-N(26)-C(11)	127.557	Zn(59)-N(25)-C(24)	109.051
Co(59)-N(25)-C(44)	120.265	Cu(59)-N(25)-C(44)	115.600	Zn(59)-O(15)-C(16)	112.492
Co(59)-N(25)-C(24)	114.600	Cu(59)-N(25)-C(24)	109.417	Zn(59)-O(15)-C(14)	139.324
Co(59)-O(15)-C(16)	126.875	Cu(59)-O(15)-C(16)	104.264		
Co(59)-O(15)-C(14)	135.084	Cu(59)-O(15)-C(14)	141.376		

4.8.2 Molecular Modeling Study of Metal Complexes of AXCPC3

Computational study of the compounds provides clear idea about the three-dimensional arrangement of different atoms in the molecules. The energy optimization of the AXCPC3 ligand and metal complexes was done by Universal Force Field (UFF) technique with minimum RMS gradient 0.100, supported in ArgusLab 4.0.1 version software (Kavitha & Anantha Lakshmi, 2015; Sharma *et al.*, 2015). The details of the bonding and energy parameters optimized by molecular modeling calculations of the metal complexes are depicted in Table 24. For AXCPC3 ligand, single point energy calculation with Hamiltonian AM1 revealed final SCF energy and heat of formation, -132288.8349 and 45.0637 kcal/mol respectively (Chaudhary & Mishra, 2015). After the geometry optimization by molecular mechanics (UFF) technique, the final geometrical energy of AXCPC3 has been reported to 139.2725 kcal/mol. In ESP mapped electron density surface of AXCPC3 (Figure A1), red colour indicates the highest electron density region which is around O-atom. The second highest electron density region is around azomethine N-atom that is shown by mixed green and yellow colours. This is the region for the stability of metal ions after coordination and supports its linkage with azomethine N-atom. It seems clear that the coordination with O-atoms is restricted due to greater electronic repulsion and field obstruction. In the Ni-AXCPC3 complex, the higher electron density around coordinated azomethine N-atom, indicated by red colour is in favor of its proposed geometry. Similar studies and computational data of the metal complexes are in good support of their proposed structures. The optimized structures of the ligand and metal complexes are reported in the Figures 81 – 85.

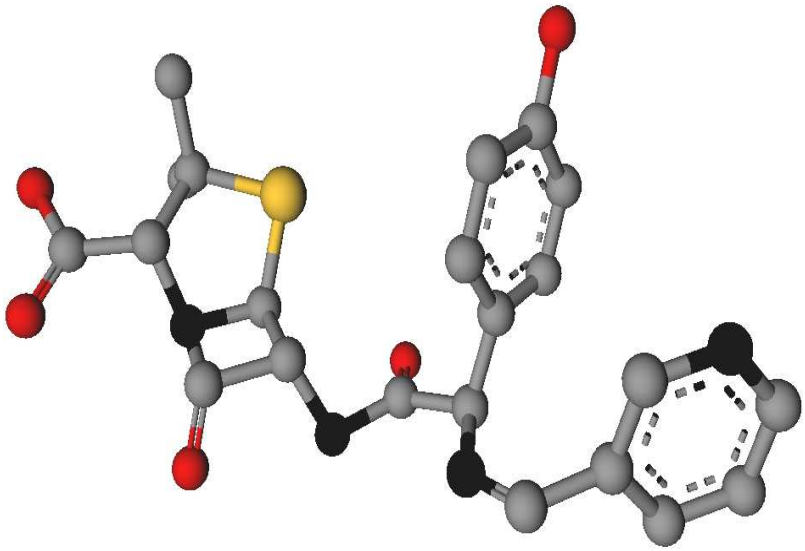

Figure 81: Molecular modeling of AXCPC3 Schiff base Ligand

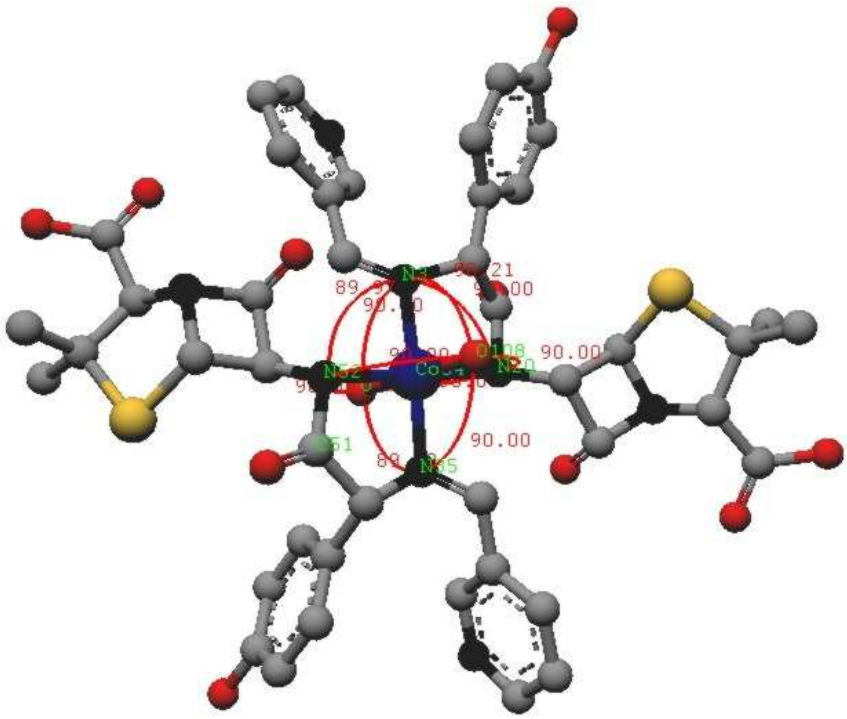

Figure 82: Molecular modeling of Co-AXCPC3

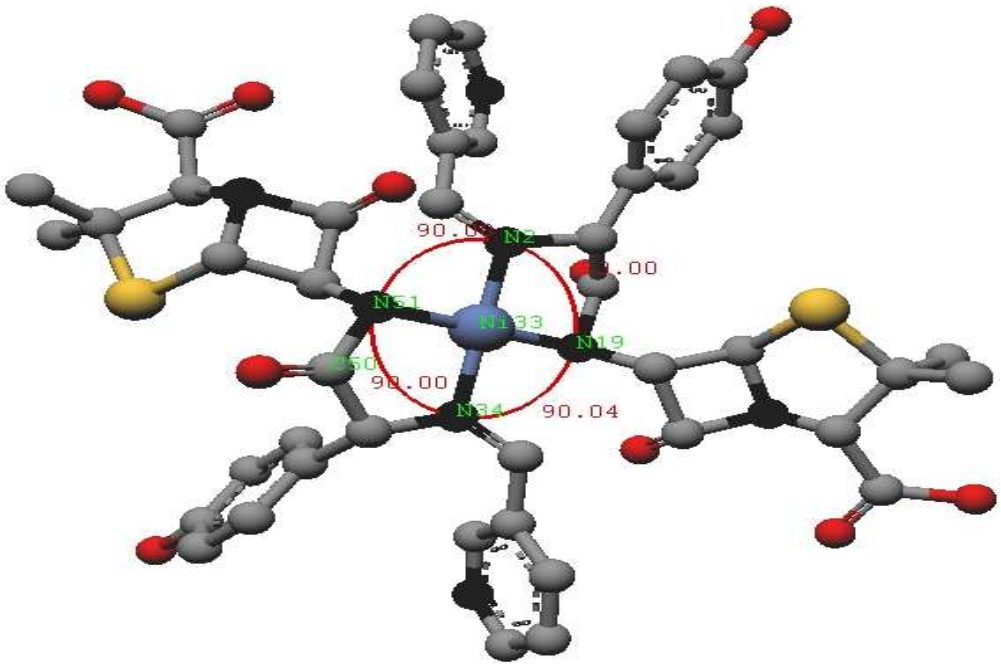

Figure 83: Molecular modeling of Ni-AXCPC3

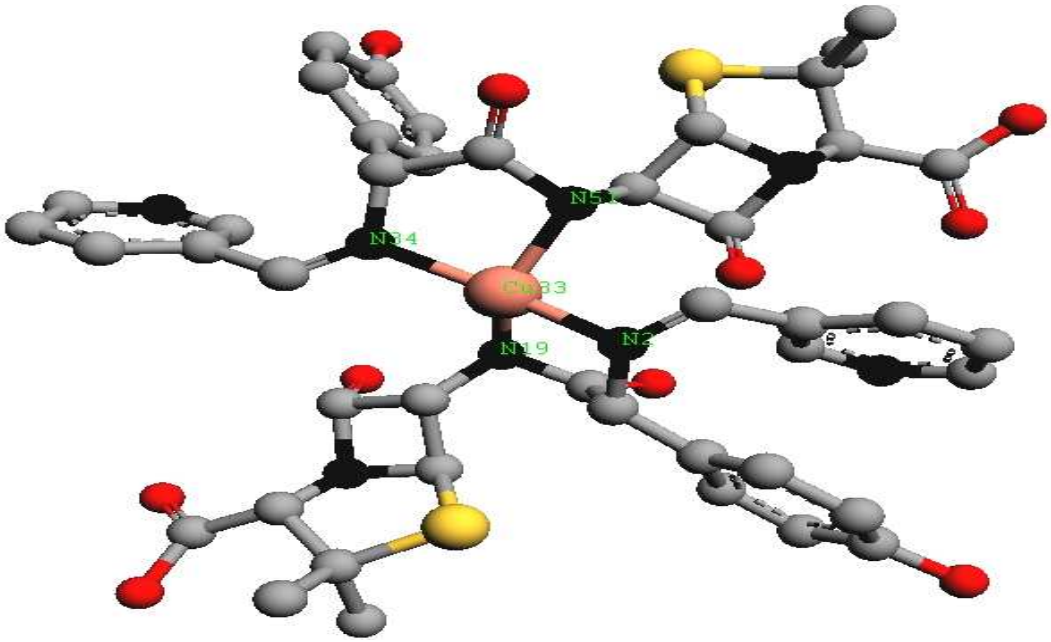

Figure 84: Molecular modeling of Cu-AXCPC3

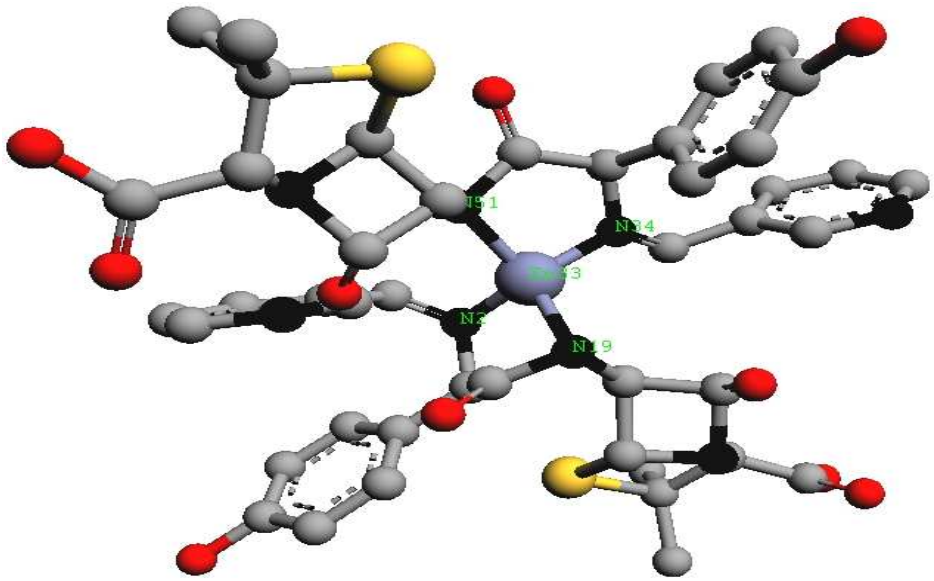

Figure 85: Molecular modeling of Zn-AXCPC3

Table 24: Selected bond lengths and bond energy parameters of metal complexes of AXCPC3 ligand

Complex	Atoms	Bond length (Å)	Bond energy (Kcal/mol)	Atoms	Bond angle	Bond angle energy (Kcal/mol)	Final Geom. Energy
Co-AXCPC3	N(3)-Co(34)	1.957	273.796	N(3)-Co(34)-N(20)	90.00	300.46	349.2538
	N(20)-Co(34)	1.972	267.453	N(3)-Co(34)-N(35)	90.00	304.025	(Kcal/mol)
	Co(34)-N(35)	1.957	273.796	N(3)-Co(34)-N(52)	90.00	300.46	(0.556 au)
	Co(34)-N(52)	1.972	267.453	N(3)-Co(34)-O(104)	90.00	273.401	
	Co(34)-O(104)	1.964	244.913	N(3)-Co(34)-O(113)	90.00	273.401	
	Co(34)-O(113)	1.964	244.913	N(35)-Co(34)-N(20)	90.00	300.46	
				N(52)-Co(34)-N(20)	90.00	296.982	
				O(104)-Co(34)-N(20)	90.00	270.214	
				O(113)-Co(34)-N(20)	90.00	270.214	
				N(35)-Co(34)-N(52)	90.00	300.46	
				N(35)-Co(34)-N(104)	90.00	273.401	
				N(35)-Co(34)-N(113)	90.00	273.401	
				N(52)-Co(34)-O(104)	90.00	270.214	
				N(52)-Co(34)-N(113)	90.00	270.214	
Ni-AXCPC3	N(2)-Ni(33)	1.870	313.824	N(2)-Ni(33)-N(19)	90.00	344.228	324.5763
	N(19)-Ni(33)	1.885	306.275	N(2)-Ni(33)-N(34)	90.00	348.473	(Kcal/mol)
	N(34)-NIi33)	1.870	313.824	N(2)-Ni(33)-N(51)	90.00	344.228	(0.517 au)
	N(51)-NI(i3)	1.885	306.275	N(34)-Ni(33)-N(19)	90.00	344.228	
				N(51)-Ni(33)-N(19)	90.00	340.090	
				N(34)-Ni(33)-N(51)	90.00	344.228	

Table 24: Contd.

Selected bond lengths and bond energy parameters of metal complexes of AXCPC3 ligand

Complex	Atoms	Bond length (Å)	Bond energy (Kcal/mol)	Atoms	Bond angle	Bond angle energy (Kcal/mol)	Final Geom. Energy
Cu-AXCPC3	N(2)-Cu(33)	2.016	181.007	N(2)-Cu(33)-N(19)	109.47	158.764	373.488
	N(19)-Cu(33)	2.031	176.938	N(2)-Cu(33)-N(34)	109.47	160.587	(Kcal/mol)
	N(34)-Cu(33)	2.016	181.007	N(2)- Cu(33)-N(51)	109.47	158.764	(0.595 au)
	N(51)-Cu(33)	2.031	176.938	N(34)- Cu(33)-N(19)	109.47	158.764	
				N(51)- Cu(33)-N(19)	109.47	156.977	
				N(34)- Cu(33)-N(51)	109.47	158.764	
Zn-AXCPC3	N(2)-Zn(33)	1.888	164.142	N(2)-Zn(33)-N(19)	109.47	193.167	352.3697
	N(19)- Zn(33)	1.903	160.260	N(2)- Zn(33)-N(34)	109.47	195.503	(Kcal/mol)
	N(34)- Zn(33)	1.888	164.142	N(2)- Zn(33)-N(51)	109.47	193.167	(0.561 au)
	N(51)- Zn(33)	1.903	160.260	N(34)- Zn(33)-N(19)	109.47	193.167	
				N(51)- Zn(33)-N(19)	109.47	190.879	
				N(34)- Zn(33)-N(51)	109.47	193.167	

4.8.3 Molecular Modeling Study of Metal Complexes of AXCPC2

The molecular modeling of AXCPC2 ligand and its four metal complexes was achieved by optimizing their structures in CsChemOffice 3D Ultra program package. The energy optimization was done several times to get minimum geometrical energy and to register the maximum stability of the complexes. The details of the bond length and bond angles of the complexes, optimized by MM2 calculations are given the Table 25 and the optimized structures are shown in the Figures 86 - 90. The Co-AXCPC2 complex exhibits maximum geometrical energy of 381.6644 Kcal/mol and is relatively less stable than others. The torsional energy for this complex is 119.7329 Kcal/mol. Due to the large size of this molecule, there has a deviation of bond angles and bond lengths from the normal for octahedral geometry. The optimized geometrical and torsional energy for the Ni-AXCPC2 complex are 233.2716 Kcal/mol and 48.383 Kcal/mol. The bond angle and bond length data supports square planar geometry of this complex. The tetrahedral geometry of Cu-AXCPC2 complex is evidenced by bond angle and bond length data that are computed in the Table 25. The optimized energy and torsional energy for this complex are measured 170.8828 Kcal/mol and 66.8742 Kcal/mol respectively. The energy data suggests maximum stability of this complex. The IR and electronic absorption spectral study reveal the octahedral geometry of Zn-AXCPC2 complex which is further supported by bond angle and bond length data. The final geometrical energy and torsional energy for this complex are 178.8377 Kcal/mol and 92.2682 Kcal.mol respectively. The stability of the complexes follows the order, Cu-AXCPC2 > Zn-AXCPC2 > Ni-AXCPC2 > Co-AXCPC2.

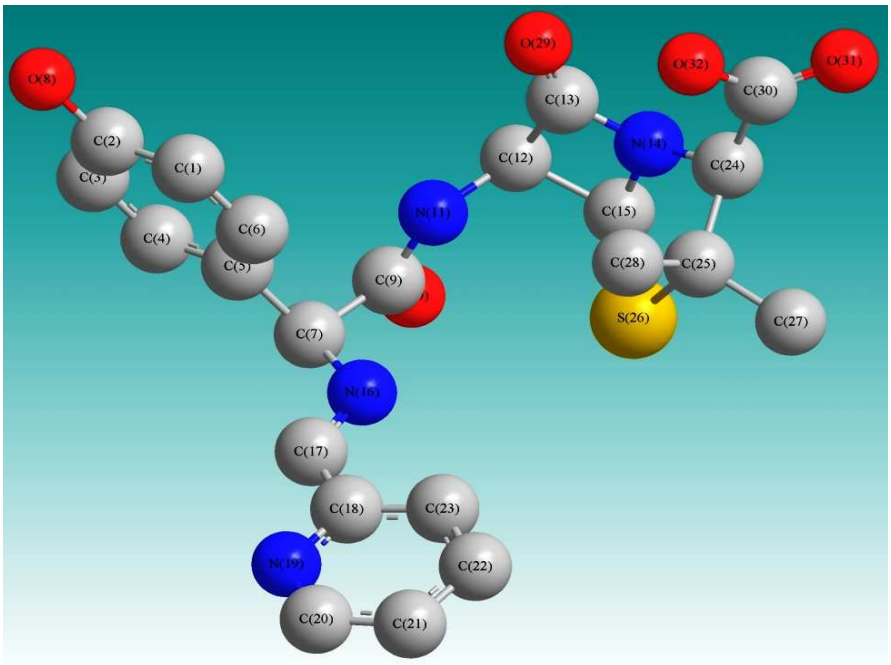

Figure 86: Molecular modeling of AXCPC2 Schiff base Ligand

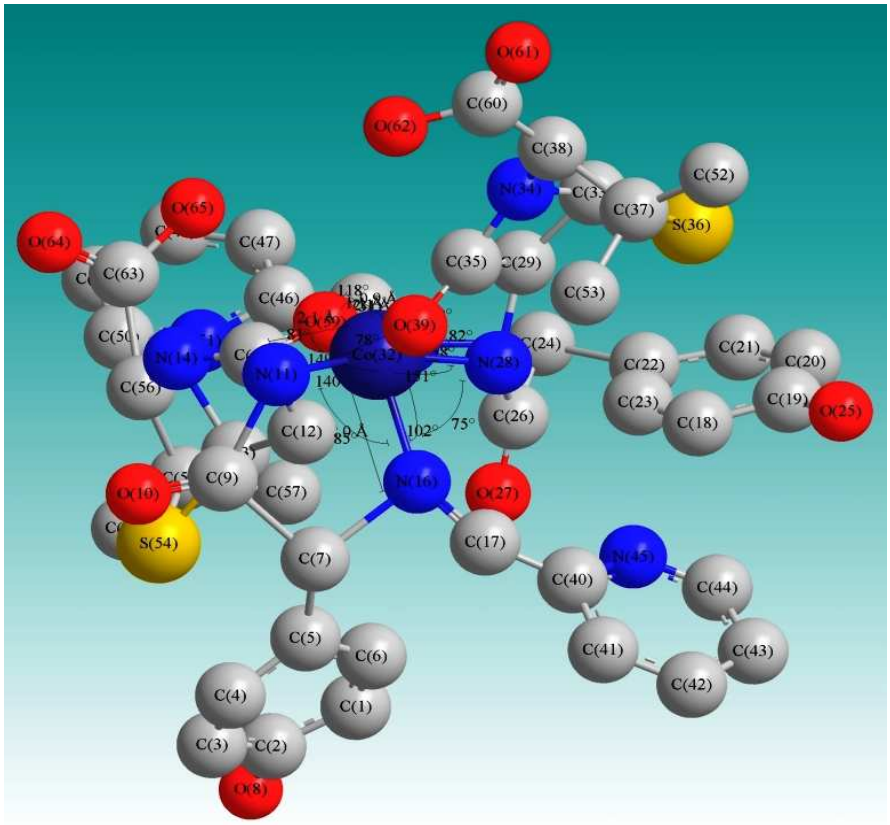

Figure 87: Molecular modeling of Co-AXCPC2

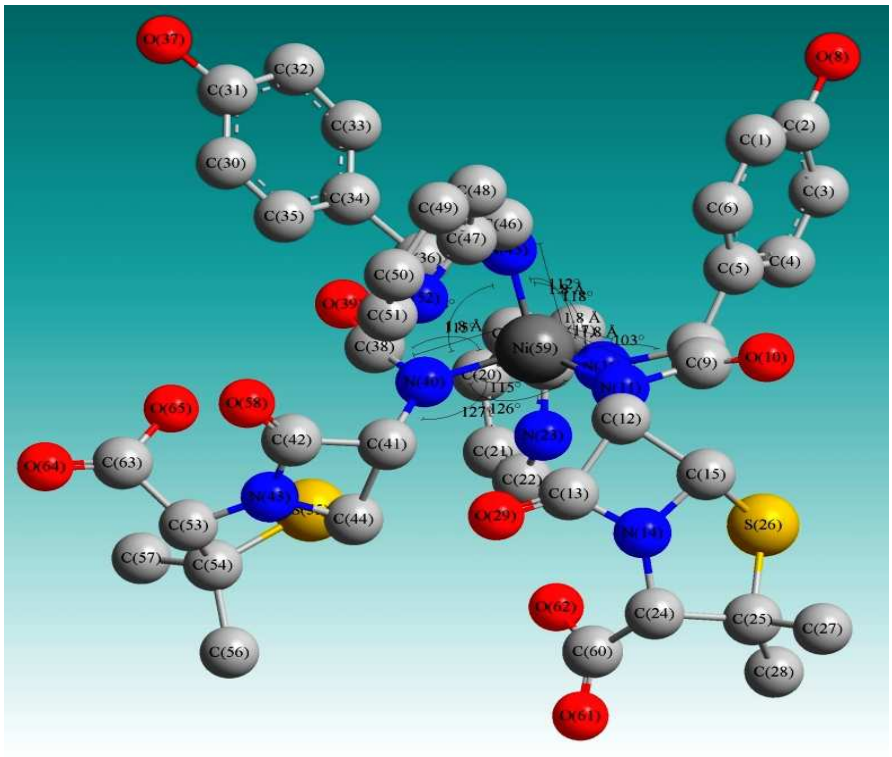

Figure 88: Molecular modeling of Ni-AXCPC2

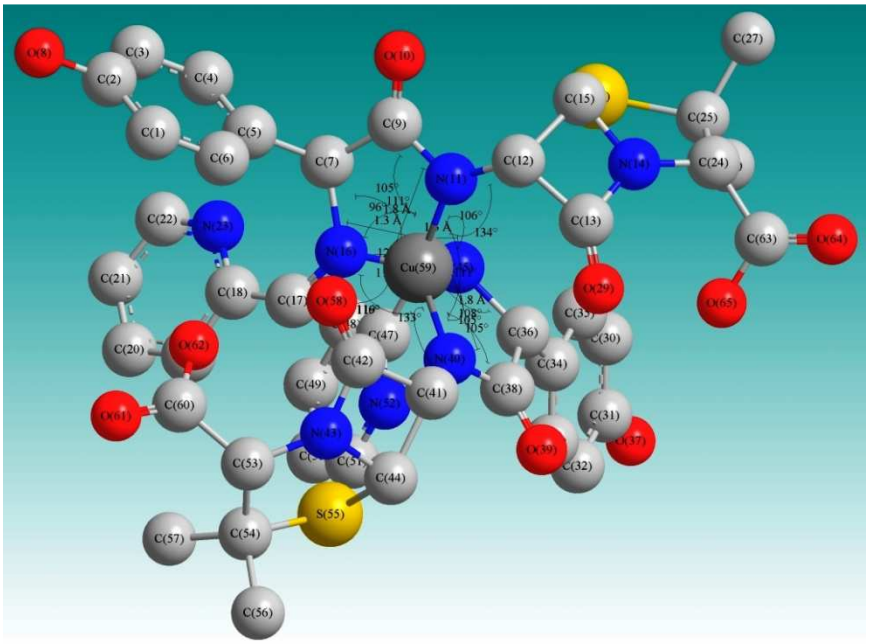

Figure 89: Molecular modeling of Cu-AXCPC2

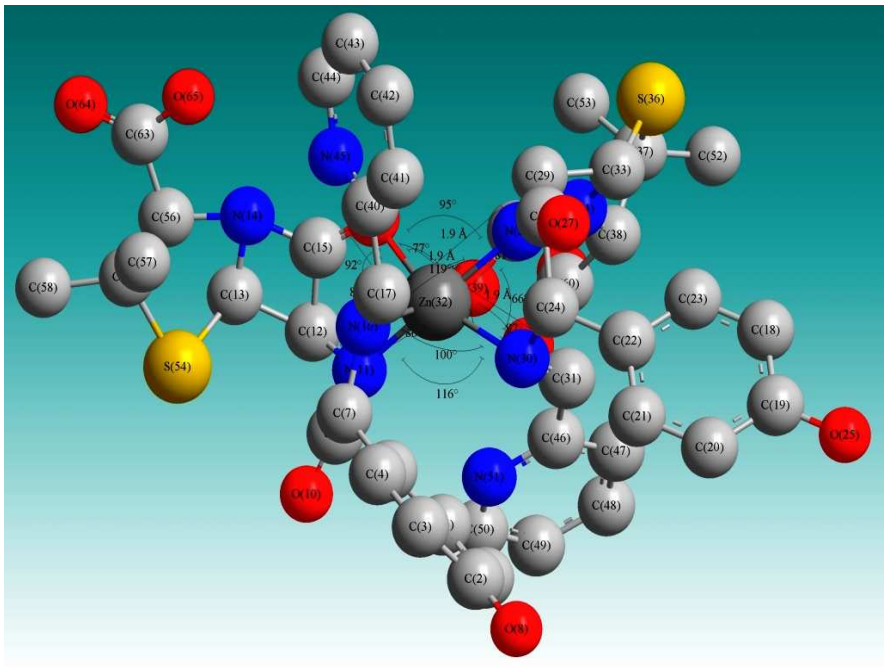

Figure 90: Molecular modeling of Zn-AXCPC2

Table 25: Selected bond lengths and bond energy parameters of metal complexes of AXCPC2 ligand

Complex	Atoms	Bond length (Å)	Atoms	Bond Angle (°)	Final Geom. Energy (Kcal/mol)
Co-AXCPC2	O(59)-Co(32)	0.6801	O(59)-Co(32)-O(39)	106.5764	381.6644
	O(39)-Co(32)	1.1215	O(59)-Co(32)-N(30)	73.3276	(Kcal/mol)
	N(30)-Co(32)	2.0047	O(59)-Co(32)-N(16)	112.7752	
	N(16)-Co(32)	2.0698	O(59)-Co(32)-N(28)	124.7521	
	Co(32)-N(28)	1.8101	O(59)-Co(32)-N(11)	78.1462	
	Co(32)-N(11)	2.1069	O(39)-Co(32)-N(30)	113.3071	
			O(39)-Co(32)-N(16)	136.8934	
			O(39)-Co(32)-N(28)	71.5159	
			O(39)-Co(32)-N(11)	84.0389	
			N(30)-Co(32)-N(16)	94.6027	
			N(30)-Co(32)-N(28)	59.4005	
			N(30)-Co(32)-N(11)	149.8053	
			N(16)-Co(32)-N(28)	98.6275	
			N(16)-Co(32)-N(11)	87.3484	
			N(28)-Co(32)-N(11)	150.0385	
Ni-AXCPC2	N(45)-Ni(59)	1.8521	N(45)-Ni(59)-N(16)	76.0495	233.2716
	N(16)-Ni(59)	1.8306	N(45)-Ni(59)-N(40)	70.0498	(Kcal/mol)
	N(40)-Ni(59)	1.8245	N(45)-Ni(59)-N(11)	91.1137	
	N(11)-Ni(59)	1.8215	N(16)-Ni(59)-N(40)	130.7710	
			N(16)-Ni(59)-N(11)	88.8005	
			N(40)-Ni(59)-N(11)	125.6416	
Cu-AXCPC2	N(45)-Cu(59)	1.3338	N(45)-Cu(59)-N(16)	120.9419	170.8828
	N(16)-Cu(59)	1.3396	N(45)-Cu(59)-N(40)	88.8246	(Kcal/mol)
	N(40)-Cu(59)	1.8536	N(45)-Cu(59)-N(11)	101.1583	
	N(11)-Cu(59)	1.8509	N(16)-Cu(59)-N(40)	105.3507	
			N(16)-Cu(59)-N(11)	104.0951	
			N(40)-Cu(59)-N(11)	137.8060	

Table 25: Contd.

Selected bond lengths and bond energy parameters of metal complexes of AXCPC2 ligand

Complex	Atoms	Bond length (Å)	Atoms	Bond Angle (°)	Final Geom. Energy (Kcal/mol)
Zn-AXCPC2	O(59)-Zn(32)	1.8804	Zn(32)-O(59)-C(15)	133.3517	178.8377
	O(39)-Zn(32)	1.8931	O(59)-Zn(32)-O(39)	132.0569	(Kcal/mol)
	N(30)-Zn(32)	1.9458	O(59)-Zn(32)-N(30)	76.3639	
	N(16)-Zn(32)	1.9358	O(59)-Zn(32)-N(28)	148.0973	
	Zn(32)-N(28)	1.9576	O(59)-Zn(32)-N(16)	87.4666	
	Zn(32)-N(11)	2.0234	O(59)-Zn(32)-N(11)	76.0839	
			O(39)-Zn(32)-N(30)	89.7547	
			O(39)-Zn(32)-N(28)	67.9057	
			O(39)-Zn(32)-N(16)	139.5210	
			O(39)-Zn(32)-N(11)	90.0544	
			N(30)-Zn(32)-N(28)	79.6744	
			N(30)-Zn(32)-N(16)	111.4034	
			N(30)-Zn(32)-N(11)	142.4048	
			N(28)-Zn(32)-N(16)	81.9590	
			N(28)-Zn(32)-N(11)	134.0984	
			N(16)-Zn(32)-N(11)	92.3833	

4.9 Antibacterial Sensitivity Study

The use of metals in the drug system, as an important chemotherapeutic agent, is the recent advances in pharmaceutical research (Wang & Chiu, 2008). Metals not only provide a template for synthesis, but they also introduce functionalities that enhance drug delivery vectors (Obaleye *et al.*, 2012). The pure metals are considered, biologically inactive. However, the activity of metal cations depends upon their bioavailability and the presence of bio-ligands (Farag *et al.*, 2013). Many organic drugs require interaction with metals for their better activity (Anacona & Diaz, 2008; Dyson, 2010). It is therefore of great interest to investigate antibacterial potency of Schiff base transition metal complexes against bacterial pathogens. So, an attempt to investigate the advancement of antibacterial activity has been carried with novel Schiff base ligands and their metal complexes.

A general survey of the experimental results of the antibacterial efficacy study revealed remarkable enhancement of activity of the ligands and metal complexes against all the bacterial pathogens. The antibacterial agents perform an action to bacterial pathogens by various mechanistic pathways, either by blocking the protein synthesis or by breaking cell wall causing the death of the organisms (Aruguete *et al.*, 2013). In the metal complexes, there is the greater extent of dispersal of positive charge of the metal ions in the chelate ring and reduces the polarity of the metal atoms. This dispersal of charge is supported by the presence of donor atoms of the ligand, after chelation. This is called Tweedy's chelation theory and this is supposed to be the convincing cause for the increased activity of the metal complexes (Anacona *et al.*, 2014; Sathya *et al.*, 2010; Sumathi & Halli, 2014). Chelation provides stability as well as increase the lipophilicity of the complexes, which favors its permeation through the lipid layers of the bacterial membranes. Chelate complexes deactivate various cellular enzymes and disturb the metabolic pathways of organisms (Shukla, 2016). Various physical properties of the complexes have been affected by the presence of metal ions and may also increase their biological activity. In our study, the experiments were conducted with clinical (Laboratory collection) strains of both gram-positive and gram-negative bacteria and the growth inhibition data was found varied in the separate experiments by the interaction with some similar compounds.

4.9.1 Antibacterial Sensitivity Study of KMAXC and metal complexes

For this investigation, four clinical strains of bacterial pathogens have been selected for their *in vitro* interaction with prepared KMAXC ligand and its metal complexes. Such bacterial pathogens were *E. coli, B. subtilis, S. aureus and K. pneumoniae*. Comparison of the inhibition zone was recorded relative to the control drug gentamicin and negative control as DMSO. The solution of the compounds was made in DMSO which exhibits no bacterial growth inhibition. The antibacterial activity results are presented in the Table 26. The results are quite promising. The prescription of the antimicrobial results shown graphically (Figure 91) reveals that they exhibited moderate to better antibacterial activity. Further, the metal complexes (Co-KMAXC, Cu-KMAXC & Zn-KMAXC) were found to possess higher antibacterial activity than the parent Schiff base KMAXC. Based on Tweedy's chelation theory, the increased lipophilicity enhances the penetration of complexes into the lipid membranes and blocks the metal binding sites in enzymes of microorganisms. These complexes also disturb the respiration process of the cell by deactivating enzymes responsible for this and thus block the synthesis of proteins, which restricts further growth of the organism. The potential activity of the complexes against bacterial pathogens may be related to cell wall structure of the bacteria which possibly occurs due to inhibition of synthesis step of the peptidoglycan layer of the bacterial cell wall (Mingeot-Leclercq & Décout, 2016; Rodríguez-Hernández, 2017). The data revealed that the activity of KMAXC enhanced on complexation comparable to the standard used. Overall comparison of observed data puts information that metal complexes are more active than KMAXC ligand against all the bacteria. Specifically, Zn-KMAXC has shown better antibacterial potency against *S. aureus*.

Table 26: Antibacterial activity of KMAXC Schiff base ligand and metal complexes

	Diameter of zone of inhibition in mm			
Compounds	*E. coli*	*B. subtilis*	*S.aureus*	*K. pneumoniae*
KMAXC	12	14	11	10
Co-KMAXC	11	15	16	14
Cu-KMAXC	18	15	17	13
Zn-KMAXC)	19	17	19	15
Control (Gentamycin)	20	24	19	21
DMSO	0	0	0	0

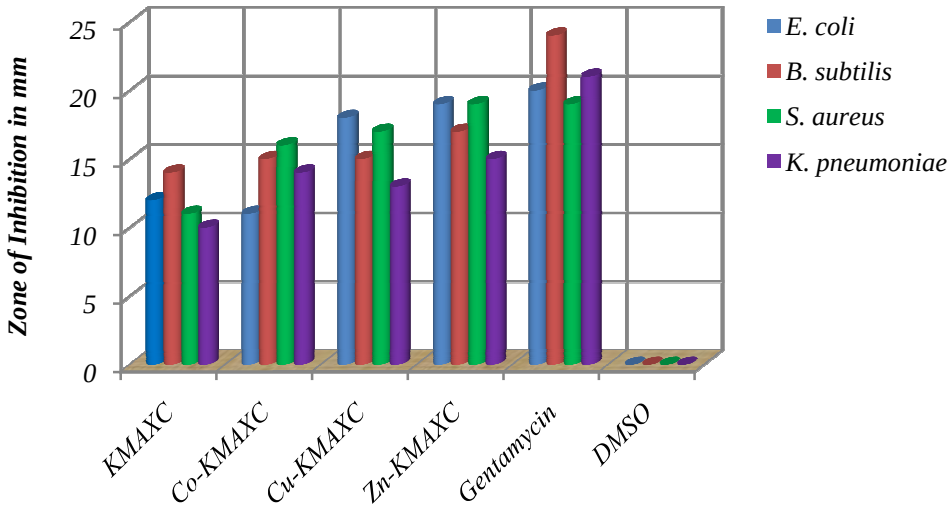

Figure 91: Bar graph showing antibacterial activity of KMAXC ligand and its metal complexes

4.9.2 Antibacterial Sensitivity Study of AXCPC3 and Metal Complexes

In this investigation, four clinical strains of bacterial pathogens *viz. E. coli, P. vulgaris, K. pneumoniae and S. aureus* have been selected for their *in vitro* interaction with prepared AXCPC3 ligand and its metal complexes. Growth inhibition zone of the prepared compounds was compared with the control drug amikacin (30 µg/disc) and parent drug amoxicillin. The solution of the compounds was made in DMSO which exhibited no bacterial growth inhibition and used as negative control.

The antibacterial results are presented in the Table 27. The results report biologically active nature of AXCPC3 ligand and its metal complexes such as Co-AXCPC3, Ni-AXCPC3, Cu-AXCPC3 & Zn-AXCPC3, with significantly enhanced antibacterial activity. Cu-AXCPC3 has shown little activity against all the bacterial pathogens compared to AXCPC3 and other metal complexes. The AXCPC3 delivers activity even greater than parent drug amoxicillin and control drug amikacin. Moreover, the complexes deliver better antibacterial activity at their higher concentration. Two different concentrations (100 & 50 µg/µL) of the compounds have been selected for antibacterial assay. Precise observation reveals that the compounds are less active against *S. aureus* and more active against *E. coli* and *P. vulgaris* bacteria. This enhanced activity may be attributed due to chelation of Schiff base with metal ions that provide stability and more susceptibility bacteriostatic effect against the bacterial pathogens (Al-Amiery *et al.*, 2012; Jesmin *et al.*, 2008). It has been suggested that the structural components possessing additional C=N bond with nitrogen and oxygen donor systems inhibit enzyme activity due to their deactivation by metal coordination. This permits their efficient permeation through the lipid layer of organisms and destroys their activity (Bagihalli *et al.*, 2008). Comparative bar graph of antibacterial sensitivity study has presented in the Figures 92 & 93.

Table 27: Antibacterial activity activity of AXCPC3 Schiff base ligand and metal complexes

Compounds	Diameter of zone of inhibition in mm							
	E. coli		*K. pneumoniae*		*P. vulgaris*		*S. aureus*	
Concentration (µg/µL)	100	50	100	50	100	50	100	50
AXCPC3	26	10	15	9	24	12	15	13
Co-AXCPC3	24	12	16	11	21	15	13	10
Ni-AXCPC3	23	10	12	8	20	16	14	13
Cu-AXCPC3	12	8	10	8	11	9	9	8
Zn-AXCPC3	22	0	11	0	18	12	8	7
Amox.	25	0	14	12	18	16	11	11
Amk.	21	21	18	18	17	17	17	17
DMSO	0	0	0	0	0	0	0	0

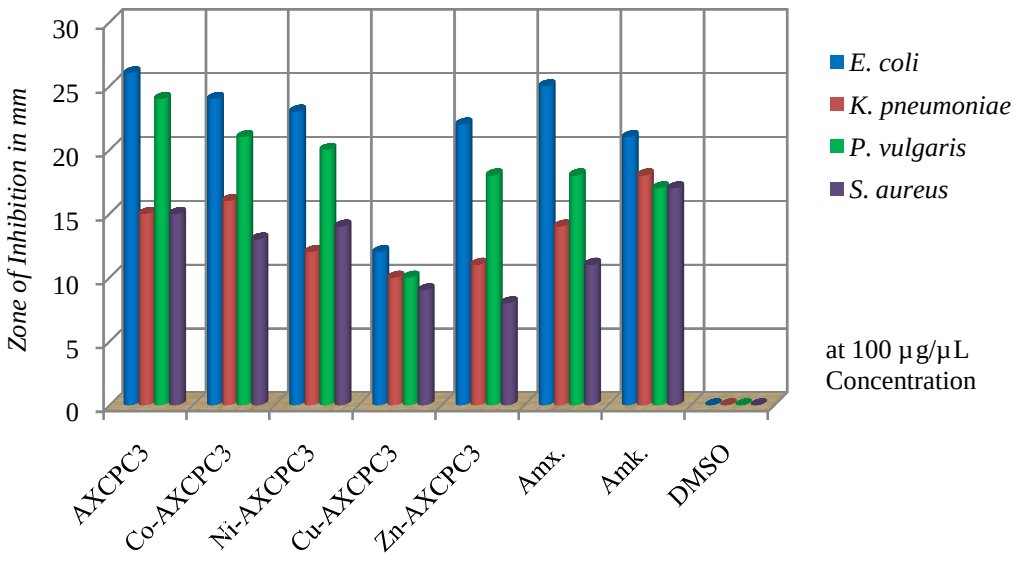

Figure 92: Bar graph showing antibacterial activity of AXCPC3 ligand and its metal complexes at 100 µg/µL concentration

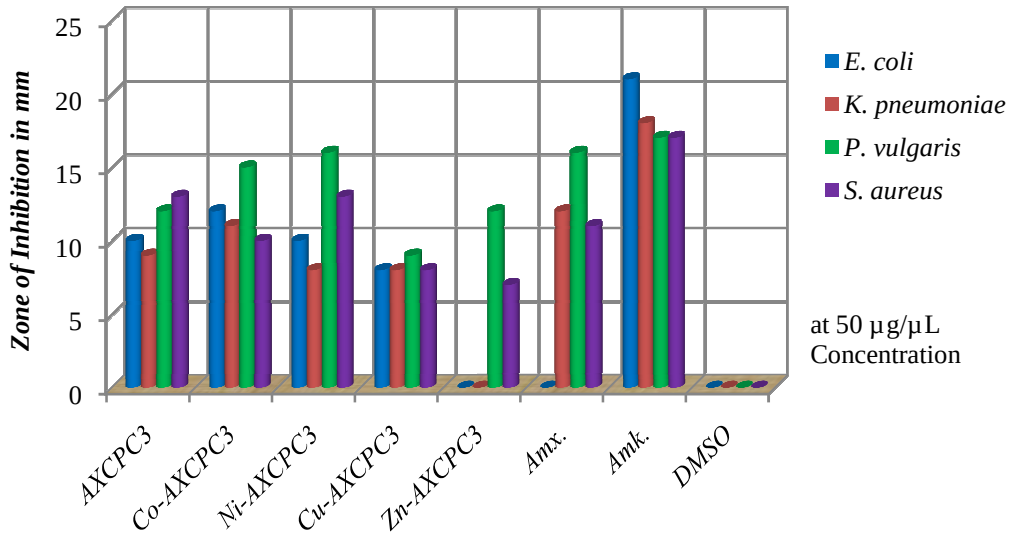

Figure 93: Bar graph showing antibacterial activity of AXCPC3 Schiff base ligand and metal complexes at 50 µg/µL concentration

4.9.3 Antibacterial Sensitivity Study of AXCPC2 and Metal Complexes

The AXCPC2 ligand and its metal complexes under this category were tested for *in vitro* to access their growth inhibitory activity against *E. coli*, *K. pneumonia, P. vulgaris* and *S. aureus* bacterial pathogens by the standard Kirby Bauer paper disc diffusion method (Abdel Aziz *et al.*, 2012; Nair *et al.*, 2012). Three different concentrations of the compounds (100, 50 and 25 µg/µL) have been used for this purpose and the growth inhibitory data are summarized in the Table 28. Amoxicillin with different concentrations was used as reference standard to compare the growth inhibition zone with synthesized complexes. The amikacin 30 µg per disc was used as control drug to compare the relative antibacterial activity of the complexes. The antibacterial results are presented in the bar graphs Figures 94 - 96. The results declare significant antibacterial activity of AXCPC2 ligand relative to parent drug amoxicillin. All the metal complexes deliver better antibacterial activity at higher concentration and they deliver considerable activity at lower concentrations. The Co-AXCPC2 complex is found less active with all the bacterial pathogens except *S. aureus* bacteria. At 25 µg/µL concentration, the Co-AXCPC2 complex is found almost resistant to *E. coli, P. vulgaris,* and *K. pneumoniae* bacteria. However, Ni-AXCPC2 and Cu-AXCPC2 complexes showed better antibacterial activity. The Zn-AXCPC2 complex also delivers considerable activity at higher concentration. The computed antibacterial data concludes greater inhibitory effect of ligand and metal complexes with *P. vulgaris* and *S. aureus* bacteria. The antibacterial activity of the metal chelates can be explained by overtone concept and the Tweedy chelation theory. The variation in the activity of complex against different organisms depends either on the impermeability of the microbial cells or difference in ribosomal parts of the organisms (Abu Ali *et al.*, 2015; Chaturvedi & Kamboj, 2016; Hasan *et al.*, 2016; Manimaran *et al.*, 2011).

Table 28: Antibacterial activity of AXCPC2 Schiff base ligand and metal complexes

Compounds	Diameter of zone of inhibition in mm											
	E. coli			*K. pneumoniae*			*P. vulgaris*			*S. aureus*		
Concentration (µg/µL)	100	50	25	100	50	25	100	50	25	100	50	25
AXCPC2	24	18	17	11	10	10	13	11	10	23	14	12
Co-AXCPC2	11	0	0	15	11	0	10	8	0	19	13	10
Ni-AXCPC2	14	13	12	15	11	0	12	11	8	16	14	14
Cu-AXCPC2	14	14	12	19	14	11	15	14	13	20	19	19
Zn-AXCPC2	12	0	0	14	11	0	15	14	12	18	18	18
Amoxicillin	24	15	12	14	12	8	18	16	10	19	15	14
Amikacin	20	20	20	18	18	18	27	27	27	26	26	26
MeOH	0	0	0	0	0	0	0	0	0	0	0	0

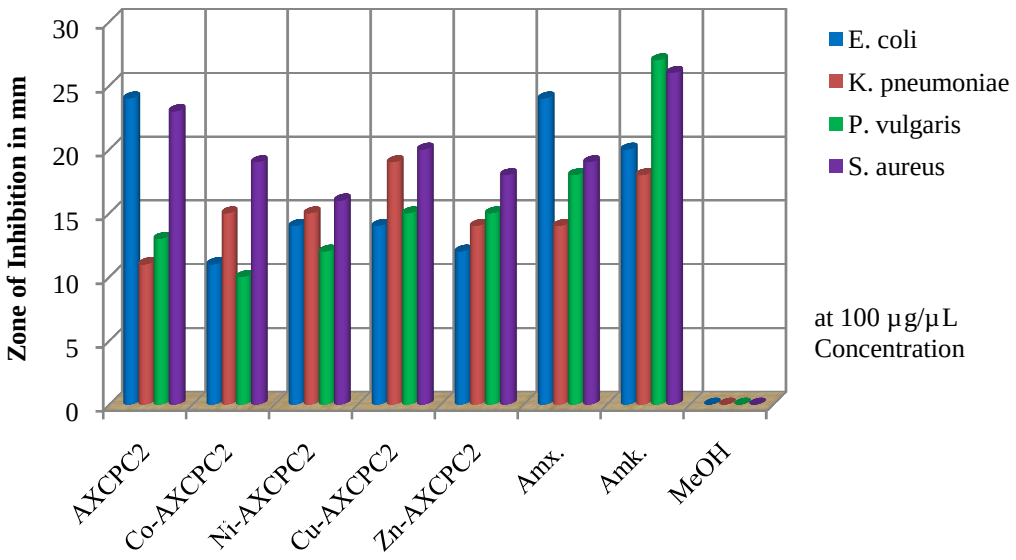

Figure 94: Bar graph showing antibacterial activity of AXCPC2 Schiff base ligand and metal complexes at 100 µg/µL concentration

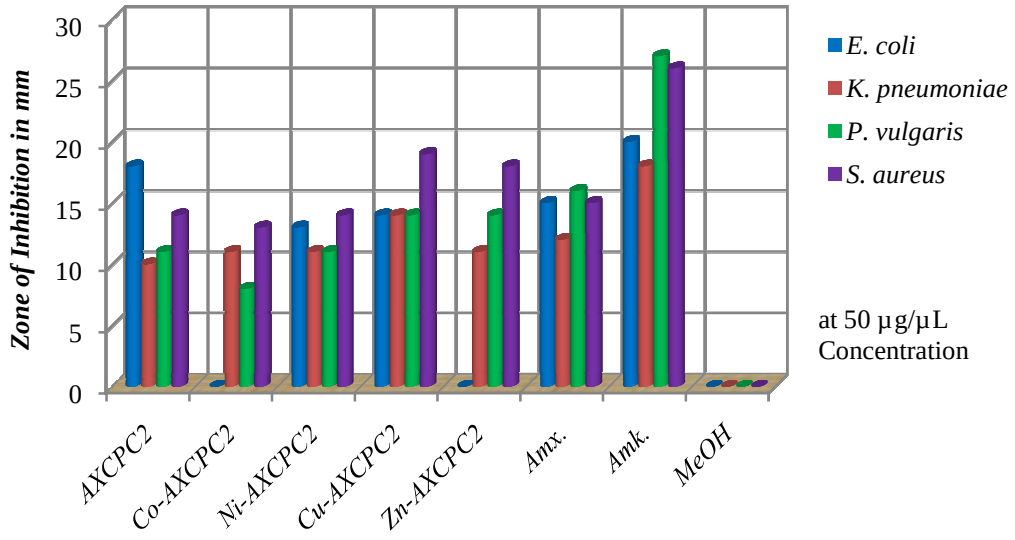

Figure 95: Bar graph showing antibacterial activity of AXCPC2 Schiff base ligand and metal complexes at 50 µg/µL concentration

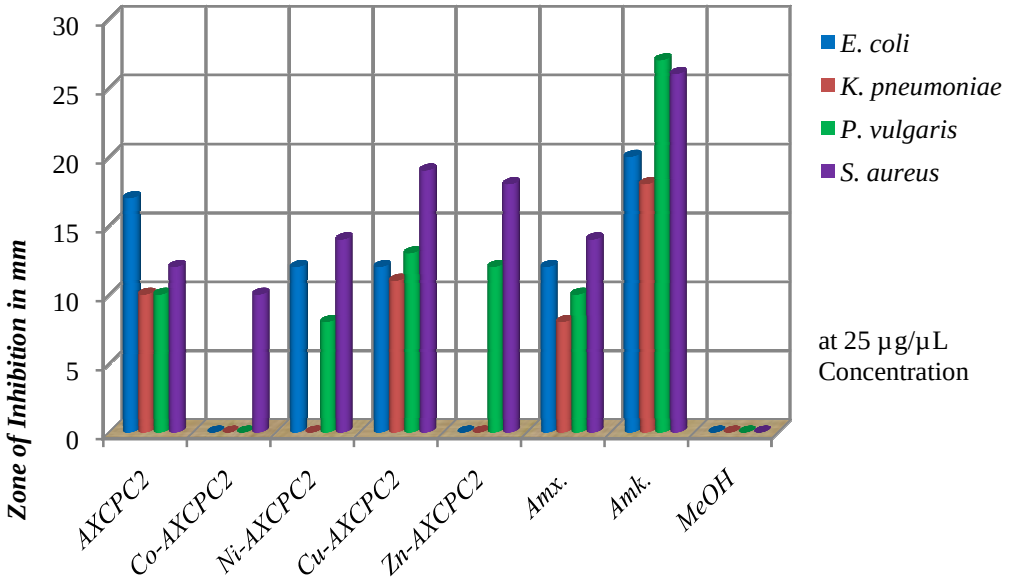

Figure 96: Bar graph showing antibacterial activity of AXCPC2 Schiff base ligand and metal complexes at 25 µg/µL concentration

CHAPTER 5

CONCLUSION AND RECOMMENDATION

The Schiff bases belong to a highly remarkable class of ligands in coordination chemistry. Simple synthetic procedure and easy coordination with metals for the formation of complexes are considered the distinctiveness of the compounds. They have gained increasing attention in recent years due to their versatile applications in various fields such as medicine, catalysis, electronics, industrial and material science. In our work, the metal complexes of Schiff bases of kanamycin and amoxicillin derivatives have focused on observing the pharmacological potency in terms of *in vitro* antibacterial evaluation test. Details of the studies on synthesis, spectral characterization, thermal, powder XRD study, the surface morphological study by SEM analysis and antibacterial evaluation by disc diffusion technique of the Schiff bases and metal complexes are presented in this thesis.

5.1 Conclusion

Growing interest in the success of metal-based drugs as chemotherapeutic agents is the basic foundation of Schiff base research. The Schiff bases and their metal complexes are the promising materials in medicinal chemistry, as most of them have biological functions. Besides of the biological interest, their applications in other fields as in the electronic field, material science and in very broad fields of chemistry, give an impetus of this investigation. The present investigation has devoted for the synthesis of three types of Schiff base ligands, KMAXC, AXCPC2, and AXCPC3. They have interacted with Co(II), Ni(II), Cu(II) and Zn(II) ions for the formation of their metal complexes. The maximum availability of donor atoms of the Schiff base ligands has made their successful coordination with metal ions. The nitrogen atom of azomethine linkage of Schiff base ligand is a core part, whose presence changes the physicochemical profile of the molecules. The legation of Schiff base ligands with metal ions further changes their various properties.

In the present thesis, the manuscript of the synthesis of various kinds of Schiff base ligands and their metal complexes has been documented in the proper sections and they have been characterized by various physical and spectral techniques, like CHNS analysis, conductivity measurement, FT-IR, ^{1}H & ^{13}C NMR, ESI-MS, electronic absorption and EPR studies. Their structure characterization has been further validated by XRPD, TGA/DTA, and molecular modeling studies. The surface morphology, which informs about the surface structure as well as crystalline structure, has been authenticated by SEM analysis study. A most illuminating part of the work is the antibacterial activity study which has been accomplished by disc diffusion technique.

Structural analysis of all the Schiff base ligands and metal complexes, by applying spectral techniques has revealed the participation of nitrogen atom of azomethine group in the legation process with metal ions. The IR absorption data, as well as ^{1}H NMR data are in support of this fact. Molar conductivity values of the compounds fall below 100 μSiemen/cm range and this has recommended non-electrolytic nature of the complexes. The electronic absorption and EPR data nicely support the concerned geometry of the complexes. This has been further assisted by molecular modeling study. The powder XRD data of the complexes and the particle size calculation through Scherrer's formula revealed their nanocrystalline nature.

In our work, the antibacterial activity study of all the synthesized ligands and complexes, against the clinical strains of bacterial pathogens, show remarkable inhibition growth. The metal complexes of KMAXC Schiff base ligands show higher bacterial inhibition growth compared to free Schiff base ligand. Moreover, the complexes delivered strong antibacterial sensitivity against *S. aureus* bacterial pathogens. This study with AXCPC3 Schiff base ligand and metal complexes also revealed the strong antibacterial potency against all the bacterial pathogens at their higher concentration. For this class of compounds, antibacterial study had been conducted at 100 and 50 μg/μL concentrations. Furthermore, AXCPC3 ligand showed greater potency than parent drug amoxicillin and control drug amikacin. This greater activity might be due to azomethine linkage and heteroatoms present in these compounds. A similar study with AXCPC2 Schiff base ligand and metal complexes also revealed better antibacterial activity. Here the study has conducted with three

different concentrations of the ligand and metal complexes. The Co-AXCPC2 complex was found less active with all the bacterial pathogens except *S.aureus* bacteria.

5.2 Recommendation

Research is a continuous process and the following objectives are planned for the future studies.

- To explore the MIC measurement of synthesized Schiff base ligands and metal complexes.
- To investigate their antioxidant, antifungal and anticancer activities.
- To obtain single crystal for all the Schiff base ligands and metal complexes and to explore their crystal structures.
- To investigate the *in vivo* antibacterial study of the compounds.
- To investigate the catalytic, surfactant and electrochemical studies of the compounds.

CHAPTER 6

SUMMARY

The thesis has documented in six chapters. These are briefly summarized as follows:

Chapter 1 presents a general introduction and chemistry of Schiff bases and their metal complexes with cobalt(II), nickel(II), copper(II) and zinc(II). The discussion on the synthetic design and various biological applications of the Schiff bases and metal complexes are presented. The structure and chemical information of the precursor compounds such as aminoglycoside (kanamycin), β-lactam antibiotic (amoxicillin) and pyridine carbaldehyde derivatives are also presented. Biometals in trace amount are essential for the regulation of metabolic activities in livings. Chemistry and biology of such metallo-elements are briefly described in this chapter. The objectives and scope of the present work are highlighted at the end of this chapter.

Chapter 2 deals the detailed literature review of the relevant work which is essential to authenticate the research. Here the literature has reviewed on the basis of various potential applications of the Schiff base and metal complexes.

Details regarding the materials used in the current study and various characterization methods used to study the synthesized ligands and metal complexes are presented in chapter 3. Experimental details for the synthesis and characterization of the Schiff bases and metal complexes are included in this chapter. The procedure used for carrying out antibacterial studies and the organism information has briefly described here.

Chapter 4 presents details of results and discussion of the experimental work. This is considered skeletal part of the thesis. The proposed molecular geometry of the Schiff base ligands and metal complexes is portrayed in this chapter. The spectral characterizations, thermal decomposition, Powder XRD, scanning electron

microscopy study and molecular modeling data have analyzed and the results have computed and discussed in this chapter. Tables and figures representing the analyzed data are positioned at the proper places in the text of this chapter. The antibacterial evaluation data of the synthesized Schiff bases and metal complexes are highlighted at the end.

.In chapter 5, the conclusion of the research work has documented. The future prospects and recommendations for the continuation of present research work are highlighted.

Chapter 6 presents a brief summary of all the chapters of the thesis.

REFERENCES

Abdallah, S. M., Mohamed, G. G., Zayed, M. A., & Abou El-Ela, M. S. (2009). Spectroscopic study of molecular structures of novel Schiff base derived from o-phthaldehyde and 2-aminophenol and its coordination compounds together with their biological activity. *Spectrochimica Acta. Part A, Molecular and Biomolecular Spectroscopy*, *73*, 833–840. doi:10.1016/j.saa.2009.04.005

Abdallah, S. M., Zayed, M. A., & Mohamed, G. G. (2010). Synthesis and spectroscopic characterization of new tetradentate Schiff base and its coordination compounds of NOON donor atoms and their antibacterial and antifungal activity. *Arabian Journal of Chemistry*, *3*, 103–113. doi:10.1016/j.arabjc.2010.02.006

Abdel-Rahman, L. H., Abu-Dief, A. M., Adam, M. S. S., & Hamdan, S. K. (2016). Some New Nano-sized Mononuclear Cu(II) Schiff Base Complexes: Design, Characterization, Molecular Modeling and Catalytic Potentials in Benzyl Alcohol Oxidation. *Catalysis Letters*, *146*, 1373-1396. doi: 10.1007/s10562-016-1755-0

Abdel-Rahman, L. H., Abu-Dief, A. M., Ismael, M., Mohamed, M. A. A., & Hashem, N. A. (2016). Synthesis, structure elucidation, biological screening, molecular modeling and DNA binding of some Cu(II) chelates incorporating imines derived from amino acids. *Journal of Molecular Structure, 1103*, 232–244. doi: 10.1016/j.molstruc.2015.09.039

Abdel-Rahman, L. H., Abu-Dief, A. M., Moustafa, H., & Hamdan, S. K. (2016). Ni(II) and Cu(II) complexes with ONNO asymmetric tetradentate Schiff base ligand: synthesis, spectroscopic characterization, theoretical calculations, DNA interaction and antimicrobial studies, *Applied Organometallic Chemistry, 31,* e3555. doi: 10.1002/aoc.3555

Abdel Aziz, A. A., Salem, A. N. M., Sayed, M. A., & Aboaly, M. M. (2012). Synthesis, structural characterization, thermal studies, catalytic efficiency and

antimicrobial activity of some M(II) complexes with ONO tridentate Schiff base N-salicylidene-o-aminophenol (saphH2). *Journal of Molecular Structure*, *1010*, 130–138. doi: 10.1016/j.molstruc.2011.11.043

Abou-Hussein, A. A., & Linert, W. (2014). Synthesis, spectroscopic, coordination and biological activities of some organometallic complexes derived from thio-Schiff base ligands. *Spectrochimica Acta. Part A, Molecular and Biomolecular Spectroscopy*, *117*, 763–771. doi: 10.1016/j.saa.2013.06.078

Abu-Dief, A. M., & Mohamed, I. M. A. (2015). A review on versatile applications of transition metal complexes incorporating Schiff bases. *Beni-Suef University Journal of Basic and Applied Sciences*, *4*, 119–133. doi: 10.1016/j.bjbas.2015.05.004

Abu Ali, H., Fares, H., Darawsheh, M., Rappocciolo, E., Akkawi, M., & Jaber, S. (2015). Synthesis, characterization and biological activity of new mixed ligand complexes of Zn(II) naproxen with nitrogen based ligands. *European Journal of Medicinal Chemistry*, *89*, 67–76. doi: 10.1016/j.ejmech.2014.10.032

Ahmed, S. K., & Khaled, S. (2015). Syntheses, spectral characterization, thermal properties and DNA cleavage studies of a series of Co(II), Ni(II) and Cu(II) polypyridine complexes with some new schiff-bases derived from 2-chloro ethyl amine. *Canadian Chemical Transactions*, *3*, 207–224. doi: 3179/canchemtrans.2015.03.02.0190

Al-Amiery, A. A., Al-Majedy, Y. K., Ibrahim, H. H., & Al-Tamimi, A. A. (2012). Antioxidant, antimicrobial, and theoretical studies of the thiosemicarbazone derivative Schiff base 2-(2-imino-1-methylimidazolidin-4-ylidene)hydrazinecarbothioamide (IMHC). *Organic and Medicinal Chemistry Letters*, *2*. doi: 10.1186/2191-2858-2-4

Al-Resayes, S. I. (2010). Kinetics analysis for non-isothermal decomposition γ-irradiated indium acetate. *Arabian Journal of Chemistry*, *3*, 191–194. doi: 10.1016/j.arabjc.2010.04.010

Al-Sha'alan, N. H. (2007). Antimicrobial activity and antimicrobial activity and

spectral, magnetic and thermal studies of some transition metal complexes of a Schiff base hydrazone containing a quinoline moiety. *Molecules*, *12*, 1080–1091. Retrieved from ncbi.nlm.nih.gov/pubmed/17873842

Altaf, A. A., Shahzad, A., Gul, Z., Rasool, N., Badshah, A., Lal, B., & Khan, E. (2015). A review on the medicinal importance of pyridine derivatives. *Journal of Drug Design and Medicinal Chemistry*, *1*, 1–11. doi: 10.11648/J.JDDMC.20150101.11

Amer, S., El-Wakiel, N., & El-Ghamry, H. (2013). Synthesis, spectral, antitumor and antimicrobial studies on Cu(II) complexes of purine and triazole Schiff base derivatives. *Journal of Molecular Structure*, *1049*, 326–335. doi: 10.1016/j.molstruc.2013.06.059

Aminov, R. I. (2010). A brief history of the antibiotic era: Lessons learned and challenges for the future. *Frontiers in Microbiology*, *1*, 1–7. doi: 10.3389/fmicb.2010.00134

Anacona, J. R., Calvo, J., & Almanza, O. A. (2013). Synthesis, spectroscopic, and magnetic studies of mono- and polynuclear Schiff base metal complexes containing salicylidene-cefotaxime ligand. *International Journal of Inorganic Chemistry*, *2013*. doi: 10.1155/2013/108740

Anacona, J. R., & Diaz, J. (2008). Synthesis, characterization and superoxide dismutase activity of the manganese(II) mixed ligand complexes containing sulphathiazole. *Journal of the Chilean Chemical Society*, 53, 1702–1704. doi: 10.4067/S0717-97072008000400014

Anacona, J. R., & Lopez, M. (2012). Mixed-ligand nickel(II) complexes containing sulfathiazole and cephalosporin antibiotics: synthesis, characterization, and antibacterial activity. *International Journal of Inorganic Chemistry*, *2012*, 1–8. doi: 10.1155/2012/106187

Anacona, J. R., Luis, J., & Camus, J. (2014). Synthesis, characterization and antibacterial activity of a Schiff base derived from cephalexin and sulphathiazole and its transition metal complexes. *Spectrochimica Acta. Part A, Molecular and*

Biomolecular Spectroscopy, *129*, 96–102. doi: 10.1016/j.saa.2014.03.019

Anacona, J. R., Noriega, N., & Camus, J. (2015). Synthesis, characterization and antibacterial activity of a tridentate Schiff base derived from cephalothin and sulfadiazine, and its transition metal complexes. *Spectrochimica Acta - Part A: Molecular and Biomolecular Spectroscopy*, *137*, 16–22. doi: 10.1016/j.saa.2014.07.091

Anand, P., Patil, V. M., Sharma, V. K., Khosa, R. L., & Masand, N. (2012). Schiff bases: A review on biological insights. *International Journal of Drug Design and Discovery*, *3*, 851–868.

Anis, I., Afza, N., Aslam, M., Noreen, Z., Hussain, A., Hussain, M. T., Sherazi, T. A., & Shah, M. R. (2013). Synthesis, characterization, antimicrobial and cytotoxic evaluation of a bidentate Schiff base ligand: {5-Chloro-2-[(4-nitrobenzylidene)amino]phenyl}(phenyl)methanone and its transition metal(II) complexes. *Journal of Chemical Society of Pakistan*, *35*, 1508–1515.

Aouniti, A., Elmsellem, H., Tighadouini, S., Elazzouzi, M., Radi, S., Chetouani, A., Hammouti, B., Zarrouk, A. (2016). Schiff's base derived from 2-acetyl thiophene as corrosion inhibitor of steel in acidic medium. *Journal of Taibah University for Science*, *10*, 774–785. doi: 10.1016/j.jtusci.2015.11.008

Aruguete, D. M., Kim, B., Hochella, M. F., Ma, Y., Cheng, Y., Hoegh, A., Liu, J., & Pruden, A. (2013). Antimicrobial nanotechnology: its potential for the effective management of microbial drug resistance and implications for research needs in microbial nanotoxicology. *Environmental Science: Processes & Impacts*, *15*, 93-102. doi: 10.1039/c2em30692a

Asadi, Z., Asadi, M., Firuzabadi, F. D., & Shorkaei, M. R. (2014). New method in synthesis of nano uranyl(VI) Schiff base complexes: characterization and electrochemical studies. *Journal of Industrial and Engineering Chemistry*, *20*, 4227–4232. doi: 10.1016/j.jiec.2014.01.025

Aziz, A. A. A., Salem, A. N. M., Sayed, M. A., & Aboaly, M. M. (2012). Synthesis, structural characterization, thermal studies, catalytic efficiency and antimicrobial

activity of some M(II) complexes with ONO tridentate Schiff base N-salicylidene-o-aminophenol (saphH2) *Journal of Molecular Structure, 1010,* 130–138. doi: 10.1016/j.molstruc.2011.11.043

Bagihalli, G. B., Avaji, P. G., Patil, S. A., & Badami, P. S. (2008). Synthesis, spectral characterization, *in vitro* antibacterial, antifungal and cytotoxic activities of Co(II), Ni(II) and Cu(II) complexes with 1,2,4-triazole Schiff bases. *European Journal of Medicinal Chemistry, 43,* 2639–2649. doi: 10.1016/j.ejmech.2008.02.013

Bandmann, O., Weiss, K. H., & Kaler, S. G. (2015). Wilson's disease and other neurological copper disorders. *The Lancet Neurology, 14,* 103–113. doi: 10.1016/S1474-4422(14)70190-5

Barnham, K. J., & Bush, A. I. (2014). Biological metals and metal-targeting compounds in major neurodegenerative diseases. *Chemical Society Reviews, 43,* 6727–6749. doi: 10.1039/c4cs00138a

Bérdy, J. (2012). Thoughts and facts about antibiotics: where we are now and where we are heading. *The Journal of Antibiotics, 65,* 385–395. doi: 10.1038/ja.2012.27

Bharti, S. K., Patel, S. K., Nath, G., Tilak, R., & Singh, S. K. (2010). Synthesis, characterization, DNA cleavage and *in vitro* antimicrobial activities of copper(II) complexes of Schiff bases containing a 2,4-disubstituted thiazole. *Transition Metal Chemistry,* doi: 10.1007/s11243-010-9412-8

Bhowon, M. G., Li Kam Wah, H., Dosieah, A., Ridana, M., Ramalingum, O., & Lacour, D. (2004). Synthesis, characterization, and catalytic activity of metal Schiff base complexes derived from Pyrrole-2-carboxaldehyde. *Synthesis and Reactivity in Inorganic and Metal-Organic Chemistry, 34,* 1–16. doi: 10.1081/SIM-120027314

Biswas, S., Sarkar, D., Kundu, S., Roy, P., & Mondal, T. K. (2015). Rhodium(III)-triphenylphosphine complex with NNS donor thioether containing Schiff base ligand: Synthesis, spectra, electrochemistry and catalytic activity. *Journal of Molecular Structure, 1099,* 297–303. doi: 10.1016/j.molstruc.2015.06.065

Boer, J. L., Mulrooney, S. B., & Hausinger, R. P. (2013). Nickel-dependent metalloenzymes. *Archives of Biochemistry and Biophysics*, doi: 10.1016/j.abb.2013.09.002

Brodowska, K., & Łodyga-Chruscinska, E. (2014). Schiff bases – interesting range of applications in various fields of science. *CHEMIK*, *68*, 129–134.

Cabral, P. C., Da Silva Diniz, A., & Grande De Arruda, I. K. (2005). Vitamin A and zinc status in patients on maintenance haemodialysis. *Nephrology*, *10*, 459–463. doi: 10.1111/j.1440-1797.2005.00469.x

Cao, Y., Yi, C., Liu, H., Li, H., Li, Q., Yuan, Z., & Wei, G. (2016). Syntheses, crystal structures and *in vitro* anticancer activities of oxovanadium(IV) complexes of amino acid Schiff base and 1,10-phenanthroline ligands. *Transition Metal Chemistry*, *41*, 531-538. doi: 10.1007/s11243-016-0049-0

Carreño, A., Gacitúa, M., Páez-Hernández, D., Polanco, R., Preite, M., Fuentes, J. A., Mora, G. C., Chavez, I, & Arratia-Pérez, R. (2015). Spectral, theoretical characterization and antifungal properties of two phenol derivative Schiff bases with an intramolecular hydrogen bond. *New Journal of Chemistry*. doi: 10.1039/c5nj01469g

Ceyhan, G., Celik, C., Serhan, U., Ibrahim, D., Elmastas, M., & Tümer, M. (2011). Antioxidant, electrochemical, thermal, antimicrobial and alkane oxidation properties of tridentate Schiff base ligands and their metal complexes. *Spectrochimica Acta - Part A: Molecular and Biomolecular Spectroscopy*, *81*, 184–198. doi: 10.1016/j.saa.2011.05.106

Ceyhan, G., Köse, M., Tümer, M., Demirtaş, İ., Şahin Yağlioğlu, A., & McKee, V. (2013). Structural characterization of some Schiff base compounds: Investigation of their electrochemical, photoluminescence, thermal and anticancer activity properties. *Journal of Luminescence*, *143*, 623–634. doi: 10.1016/j.jlumin.2013.06.002

Chakraborty, A., Kumar, P., Ghosh, K., & Roy, P. (2010). Evaluation of a Schiff base copper complex compound as potent anticancer molecule with multiple targets of

action. *European Journal of Pharmacology*, *647*, 1–12. doi:10.1016/j.ejphar.2010.08.003

Chaturvedi, D., & Kamboj, M. (2016). Role of Schiff base in drug discovery research. *Chemical Sciences Journal, 7*. doi: 10.4172/2150-3494.1000e114

Chaudhary, N. K. (2013). Bio-coordination of Schiff base derived from amoxicillin trihydrate and pyrrole-2-carbaldehyde with Cu(II), Co(II) & Zn(II) ions: synthesis, characterization and antibacterial evaluation. *World Journal of Pharmacy and Pharmaceutical Sciences, 2*, 6016–6025.

Chaudhary, N. K., & Mishra, P. (2014). *In vitro* antimicrobial screening of metal complexes of Schiff base derived from streptomycin and amoxicillin: Synthesis, characterization and molecular modeling. *American Journal of Applied Chemistry*, *2*, 19–26. doi: 10.11648/j.ajac.20140201.15

Chaudhary, N. K., & Mishra, P. (2015). Spectral investigation and *in vitro* antibacterial evaluation of Ni^{II} and Cu^{II} complexes of Schiff base derived from amoxicillin and α-formylthiophene (αft). *Journal of Chemistry, 2015*. doi: 10.1155/2015/136285

Chaudhary, N. K., & Mishra P. (2015). Synthesis, structure delineation and antibacterial activity study of metal(II) complexes of Schiff base derived from kanamycin and methyl ester of amoxicillin. *International Research Journal of Pure and Applied Chemistry,* 7, 165–180. doi:10.9734/IRJPAC/2015/17013

Chaudhary, N. K., & Mishra P. (2017). Metal complexes of a novel Schiff base based on penicillin: characterization, molecular modeling, and antibacterial activity study. *Bioinorganic Chemistry and Applications*, 2017. doi:10.1155/2017/6927675

Chaudhary, N. K., & Mishra P. (2018). Bioactivity of some divalent M(II) complexes of penicillin based Schiff base ligand: synthesis, spectroscopic characterization, and thermal study. *Journal of Saudi Chemical Society*, *22*, 601-613. doi:10.1016/j.jscs.2017.10.003

Chen, W., Li, Y., Cui, Y., Zhang, X., Zhu, H.-L., & Zeng, Q. (2010). Synthesis,

molecular docking and biological evaluation of Schiff base transition metal complexes as potential urease inhibitors. *European Journal of Medicinal Chemistry*, *45*, 4473–4478. doi:10.1016/j.ejmech.2010.07.007

Claridge, T. D. (1999). *High-resolution NMR techniques in organic chemistry*. (First Edition). Tetrahedron organic chemistry series.

Coates, J. (2000). *Interpretation of Infrared Spectra, A practical approach.* encyclopedia of analytical chemistry, John Wiley & Sons Ltd, Chichester, 10815–10837.

Coats, A., & Redfern, J. P. (1963). Thermogravimetric analysis. *Analyst*, *88*.

Cozzi, P. G. (2004). Metal-salen Schiff base complexes in catalysis: practical aspects. *Chemical Society Reviews*, *33*, 410–421. doi: 10.1039/b307853c

Da Silva, C. M., Da Silva, D. L., Modolo, L. V., Alves, R. B., De Resende, M. A., Martins, C. V. B., & De Fátima, Â. (2011). Schiff bases: A short review of their antimicrobial activities. *Journal of Advanced Research*, *2*, 1–8. doi: 10.1016/j.jare.2010.05.004

Dey, D., Kaur, G., Ranjani, A., Gayathri, L., Chakraborty, P., Adhikary, J., Pasan, J., Dhanasekaran, D., Choudhury, R. A., Akbarsha, A. M., Kole, N., & Biswas, B. (2014). A trinuclear zinc–Schiff base complex: biocatalytic activity and cytotoxicity. *European Journal of Inorganic Chemistry*, doi: 10.1002/ejic.201402158

Dias, D. A., Urban, S., & Roessner, U. (2012). A historical overview of natural products in drug discovery. *Metabolites*, *2*, 303–336. doi:10.3390/metabo2020303

Doğan, F., Ulusoy, M., Öztürk, Ö. F., Kaya, İ., & Salih, B. (2009). Synthesis, characterization and thermal study of some tetradentate Schiff base transition metal complexes. *Journal of Thermal Analysis and Calorimetry*, *98* , 785–792. doi:10.1007/s10973-009-0205-2

Dyson, P. J. (2010). Metal-based drugs. *Australian. Journal of Chemistry*, *63*, 1503–

1504. doi: 10.1071/CH10382

Ebrahimi-Kahrizsangi, R., & Abbasi, M. H. (2008). Evaluation of reliability of Coats-Redfern method for kinetic analysis of non-isothermal TGA. *Transactions of Nonferrous Metals Society of China*, *18*, 217–221. doi: 10.1016/S1003-6326(08)60039-4

El-Baradie, K. Y., El-Wakiel, N. A., & El-Ghamry, H. A. (2014). Synthesis, characterization and corrosion inhibition in acid medium of L-histidine Schiff base complexes. *Applied Organometallic Chemistry*, *29*, 117-125. doi:10.1002/aoc.3255

El-Gammal, O. A., El-Reash, G. M. A., Yousef, T. A., & Mefreh, M. (2015). Synthesis, spectral characterization, computational calculations and biological activity of complexes designed from NNO donor Schiff-base ligand. *Spectrochimica Acta Part A: Molecular and Biomolecular Spectroscopy*, *146*, 163–176. doi:10.1016/j.saa.2015.01.043

El-Sherif, A. A., Shehata, M. R., Shoukry, M. M., & Barakat, M. H. (2012). Synthesis, characterization, equilibrium study and biological activity of Cu(II), Ni(II) and Co(II) complexes of polydentate Schiff base ligand. *Spectrochimica Acta. Part A, Molecular and Biomolecular Spectroscopy*, *96*, 889–897. doi:10.1016/j.saa.2012.07.047

Farag, A. M., Guan, T. S., Osman, H., Majid, A. M. S. A., Iqbal, M. A., & Ahamed, M. B. K. (2013). Synthesis of metal(II) [M = Cu, Mn, Zn] Schiff base complexes and their pro-apoptotic activity in liver tumor cells via caspase activation. *Medicinal Chemistry Research*, *22*, 4727–4736. doi:10.1007/s00044-013-0482-y

Farrell, N. (2002). Biomedical uses and applications of inorganic chemistry. An overview. *Coordination Chemistry Reviews*, *232*, 1–4. doi: 10.1016/S0010-8545(02)00100-5

Field, L. D., Sternhell, S., & Kalman, J. R. (2007). *Organic structures from spectra* (Fourth Edition). John Wiley and Sons Ltd.

Fosso, M. Y., Shrestha, S. K., Green, K. D., & Garneau-Tsodikova, S. (2015).

Synthesis and bioactivities of kanamycin B-derived cationic amphiphiles. *Journal of Medicinal Chemistry, 58,* 9124-9132. doi:10.1021/acs.jmedchem.5b01375

Gaber, M., El-Ghamry, H., Atlam, F., & Fathalla, S. (2015). Synthesis, spectral and theoretical studies of Ni(II), Pd(II) and Pt(II) complexes of 5-mercapto-1,2,4-triazole-3-imine-2′-hydroxynaphyhaline. *Spectrochimica Acta Part A: Molecular and Biomolecular Spectroscopy*, *137*, 919–929. doi:10.1016/j.saa.2014.09.015

Garcia-Migura, L., Sunde, M., Karlsmose, S., Veldman, K., Schroeter, A., Guerra, B., Granier, S. A., Perrin-Guyomard, A., Gicquel-Bruneau, M., Franco, A., Englumd, S., Teale, C., heiska, H., Clemente, L., Boerlin, P., Moreno, M. A., Daignault, D., Mevius, D., Hendriksen, R. S., & Aarestrup, F. M. (2011). Establishing streptomycin epidemiological Cut-Off values for *Salmonella* and *Escherichia coli*. *Microbial Drug Resistance, 18,* 88-93, doi:10.1089/mdr.2011.0064

Geddes, A. M., Klugman, K. P., & Rolinson, G. N. (2007). Introduction: historical perspective and development of amoxicillin/clavulanate. *International Journal of Antimicrobial Agents, 30S,* S109–S112. doi:10.1016/j.ijantimicag.2007.07.015

Ghosh, A. K., Mitra, M., Fathima, A., Yadav, H., Choudhury, A. R., Nair, B. U., & Ghosh, R. (2016). Antibacterial and catecholase activities of Co(III) and Ni(II) Schiff base complexes. *Polyhedron*, *107*, 1–8. doi:10.1016/j.poly.2016.01.015

Gibson, D. (2016). Platinum(IV) anticancer prodrugs - hypotheses and facts. *Dalton Transactions, 45,* 12983-12991, doi:10.1039/C6DT01414C

Grivani, G., Tahmasebi, V., Khalaji, A. D., Eigner, V., & Dušek, M. (2014). Synthesis, characterization, crystal structure, catalytic activity in oxidative bromination, and thermal study of a new oxidovanadium Schiff base complex containing O, N-bidentate Schiff base ligand. *Journal of Coordination Chemistry*, *67,* 3664-3677, doi:10.1080/00958972.2014.960405

Haas, K. L., & Franz, K. J. (2009). Application of metal coordination chemistry to explore and manipulate cell biology. *Chemical Reviews*, *109*, 4921–4960. doi:

10.1021/cr900134a

Hafner, B. (2007). Scanning Electron Microscopy Primer. *Cities*, 1–29.

Hamak, K., & Eissa, H. (2013). Synthesis, characterization, biological evaluation and anti corrosion activity of some heterocyclic compounds oxazepine derivatives from Schiff bases. *Organic Chemistry Current Research*, *2*. doi:10.4172/2161-0401.1000121

Hameed, A., Al-Rashida, M., Uroos, M., Ali, S. A., & Khan, K. M. (2017). Schiff bases in medicinal chemistry: a patent review (2010-2015). *Expert Opinion on Therapeutic Patents*, *27*, 63–79. doi:10.1080/13543776.2017.1252752

Hannon, M. J. (2007). Metal-based anticancer drugs: From a past anchored in platinum chemistry to a post-genomic future of diverse chemistry and biology. *Pure and Applied Chemistry*, *79*(12), 2243–2261. doi:10.1351/pac200779122243

Hasan, M. R., Hossain, M. A., Salam, M. A., & Uddin, M. N. (2016). Nickel complexes of Schiff bases derived from mono/diketone with anthranilic acid: synthesis, characterization and microbial evaluation. *Journal of Taibah University for Science*, doi:10.1016/j.jtsci.2015.11.007

Hecht, D. W. (2004). Prevalence of antibiotic resistance in anaerobic bacteria: worrisome developments. *Clinical Infectious Disease*, *39*, 92–97. doi: 10.1086/421558

Hien, B. T. T., Scheutz, F., Cam, P. D., Serichantalergs, O., Huong, T. T., Thu, T. M., & Dalsgaard, A. (2008). Diarrheagenic *Escherichia coli* and Shigella strains isolated from children in a hospital case-control study in Hanoi, Vietnam. *Journal of Clinical Microbiology*, *46*, 996–1004. doi:10.1128/JCM.01219-07

Holm, R. H., Kennepohl, P., & Solomon, E. I. (1996). Structural and functional aspects of metal sites in biology. *Chemical Reviews*, *96*, 2239–2314. doi:10.1021/cr9500390

Imani, N., Behzad, M., Rudbari, H. A., Bruno, G., Samari Jahromi, H., & Khaleghian, A. (2015). Crystal structures, spectroscopic, electrochemical, and antibacterial

properties of a series of new copper(II) Schiff base complexes. *Journal of Coordination Chemistry*, *68*, 2296-2306, doi:10.1080/00958972.2015.1051476

Iqbal, M. S., Bukhari, I. H., & Arif, M. (2005). Preparation, characterization and biological evaluation of copper(II) and zinc(II) complexes with Schiff bases derived from amoxicillin and cephalexin. *Applied Organometallic Chemistry*, *19*, 864–869. doi:10.1002/aoc.918

Jabali, B., & Abu Ali, H. (2016). New zinc(II) complexes of the non-steroidal anti-inflammatory drug (indomethacin) and various nitrogen donor ligands. synthesis, characterization and biological activity. *Polyhedron*, *117*, 249–258. doi:10.1016/j.poly.2016.06.003

Jain, R. K., & Mishra, A. P. (2012). Microwave synthesis and spectral, thermal and antimicrobial activities of some novel transition metal complexes with tridentate Schiff base ligands. *Journal of the Serbian Chemical Society*, *77*, 1013–1029. doi:10.2298/JSC111001023J

Jana, S., Bhowmik, P., Das, M., Jana, P. P., Harms, K., & Chattopadhyay, S. (2012). Synthesis and characterisation of two double EE azido and thiocyanato bridged dimeric Cu(II) complexes with tridentate Schiff bases as blocking ligands. *Polyhedron*, *37*, 21–26. doi:10.1016/j.poly.2012.01.031

Jarrahpour, A. A., Motamedifar, M., Pakshir, K., Hadi, N., & Zarei, M. (2004). Synthesis of novel azo Schiff bases and their antibacterial and antifungal activities. *Molecules*, *9*, 815–824. Retrieved from http://www.ncbi.nlm.nih.gov/pubmed/18007481

Jayaseelan, P., Prasad, S., Vedanayaki, S., & Rajavel, R. (2016). Synthesis, characterization, anti-microbial, DNA binding and cleavage studies of Schiff base metal complexes. *Arabian Journal of Chemistry*, 9, S668-S677. doi:10.1016/j.arabjc.2011.07.029

Jeevadason, A. W., Murugavel, K. K., & Neelakantan, M. A. (2014). Review on Schiff bases and their metal complexes as organic photovoltaic materials. *Renewable and Sustainable Energy Reviews*, *36*, 220–227.

doi:10.1016/j.rser.2014.04.060

Jesmin, M., Ali, M. M., Salahuddin, M. S., Habib, M. R., & Khanam, J. A. (2008). Antibacterial activity of some Schiff bases derived from benzoin, salicylaldehyde, aminophenol and 2,4-dinitrophenyl Hydrazine. *Mycology*, *36*, 70–73. doi: 10.4489/MYCO.2008.36.1.070

Jia, Y., & Li, J. (2013). Molecular assembly of Schiff base interactions: construction and application. *Chemical Reviews*. doi:10.1021/cr400559g

Joshi, S. R., & Habib, S. I. (2014). Synthesis, spectral study of Ni(II) and Cu(II) metal ions with heterocyclic ligands. *International Journal of Drug Development & Research*, *6*, 32–38.

Justin Dhanaraj, C., & Johnson, J. (2014). Synthesis, characterization, electrochemical and biological studies on some metal(II) Schiff base complexes containing quinoxaline moiety. *Spectrochimica Acta - Part A: Molecular and Biomolecular Spectroscopy*, *118*, 624–631. doi:10.1016/j.saa.2013.09.007

Kaban, S., & Fidaner, Z. (1990). Synthesis of Schiff bases by condensation of hetarylearboxaldehydes with p-Phenetidine. *Monatshefte Fur Chemie*, *121*, 525–528. doi: 10.1007/BF00810861

Kajal, A., Bala, S., Kamboj, S., Sharma, N., & Saini, V. (2013). Schiff bases : A versatile pharmacophore. *Journal of Catalysts*, *2013*. doi:10.1155/2013/893512

Kalkandelen, S., Selimoglu, E., Erdogan, F., Ucuncu, H., & Altas, E. (2002). Comparative cochlear toxicities of streptomycin, gentamicin, amikacin and netilmicin in Guinea-Pigs. *Journal of International Medical Research*, *30*, 406–412. doi:10.1177/147323000203000407

Kareem, A., Laxmi, Arshad, M., Nami, S. A. A., & Nishat, N. (2016). Herbo-mineral based Schiff base ligand and its metal complexes: synthesis, characterization, catalytic, potential and biological applications. *Journal of Photochemistry and Photobiology B: Biology*, *160*, 163–171. doi: 10.1016/j.jphotobiol.2016.03.030

Kasselouri, S., Garoufis, A., Kalkanis, G., Perlepes, S. P., & Hadjiliadis, N. (1993).

Complexes of divalent transition metal chlorides with the tetradentate Schiff base ligand 1,2-bis(2'-pyridylmethyleneimino)-benzene. *Transition Metal Chemistry, 18* , 531–536. doi.org/10.1007/BF00136621

Kavitha, N., & Anantha Lakshmi, P. V. (2015). Synthesis, characterization and thermogravimetric analysis of Co(II), Ni(II), Cu(II) and Zn(II) complexes supported by ONNO tetradentate Schiff base ligand derived from hydrazino benzoxazine. *Journal of Saudi Chemical Society, 21,* S457-S466, doi 10.1016/j.jscs.2015.01.003

Kaya, İ., & Kamacı, M. (2012). Synthesis, optical, electrochemical, and thermal stability properties of poly(azomethine-urethane)s. *Progress in Organic Coatings*, *74*, 204–214. doi: 10.1016/j.porgcoat.2011.12.010

Kaya, İ., Kartal, E., & Şenol, D. (2015). Synthesis and characterization of polyphenol derived from Schiff bases containing methyl and carboxyl groups in the structure. *Designed Monomers and Polymers*, doi: 10.1080/15685551.2015.1041084

Keypour, H., Liyaghati-Delshad, M., Rezaeivala, M., & Bayat, M. (2014). Synthesis, characterization, antibacterial activities and theoretical studies of Mn(II) and Cd(II) complexes with new macrocyclic Schiff base ligands incorporating a phenanthroline head unit. *Journal of the Iranian Chemical Society*, *12,* 621-630. doi: 10.1007/s13738-014-0520-9

Khan, M. I., Khan, A., Hussain, I., Khan, M. A., Gul, S., Iqbal, M., Inayat-Ur-Rahman, & Khuda F. (2013). Spectral, XRD, SEM and biological properties of new mononuclear Schiff base transition metal complexes. *Inorganic Chemistry Communications*, *35*, 104–109. doi: 10.1016/j.inoche.2013.06.014

Kianfar, A. H., Farrokhpour, H., Dehghani, P., & Khavasi, H. R. (2015). Experimental and theoretical spectroscopic study and structural determination of nickel(II) tridentate Schiff base complexes. *Spectrochimica Acta Part A: Molecular and Biomolecular Spectroscopy*, *150,* 220–229. doi: 10.1016/j.saa.2015.05.084

Kostova, I., & Saso, L. (2013). Advances in research of Schiff-base metal complexes as potent antioxidants. *Current Medicinal Chemistry, 20*, 4609–4632. doi: 10.2174/09298673113209990149

Krishnapriya, K. R., Saravanakumar, D., Arunkumar, P., & Kandaswamy, M. (2008). Synthesis of new oxamide-based ligand and its coordination behavior towards copper(II) ion: spectral and electrochemical studies. *Spectrochimica Acta - Part A: Molecular and Biomolecular Spectroscopy*, *69*, 1077–1081. doi: 10.1016/j.saa.2007.06.006

Kundu, S., Pramanik, A. K., Mondal, A. S., & Mondal, T. K. (2016). Ni(II) and Pd(II) complexes with new N,O donor thiophene appended Schiff base ligand: synthesis, electrochemistry, X-ray structure and DFT calculation. *Journal of Molecular Structure, 1116*, 1–8. doi: 10.1016/j.molstruc.2016.03.013

Lakshmipraba, J., & Arunachalam, S. (2010). Studies on the interactions of polymer-anchored copper(II) complexes with tRNA. *Transition Metal Chemistry, 35*, 477–482. doi: 10.1007/s11243-010-9352-3

Leelavathy, C., & Arulantony. (2013). Synthesis, spectral characterization and biological activity of metal(II) complexes with 4-aminoantipyrine derivatives. *Spectrochimica Acta. Part A, Molecular and Biomolecular Spectroscopy, 113*, 346-355. doi: 10.1016/j.saa.2013.04.055

Lewis, K. (2013). Platforms for antibiotic discovery. *Nature Reviews. Drug Discovery, 12*, 371–387. doi: 10.1038/nrd3975

Li, J. W.-H., & Vederas, J. C. (2009). Drug discovery and natural products: end of an era or an endless frontier? *Science, 325*, 161–165. doi: 10.1126/science.1168243

Liang, Z., Liu, Z., & Gao, Y. (2007). Synthesis, characterization and photochromic studies of three novel calix[4]arene-Schiff bases. *Spectrochimica Acta - Part A: Molecular and Biomolecular Spectroscopy*, *68*, 1231–1235. doi: 10.1016/j.saa.2007.01.026

Ligon, B. L. (2004). Penicillin: its discovery and early development. *Seminars in Pediatric Infectious Diseases, 15*, 52–57. doi: 10.1053/j.spid.2004.02.001

Liou, G.-S., Hsiao, S.-H., & Su, T.-H. (2005). Synthesis, luminescence and electrochromism of aromatic poly(amine–amide)s with pendent triphenylamine moieties. *Journal of Materials Chemistry*, *15*, 1812-1820. doi: 10.1039/b419183h

Maclachlan, M. J., Park, M. K., & Thompson, L. K. (1996). Coordination compounds of Schiff base ligands derived from diaminomaleonitrile (DMN): mononuclear, dinuclear, and macrocyclic derivatives. *Inorganic Chemistry*, *35*, 5492–5499. doi: 10.1021/ic960237p

Madkour, L. H., & Elroby, S. K. (2015). Inhibitive properties, thermodynamic, kinetics and quantum chemical calculations of polydentate Schiff base compounds as corrosion inhibitors for iron in acidic and alkaline media. *International Journal of Industrial Chemistry*, *6*, 165–184. doi: 10.1007/s40090-015-0039-7

Mahalakshmi, N., & Rajavel, R. (2010). Synthesis, spectroscopic, DNA cleavage and antibacterial activity of binuclear Schiff base complexes. *Arabian Journal of Chemistry*, *7*, 509-517. doi: 10.1016/j.arabjc.2010.11.010

Mahapatra, B. B., Mishra, R. R., & Sarangi, A. K. (2013). Synthesis, characterisation, XRD, molecular modelling and potential antibacterial studies of Co(II), Ni(II), Cu(II), Zn(II), Cd(II) and Hg(II) complexes with bidentate azodye ligand. *Journal of Saudi Chemical Society*, *20*, 635-643. doi: 10.1016/j.jscs.2013.07.002

Mahmoud, W. H., Deghadi, R. G., & Mohamed, G. G. (2016). Spectroscopic and thermal characterization of biologically and anticancer active novel Schiff base metal complexes. *Research on Chemical Intermediates*, *42*, 7869-7907. doi: 10.1007/s11164-016-2567-y

Mahmoud, W. H., Mohamed, G. G., & El-dessouky, M. M. I. (2014). Synthesis, characterization and *in vitro* biological activity of mixed transition metal complexes of lornoxicam with 1,10- phenanthroline. *International Journal of Electrochemical Science*, *9*, 1415–1438.

Majumder, S., Panda, G. S., & Choudhuri, S. K. (2003). Synthesis, characterization

and biological properties of a novel copper complex. *European Journal of Medicinal Chemistry*, *38*, 893–898. doi: 10.1016/j.ejmech.2003.08.002

Manimaran, A., Chinnusamy, V., & Jayabalakrishnan, C. (2011). Synthesis, spectral characterization, C-C coupling, oxidation reactions and antibacterial activities of new ruthenium(III) Schiff base complexes. *Applied Organometallic Chemistry*, *25*, 87–97. doi: 10.1002/aoc.1720

Manjunath, M., Kulkarni, A. D., Bagihalli, G. B., Malladi, S., & Patil, S. A. (2016). Bio-important antipyrine derived Schiff bases and their transition metal complexes: synthesis, spectroscopic characterization, antimicrobial, anthelmintic and DNA cleavage investigation. *Journal of Molecular Structure*, *1127*, 314-321. doi: 10.1016/j.molstruc.2016.07.123

Matak, P., Zumerle, S., Mastrogiannaki, M., El Balkhi, S., Delga, S., Mathieu, J. R. R., Cannonne-Hergaux, F., Poupon, J., Sharp, P. A., Vaulont, S., & Peyssonnaux, C. (2013). Copper deficiency leads to anemia, duodenal hypoxia, upregulation of HIF-2α and altered expression of iron absorption genes in mice. *PLoS ONE*, *8*. doi: 10.1371/journal.pone.0059538

Migahed, M. A., Farag, A. A., Elsaed, S. M., Kamal, R., Mostfa, M., & El-Bary, H. A. (2011). Synthesis of a new family of Schiff base nonionic surfactants and evaluation of their corrosion inhibition effect on X-65 type tubing steel in deep oil wells formation water. *Materials Chemistry and Physics*, *125*, 125–135. doi: 10.1016/j.matchemphys.2010.08.082

Mingeot-Leclercq, M. P., & Décout, J.-L. (2016). Bacterial lipid membranes as promising targets to fight antimicrobial resistance, molecular foundations and illustration through the renewal of aminoglycoside antibiotics and emergence of amphiphilic aminoglycosides. *Medicinal Chemistry Communication*, *7*, 586–611. doi: 10.1039/c5md00503e

Mingeot-Leclercq, M. P., Glupczynski, Y., & Tulkens, P. M. (1999). Aminoglycosides: activity and resistance. *Antimicrobial Agents and Chemotherapy*, *43*, 727–737.

Mishra, A. P., Sharma, N., & Jain, R. K. (2013). Microwave synthesis, spectral, thermal and antimicrobial studies of some Ni(II) and Cu(II) Schiff base complexes. *Open Journal of Synthesis Theory and Applications*, *2*, 56–62. doi: 10.4236/ojsta.2013.22007

Modi, C. K., Gade, B. G., Chudasama, J. A., Parmar, D. K., Nakum, H. D., & Patel, A. L. (2015). Synthesis, spectral investigation and catalytic aspects of entrapped VO(IV) and Cu(II) complexes into the supercages of zeolite-Y. *Spectrochimica Acta Part A: Molecular and Biomolecular Spectroscopy*, *140*, 174–184. doi: 10.1016/j.saa.2014.12.028

Montazerozohori, M., Zahedi, S., Naghiha, A., & Zohour, M. M. (2014). Synthesis, characterization and thermal behavior of antibacterial and antifungal active zinc complexes of bis (3(4-dimethylaminophenyl)-allylidene-1,2-diaminoethane. *Materials Science & Engineering. C*, *35*, 195–204. doi: 10.1016/j.msec.2013.10.030

Murphy, D. M. (2009). EPR (electron paramagnetic resonance) spectroscopy of polycrystalline oxide systems. *Metal Oxide Catalysis*

Murtaza, G., Rauf, M. K., Badshah, A., Ebihara, M., Said, M., Gielen, M., de Vos, D., Dilshad, E., & Mirza, B. (2012). Synthesis, structural characterization and *in vitro* biological screening of some homoleptic copper(II) complexes with substituted guanidines. *European Journal of Medicinal Chemistry*, *48*, 26–35. doi: 10.1016/j.ejmech.2011.11.029

Naber, C. K. (2009). *Staphylococcus aureus* bacteremia: epidemiology, pathophysiology, and management strategies. *Clinical Infectious Diseases*, *48*, S231–S237. doi: 10.1086/598189

Naeimi, H., Nazifi, Z. S., Amininezhad, S. M., & Amouheidari, M. (2013). Synthesis, characterization and *in vitro* antimicrobial activity of some new Schiff bases and their complexes. *The Journal of Antibiotics*, *66*, 687–689. doi: 10.1038/ja.2013.73

Naglah, A. M., Awad, H. M., Bhat, M. A., Al-omar, M. A., & Amr, A. E. E. (2015).

Microwave-assisted synthesis and antimicrobial activity of some novel isatin Schiff bases linked to nicotinic acid via certain amino acid bridge. *Journal of Chemistry, 2015*. doi: 10.1155/2015/364841

Nair, M. S., Arish, D., & Joseyphus, R. S. (2012). Synthesis, characterization, antifungal, antibacterial and DNA cleavage studies of some heterocyclic Schiff base metal complexes. *Journal of Saudi Chemical Society*, *16*, 83–88. doi: 10.1016/j.jscs.2010.11.002

Negm, N. A., El Farargy, A. F., Al Sabagh, A. M., & Abdelrahman, N. R. (2011). New Schiff base cationic surfactants: surface and thermodynamic properties and applicability in bacterial growth and metal corrosion prevention. *Journal of Surfactants and Detergents*, *14*, 505–514. doi: 10.1007/s11743-011-1258-3

Obaleye, J. A., Tella, A. C., & Bamigboye, M. O. (2012). Metal complexes as prospective antibacterial agents, a search for antibacterial agents. Dr. Varaprasad Bobbarala (Ed.), InTech, doi: 10.5772/34282

Osowole, A. A., & Balogun, S. A. (2012). Spectral, magnetic, thermal and antibacterial properties of some metal(II) complexes of aminoindanyl Schiff base. *European Journal of Applied Sciences*, *4*, 6–13.

Osowole, A. A., & Daramola, A. O. (2011). Synthesis, physicochemical and biological activities of some metal(II) complexes of (methylsulfanyl)-2,4-benzenediol Schiff base. *Elixir Applied Chemistry*, *39*, 4876–4879.

Padmaja, M., Pragathi, J., & Kumari, C. G. (2011). Synthesis, spectral characterization, molecular modelling and biological activity of first row transition metal complexes with Schiff base ligand derived from chromone-3-carbaldehyde and o-amino benzoic acid. *Journal of Chemical and Pharmaceutical Research*, *3*, 602–613.

Pahontu, E., Fala, V., Gulea, A., Poirier, D., Tapcov, V., & Rosu, T. (2013). Synthesis and characterization of some new Cu(II), Ni(II) and Zn(II) Ccomplexes with salicylidene thiosemicarbazones: antibacterial, antifungal and *in vitro* antileukemia activity. *Molecules*, *18*, 8812–8836. doi:

10.3390/molecules18088812

Panda, J., Patro, V. J., Sahoo, B. M., & Mishra, J. (2013). Green chemistry approach for efficient synthesis of Schiff bases of isatin derivatives and evaluation of their antibacterial activities. *Journal of Nanoparticles, 2013*. doi:10.1155/2013/549502

Patil, S. A., Unki, S. N., Kulkarni, A. D., Naik, V. H., Kamble, U., & Badami, P. S. (2011). Spectroscopic, *in vitro* antibacterial, and antifungal studies of Co(II), Ni(II), and Cu(II) complexes with 4-chloro-3-coumarinaldehyde Schiff bases. *Journal of Coordination Chemistry*, *64*(2), 323–336. doi:10.1080/00958972.2010.541240

Pirhadi, S., Sunseri, J., & Koes, D. R. (2016). Open source molecular modeling. *Journal of Molecular Graphics and Modelling, 69,* 127–143. doi:10.1016/j.jmgm.2016.07.008

Prakash, A., & Adhikari, D. (2011). Application of Schiff bases and their metal complexes-A review. *International Journal of ChemTech Research*, *3*, 1891–1896.

Prashanth, L., Kattapagari, K. K., Chitturi, R., Baddam, V. R. R., & Prasad, L. K. (2015). A review on role of essential trace elements in health and disease. *Journal of Dr. NTR University of Health Sciences*, *4*, 75–85. doi:10.4103/2277-8632.158577

Qin, W., Long, S., Panunzio, M., & Biondi, S. (2013). Schiff bases: A short survey on an evergreen chemistry tool. *Molecules*, *18*, 12264–12289. doi:10.3390/molecules181012264

Rahaman, F., & Mruthyunjayaswamy, B. H. M. (2014). Synthesis, spectral characterization and biological activity studies of transition metal complexes of Schiff base ligand containing indole moiety. *Complex Metals*, *1*, 88–95. doi:10.1080/2164232X.2014.889580

Rajasekar, M., Sreedaran, S., Prabu, R., Narayanan, V., Jegadeesh, R., Raaman, N., & Kalilur Rahiman, A. (2010). Synthesis, characterization, and antimicrobial

activities of nickel(II) and copper(II) Schiff-base complexes. *Journal of Coordination Chemistry*, *63*, 136–146. doi: 10.1080/00958970903296362

Rajendra, J., & Anand, P. M. (2012). Microwave assisted synthesis, spectroscopic, thermal and antimicrobial studies of some transition metal complexes of Schiff base ligands containing thiazole moiety. *Jordan Journal of Chemistry*, *7*, 9–21.

Rama, I., & Selvameena, R. (2015). Synthesis, structure analysis, anti-bacterial and *in vitro* anti-cancer activity of new Schiff base and its copper complex derived from sulfamethoxazole. *Journal of Chemical Science*, *127*, 671–678. doi: 10.1007/s12039-015-0824-z

Raman, N., Sakthivel, A., & Rajasekaran, K. (2007). Synthesis and spectral characterization of antifungal sensitive Schiff base transition metal complexes. *Mycobiology*, *35*, 150–153. doi: 10.4489/MYCO.2007.35.3.150

Rani, A., Kumar, M., Khare, R., & Tuli, H. S. (2015). Schiff bases as an antimicrobial agent : A review. *Journal of Biological and Chemical Sciences*, *2*, 62–91.

Rawat, M. S. M., Mal, S., & Singh, P. (2015). Photochromism in anils - A review. *Open Chemistry Journal*, *2*, 7–19. doi: 10.2174/1874842201502010007

Reedijk, J. (2008). Medicinal applications of metal complexes binding to biological macromolecules. *Macromolecular Symposia*, *270*, 193–201. doi: 10.1002/masy.200851023

Reiss, A., Chifiriuc, M. C., Amzoiu, E., & Spînu, C. I. (2014). Transition metal(II) complexes with cefotaxime-derived schiff base: synthesis, characterization, and antimicrobial studies. *Bioinorganic Chemistry and Applications*, *2014*. doi: 10.1155/2014/926287

Rodríguez-Hernández, J. (2017). Bacterial infections: few concepts. *Polymers against Microorganisms*, *Springer, Cham.* doi: 10.1007/978-3-319-47961-3_2

Romero-Canelón, I., & Sadler, P. J. (2013). Next-generation metal anticancer complexes: multitargeting via redox modulation. *Inorganic Chemistry*, *52*, 12276-12291. doi: 10.1021/ic400835n

Rudbari, H. A., Iravani, M. R., Moazam, V., Askari, B., Khorshidifard, M., Habibi, N., & Bruno, G. (2016). Synthesis, characterization, X-ray crystal structures and antibacterial activities of Schiff base ligands derived from allylamine and their vanadium(IV), cobalt(III), nickel(II), copper(II), zinc(II) and palladium(II) complexes. *Journal of Molecular Structure*, *1125*, 113–120. doi: 10.1016/j.molstruc.2016.06.055

Sahu, I. D., McCarrick, R. M., & Lorigan, G. A. (2013). Use of electron paramagnetic resonance to solve biochemical problems. *Biochemistry*, *52*, 5967–5984. doi: 10.1021/bi400834a

Sahu, R., Thakur, D. S., & Kashyap, P. (2012). Schiff base: an overview of its Mmedicinal chemistry potential for new drug molecules. *International Journal of Pharmaceutical Science and Nanotechnology*, *5*, 1757–1764.

Samanta, B., Chakraborty, J., Choudhury, C. R., Dey, S. K., Dey, D. K., Batten, S. R., Jensen, P., Yap, G. P. A., & Mitra, S. (2007). New Cu(II) complexes with polydentate chelating Schiff base ligands: synthesis, structures, characterisations and biochemical activity studies. *Structural Chemistry*, *18*, 33–41. doi: 10.1007/s11224-006-9115-0

Samide, A., & Tutunaru, B. (2011). Adsorption and inhibitive properties of a Schiff base for the corrosion control of carbon steel in saline water. *Journal of Environmental Science and Health, Part A: Toxic/Hazardous Substances and Environmental Engineering*, *46*, 1713–1720. doi: 10.1080/10934529.2011.623972

Sathya, N., Raja, G., Padma Priya, N., & Jayabalakrishnan, C. (2010). Ruthenium(II) complexes incorporating tridentate schiff base ligands: synthesis, spectroscopic, redox, catalytic and biological properties. *Applied Organometallic Chemistry*, *24*, 366–373. doi: 10.1002/aoc.1621

Schweitzer, V. G., Hawkins, J. E., Lilly, D. J., Litterst, C. J., Abrams, G., Davis, J. A., & Christy, M. (1984). Ototoxic and nephrotoxic effects of combined treatment with cis-diamminedichloroplatinum and kanamycin in the guinea pig. *Otolaryngol Head Neck Surgery*, *92*, 38–49.

Shakir, M., Abbasi, A., Faraz, M., & Sherwani, A. (2015). Synthesis, characterization and cytotoxicity of rare earth metal ion complexes of N,N'-bis-(2-thiophenecarboxaldimine)-3,3'-diaminobenzidene, Schiff base ligand. *Journal of Molecular Structure, 1102,* 108–118. doi: 10.1016/j.molstruc.2015.08.061

Shakir, M., Hanif, S., Sherwani, M. A., Mohammad, O., & Al-Resayes, S. I. (2015). Pharmacologically significant complexes of Mn(II), Co(II), Ni(II), Cu(II) and Zn(II) of novel Schiff base ligand, (E)-N-(furan-2-yl methylene) quinolin-8-amine : synthesis, spectral, XRD, SEM, antimicrobial, antioxidant and *in vitro*. *Journal of Molecular Structure*, 1092, 143-159. doi: 10.1016/j.molstruc.2015.03.012

Sharaby, C. M. (2007). Synthesis, spectroscopic, thermal and antimicrobial studies of some novel metal complexes of Schiff base derived from [N^1-(4-methoxy-1,2,5-thiadiazol-3-yl)sulfanilamide] and 2-thiophene carboxaldehyde. *Spectrochimica Acta - Part A: Molecular and Biomolecular Spectroscopy, 66,* 1271–1278. doi: 10.1016/j.saa.2006.05.030

Sharma, V., Arora, E. K., & Cardoza, S. (2015). 4-Hydroxy-benzoic acid (4-diethylamino-2-hydroxy-benzylidene)hydrazide: DFT, antioxidant, spectroscopic and molecular docking studies with BSA. *Luminescence*, *31*, 738-745. doi: 10.1002/bio.3018

Shebl, M. (2014). Synthesis, spectroscopic characterization and antimicrobial activity of binuclear metal complexes of a new asymmetrical Schiff base ligand: DNA binding affinity of copper(II) complexes. *Spectrochimica Acta - Part A: Molecular and Biomolecular Spectroscopy*, *117*, 127–137. doi: 10.1016/j.saa.2013.07.107

Sherif, O. E., & Abdel-Kader, N. S. (2014). Spectroscopic and biological activities studies of bivalent transition metal complexes of Schiff bases derived from condensation of 1,4-phenylenediamine and benzopyrone derivatives. *Spectrochimica Acta. Part A, Molecular and Biomolecular Spectroscopy, 117,* 519–526. doi: 10.1016/j.saa.2013.08.037

Sherif, O. E., & Abdel-Kader, N. S. (2015). DFT calculations, spectroscopic studies,

thermal analysis and biological activity of supramolecular Schiff base complexes. *Arabian Journal of Chemistry*. doi: 10.1016/j.arabjc.2015.07.008

Shivakumar, S. S., & Mohana, K. N. (2013). Corrosion behavior and adsorption thermodynamics of some Schiff bases on mild steel corrosion in industrial water medium. *International Journal of Corrosion, 2013*. doi: 10.1155/2013/543204

Shoaib, K., Rehman, W., Mohammad, B., & Ali, S. (2013). Synthesis, characterization and biological applications of transition metal complexes of [NO] donor Schiff bases. *Journal of Proteomics & Bioinformatics, 6*, 153–157. doi: 10.4172/jpb.1000274

Shukla, S. (2016). Synthesis and anti-bacterial application of copper(II) salicylaldehyde Schiff base complex. *Austin Journal of Analytical and Pharmaceutical Chemistry 3*, 1077.

Silverstein, R. M., Webster, F. X., & Kiemle, D. (2005). *Spectrometric identification of organic compounds, 7th Edition*. John Wiley & Sons.

Singh, A. K., & Quraishi, M. A. (2012). Study of some bidentate schiff bases of isatin as corrosion inhibitors for mild steel in hydrochloric acid solution. *International Journal of Electrochemical Science, 7*, 3222–3241.

Singh, H. L., & Singh, J. (2014). Synthesis, spectroscopic, molecular structure, and antibacterial studies of dibutyltin(IV) Schiff base complexes derived from phenylalanine, isoleucine, and glycine. *Bioinorganic Chemistry and Applications, 2014*. doi: 10.1155/2014/716578

Singh, H. L., Singh, J., Chauhan, S. S., Mukherjee, A., & Dewa, T. (2014). Synthetic, structural, theoretical and biological study of triorganotin(IV) Schiff base complexes derived from amino acids. *Journal of Chemical and Pharmaceutical Research, 6*, 248–257.

Singh, J., & Singh, P. (2012). Synthesis, spectroscopic characterization, and *in vitro* antimicrobial studies of pyridine-2-carboxylic acid N'-(4-Chloro-Benzoyl)-hydrazide and its Co(II), Ni(II), and Cu(II) complexes. *Bioinorganic Chemistry and Applications, 2012*, doi: 10.1155/2012/104549

Singh, K., Kumar, Y., Puri, P., Sharma, C., & Aneja, K. R. (2013). Antimicrobial, spectral and thermal studies of divalent cobalt, nickel, copper and zinc complexes with triazole Schiff bases. *Arabian Journal of Chemistry, 10,* S978-S987. doi: 10.1016/j.arabjc.2012.12.038

Sinha, S.K. (2014). Trace elements deficiency & cancer. *Journal of Pharmacy and Biological Sciences, 9,* 21–32.

Souza, V. R., Rechenberg, H. R., Bonacin, J. A., & Toma, H. E. (2008). Spectroscopic and electrochemical properties of iron(II) complexes of polydentate Schiff bases containing pyrazine, pyridine and imidazole groups. *Spectrochimica Acta. Part A, Molecular and Biomolecular Spectroscopy, 71,* 1296–1301. doi: 10.1016/j.saa.2008.04.001

Sumathi, R. B., & Halli, M. B. (2014). Metal(II) complexes derived from naphthofuran-2-carbohydrazide and diacetylmonoxime Schiff base: synthesis, spectroscopic, electrochemical, and biological investigation. *Bioinorganic Chemistry and Applications, 2014*. doi: 10.1155/2014/942162

Sumrra, S. H., Ibrahim, M., Ambreen, S., Imran, M., Danish, M., & Rehmani, F. S. (2014). Synthesis, spectral characterization, and biological evaluation of transition metal complexes of bidentate N, O donor Schiff bases. *Bioinorganic Chemistry and Applications, 2014*. doi: 10.1155/2014/812924

Tahmasebi, V., Grivani, G., & Bruno, G. (2016). Synthesis, characterization, crystal structure determination and catalytic activity in epoxidation reaction of two new oxidovanadium(IV) Schiff base complexes. *Journal of Molecular Structure, 1123,* 367-374. doi: 10.1016/j.molstruc.2016.06.038

Tanaka, K., Shimoura, R., & Caira, M. R. (2010). Synthesis, crystal structures and photochromic properties of novel chiral Schiff base macrocycles. *Tetrahedron Letters, 51,* 449–452. doi: 10.1016/j.tetlet.2009.11.062

Tyagi, P., Chandra, S., & Saraswat, B. S. (2015). Ni(II) and Zn(II) complexes of 2-(thiophen-2-ylmethylene)amino)benzamide: synthesis, spectroscopic characterization, thermal, DFT and anticancer activities. *Spectrochimica Acta*

Part A: Molecular and Biomolecular Spectroscopy, *134*, 200–209. doi: 10.1016/j.saa.2014.06.112

Vardhan, H., Mehta, A., Nath, I., & Verpoort, F. (2015). Dynamic imine chemistry in metal-organic polyhedra. *RSC Advances*, *5*, 67011-67030. doi: 10.1039/C5RA10801B

Venkatachalam, G., & Ramesh, R. (2006). Ruthenium(III) bis-bidentate Schiff base complexes mediated transfer hydrogenation of imines. *Inorganic Chemistry Communications*, *9*, 703–707. doi: 10.1016/j.inoche.2006.04.012

Ventola, C. L. (2015). The antibiotic resistance crisis: part 1: causes and threats. *Pharmacy and Therapeutica*, *40*, 277–283.

Walsh, C. T., & Wencewicz, T. A. (2013). Prospects for new antibiotics: a molecule-centered perspective. *The Journal of Antibiotics*, *67*, 7-22. doi: 10.1038/ja.2013.49

Wang, Y., & Chiu, J. F. (2008). Proteomic approaches in understanding action mechanisms of metal-based anticancer drugs. *Metal-Based Drugs*, *2008*. doi: 10.1155/2008/716329

Wilson, D. N. (2014). Ribosome-targeting antibiotics and mechanisms of bacterial resistance. *Nature Reviews/Microbiology*, *12*, 35–48. doi: 10.1038/nrmicro3155

Yang, Z., & Sun, P. (2006). Compare of three ways of synthesis of simple Schiff base. *Molbank*, *2006*. doi: 10.3390/M514

Zhang, X., Han, J. J., Huang, M., & Zhang, G. Y. (2012). Synthesis, crystal structures and antibacterial activities of Schiff base ligand and its cobalt(II) complex. *Russian Journal of Coordination Chemistry*, *38*, 560–566. doi: 10.1134/S1070328412080106

Zhu, S., Chen, Y., Sun, J., Yang, Y., & Yue, C. (2016). Synthesis, characterization, thermochromism, and photochromism of aromatic aldehyde hydrazone derivatives. *Journal of Chemistry*, *2016*. doi: 10.1155/2016/8460462

Živec, P., Perdih, F., Turel, I., Giester, G., & Psomas, G. (2012). Different types of

copper complexes with the quinolone antimicrobial drugs ofloxacin and norfloxacin: structure, DNA- and albumin-binding. *Journal of Inorganic Biochemistry, 117*, 35–47. doi: 10.1016/j.jinorgbio.2012.08.008

APPENDIX

Table A1: List of chemicals and reagents

S.N.	Chemicals and reagents	Source
1	Amoxicillin trihydrate	Duchefa Biochemie, Netherlands
2	Kanamycin	Alfa-Aesar
3	Pyridine-3-carboxaldehyde	Spectrochem Mumbai India
4	Pyridine-2-carbaldehyde	Spectrochem Mumbai India
5	Thiophene-2-carboxaldehyde	Spectrochem Mumbai India
6	Methanol	Merck
7	Ethanol	Merck
8	$CoCl_2$. $6H_2O$	Qualigens
9	$NiCl_2$. $6H_2O$	Qualigens
10	$CuCl_2$. $2H_2O$	Qualigens
11	$ZnCl_2$	Qualigens
12	Acetone	Merck
13	Dimethylsulphoxide (DMSO)	Qualigens
14	Sodium hydroxide	Himedia co.
15	Nutrient agar	Himedia co.
16	MHN agar	Himedia co.
17	pH buffer capsule	Merck
18	Hydrochloric acid	Merck
19	Tryptone soya broth	Himedia co.
20	Peptone water	Himedia co.

Table A2: List of instruments and glass apparatus

S.N.	Instruments and glass apparatus	Source
1	Magnetic stirrer	Vitco co. India
2	Heating mantle	Local company
3	Digital balance (4 digits)	
4	Conical flask (100 mL)	Borosil
5	Beaker (100 mL)	Borosil
6	Magnetic beads	Local
7	Condenser	Borosil
8	Pipette	Borosil
9	Measuring cylinder	Borosil
10	Pipette pump	Polylab
11	Glass adaptors	Borosil

Table A3: Solubility data of Schiff base ligands and metal complexes

S.N.	Compounds	Methanol	Water	Ethanol	$CHCl_3$	DMSO	DMF
1	KMAXC	IS	IS	IS	IS	S	S
2	AXCPC3	S	IS	IS	IS	S	S
3	AXCPC2	S	IS	IS	IS	S	S
4	Co-KMAXC	IS	IS	IS	IS	S	S
5	Cu-KMAXC	IS	IS	IS	IS	S	S
6	Zn-KMAXC	IS	IS	IS	IS	S	S
7	Co-AXCPC3	IS	IS	IS	IS	S	S
8	Ni-AXCPC3	IS	IS	IS	IS	S	S
9	Cu-AXCPC3	IS	IS	IS	IS	S	S
10	Zn-AXCPC3	IS	IS	IS	IS	S	S
11	Co-AXCPC2	IS	IS	IS	IS	S	S
12	Ni-AXCPC2	IS	IS	IS	IS	S	S
13	Cu-AXCPC2	IS	IS	IS	IS	S	S
14	Zn-AXCPC2	IS	IS	IS	IS	S	S

IS = Insoluble

S = Soluble

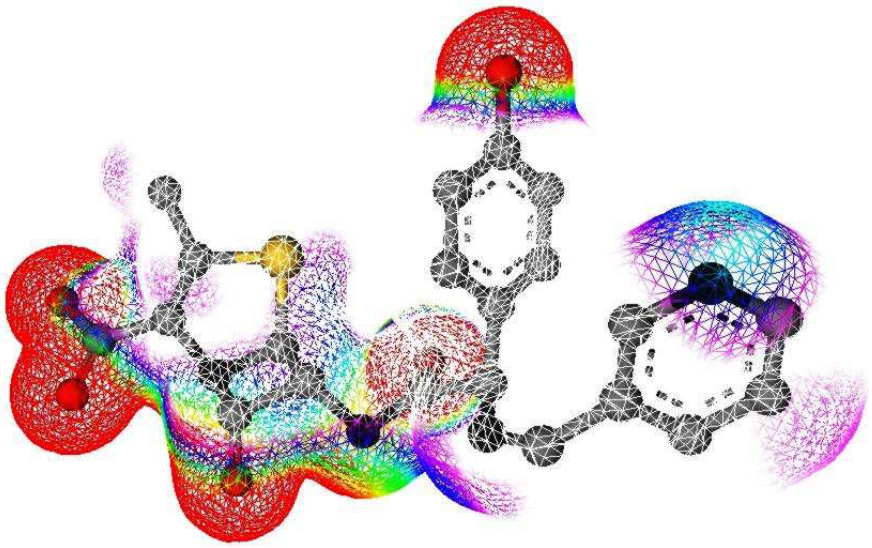

Figure A1: Electrostatic potential mapped electron density surface of AXCPC3 ligand

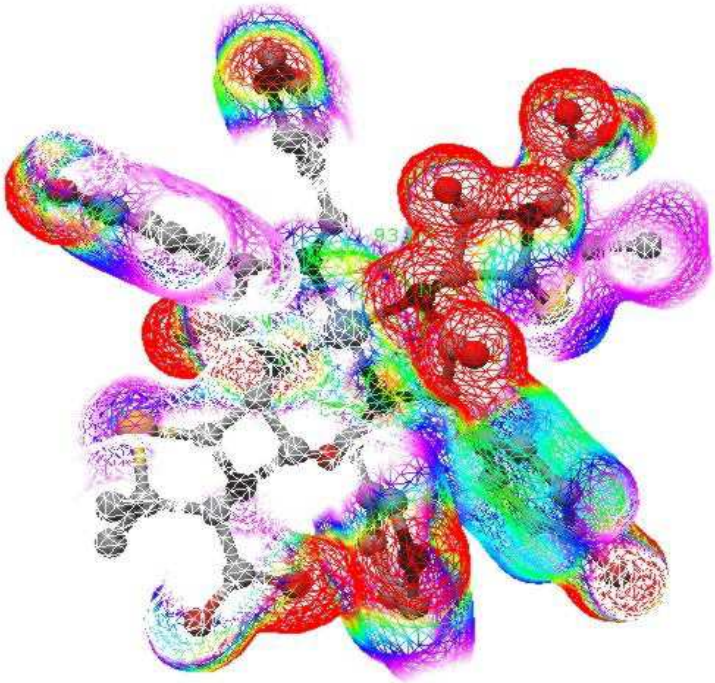

Figure A2: Electrostatic potential mapped electron density surface of Ni-AXCPC3

Figure A3: Antibacterial activity against pathogenic bacteria with AXCPC3 Schiff base ligand and metal complexes

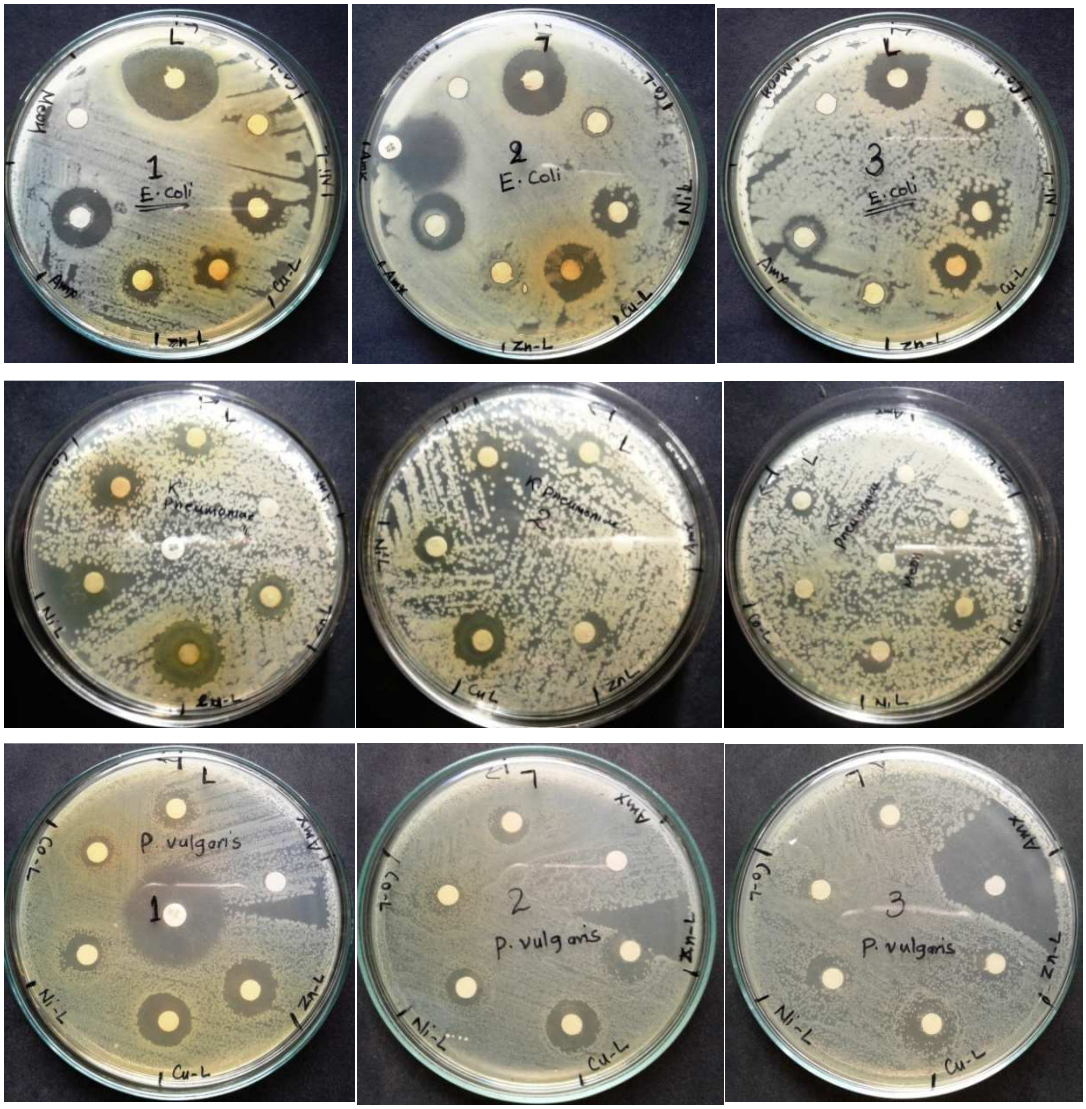

Figure A4: Antibacterial activity against pathogenic bacteria with AXCPC2 Schiff base ligand and metal complexes

Figure A5: Sample picture of AXCPC3 Ligand and metal complexes

Figure A6: Sample picture of AXCPC2 Ligand and metal complexes

LIST OF PUBLICATIONS AND SCIENTIFIC PAPER PRESENTATIONS

List of Publications

1. **Chaudhary, N. K.,** & Mishra, P. (2017). Bioactivity of some divalent M(II) complexes of penicillin based Schiff base ligand: synthesis, spectroscopic characterization, and thermal study. *Journal of Saudi Chemical Society*, Vol. 22, 2018, pp. 601-613. doi: 10.1016/j.jscs.2017.10.003
2. **Chaudhary, N. K.,** & Mishra, P. (2017). Metal complexes of a novel Schiff base based on penicillin: characterization, molecular modeling and antibacterial activity study. *Bioinorganic Chemistry and Applications*, Vol. 2017, doi: 10.1155/2017/6927675
3. **Chaudhary, N. K.,** & Mishra, P. (2015). Spectral investigation and *in vitro* antibacterial evaluation of Ni^{II} and Cu^{II} complexes of Schiff base derived from amoxicillin and α-formylthiophene (αft). *Journal of Chemistry*, Vol. 2015, Article ID 136585. doi: 10.1155/2015/136285
4. **Chaudhary, N. K.,** & Mishra, P. (2015). Synthesis, structure delineation and antibacterial activity study of metal(II) complexes of Schiff base derived from kanamycin and methyl ester of amoxicillin. *International Research Journal of Pure and Applied Chemistry*, Vol. 7(4), 2015, pp. 165-180. doi: 10.9734/IRJPAC/2015/17013

Scientific Paper Presentations

1. Scientific paper presentation entitled **"Bioactivity of some divalent M(II) complexes of Penicillin based Schiff base ligand: Synthesis, Spectroscopic characterization and Thermal study"** at the National Conference on Recent Innovations in Science, Engineering and Technology (NCRISET) held at New Delhi, India on 24th September, 2017.
2. Scientific paper presentation entitled **"Coordination chemistry and antimicrobial screening of Ni^{II} and Cu^{II} complexes of asymmetric Schiff base of Streptomycin and aniline"** in the 7th National conference on Science and Technology, organized by NAST, Nepal on 29-31 March, 2016.

3. Scientific paper presentation entitled **"UV/visible investigation and antibiotic study of metal complexes of Schiff base derived from Amoxicillin and Thiophene-2-carbaldehyde"** in the 16th International Symposium on Eco-materials Processing and Design (ISEPD-2015), held at Kathmandu, Nepal.
4. Scientific paper presentation entitled **"Bio-coordination and Antibacterial screening of Cu(II), Co(II) and Zn(II) Complexes of Schiff base derived from Kanamycin and Amoxicillin"** in the International conference on Emerging Trends in Science and Technology on March 22-23, 2014 at Biratnagar, Nepal.
5. Scientific paper presentation entitled **"Bio-coordination behavior of Cu(II) and Ni(II) ions with biologically active Streptomycin and Amoxicillin mixed ligands: Synthesis, spectroscopic characterization and molecular modeling"** in the scientific seminar of "Modern trends in Science and Technology" on 28th - 29th December-2012, at Biratnagar, Nepal.

Journal of Saudi Chemical Society (2018) **22**, 601–613

King Saud University

Journal of Saudi Chemical Society

www.ksu.edu.sa
www.sciencedirect.com

ORIGINAL ARTICLE

Bioactivity of some divalent M(II) complexes of penicillin based Schiff base ligand: Synthesis, spectroscopic characterization, and thermal study

N.K. Chaudhary, P. Mishra *

Bio-inorganic and Materials Chemistry Research Laboratory, Tribhuvan University, M.M.A.M. Campus, Biratnagar, Nepal

Received 5 August 2017; revised 17 September 2017; accepted 17 October 2017
Available online 31 October 2017

KEYWORDS

Schiff base metal complexes;
Kinetic parameters;
Antibacterial activity;
Molecular modeling;
Penicillin

Abstract A series of four novel metal complexes of Co(II), Ni(II), Cu(II) and Zn(II) were synthesized from Schiff base derived from amoxicillin (AMX) and picolinaldehyde (PC2). The ligand and metal complexes were fully characterized by physical and spectral techniques such as elemental microanalysis, conductivity, FT-IR, ^{1}H & ^{13}C NMR, UV–vis, mass spectra, EPR, magnetic moment measurement, TGA/DTA, PXRD and antibacterial activity study. The spectroscopic study revealed 1:2 metal ligand ratio and coordination sites in the ligand for metal ions were evaluated by analysis of the spectral results. The surface morphology of the complexes was evaluated by SEM analysis. Molar conductivity implies non-electrolytic nature of the complexes. UV–vis. spectral study nicely supports octahedral geometry for Co(II) and Zn(II) complexes and tetrahedral geometry for Cu(II) complex. The kinetic parameters were extracted from Coats-Redfern equation. The PXRD study revealed nano-crystalline nature of Co(II), Ni(II) & Cu(II) complexes and amorphous nature of Zn(II) complex. The proposed geometry of the complexes was optimized by MM2 calculation supported in Cs-ChemOffice Ultra-11 program. The ligand and metal complexes were screened for antibacterial potency against four human pathogenic clinical strains of bacteria and the data revealed their promising antibacterial activity.

1. Introduction

Schiff bases and related complexes cover a wide range of applications in medicinal and pharmaceutical fields and are of great research interest [1]. Due to the formation of stable complexes with transition metal ions and participation of azomethine linkage in the chelation process, Schiff bases are considered as a model compound and play an active role in the development of coordination chemistry [2]. The lone pair electron of N-atom in azomethine group has significant ability to chelate

* Corresponding author.
E-mail address: prmmishra@rediffmail.com (P. Mishra).
Peer review under responsibility of King Saud University.

ELSEVIER Production and hosting by Elsevier

https://doi.org/10.1016/j.jscs.2017.10.003
1319-6103

various metal ions, leading to potential biomedical applications, easy removal of toxic metals from the biological systems and also from waste materials [3,4]. Metal ions make bridge between the drug substances and pathogenic organisms and thus the field of metal drug interaction chemistry is growing rapidly in the medical and chemical sciences [5]. Chemically Schiff base is an imine group containing compound whose clinical profile attribute it a versatile pharmacophore in the biomedical field [6]. The applications in electronics as a very good sensor, catalytic activity in various reaction pathways in chemical science [7,8] and as dyes and paints in industries further increase the importance of this class of compound [9,10]. Recent progress in the field of coordination chemistry including Schiff base metal complexes offers a big platform for the advancement of chemical research. The Schiff bases containing heterocyclic moiety prove special attention because of their significant role in biological processes as a very good chemotherapeutic agent and also an important antioxidant chemical [11,12]. Their role in removing toxic chemicals from the biological system is fantabulous. This research is mainly focused on the antibacterial evaluation of amoxicillin derived Schiff base and its metal complexes. The current literature search has highlighted antibacterial resistance in community pathogens as a major problem and to overcome from this, the antibiotics of the new generation should be revived [13,14].

In continuation of our ongoing interest in the design and development of novel bioactive Schiff base materials [15,16], we have focused the attention in deriving novel Schiff base ligand from amoxicillin and picolinaldehyde, and its four metal derivatives with divalent 3d-metal (Co^{+2}, Ni^{+2}, Cu^{+2} and Zn^{+2}) ions. This investigation has extended to spectral characterization, thermal stability study, powder X-ray diffraction study and molecular modeling of the synthesized compounds. Several research papers computed amoxicillin as an old generation antibiotic because of its resistance to various bacterial pathogens [17]. Picolinaldehyde (also called pyridine-2-carbaldehyde) is a pyridine based aromatic aldehyde that bears potential ability for the synthesis of many drug candidates [18]. We report here a simple condensation reaction between the aldehyde moiety of picolinaldehyde and the inner amino group of amoxicillin for the formation of Schiff base.

2. Experimental section

2.1. Materials and reagents

Amoxicillin trihydrate was purchased from Duchefa Biochemie, Netherland. Picolinaldehyde in extra pure form was procured from Spectrochem Mumbai, India. M(II) chloride (M = Co^{+2}, Ni^{+2}, Cu^{+2} and Zn^{+2}) salts were purchased from Merck. Double distilled methanol was used as a solvent for the synthesis. Triple distilled water was used for rinsing the required apparatus and they were dried in the oven before use. All the chemicals used in this research were of analytical reagent grade and used as commercially obtained without further purification.

2.2. Instruments

The molar conductance of solid complexes in 10^{-3} (M) DMSO was measured in Labtronics auto digital conductivity meter (LT 16 model). The CHNS micro-elemental analysis of the compounds was performed on Elementar Vario EL III model analyzer. The infrared spectra were recorded on a Perkin-Elmer FT-IR spectrophotometer as a KBr discs in the range of 400–4000 cm^{-1}. The ^{1}H NMR and ^{13}C NMR spectra were recorded on Bruker Avance III, 400 MHz spectrometer, using DMSO-d_6 as solvent and tetramethylsilane as an internal standard. The electronic spectra of the complexes were recorded on single beam microprocessor Labtronics UV–Vis spectrophotometer (LT-290 model) in the range 200–1000 nm in DMSO solvent. X-band electron spin resonance (ESR) measurement of solid Cu(II) complex was recorded on JES-FA200 ESR spectrometer with no marker lines used. The positive mode ESI-MS spectra of the compounds were analyzed on Agilent Q-TOF mass spectrometer. The X-ray powder diffraction study was accomplished in Bruker AXS D8 Advance X-ray diffractometer with the monochromatised Cu-Kα line at wavelength 1.5406 Å as the radiation source. The TGA/DTA study was performed in Perkin-Elmer thermal analyzer with a linear heating rate of 10 °C min^{-1} in the range of 40–750 °C. JEOL JSM-6390 LV scanning electron microscope was used to record the micrograph of the compounds. The molecular modeling of the synthesized compounds was accomplished by running energy optimization job through MM2 calculation supported in ChemOffice software program.

2.3. Synthesis of ligand (AXCPC2)

The Schiff base ligand (AXCPC2) ((E)-6-(2-(4-hydroxyphenyl)-2-(pyridine-2-methyleneamino) acetamido)-3,3-dimethyl-7-oxo-4-thia-1-aza—bicyclo[3.2.0] heptanes-2-carboxylic acid) was prepared by refluxing the equimolar mixture (1:1) of amoxicillin trihydrate and Pyridine-2-carbaldehyde in methanol solvent media. For this purpose, 5 mmol (2.09725 gm) amoxicillin trihydrate in 30 ml methanol was stirred under hot condition over the magnetic stirrer for several hours and 5 mmol (0.471 ml) pyridine-2-carbaldehyde was added dropwise. The pH of the mixture was checked and maintained neutral by adding 0.1 N NaOH solution. The resulting mixture was refluxed for 4 h till it became clear yellow color. The solution was left undisturbed for better crystal formation and bright yellow solid was separated after volume reduction. The solid was recrystallized from hot methanol and dried in the desiccators using anhydrous $CaCl_2$. The ligand was stored in the airtight vial in the refrigerator until its further use.

2.4. General method for synthesis of metal complexes

The solid metal complexes were prepared by adding hot methanolic solution of metal salts containing 0.5 mmol of $CoCl_2{\cdot}6H_2O$ (0.1189 gm), $NiCl_2{\cdot}6H_2O$ (0.1188 gm), $CuCl_2{\cdot}2H_2O$ (0.085 gm) and $ZnCl_2$ (0.0681 gm) to the hot and homogeneously stirred solution of AXCPC2 ligand (1 mmol, 0.454 gm) in 20 ml methanol. The solution was refluxed for several hours under hot water bath with constant stirring. The stirring is done to homogenize the molecules and to facilitate the bonding of the ligand with metal ions. Different colored solid M-AXCPC2 (M = Co^{+2}, Ni^{+2}, Cu^{+2} & Zn^{+2}) complexes were obtained by volume reduction of the solution. The solid was separated, washed with methanol and dried in the desiccators.

The solid was stored in the airtight vial in the refrigerator, until its further use.

2.5. Antibacterial assessment

The synthesized Schiff base and its corresponding metal(II) complexes were screened for antibacterial activity against some human pathogenic organisms. Four different bacterial organisms were selected for this study purpose. The organisms were very carefully revived in MHN agar media and diffused in tryptone water before seeding in the agar plate. Kirby-Bauer paper disc diffusion technique was applied in order to show the antibacterial potency of the compounds. The fresh clinical culture of organisms was procured from biochemistry laboratory of Suraksha Hospital, Biratnagar. It's detailed and the minute study was done in Bio-inorganic and Materials Chemistry Research Laboratory of Mahendra Morang Adarsh Multiple Campus, Biratnagar. The organisms selected for the study were *E. coli, P. vulgaris, K. pneumoniae,* and *S. aureus*. They were tested against three different concentrations of the synthesized compounds.

3. Results and discussion

3.1. Physical characterization

Micro analytical, molar conductance and other physical properties of the ligand and metal complexes are presented in Table 1. The molar conductance values clearly indicate non-electrolytic nature of the ligand and its metal complexes. The micro analytical data of the complexes revealed ML_2 type geometry with 1:2 metal ligand ratios. The ligand was soluble in methanol and the metal complexes were soluble only in mild polar organic solvents like DMSO and DMF. They were found insoluble in water. The proposed structure determination and confirmation of the complexes (Fig. 1) is well explained on the basis of the rigorous study of their physical data in combination with spectral results.

3.2. Spectral characterization

3.2.1. FT-IR spectroscopy

The significant IR spectral bands of Schiff base (AXCPC2) ligand and its corresponding metal complexes are documented in Table 2. These bands deliver valuable information about the nature of functional groups attached to the metal atoms. The IR spectrum of AXCPC2 ligand exhibits broad absorption band in the region between 3600 and 2800 cm^{-1} with a peak at 3336 cm^{-1} and two shoulder peaks at 2963 and 2928 cm^{-1} correspond to ν(NH), ν(OH) and ν(CH) overlapping stretching vibrations. The shoulder peaks associated with this broad absorption band are attributed to methyl ν(C—H) symmetric and asymmetric stretch. The metal complexes also exhibit broad absorption band which corresponds to ν(NH), ν(OH) and ν(CH) overlapping stretching vibrations in the similar regions, with highest peak intensity at 3397, 3391, 3395 and 3308 cm^{-1} for respective Co-AXCPC2, Ni-AXCPC2, Cu-AXCPC2 and Zn-AXCPC2 complexes. The ν(C═N) stretch attributed to azomethine bond for AXCPC2 at 1657 cm^{-1} has observed to an experience downward shift of 7–13 cm^{-1} upon complexation with metal ions [19,20]. The related ν(C═N) stretch peak for Co-AXCPC2, Ni-AXCPC2, Cu-AXCPC2 and Zn-AXCPC2 complexes are observed at 1650, 1644, 1647 and 1651 cm^{-1} respectively. The IR spectrum of AXCPC2 exhibits ν(COOH) symmetric and asymmetric stretch vibration bands at 1439 and 1514.8 cm^{-1} and no appreciable change of this value is observed in the IR spectra of metal complexes. The carboxylic ν(C═O) stretch for the ligand is observed at 1737 cm^{-1} and this value has shifted to 1710, 1740, 1725 and 1740 cm^{-1} for Co-AXCPC2, Ni-AXCPC2, Cu-AXCPC2 and Zn-AXCPC2 complexes. This shift in positions may be attributed to change in electronic environment after complexation [21]. Most of the IR absorption bands of the complexes in the fingerprint region are similar, providing their identity. Metal-nitrogen ν(M—N) bonding in the complexes is ascribed by the appearance of less intense peaks in the region of 418–463 cm^{-1}. The Co-AXCPC2 and Zn-AXCPC2 complexes also exhibit less intense IR absorption peaks at 568 and 525 cm^{-1}, which corresponds to metal-oxygen ν(M—O) bonding.

3.2.2. ^{1}H & ^{13}C NMR spectral analysis

The ^{1}H NMR spectral comparison of AXCPC2 ligand and its diamagnetic Zn-AXCPC2 complex furnishes information about the proton environment of the molecule and their chemical shift data are reported in Table 3. The azomethine proton of ligand resonated as a sharp singlet at 9.225 ppm and on complexation, this signal was shifted to 9.440 ppm. This indicates the involvement of azomethine group in chelation pro-

Table 1 Physical properties and micro analytical data of ligand and metal complexes.

Complex	Empirical formula	Formula weight	Color	Calculated (found) (%)				
				C	H	N	O	S
AXCPC2	$C_{22}H_{22}N_4O_5S$	454.13	Cocoa brown	58.14 (58.18)	4.88 (4.82)	12.33 (12.29)	17.60 (17.62)	7.06 (7.01)
Co-AXCPC2	$C_{44}H_{42}CoN_8O_{10}S_2$	965.18	Coffee	54.71 (54.69)	4.38 (4.40)	11.60 (11.58)	16.56 (16.51)	6.64 (6.67)
Ni-AXCPC2	$C_{44}H_{42}N_8NiO_{10}S_2$	964.18	Beaver	54.73 (54.69)	4.38 (4.37)	11.60 (11.55)	16.57 (16.55)	6.64 (6.60)
Cu-AXCPC2	$C_{44}H_{42}CuN_8O_{10}S_2$	969.18	Rifle green	54.45 (54.39)	4.36 (4.41)	11.55 (11.48)	16.49 (16.52)	6.61 (6.56)
Zn-AXCPC2	$C_{44}H_{46}N_8O_{12}S_2Zn$	1006.2	Ruddy brown	52.41 (52.42)	4.60 (4.63)	11.11 (11.15)	19.04 (19.12)	6.36 (6.32)

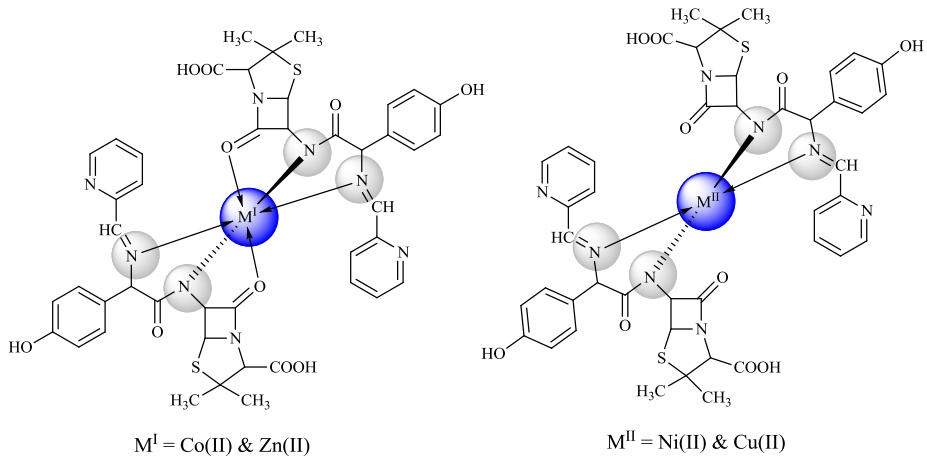

Fig. 1 Structure of metal complexes.

Table 2 FTIR spectral data of AXCPC2 Schiff base and metal complexes.

Complex	ν(NH) & ν(OH)	ν(C—H) methyl	ν(C=N) (imine)	ν_{asym} (COOH)	ν_{sym} (COOH)	ν(C=O) carboxylic	ν(M—N)	ν(M—O)
AXCPC2	3336	2963, 2928	1657	1514.8	1439	1737	–	–
Co-AXCPC2	3397 (b)	2959, 2927	1650	1514.42	1440	1710	463.47	567.92
Ni-AXCPC2	3391		1644	1514.49	1440.96	1740	422	–
Cu-AXCPC2	3395	2957,	1647	1513.52	1440.24	1725	418	–
Zn-AXCPC2	3308	2960, 2926	1651	1514.35	1438	1740	418.32	525.21

Table 3 ^{1}H NMR spectral data of AXCPC2 ligand and Zn-complex.

Comp.	Chemical shift (δ) ppm	Assignment
AXCPC2	10.122 (s)	Carboxylic proton
	9.723 broad	Phenolic OH proton (may be due to H-bond)
	9.225 (s)	Azomethine proton
	8.197–8.443	Pyridine ring protons
	8.008–8.130	Amide NH proton
	6.691–7.767	Ar-H protons
	1.146–1.495	Methyl protons
Zn-AXCPC2	10.123 (S)	Carboxylic proton
	9.75 broad	Phenolic OH proton (May be due to H-bond)
	9.440 (s)	Azomethine proton
	8.187–8.594	Pyridine ring protons
	6.713–7.784	Ar-H protons
	1.229–1.521	Methyl protons

cess. The pyridine ring protons of ligand resonate in the range of 8.197–8.443 ppm and these signals were found between 8.187 and 8.594 ppm in the ^{1}H NMR of the Zn-AXCPC2 complex. The signal for amide NH proton has appeared between 8.008 and 8.130 ppm in the ^{1}H NMR of ligand which has almost vanished in the ^{1}H NMR spectrum of Zn-AXCPC2 complex and this indicated its participation in the coordination with the metal atom. Phenolic proton signal at 9.723 ppm as a broad signal for ligand has almost resumed in the Zn-AXCPC2 complex. Other aromatic and methyl proton signals have appeared at similar positions in ^{1}H NMR spectra of ligand and complex.

^{13}C NMR spectral study furnishes idea about the different kinds of carbon atoms and their electronic environment in the molecules. The ^{13}C NMR spectrum of AXCPC2 ligand delivers a signal for carboxylic carbon at 174.05 ppm. The signal for azomethine carbon appeared at 152.279 ppm. The signal at 171.043 ppm is attributed to lactam carbonyl carbon and the signal for other carbons of lactam and thiazole ring appeared in the range of 40.229–55.177 ppm. The aromatic ring carbons deliver the signal in the range of 115.622–131.259 ppm and the signals in the range of 137.492–149.636 are attributed to pyridine ring carbons. The methyl carbons showed a signal at 29.450 ppm. The recorded spectrum of AXCPC2 ligand is given in Fig. 2 and the spectral data are reported in Table 4. Due to resonance effect in diamagnetic and paramagnetic nature of the complexes, there was no marked change in ^{13}C NMR spectrum of Zn-AXCPC2, compared to the ligand.

3.2.3. Mass spectral analysis

The mass spectra of AXCPC2 ligand and its four metal complexes revealed the peaks at various positions of m/z values. The peak at m/z 456 in the mass spectrum of AXCPC2 ligand signifies molecular ion peak $[M + H]^{\cdot +}$. The metal complexes, such as, Co-AXCPC2, Ni-AXCPC2, Cu-AXCPC2 and Zn-AXCPC2 deliver respective molecular ion peaks at m/z 966, 965, 970 and 1006.2, which strongly support proposed molecular formula of the complexes. These molecular mass values combined with other spectral studies are essential to generate the structure of the compounds.

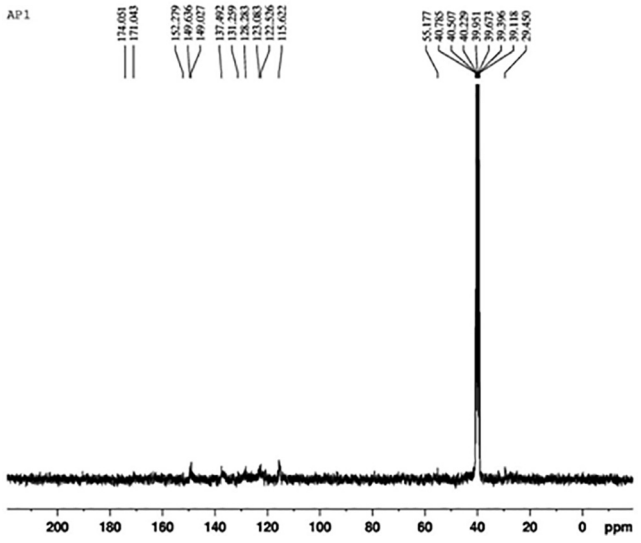

Fig. 2 ^{13}C NMR spectrum of AXCPC2 ligand.

3.2.4. *Electronic absorption and conductivity measurement*

The electronic absorption spectral data for AXCPC2 ligand and its corresponding metal(II) complexes are presented in Table 5. The electronic spectrum of AXCPC2 ligand shows a broad peak at 266 nm assignable to $\pi \rightarrow \pi^*$ transition and a peak at 301 nm is assignable to $n \rightarrow \pi^*$ transition. The intra ligand charge transfer band for the ligand appears at 361 nm. The $\pi \rightarrow \pi^*$ and $n \rightarrow \pi^*$ transitions in metal complexes appear at the similar wavelength regions with minor variations in the data and this may be due to change in electron density around the target group. Besides these absorption peaks, metal complexes deliver peaks in the high wavelength regions and this probably describes the geometry around metal ions. The octahedral Co-AXCPC2 complex displays three absorption peaks at 465, 590 and 853 nm, assignable to $^4T_{1g}(F) \rightarrow {}^4T_{1g}(P)$, $^4T_{1g}(F) \rightarrow {}^4A_{2g}$, and $^4T_{1g} \rightarrow {}^4T_{2g}$ transitions respectively [22]. The ligand metal charge transfer band (LMCT) is attributed by the absorption peak at 409 nm. The magnetic moment value (5.32 BM) further confirms octahedral geometry of this complex [23,24]. The Ni-AXCPC2 complex exhibits two absorption bands at higher wavelength region at 516 and 690 nm due to $^1A_{1g} \rightarrow {}^1B_{1g}$ and $^1A_{1g} \rightarrow {}^1B_{2g}$ transitions respectively and these assign square planar of the complex. The tetrahedral geometry of the Cu-AXCPC2 complex has been demonstrated by $^2T_{2g} \rightarrow {}^2E_g$ transition with corresponding absorption band appeared at 508 and 625 nm. This is further supported by magnetic moment value (1.75 BM), with one unpaired electron [25]. The diamagnetic Zn-AXCPC2 complex delivers high energy bands at 269, 308 and 402 nm, which correspond to $\pi \rightarrow \pi^*$, $n \rightarrow \pi^*$ and LMCT band. Due to the complete d^{10} electronic configuration, d-d transition band was not observed. Association of two H_2O molecules in the zinc complex has been suggested by thermal analysis study and coordination number six has favored around Zn^{+2} ion in the complex. Based on the experimental evidence, microanalytical, spectral and thermal studies, an outer orbital octahedral geometry has assigned for zinc complex [26].

The molar conductivity data of the complexes are reported in Table 5 and the data reveals their non-electrolytic nature. This also reflects non-ionic nature of the complexes [27].

Table 4 The ^{13}C NMR spectral data (δ ppm) of AXCPC2 ligand.

AXCPC2 ligand	Assignment	Chemical shift δ ppm
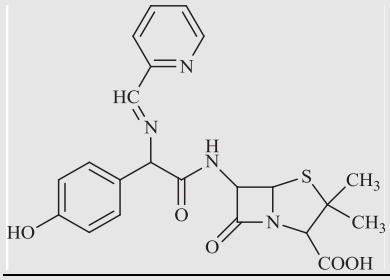	COOH	174.05
	C═O	171.043
	CH═N	152.279
	Pyridine ring carbon	149.636, 149.027, 137.492
	Aromatic ring carbon	131.259, 128.283, 123.083, 122.526, 115.622
	Lactam & thiazole ring carbon	55.177, 40.785, 40.507, 40.229, 39.951, 39.673, 39.396, 39.118
	DMSO	
	CH_3	29.450

Table 5 Electronic spectra, magnetic moments and molar conductivity data of ligand and its metal complexes.

No.	Comp.	Peak positions (nm)	Assignment	Magnetic moment (BM)	Conductance (μ siemen/cm)
1	AXCPC2	266, 304, 361	$\pi \rightarrow \pi^*$, $n \rightarrow \pi^*$, intraligand CT band		
2	Co-AXCPC2	268, 309, 410,	$\pi \rightarrow \pi^*$, $n \rightarrow \pi^*$, LMCT band	5.32	25.6
		465,	$^4T_{1g}(F) \rightarrow {}^4T_{1g}(P)$		
		590,	$^4T_{1g}(F) \rightarrow {}^4A_{2g}$		
		853,	$^4T_{1g} \rightarrow {}^4T_{2g}$		
3	Ni-AXCPC2	268, 307, 420,	$\pi \rightarrow \pi^*$, $n \rightarrow \pi^*$, LMCT band	–	20.9
		516,	$^1A_{1g} \rightarrow {}^1B_{1g}$		
		690,	$^1A_{1g} \rightarrow {}^1B_{2g}$		
4	Cu-AXCPC2	269, 310, 396,	$\pi \rightarrow \pi^*$, $n \rightarrow \pi^*$, LMCT band	1.75	31.1
		508, 625,	$^2T_{2g} \rightarrow {}^2E_g$		
5	Zn-AXCPC2	269, 308, 402	$\pi \rightarrow \pi^*$, $n \rightarrow \pi^*$, LMCT band	–	8.7

3.2.5. EPR analysis

The solid state X-band EPR spectrum of the Cu-AXCPC2 complex is presented in Fig. 3. The EPR spectrum was recorded at room temperature under the frequency of 9445.144 MHz with center line at 314.187 mT. The g tensor and G values are the useful parameters of ESR spectrum which are used for gaining information about the electronic environment and the possible geometry of the complex. The exchange coupling interaction parameter (G) has been calculated by Hathaway expression [28,29]. The g tensor data for this complex displays g|| value 2.149 and $g_{\perp}$ value 2.04. The order of splitting factor $g|| > g_{\perp} > g_e$ (2.0023) is the characteristic feature of axial symmetry of the complex and also indicates the presence of the unpaired electron in the d-orbital of Cu(II) ion. The calculated g_{ave} value is 2.076 and exchange coupling interaction parameter value (G) is 3.72. Since G value is less than 4, this shows appreciable exchange interaction in the complex [30].

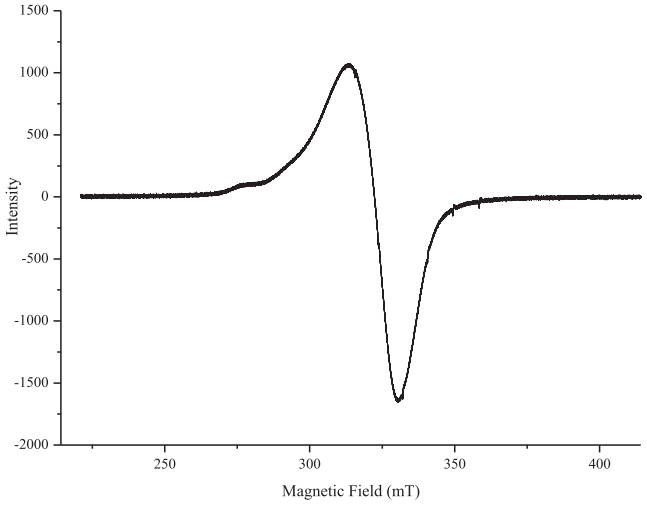

Fig. 3 EPR spectrum of Cu-AXCPC2.

3.3. Thermal properties

The TGA/DTA of the AXCPC2 ligand and its metal complexes were carried within the temperature range from room temperature to 750 °C in the nitrogen atmosphere with the linear heating rate of 10 °C/min. The thermal data have been extracted from the intimate analysis of their thermogram and the data are presented in Table 6. The following findings have been achieved in our research analysis.

The thermogram of AXCPC2 Schiff base ligand showed continuous decomposition from 54 °C to 619.73 °C with major four decomposition steps and after this temperature, the ligand leaves no residue. The decomposition step in the temperature range of 53.89–101.43 °C with the small mass loss of 0.162 mg (2.849%) is associated with loss of moisture and makes no sense for the thermal stability. The second decomposition step in the temperature range of 172.94–232.11 °C with mass loss of 0.954 mg (16.842%) may be attributed to the loss of ligand moiety. Two small shoulder peaks are associated with second decomposition step. The mass loss of 2.46 mg (43.529%) is associated with third decomposition step with a temperature range of 276.47–298.54 °C (T_{DTG} = 284.35 °C). This decomposition step is also attributed to the loss of ligand moiety. T_{DTA} peak at 296.5 °C for this step concludes endo thermal effect. The last decomposition step represents complete loss of ligand molecule in the temperature range of 528.17–619.73 °C with T_{DTG} = 574.22 °C. T_{DTA} peak at 551 °C for this step shows exo thermal effect.

The Co-AXCPC2 complex exhibits decomposition in two steps. The first decomposition step with mass loss of 0.571 mg (16.525%) occurred in the temperature range of 194.91–309.61 °C and this is assigned to the loss of organic moiety of the ligand. The second decomposition step involves the mass loss of 2.406 mg (69.647%) in the temperature range of 527.36–585.06 °C with T_{DTG} peak at 547.88 °C and this may be attributed to the complete loss of ligand part. The thermogram after this temperature gave horizontal platue, indicating cobalt oxide as stable residue. The associated T_{DTA} peak at 510 °C shows exo thermal effect. The thermogram of Ni-AXCPC2 complex exhibits decomposition in two steps, very much similar to Co-AXCPC2 complex. The first step involves

Table 6 Thermal decomposition data of ligand and metal complexes.

Complex	Steps	TG range (^{0}C)				DTA		
		$\Delta_{m\%}$ *found (Cal.)*	T_i	T_f	T_{DTG}	Mass loss	T_{DTA}	Peak
AXCPC2	1	2.849	53.89	101.43	74.39	0.162	–	–
	2	16.842	172.94	232.11	193.53	0.954	–	–
	3	43.529	276. 47	298.54	284.35	2.46	296.5	Endo
	4	81.667	528.17	619.73	574.22	4.631	551	Exo
Co-AXCPC2	1	16.525	194.91	309.61	208.77	0.571	–	–
	2	69.647	527.36	585.06	547.88	2.406	510	Exo
Ni-AXCPC2	1	16.454	191.4	267.04	211.37	0.564	–	–
	2	74.754	489.65	551.22	513.88	2.566	511.16	Exo
Cu-AXCPC2	1	23.733	175.76	244.81	205.71	2.062	–	–
	2	44.964	271.37	2992.93	281.73	3.927	–	–
	3	69.336	441.02	502.57	456.89	6.056	458	Exo
Zn-AXCPC2	1	12.557	189.04	226.83	209.54	0.865	–	–
	2	27.928	262.92	284.46	270.89	1.922	–	–
	3	75.299	582.67	672.77	618.27	5.189	619	Exo

the decomposition in the temperature range of 191.4–267.04 °C with T_{DTG} peak at 211.37 °C. The second step involves the decomposition in the temperature range of 489.65–551.22 °C with T_{DTG} peak at 513.88 °C and T_{DTA} peak at 511.16 °C. This step shows exo thermal effect. After the second decomposition step, the thermogram shows horizontal platue, indicating nickel oxide as stable residue. The thermogram of Cu-AXCPC2 complex showed decomposition in three major steps. The first step involves the mass loss of 2.062 mg (23.733%) in the temperature range of 175.76–244.81 °C and this may be attributed to the loss of ligand moiety. The second step involves the mass loss of 3.927 mg (44.964%) in the temperature range of 271.37–299.93 °C with T_{DTG} peak at 281.73 °C. The third step involves major mass loss of the substance with 6.056 mg (69.336%) in the temperature range of 441.02–502.57 °C and after this the thermogram became horizontal, indicating complete loss of organic moiety and leaves copper oxide as stable residue. The T_{DTA} peak associated with this step is 458 °C and shows exo thermal effect. The thermogram of the Zn-AXCPC2 complex also exhibits major three decomposition steps as like Co-AXCPC2 complex but with several shoulder peaks. Nearly 3.5% weight loss at T_{DTG} = 86.01 °C is associated to loss of two molecules of lattice water in the thermogram of the Zn-AXCPC2 complex [31]. The first decomposition step involves the mass loss of 0.865 mg (12.557%) in the temperature range of 189.04–226.83 °C with T_{DTG} = 209.54 °C. This may be attributed to the loss of organic parts of the ligand. The second decomposition step involves the mass loss of 1.922 mg (27.928%) in the temperature range of 262.92–284.46 °C. This step is associated with one shoulder peak at T_{DTG} = 307.37 °C. This step of the thermogram involves the loss of ligand moiety. The third and final

Table 7 Thermodynamic and kinetic parameters of ligand and metal complexes.

Comp.	Step	r	A (s^{-1})	T_{max} (K)	E^* kJ/mol)	ΔS^* (J/K.mol)	ΔH^* (kJ/mol)	ΔG^* (kJ/mol)
AXCPC2	1	−0.98242	3.94×10^{8}	347.39	71.9763	−82.425	69.087	28.702
	2	−0.98265	2.93×10^{10}	466.53	108.96	−49.05	105.081	22.988
	3	−0.99165	1.897×0^{30}	557.35	332.7696	328.75	328.135	−182.9
	4	−0.98539	1.56×10^{11}	847.22	221.028	−40.106	213.983	34.19
CoAXCPC2	1	−0.98253	9.2×10^{2}	481.77	51.091	−192.96	47.086	93.009
	2	−0.98148	2.23×10^{24}	820.88	419.258	212.009	412.43	−173.6
NiAXCPC2	1	−0.98108	1.16×10^{6}	484.37	80.665	−133.64	76.63	64.8
	2	−0.98349	1.86×10^{19}	786.88	325.358	115.128	318.81	−90.27
Cu−AXCPC2	1	−0.981	3.13×10^{8}	478.71	99.86	−87.005	95.88	41.74
	2	−0.98863	4.66×10^{36}	554.73	408.458	451.134	403.84	−249.8
	3	−0.98164	$1{,}5 \times 10^{17}$	729.89	275.889	75.675	269.82	−54.9
Zn-AXCPC2	1	−0.98843	1.3×10^{21}	482.54	213.025	154.5	209.01	−74.34
	2	0.98989	2.089×10^{27}	543.89	305.09	272.32	300.57	−147.8
	3	0.98545	5.93×10^{13}	891.27	277.84	8.864	270.43	−7.629

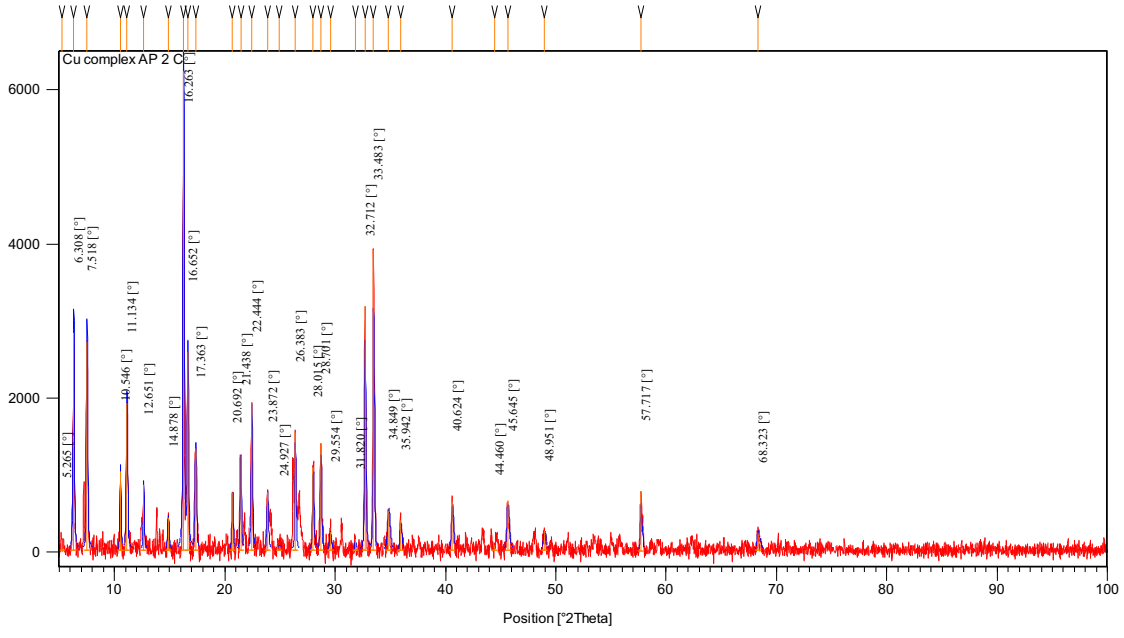

Fig. 4 X-ray diffractogram of Cu-AXCPC2.

step in the temperature range of 582.67–672.77 °C with T_{DTG} = 618.27 °C is associated with the complete loss of ligand moiety and leaves zinc oxide as stable residue. This can be concluded by the horizontal portion of thermogram after 672.77 °C. The T_{DTA} peak for this step at 619 °C concludes exothermal effect.

3.3.1. Kinetic parameter

The thermodynamic and kinetic parameters of the ligand and metal complexes have been extracted from thermogravimetric (TG) and differential thermal analysis (DTA) curves and the computed values are presented in Table 7. These parameters were evaluated graphically by employing the Coats-Redfern method [32,33].

$$\ln\left[-\frac{ln(1-\alpha)}{T^2}\right] = ln\left[\frac{AR}{\beta E^*}\right] - \frac{E^*}{RT}$$

where, α represents the decomposition fraction at temperature T K, β denotes linear heating rate (dT/dt). E^* and A denote the activation energy and Arrhenius pre-exponential factor respectively. R represents gas constant. A linear plot of left side versus $1/T$ of Coats-Redfern equation gives a straight line, whose slope E^*/R furnishes activation energy parameter and the pre-exponential factor (A) can be determined from the intercept. The other thermodynamic parameters such as entropy of activation (ΔS^*), enthalpy of activation (ΔH^*) and free energy of activation (ΔG^*) have been calculated by using the following relation:

$$\Delta S^* = Rln\left[\frac{Ah}{k_B T}\right]$$

$$\Delta H^* = E^* - RT$$

$$\Delta G^* = \Delta H^* - T\Delta S^*$$

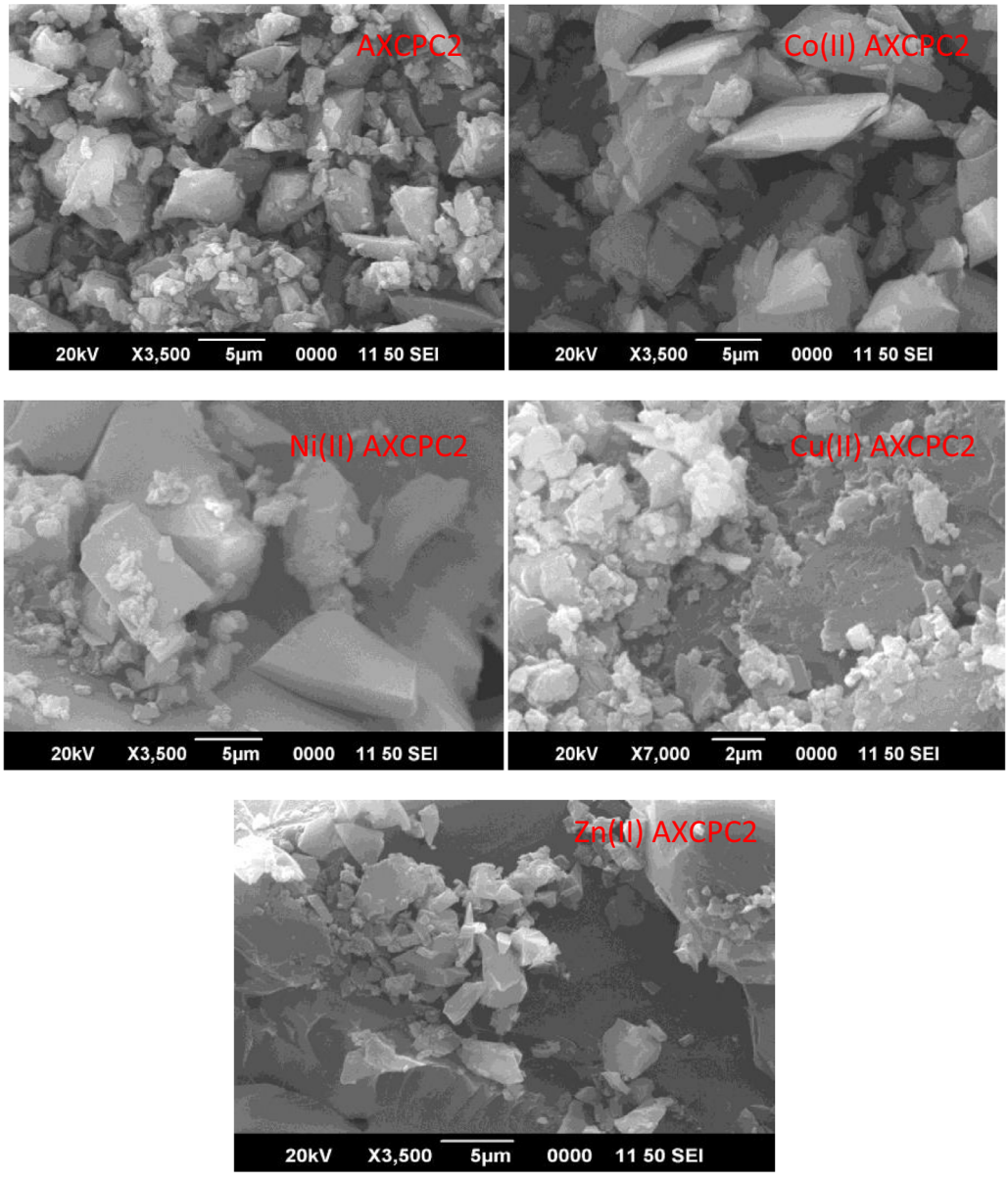

Fig. 5 SEM micrograph images of AXCPC2 ligand and its metal complexes.

Following remarks can be pointed out:

(1) The activation energy (E^*) values of the subsequent steps are increasing on going from one to another decomposition steps and this reveals the decreasing rate of decomposition of complexes. The rate of decomposition of ligand parts from the complex is becoming slow and this reflects the greater stability of the complex [34].

(2) The negative entropy of activation, ΔS^*, values in the most of the decomposition steps reveals slow reaction process with more ordered activated complex. Moreover, positive values of ΔS^* are also seen in some decomposition steps and this reflects spontaneous decomposition process [35].

(3) The positive value of enthalpy, ΔH^*, in all the decomposition steps means that the decomposition processes are endothermic [36].

(4) The endothermic decomposition processes of various decomposition steps are further supported by positive values of ΔG^* in most of the steps and justify non-spontaneous nature.

3.4. XRPD study

The crystal parameters of metal complexes of AXCPC2 ligand were studied by powder X-ray diffraction technique. The diffractogram of Co-AXCPC2 ligand displays 12 reflection peaks with a most intense peak at 15.992° with corresponding d spacing value of 5.54217 Å. The cell dimensions $\alpha = b = 8.29$ Å, $c = 16.71$ Å, $\alpha = \beta = \gamma = 90°$, represent tetragonal crystal system with p3 space group. The calculated unit cell volume for this complex is 1147.36 Å^3. The average crystallite size of 51.02825 nm executes nanocrystalline nature of this complex. The diffractogram of the Ni-AXCPC2 complex registered 24 well-resolved reflection peaks with peak maxima at 18.5777° with corresponding interplanar d spacing value of

Table 8 Selected bond lengths and bond energy parameters of metal complexes of AXCPC2 ligand.

Complex	Atoms	Bond length (Å)	Atoms	Bond angle (°)	Optimized energy
Co-AXCPC2	O(59)-Co(32)	0.6801	O(59)-Co(32)-O(39)	106.5764	381.6644
	O(39)-Co(32)	1.1215	O(59)-Co(32)-N(30)	73.3276	Tor. 119.7329
	N(30)-Co(32)	2.0047	O(59)-Co(32)-N(16)	112.7752	
	N(16)-Co(32)	2.0698	O(59)-Co(32)-N(28)	124.7521	VDW
	Co(32)-N(28)	1.8101	O(59)-Co(32)-N(11)	78.1462	198.1346
	Co(32)-N(11)	2.1069	O(39)-Co(32)-N(30)	113.3071	
			O(39)-Co(32)-N(16)	136.8934	
			O(39)-Co(32)-N(28)	71.5159	
			O(39)-Co(32)-N(11)	84.0389	
			N(30)-Co(32)-N(16)	94.6027	
			N(30)-Co(32)-N(28)	59.4005	
			N(30)-Co(32)-N(11)	149.8053	
			N(16)-Co(32)-N(28)	98.6275	
			N(16)-Co(32)-N(11)	87.3484	
			N(28)-Co(32)-N(11)	150.0385	
Ni-AXCPC2	N(45)-Ni(59)	1.8521	N(45)-Ni(59)-N(16)	76.0495	233.2716
	N(16)-Ni(59)	1.8306	N(45)-Ni(59)-N(40)	70.0498	Tor. 48.383
	N(40)-Ni(59)	1.8245	N(45)-Ni(59)-N(11)	91.1137	VDW
	N(11)-Ni(59)	1.8215	N(16)-Ni(59)-N(40)	130.7710	25.8868
			N(16)-Ni(59)-N(11)	88.8005	
			N(40)-Ni(59)-N(11)	125.6416	
Cu-AXCPC2	N(45)-Cu(59)	1.3338	N(45)-Cu(59)-N(16)	120.9419	170.8828
	N(16)-Cu(59)	1.3396	N(45)-Cu(59)-N(40)	88.8246	Tor. 66.8742
	N(40)-Cu(59)	1.8536	N(45)-Cu(59)-N(11)	101.1583	Dip. 11.1601
	N(11)-Cu(59)	1.8509	N(16)-Cu(59)-N(40)	105.3507	VDW 40.2188
			N(16)-Cu(59)-N(11)	104.0951	
			N(40)-Cu(59)-N(11)	137.8060	
Zn-AXCPC2	O(59)-Zn(32)	1.8804	Zn(32)-O(59)-C(15)	133.3517	178.8377
	O(39)-Zn(32)	1.8931	O(59)-Zn(32)-O(39)	132.0569	Tor. 92.2682
	N(30)-Zn(32)	1.9458	O(59)-Zn(32)-N(30)	76.3639	Dip./Dip.
	N(16)-Zn(32)	1.9358	O(59)-Zn(32)-N(28)	148.0973	16.2998
	Zn(32)-N(28)	1.9576	O(59)-Zn(32)-N(16)	87.4666	VDW
	Zn(32)-N(11)	2.0234	O(59)-Zn(32)-N(11)	76.0839	45.9981
			O(39)-Zn(32)-N(30)	89.7547	
			O(39)-Zn(32)-N(28)	67.9057	
			O(39)-Zn(32)-N(16)	139.5210	
			O(39)-Zn(32)-N(11)	90.0544	
			N(30)-Zn(32)-N(28)	79.6744	
			N(30)-Zn(32)-N(16)	111.4034	
			N(30)-Zn(32)-N(11)	142.4048	
			N(28)-Zn(32)-N(16)	81.9590	
			N(28)-Zn(32)-N(11)	134.0984	
			N(16)-Zn(32)-N(11)	92.3833	

4.7762 Å. The cell dimensions $a = b = 12.333$ Å, $c = 20.713$ Å, $\alpha = \beta = \gamma = 90°$, represents tetragonal crystal system and the space group is P42BC. The calculated unit cell volume is 3150.7 Å^3 and the average crystallite size is 46.5554 nm and this represents nanocrystalline nature of the complex. Thirty reflection peaks have been registered in the diffractogram of the Cu-AXCPC2 complex (Fig. 4). The most intense peak with 100% intensity has recorded at 16.2628° with interplanar d spacing value 5.4505 Å. The unit cell dimensions $a = 13.179$ Å, $b = 16.931$ Å, $c = 7.274$ Å, $\alpha = \gamma = 90°$, $\beta = 102°$, suggest monoclinic crystal system with space group p21. The calculated unit cell volume of this complex is 1581 Å^3. The average crystallite size 57.3205 nm suggests nanocrystalline nature of this complex. The diffractograms of AXCPC2 and the Zn-AXCPC2 revealed their amorphous nature.

3.5. SEM study of AXCPC2 and metal complexes

An intimate observation of SEM micrographs of AXCPC2 ligand and metal complexes reveals the fact that there is a significant difference in their images, which may be attributed to change in the metal ions. The SEM images of AXCPC2 ligand and metal complexes are shown in Fig. 5. The SEM micrograph of AXCPC2 ligand displays non-uniform sized and irregularly shaped crystalline structure. However, Co-AXCPC2 complex shows sharp edged needle like crystal. The Ni-AXCPC2 complex reveals ice like crystalline structure and agglomerated morphology is seen for the Cu-AXCPC2 complex. The broken rock like structure with layered morphology has observed in the SEM micrograph of the Zn-AXCPC2 complex [37].

3.6. Molecular modeling study

The molecular modeling of AXCPC2 ligand and its four metal complexes was achieved by optimizing their structures in CsChem Office 3D Ultra-11 program package. The energy optimization was done several times to get minimum geometrical energy and to register the maximum stability of the complexes [38]. The details of the bond length and bond angles of the complexes, optimized by MM2 calculations are given Table 8. The Co-AXCPC2 complex exhibits maximum geometrical energy of 381.6644 kcal/mol and is relatively less stable than others. The torsional energy for this complex is 119.7329 kcal/mol. Due to the large size of this molecule, there has a deviation of bond angles and bond lengths from the normal value of octahedral geometry [39]. The optimized geometrical and torsional energy for the Ni-AXCPC2 complex are 233.2716 kcal/mol and 48.383 kcal/mol. The bond angle and bond length data support square planar geometry of this complex. The tetrahedral geometry of Cu-AXCPC2 complex is evidenced by bond angle and bond length data that are computed in Table 8. The optimized energy and torsional energy for this complex have measured 170.8828 kcal/mol and 66.8742 kcal/-mol respectively. The energy data suggests maximum stability of this complex. The IR and electronic absorption spectral study reveal the octahedral geometry of Zn-AXCPC2 complex which is further supported by bond angle and bond length data. The final geometrical and torsional energy for this complex are 178.8377 kcal/mol and 92.2682 kcal.mol respectively. The stability of the complexes follows the order, Cu-AXCPC2 > Zn-AXCPC2 > Ni-AXCPC2 > Co-AXCPC2.

3.7. Antibacterial sensitivity studies

The AXCPC2 ligand and its metal complexes under this category were tested for *in vitro* to access their growth inhibitory activity against *E. coli*, *K. pneumoniae*, *P. vulgaris* and *S. aureus* bacterial pathogens by the standard Kirby Bauer paper disc diffusion method [40,41]. Three different concentrations of the compounds (100, 50 and 25 mcg/mcl) have been used for this purpose and the growth inhibitory data are summarized in Table 9. Amoxicillin with different concentrations was used as reference standard to compare the growth inhibition zone with synthesized complexes. The amikacin 30 mcg per disc was used as control drug to compare the relative antibacterial activity of the complexes. The antibacterial results are presented in the bar graphs Figs. 6–8. The results declare the higher antibacterial activity of AXCPC2 ligand relative to parent drug amoxicillin. All the metal complexes deliver better antibacterial activity at higher concentration and they deliver considerable activity at lower concentrations. The Co-AXCPC2 complex is found less active with all the bacterial pathogens except *S. aureus* bacteria. At 25 mcg/mcl concentration, the Co-AXCPC2 complex is found almost resistant to *E. coli*, *P. vulgaris*, and *K. pneumoniae* bacteria. However, Ni-AXCPC2 and Cu-AXCPC2 complexes showed better antibacterial activity. The Zn-AXCPC2 complex also delivers considerable activity at higher concentration. The computed antibacterial data concludes greater inhibitory effect of ligand and metal complexes with *P. vulgaris* and *S. aureus* bacteria. The antibacterial activity of the metal chelates can be

Table 9 Antibacterial data of AXCPC2 Schiff base ligand and metal complexes.

Compounds	Diameter of zone of inhibition in mm											
	E. coli			*K. pneumoniae*			*P. vulgaris*			*S. aureus*		
Concentration (mcg/mcl)	100	50	25	100	50	25	100	50	25	100	50	25
AXCPC2	24	18	17	11	10	10	13	11	10	23	14	12
Co-AXCPC2	11	–	–	15	11	–	10	8	–	19	13	10
Ni-AXCPC2	14	13	12	15	11	–	12	11	8	16	14	14
Cu-AXCPC2	14	14	12	19	14	11	15	14	13	20	19	19
Zn-AXCPC2	12	–	–	14	11	–	15	14	12	18	18	18
Amoxicillin	24	15	12	14	12	8	18	16	10	19	15	14
Amikacin	20	20	20	18	18	18	27	27	27	26	26	26
MeOH	0	0	0	0	0	0	0	0	0	0	0	0

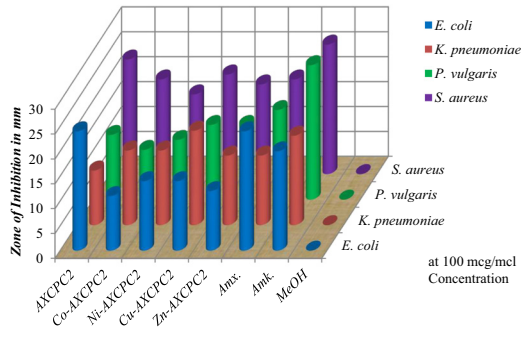

Fig. 6 Bar graph showing antibacterial activity of AXCPC2 Schiff base ligand and metal complexes at 100 mcg/mcl concentration.

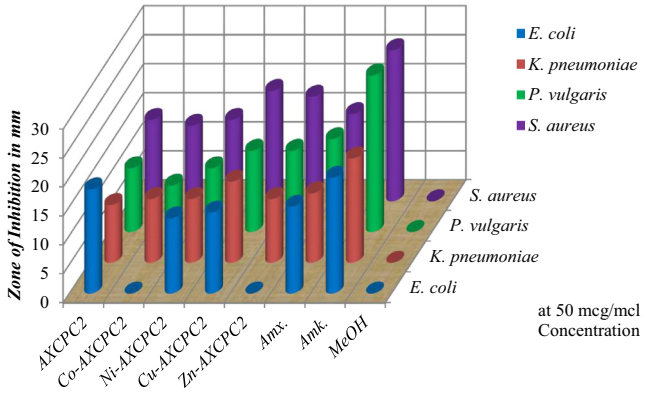

Fig. 7 Bar graph showing antibacterial activity of AXCPC2 Schiff base ligand and metal complexes at 50 mcg/mcl concentration.

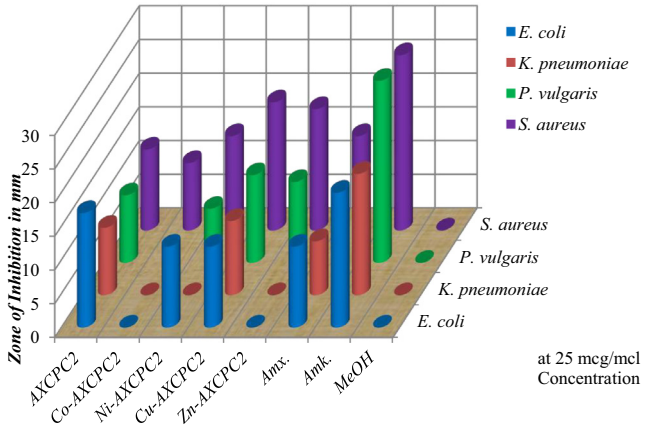

Fig. 8 Bar graph showing antibacterial activity of AXCPC2 Schiff base ligand and metal complexes at 25 mcg/mcl concentration.

explained by overtone concept and the Tweedy's chelation theory [42]. The variation in the activity of complex against different organisms depends either on the impermeability of the microbial cells or difference in ribosomal parts of the organisms [39,43–45].

4. Conclusion

The penicillin based Schiff base ligand derived from amoxicillin and pyridine-2-carbaldehyde is of promising research interest and its coordination with metals (M = Co(II), Ni (II), Cu(II), & Zn(II)) has afforded variable structural geometry of the complexes. From the analytical and spectral data analysis, it has observed the octahedral geometry for Co-AXCPC2 and Zn-AXCPC2 complexes, square planar geometry for Ni-AXCPC2 and tetrahedral geometry for the Cu-AXCPC2 complex. Theoretical data obtained from the energy optimization through molecular modeling software and the analysis of the bond lengths and bond angles data nicely interprets the concerned geometry and provides in line support. The antibacterial screening showed that the ligand and the complexes have well antibacterial potency against all the tested human pathogenic organisms. Furthermore, the growth inhibitory effect of the complexes is seen higher at 100 mcg/mcl concentration of the complexes. However, the interaction of the ligand and metal complexes with *P. vulgaris* and *S. aureus* bacteria is highly noticeable. These biological findings of our study would be the new hope for the development of more potent metal based therapeutic drugs.

Acknowledgement

This research work has financially supported by Nepal Academy of Science and Technology (NAST), so one of the authors is highly indebted to acknowledge this organization.

References

[1] K. Brodowska, E. Łodyga-Chruścińska, Schiff bases – interesting range of applications in various fields of science, Chemik. 68 (2014) 129–134, https://doi.org/10.1002/chin.201511346.

[2] A.A. Abdel Aziz, I.S.A. El-Sayed, M.M.H. Khalil, Some divalent metal(II) complexes of novel potentially tetradentate Schiff base N, N′-bis(2-carboxyphenylimine)-2,5-thiophenedicarboxaldhyde: Synthesis, spectroscopic characterization and bioactivities, Appl. Organometalllic Chem. (2017), https://doi.org/10.1002/aoc.3730.

[3] A. Ganguly, S. Ghosh, S. Kar, N. Guchhait, Selective fluorescence sensing of Cu(II) and Zn(II) using a simple Schiff base ligand: Naked eye detection and elucidation of photoinduced electron transfer (PET) mechanism, Spectrochim. Acta Part A Mol. Biomol. Spectrosc. 143 (2015) 72–80, https://doi.org/10.1016/j.saa.2015.02.013.

[4] M.A. Ashraf, K. Mahmood, A. Wajid, Synthesis, characterization and biological activity of schiff bases, Int. Conf. Chem. Chem. Process. 10 (2011) 1–7.

[5] M.S. Refat, H.M.A. Al-Maydama, F.M. Al-Azab, R.R. Amin, Y.M.S. Jamil, Synthesis, thermal and spectroscopic behaviors of metal-drug complexes: La(III), Ce(III), Sm(III) and Y(III) amoxicillin trihydrate antibiotic drug complexes, Spectrochim. Acta - Part A: Mol. Biomol. Spectrosc. 128 (2014) 427–446, https://doi.org/10.1016/j.saa.2014.02.160.

[6] O.E. Sherif, N.S. Abdel-Kader, DFT calculations, spectroscopic studies, thermal analysis and biological activity of

supramolecular Schiff base complexes, Arabian J. Chem. (2015), https://doi.org/10.1016/j.arabjc.2015.07.008.
[7] A.M. Abu-Dief, I.M.A. Mohamed, A review on versatile applications of transition metal complexes incorporating Schiff bases, Beni-Suef Univ. J. Basic Appl. Sci. 4 (2015) 119–133, https://doi.org/10.1016/j.bjbas.2015.05.004.
[8] P.G. Cozzi, Metal-Salen Schiff base complexes in catalysis: practical aspects, Chem. Soc. Rev. 33 (2004) 410–421, https://doi.org/10.1039/b307853c.
[9] W. Qin, S. Long, M. Panunzio, S. Biondi, Schiff bases: a short survey on an evergreen chemistry tool, Molecules 18 (2013) 12264–12289, https://doi.org/10.3390/molecules181012264.
[10] L.H. Abdel-Rahman, A.M. Abu-dief, S.K. Hamdan, A.A. Sellem, Nano structure iron (II) and copper (II) Schiff base complexes of a NNO-tridentate ligand as new antibiotic agents: spectral, thermal behaviors and DNA binding ability, Int. J. Nanomater. Chem. 1 (2015) 65–77, https://doi.org/10.12785/ijnc/010204.
[11] S.G. Shirodkar, P.S. Mane, T.K. Chondhekar, Synthesis and fungitoxic studies of Mn(II), Co(II), Ni(II) and Cu(II) with some heterocyclic schiff base ligands, Indian J. Chem. 40 (2001) 1114–1117.
[12] M. Sönmez, A. Levent, M. Şekerci, Synthesis, characterization, and thermal investigation of some metal complexes containing polydentate ONO-donor heterocyclic Schiff base ligand, Russ. J. Coord. Chem. 30 (2004) 695–699. http://link.springer.com/10.1023/B:RUCO.0000040726.57728.a3.
[13] M.S. Butler, M.A. Blaskovich, M.A. Cooper, Antibiotics in the clinical pipeline in 2013, J. Antibiot. 66 (2013) 571–591, https://doi.org/10.1038/ja.2013.86.
[14] I.O. Okonko, E.A. Fajobi, T.A. Ogunnusi, A.A. Ogunjobi, C.H. Obiogbolu, Antimicrobial chemotherapy and sustainable development: The past, the current trend, and the future, Afr. J. Biomed. Res. 11 (2008) 235–250, https://doi.org/10.4314/ajbr.v11i3.50752.
[15] N.K. Chaudhary, P. Mishra, Metal complexes of a novel Schiff base based on penicillin: characterization, molecular modeling, and antibacterial activity study, Bioinorg. Chem. Appl. 2017 (2017), https://doi.org/10.1155/2017/6927675.
[16] N.K. Chaudhary, P. Mishra, Spectral investigation and in vitro antibacterial evaluation of Ni II and Cu II complexes of Schiff base derived from amoxicillin and α-formylthiophene (α-ft), J. Chem. 2015 (2015), https://doi.org/10.1155/2015/136285.
[17] D. Sevillano, A. Calvo, M.J. Gimenez, L. Alou, L. Aguilar, E. Valero, A. Carcas, J. Prieto, Bactericidal activity of amoxicillin against non-susceptible Streptococcus pneumoniae in an in vitro pharmacodynamic model simulating the concentrations obtained with the 2000/125 mg sustained-release co-amoxiclav formulation, J. Antimicrob. Chemother. 54 (2004) 1148–1151, https://doi.org/10.1093/jac/dkh463.
[18] P.F. Rapheal, E. Manoj, M.R.P. Kurup, Copper(II) complexes of N(4)-substituted thiosemicarbazones derived from pyridine-2-carbaldehyde: Crystal structure of a binuclear complex, Polyhedron 26 (2007) 818–828, https://doi.org/10.1016/j.poly.2006.09.091.
[19] A. Reiss, M.C. Chifiriuc, E. Amzoiu, C.I. Spînu, Transition metal(II) complexes with cefotaxime-derived schiff base: Synthesis, characterization, and antimicrobial studies, Bioinorg. Chem. Appl. 2014 (2014), https://doi.org/10.1155/2014/926287.
[20] I. Anis, N. Afza, M. Aslam, Z. Noreen, A. Hussain, M.T. Hussain, T.A. Sherazi, M.R. Shah, Synthesis, characterization, antimicrobial and cytotoxic evaluation of a bidentate Schiff base ligand: {5-chloro-2-[(4-nitrobenzylidene)amino]phenyl}(phenyl) methanone and its transition metal (II) complexes, J. Chem. Soc. Pakistan 35 (2013) 1508–1515.
[21] P. Živec, F. Perdih, I. Turel, G. Giester, G. Psomas, Different types of copper complexes with the quinolone antimicrobial drugs ofloxacin and norfloxacin: Structure, DNA- and albumin-binding, J. Inorg. Biochem. 117 (2012) 35–47, https://doi.org/10.1016/j.jinorgbio.2012.08.008.
[22] X. Zhang, J.J. Han, M. Huang, G.Y. Zhang, Synthesis, crystal structures and antibacterial activities of Schiff base ligand and its cobalt (II) complex, Russ. J. Coord. Chem. 38 (2012) 560–566, https://doi.org/10.1134/S1070328412080106.
[23] A.A. El-Sherif, M.R. Shehata, M.M. Shoukry, M.H. Barakat, Synthesis, characterization, equilibrium study and biological activity of Cu(II), Ni(II) and Co(II) complexes of polydentate Schiff base ligand, Spectrochim. Acta Part A, Mol. Biomol. Spectrosc. 96 (2012) 889–897, https://doi.org/10.1016/j.saa.2012.07.047.
[24] K. Singh, Y. Kumar, P. Puri, C. Sharma, K.R. Aneja, Antimicrobial, spectral and thermal studies of divalent cobalt, nickel, copper and zinc complexes with triazole Schiff bases, Arabian J. Chem. (2013), https://doi.org/10.1016/j.arabjc.2012.12.038.
[25] A.A. Dehghani-firouzabadi, S. Firouzmandi, Synthesis and characterization of a new unsymmetrical potentially pentadentate Schiff base ligand and related complexes with manganese(II), nickel(II), copper(II), zinc(II) and cadmium(II), J. Braz. Chem. Soc. (2016) 1–7, https://doi.org/10.21577/0103-5053.20160226.
[26] M.S. Iqbal, I.H. Bukhari, M. Arif, Preparation, characterization and biological evaluation of copper(II) and zinc(II) complexes with Schiff bases derived from amoxicillin and cephalexin, Appl. Organomet. Chem. 19 (2005) 864–869, https://doi.org/10.1002/aoc.918.
[27] X. Ran, L. Wang, Y. Lin, J. Hao, D. Cao, Syntheses, characterization and biological studies of zinc(II), copper(II) and cobalt(II) complexes with Schiff base ligand derived from 2-hydroxy-1-naphthaldehyde and selenomethionine, Appl. Organomet. Chem. 24 (2010) 741–747, https://doi.org/10.1002/aoc.1678.
[28] S.K. Bharti, S.K. Patel, G. Nath, R. Tilak, S.K. Singh, Synthesis, characterization, DNA cleavage and in vitro antimicrobial activities of copper(II) complexes of Schiff bases containing a 2,4-disubstituted thiazole, Transition Met. Chem. 35 (2010) 917–925, https://doi.org/10.1007/s11243-010-9412-8.
[29] B. Manjula, S.A. Antony, C.J. Dhanaraj, Synthesis, spectral characterization, and antimicrobial activities of Schiff base complexes derived from 4-aminoantipyrine, Spectros. Lett.: Int. J. Rapid Commun. 47 (2014) 518–526, https://doi.org/10.1080/00387010.2013.820196.
[30] H.F. Abd El-Halim, G.G. Mohamed, E.A.M. Khalil, Synthesis, spectral, thermal and biological studies of mixed ligand complexes with newly prepared Schiff base and 1,10-phenanthroline ligands, J. Mol. Struct. 1146 (2017) 153–163, https://doi.org/10.1016/j.molstruc.2017.05.092.
[31] A. Dylong, M. Sowa, W. Goldeman, K. Ślepokura, P. Drozdzewski, B. Szponar, E. Matczak-Jon, Zinc(II) complexes derived from imidazo [1,2-a] pyridin-2- ylacetic acid (HIP-2-ac): [Zn(IP-2-ac)2(H_2O)] and unexpectedly, [Zn3(IP-2-ac)$_6$(H_2O)]·11H_2O, J. Coord. Chem. (2015), https://doi.org/10.1080/00958972.2015.1048241.
[32] A.W. Coats, J.P. Redfern, Thermogravimetric analysis, Analyst. 88 (1963).
[33] N. Kavitha, P.V. Anantha, Lakshmi, Synthesis, characterization and thermogravimetric analysis of Co(II), Ni(II), Cu(II) and Zn (II) complexes supported by ONNO tetradentate Schiff base ligand derived from hydrazino benzoxazine, J. Saudi Chem. Soc. 21 (2017) S457–S466, https://doi.org/10.1016/j.jscs.2015.01.003.
[34] M. Gaber, H. El-Ghamry, F. Atlam, S. Fathalla, Synthesis, spectral and theoretical studies of Ni(II), Pd(II) and Pt(II) complexes of 5-mercapto-1,2,4-triazole-3-imine-2′-hydroxynaphyhaline, Spectrochim. Acta Part A Mol. Biomol. Spectrosc. 137 (2015) 919–929, https://doi.org/10.1016/j.saa.2014.09.015.

[35] M. Montazerozohori, S. Zahedi, A. Naghiha, M.M. Zohour, Synthesis, characterization and thermal behavior of antibacterial and antifungal active zinc complexes of bis (3(4-dimethylaminophenyl)-allylidene-1,2-diaminoethane, Mater. Sci. Eng., C 35 (2014) 195–204, https://doi.org/10.1016/j.msec.2013.10.030.

[36] W.H. Mahmoud, G.G. Mohamed, M.M.I. El-dessouky, Synthesis, characterization and in vitro biological activity of mixed transition metal complexes of lornoxicam with 1,10-phenanthroline, Int. J. Electrochem. Sci. 9 (2014) 1415–1438.

[37] M. Shakir, S. Hanif, M.A. Sherwani, O. Mohammad, S.I. Al-Resayes, Pharmacologically significant complexes of Mn(II), Co (II), Ni(II), Cu(II) and Zn(II) of novel Schiff base ligand, (E)-N-(furan-2-yl methylene) quinolin-8-amine : Synthesis, spectral, XRD, SEM, antimicrobial, antioxidant and in vitro cytotoxic studies, J. Mol. Struct. (2015), https://doi.org/10.1016/j.molstruc.2015.03.012.

[38] U. El-Ayaan, A.A.-M. Abdel-Aziz, Synthesis, antimicrobial activity and molecular modeling of cobalt and nickel complexes containing the bulky ligand: bis[N-(2,6-diisopropylphenyl) imino] acenaphthene, Eur. J. Med. Chem. 40 (2005) 1214–1221, https://doi.org/10.1016/j.ejmech.2005.06.009.

[39] M.R. Hasan, M.A. Hossain, M.A. Salam, M.N. Uddin, Nickel complexes of Schiff bases derived from mono/diketone with anthranilic acid: Synthesis, characterization and microbial evaluation, J. Taibah Univ. Sci. (2015), https://doi.org/10.1016/j.jtsci.2015.11.007.

[40] A.A. Abdel Aziz, A.N.M. Salem, M.A. Sayed, M.M. Aboaly, Synthesis, structural characterization, thermal studies, catalytic efficiency and antimicrobial activity of some M(II) complexes with ONO tridentate Schiff base N-salicylidene-o-aminophenol ($saphH_2$), J. Mol. Struct. 1010 (2012) 130–138, https://doi.org/10.1016/j.molstruc.2011.11.043.

[41] M.S. Nair, D. Arish, R.S. Joseyphus, Synthesis, characterization, antifungal, antibacterial and DNA cleavage studies of some heterocyclic Schiff base metal complexes, J. Saudi Chem. Soc. 16 (2012) 83–88, https://doi.org/10.1016/j.jscs.2010.11.002.

[42] S.W. Smith, The role of chelation in the treatment of other metal poisonings, J. Med. Toxicol. 9 (2013) 355–369, https://doi.org/10.1007/s13181-013-0343-6.

[43] D. Chaturvedi, M. Kamboj, Role of Schiff Base in drug discovery research, Chem. Sci. J. 7 (2016), https://doi.org/10.4172/2150-3494.1000e114.

[44] A. Manimaran, V. Chinnusamy, C. Jayabalakrishnan, Synthesis, spectral characterization, C-C coupling, oxidation reactions and antibacterial activities of new ruthenium(III) Schiff base complexes, Appl. Organomet. Chem. 25 (2011) 87–97, https://doi.org/10.1002/aoc.1720.

[45] H.A. Ali, H. Fares, M. Darawsheh, E. Rappocciolo, M. Akkawi, S. Jaber, Synthesis, characterization and biological activity of new mixed ligand complexes of Zn(II) naproxen with nitrogen based ligands, Eur. J. Med. Chem. 89 (2015) 67–76, https://doi.org/10.1016/j.ejmech.2014.10.032.

Hindawi
Bioinorganic Chemistry and Applications
Volume 2017, Article ID 6927675, 13 pages
https://doi.org/10.1155/2017/6927675

Research Article

Metal Complexes of a Novel Schiff Base Based on Penicillin: Characterization, Molecular Modeling, and Antibacterial Activity Study

Narendra Kumar Chaudhary and Parashuram Mishra

Bio-Inorganic and Materials Chemistry Research Laboratory, Tribhuvan University, M. M. A. M. Campus, Biratnagar, Nepal

Correspondence should be addressed to Parashuram Mishra; prmmishra@rediffmail.com

Received 11 January 2017; Revised 4 April 2017; Accepted 12 April 2017; Published 8 June 2017

Academic Editor: Spyros P. Perlepes

A novel Schiff base ligand of type HL was prepared by the condensation of amoxicillin trihydrate and nicotinaldehyde. The metal complexes of Co^{+2}, Ni^{+2}, Cu^{+2}, and Zn^{+2} were characterized and investigated by physical and spectral techniques, namely, elemental analysis, melting point, conductivity, ^{1}H NMR, IR, UV-Vis spectra, ESR, SEM, and mass spectrometry measurements. They were further analyzed by thermal technique (TGA/DTA) to gain better insight about the thermal stability and kinetic properties of the complexes. Thermal data revealed high thermal stability and nonspontaneous nature of the decomposition steps. The Coats-Redfern method was applied to extract thermodynamic parameters to explain the kinetic behavior. The molar conductance values were relatively low, showing their nonelectrolytic nature. The powder XRD pattern revealed amorphous nature except copper complex (1c) that crystallized in the triclinic crystal system. The EPR study strongly recommends the tetrahedral geometry of 1c. The structure optimization by MM force field calculation through ArgusLab 4.0.1 software program supports the concerned geometry of the complexes. The in vitro antibacterial activity of all the compounds, at their two different concentrations, was screened against four bacterial pathogens, namely, *E. coli, P. vulgaris, K. pneumoniae, and S. aureus,* and showed better activity compared to parent drug and control drug.

1. Introduction

Schiff bases containing penicillin and heterocyclic structural units with N, N donor atoms are considered the most prominent research area in the field of coordination chemistry [1–3]. The various donor atoms in them offer special ability for binding metals. The incorporated metals in the lattice of donor atoms of Schiff base change the physiological, morphological, and pharmacological activities of the compounds. The penicillin based Schiff base is of promising research interest owing to the widespread antibacterial resistance of the medical science. Moreover, the revival of research is essential to generate new Schiff base metal complexes with a diverse range of applications. Schiff base complexes have been used as drugs and have valuable antibacterial [4, 5], antifungal [6–8], antiviral [9, 10], anti-inflammatory [11], and antitumor activities [12]. Besides these, they also bear strong catalytic activity in various chemical reactions in chemistry [13] and surfactant activities [14] and as memory storage devices in electronics [15–17]. One of the compounds used to prepare ligand is amoxicillin, a β-lactam antibiotic. It is a broad spectrum, semisynthetic penicillin type antibiotic that has potent bactericidal activity against many gram positive and gram negative bacterial pathogens [18]. It takes action against bacteria by preventing them from forming the cell wall and stopping them from growing. In medical science, it has important application for the treatment of bronchitis, ear infection, pneumonia, throat infections, tonsillitis, typhoid, and urinary tract infections. In combination with other antibiotics, it bears potential applications for the successful treatment of many pathogenic infections. However, synthetic modification in amoxicillin by coordination with metal ions of various types has been found to bear enhanced credibility, as documented in several research papers. Cisplatin is the

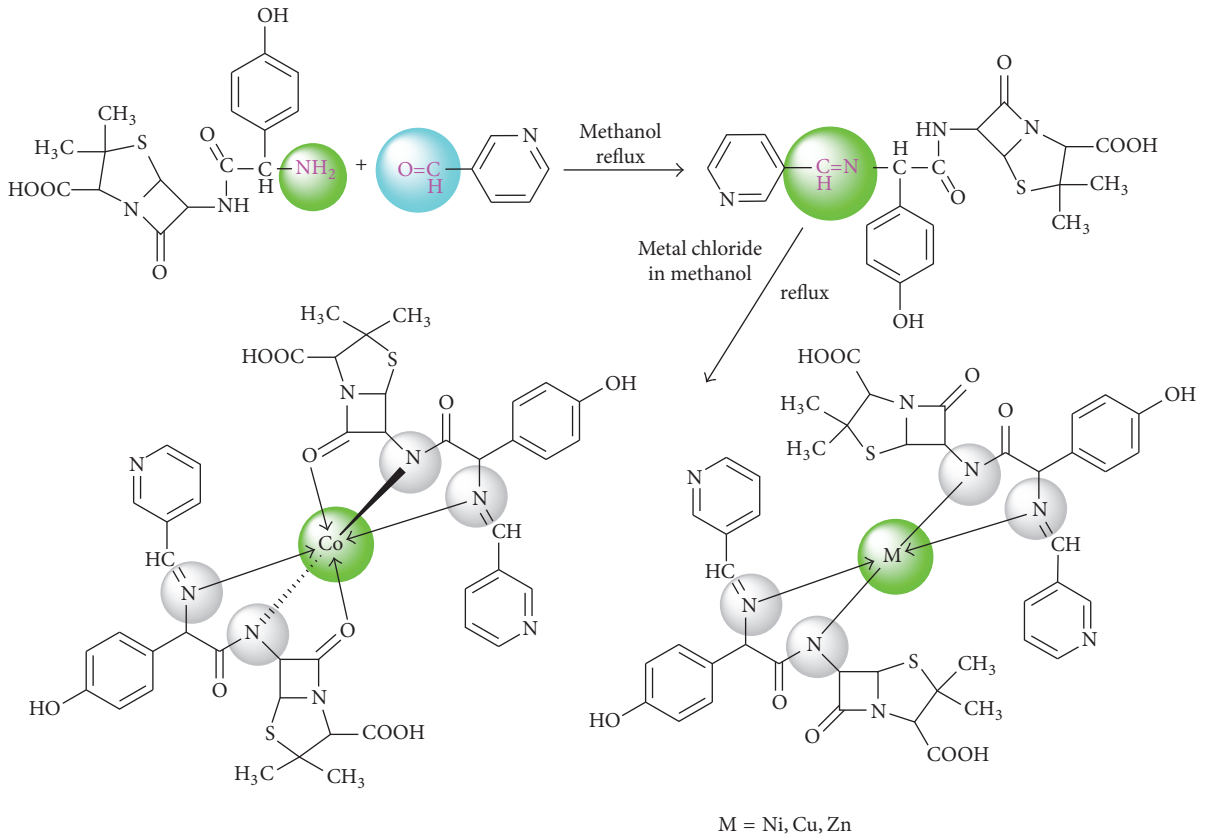

Scheme 1: Synthetic scheme for the ligand (HL) and its metal complexes.

first metal based drug that emerged in the 20th century and enlightened the world as a promising anticancer drug [19]. Since then several research findings culminated the ideas of inclusion of metals in medicine. Many biological molecules containing pyridine moiety as a part of their structural unit bear enzymatic functions as well as the compounds of diverse biological interest. The pyridine derivatives are reported to have herbicidal, fungicidal, and insecticidal activities and also constitute the major core part of biological enzymes, important vitamins, and toxic alkaloids. Its wide applications in agroindustry and as pharmaceutical ingredients in drug discovery are the key points for this research investigation. Nicotinaldehyde (also called pyridine-3-carboxaldehyde) is a class of heterocyclic compound that has pyridine ring and an aldehyde group at meta-position [20]. Among the other pyridine aldehydes, nicotinaldehyde is suitably preferred for the prevention and treatment of *Acne vulgaris*, a kind of skin disease [21].

In the present paper, we have focused on the synthesis of novel Schiff base ligand, by the condensation of amoxicillin trihydrate and nicotinaldehyde and its four metal complexes with cobalt(II), nickel(II), copper(II), and zinc(II) salts (Scheme 1). The coordination behavior of the ligand towards transition metal ions was fully investigated by various spectral and thermal techniques. The geometry of the complexes was confirmed by energy optimization through MM2 calculation supported in ChemOffice and ArgusLab software program. In continuation of our antibiotic research, we have also evaluated the antibacterial efficacy of ligand and its metal complexes against *S. aureus, E. coli, K. pneumoniae,* and *P. vulgaris* bacteria.

2. Experimental Section

2.1. Materials. All the chemicals and solvents used were of analytical reagent grade. The title compounds amoxicillin trihydrate and nicotinaldehyde in extra pure form were procured from Duchefa Biochemie, Netherlands, and Spectrochem, Mumbai, India, and used without further purification. Distilled methanol (Qualigen) was used as solvent for the synthesis. The metal salts (Co^{+2}, Ni^{+2}, Cu^{+2}, and Zn^{+2} chlorides) (Merck) were used for the synthesis of metal complexes.

2.2. Physical Measurements. Elemental microanalysis of the compounds was performed on EURO VECTOR EA 3000 micro analyzer. Melting points of the ligand and its complexes were recorded on an OMEGA melting point apparatus. The pH measurement was done on the Elico-16 pH meter. The infrared (FTIR) spectra of the prepared ligand and metal complexes were recorded on Perkin-Elmer Spectrum version 10.03.06 FT-IR spectrometer that was run as KBr discs in the range 4000–400 cm^{-1}. The ^1H NMR spectra were recorded on Bruker Avance III, 400 MHz spectrometer, using

DMSO-d_6 as solvent. The electronic absorption spectra of the complexes were recorded on single beam microprocessor Labtronics UV-Vis spectrophotometer (LT-290 model) in the range 200–1000 nm in DMSO solvent. EPR-JEOL spectra of the complexes were recorded on JES-FA200 ESR spectrometer with X-band at room temperature. ESI-MS spectra were recorded in positive mode on Agilent Q-TOF mass spectrometer equipped with an electron spray ionization source in the mass range of 200 to 1100. X-ray powder diffraction determinations were accomplished using Bruker AXS D8 Advance X-ray diffractometer with monochromatized Cu-Kα line at wavelength 1.5406 Å as the radiation source and the measurements were taken over the range of 2θ (10 to 70°). The thermal events of the compounds (TGA/DTA) were recorded on a Perkin-Elmer thermal analyzer with a linear heating rate of 20°C min^{-1} in the range of 40–730°C. The surface morphology of the synthesized ligand and metal complexes was analyzed by scanning electron microscopy technique. JEOL JSM-6390 LV scanning electron microscope was used for this investigation.

2.3. Synthesis of Ligand (HL). Amoxicillin trihydrate (2.097 g, 5 mmol) in distilled methanol (30 ml) was stirred under hot conditions for 3 hs. Solubility in methanol was marked at the temperature elevation state. Its pH was adjusted to neutral by adding 0.1 N NaOH solution. Nicotinaldehyde (0.5378 g, 5 mmol) was added slowly to the well stirred amoxicillin trihydrate solution and refluxed under stirring condition for 4 hs. A clear bright yellow solution was left undisturbed for crystallization by slow solvent evaporation process for three days. The resulting solid product was separated, recrystallized with methanol, and dried in desiccator over anhydrous $CaCl_2$. The ligand was stored in the airtight vial in the refrigerator till its further use. M. pt. 140°C. *Anal.* $C_{22}H_{22}N_4O_5S$ (454.13): Calcd. C 58.14, H 4.88, N 12.33, O 17.60, S 7.06; Found C 58.21, H 4.81, N 12.25, O 17.57, S 6.95. IR (KBr pellet, selected bands): $\overline{\upsilon}_{max}$ = 3303 (b, N-H and O-H str.), 1640 (s, C=N), 1510, 1443 (s, COOH). ^{1}H NMR (400 MHz, [D_6] DMSO): δ = 10.122 (s, 1 H, COOH), 9.425 (b, 1H, Ar-OH), 9.094 (s, 1H imine), 8.535–8.864 (m, 4H pyridine ring), 8.241–8.271 (s, 1H NH-amide), 6.718–7.625 (d, C-H aromatic), 1.118–1.562 (C-H methyl) ppm. UV/Vis: λ_{max} = 206, 262, 356 nm. ESI-MS, positive: m/z = 455 $[M + H]^+$. Conductivity: Λ_M = 10.8 μS/cm.

2.4. Synthesis of Metal Complexes

2.4.1. Co(II) Complex (1a). A solution of ligand (HL) (0.454 g, 1 mmol) in 10 ml methanol was stirred for 1 h under warm condition and a solution of $CoCl_2{\cdot}6H_2O$ (0.119 g, 0.5 mmol) in 5 ml methanol was added dropwise with continuous stirring condition. Then after the mixture solution was refluxed for 1 h over water bath with stirring, till blue colored precipitate resulted. The precipitate was filtered from the supernatant liquid, washed with methanol, and dried over anhydrous calcium chloride, yield (65%). M. pt. 285°C. *Anal.* $C_{44}H_{46}CoN_8O_{12}S_2$ (1001.2): Calcd. C 52.74, H 4.63, N 11.18, O 19.16, S 6.40; Found C 52.69, H 4.69, N 11.26, O 19.20, S 6.64. IR (KBr pellet, selected bands): $\overline{\upsilon}_{max}$ = 3417 (b, O-H str.), 1633 (s, C=N), 1510, 1443 (s, COOH), 606 (ρ_w H_2O), 526 (Co-O), 425 (Co-N). UV/Vis: λ_{max} = 263, 346–371, 457–488, 549 nm. ESI-MS, positive: m/z = 1001.2 $[M + H]^+$. Conductivity: Λ_M = 21.8 μS/cm.

2.4.2. Ni(II) Complex (1b). The nickel complex (1b) was prepared according to the procedure adopted for the preparation of 1a. A solution of $NiCl_2{\cdot}6H_2O$ (0.1188 g, 0.5 mmol) in 5 ml methanol was used for this purpose. The mixed solution of ligand (HL) and Ni^{+2} salt was refluxed for 1 and 1/2 h over water bath which resulted in green colored complex, yield (62%). M. pt. 270°C. *Anal.* $C_{44}H_{42}N_8NiO_{10}S_2$ (964.18): Calcd. C 54.73, H 4.38, N 11.60, O 16.57, S 6.64; Found C 54.55, H 4.59, N 11.59, O 16.45, S 6.44. IR (KBr pellet, selected bands): $\overline{\upsilon}_{max}$ = 3337 (b, O-H str.), 1625 (s, C=N), 1513, 1435 (s, COOH), 687 (ρ_w H_2O), 429 (Ni-N). UV/Vis: λ_{max} = 261, 346, 460, 549 nm. ESI-MS, positive: m/z = 964.18 $[M + H]^+$. Conductivity: Λ_M = 19.9 μS/cm.

2.4.3. Cu(II) Complex (1c). The copper complex (1c) was also prepared according to the procedure adopted for the preparation of 1a and 1b. A solution of $CuCl_2{\cdot}2H_2O$ (0.085 g, 0.5 mmol) in 5 ml methanol was used for this purpose. The mixed solution of ligand (HL) and Cu^{+2} salt was refluxed for 1 and 1/2 h over water bath which resulted in green colored complex, yield (65%). M. pt. 260°C. *Anal.* $C_{44}H_{42}CuN_8O_{10}S_2$ (969.18): Calcd. C 54.45, H 4.36, N 11.55, O 16.49, S 6.61; Found C 54.52, H 4.49, N 11.63, O 16.55, S 6.73. IR (KBr pellet, selected bands): $\overline{\upsilon}_{max}$ = 3379 (b, O-H str.), 1636 (s, C=N), 1512, 1436 (s, COOH), 686 (ρ_w H_2O), 444 (Ni-N). UV/Vis: λ_{max} = 227, 259, 337, 344, 485 nm. ESI-MS, positive: m/z = 969 $[M + H]^+$. Conductivity: Λ_M = 35.2 μS/cm.

2.4.4. Zn(II) Complex (1d). The zinc complex (1d) was prepared according to the above procedure and by using Zn^{+2} salt (0.07 g, 0.5 mmol). The mixed solution was refluxed for 2 h over water bath which resulted in light yellow colored complex, yield (57%). M. pt. 250°C. *Anal.* $C_{44}H_{42}N_8O_{10}S_2Zn$ (970.18): Calcd. C 54.35, H 4.35, N 11.52, O 16.45, S 6.60; Found C 54.41, H 4.43, N 11.57, O 16.49, S 6.57. IR (KBr pellet, selected bands): $\overline{\upsilon}_{max}$ = 3340 (b, O-H str.), 1629 (s, C=N), 1512, 1437 (s, COOH), 657 (ρ_w H_2O), 415 (Zn-N). ^{1}H NMR (400 MHz, [D_6] DMSO): δ = 10.123 (s, 1 H, COOH), 9.425 (b, 1H, Ar-OH), 9.295 (s, 1H imine), 8.534–8.865 (m, 4H pyridine ring), 6.720–7.66 (d, C-H aromatic), 1.118–1.571 (C-H methyl) ppm. UV/Vis: λ_{max} = 263, 346 nm. ESI-MS, positive: m/z = 970 $[M + H]^+$. Conductivity: Λ_M = 5.6 μS/cm.

2.5. Antibacterial Susceptibility Test. The antimicrobial potency of the synthesized compounds was done by assaying antibacterial activity study. The experimental portion of the study was accomplished in the laboratory of the Department of Microbiology at Mahendra Morang Adarsh Multiple Campus, Biratnagar. The compounds (HL and 1a–1d) were tested in vitro by standard Kirby-Bauer paper disc diffusion method against some gram positive and gram negative human pathogenic bacteria [12, 22, 23]. The recommended NCCLS guideline was followed for the study [24]. Well sterilized filter paper discs of 5 mm size (Whatman-model)

were used as antibiotic assay discs for testing of compounds. The discs were loaded with test compounds at two different concentrations (100 and 50 mcg/mcl in DMSO) under UV laminar flow to reduce bacterial contamination [25]. The loaded discs were dried in the laminar flow chamber by blowing hot air through hair drier. Sterilized nutrient agar media were carefully poured in the Petri plate and kept in rest for few hours in the sterilized zone for solidification. Fresh bacterial culture, revived before injection, was swabbed on the media and the loaded discs were stuck over it. One disc soaked with DMSO was used as the solvent control and amikacin (30 mcg/disc) was used as positive control. Inoculated plates were incubated at 37°C for 24 hs, and the diameter of the zone of inhibition was measured by antibiogram zone measuring scale [26].

3. Results and Discussion

3.1. Physical Characterization. The physical properties and the microanalytical data of the ligand (HL) and metal complexes (1a–1d) are summarized in the experimental section. The analytical results show (1 : 2) metal ligand ratio, that is, ML_2 type. The color change from ligand to metal complexes is in support of metal ligand interaction which is further reinforced by conductivity and pH change. The ligand (HL) was soluble in methanol. The complexes were soluble in DMSO and DMF. The nickel complex (1b) was found to be hygroscopic. The suggested molecular formulae of the ligand (HL) and metal complexes (1a–1d) have been achieved by microanalytical results in combination with various spectral techniques. The experimental molar conductivity data of HL and metal complexes was found in the range of 5.6–35.2 μS/cm and suggests their nonelectrolytic nature. The pH of ligand and complexes was almost in the neutral range.

3.2. Spectral Characterization. The formation of HL was confirmed by ESI mass spectrometry, which showed peaks at m/z = 455, attributable to $[M + H]^+$. The FTIR spectrum is also in line with the proposed structure of HL, with characteristic stretching vibrations at 1640 cm^{-1} assignable to azomethine group [27]. A broadband with absorption maximum of 3303 cm^{-1} is possibly due to collapse of N-H and O-H stretching peaks. Other significant strong bands at 1510 and 1433 cm^{-1} for HL are attributed to ν(COOH) asymmetric and symmetric stretch. The ^{1}H NMR spectrum of HL executes a sharp singlet at 9.09 ppm corresponding to azomethine proton. On complexation, ν(C=N) stretching band for HL has shifted to lower absorption frequency of 1633 cm^{-1} (1a), 1625 cm^{-1} (1b), 1636 cm^{-1} (1c), and 1629 cm^{-1} (1d), indicating the coordination of azomethine nitrogen atom to the metal ion [28]. This lower frequency shift of azomethine group in the complexes is due to the decrease in electron density and force constant of the metal with the azomethine nitrogen lone pair. In all the complexes, FTIR absorption bands corresponding to ν(O-H) execute in the range 3337–3417 cm^{-1} relative to 3303 cm^{-1} for HL. The complexes exhibit ν(COOH) stretching vibrations at the equivalent positions of the ligand, suggesting their noncoordination with the metal centers. The formation of cobalt complex (1a) was confirmed by ESI-MS peak at m/z = 1002, attributable to $[M + H]^+$. The well resolved IR band at 3417 cm^{-1}, for complex (1a), corresponds to the ν(O-H) stretching vibration (Figure 1) [29]. The evidence of bonding in 1a is also shown by the observation of new bands in the lower frequency regions at 425 and 526 cm^{-1} characteristic to ν(Co-N) and ν(Co-O) stretching vibrations that are not observed in the IR spectrum of ligand. The less intense IR band at 606 cm^{-1} is assignable to bending vibration of two lattice water molecules of the outer sphere region. The observed molecular mass of nickel complex (1b) was evidenced by ESI mass spectrum peak value at m/z = 964, assignable to molecular ion peak. The formation of this complex was verified by FTIR spectroscopy, where specific bands are observed at 1625 cm^{-1} ν(CH=N), 3337 cm^{-1} ν(O-H), 429 cm^{-1} ν(Ni-N), and 687 cm^{-1} for outer sphere lattice water molecules. The copper complex (1c) executes a strong azomethine band at 1636 cm^{-1} which has undergone a negative shift by 4 cm^{-1} relative to that of the free ligand. The other significant FTIR bands are observed at 3379 cm^{-1} ν(O-H), 444 cm^{-1} ν(Cu-N), and 686 cm^{-1} for outer sphere lattice water molecules. The formation of the complex 1c is further evidenced by the ESI-MS peak at m/z = 970, attributed to $[M + H]^+$. The positive ion ESI mass spectrum showed peaks at m/z = 971 for zinc complex (1d), attributed to $[M + H]^+$. Its formation was strongly evidenced by FTIR and ^{1}H NMR spectral data. The strong azomethine band at 1629 cm^{-1} ν(CH=N) for this complex has shifted by 11 cm^{-1} towards a lower wave number relative to that of the free ligand, indicating metal coordination with azomethine nitrogen. The metal nitrogen coordination is further evidenced by a sharp peak at 415 cm^{-1} in the FTIR spectrum of 1d. The ^{1}H NMR spectrum is also consistent with the suggested structure. The downfield shift of ^{1}H NMR signal for azomethine proton from δ 9.094 ppm for ligand to δ 9.295 ppm for zinc complex (1d) also supports coordination of the azomethine nitrogen to the zinc(II) ion. Two doublets observed at δ 6.718–7.625 for HL and δ 6.72–7.66 ppm for zinc complex 1d are attributed to aromatic ring protons. The methyl protons of amoxicillin moiety in both HL and 1d appear as a singlet peak in the region of δ 1.118–1.562 ppm. Amide NH proton for HL executes signal at 8.241–8.271 ppm, which is absent in the spectrum of 1d, and this confirms the coordination of amide N-atom with metal center via deprotonation [30]. In the spectrum of HL, the signal due to carboxylic proton appears at δ 10.122 ppm, which is still present in the ^{1}H NMR spectrum of zinc complex (1d).

3.3. Electronic Absorption Spectra and Magnetic Moment Measurement. The electronic absorption spectrum of ligand (HL) displays high energy bands in the ultraviolet region at 206 and 262 nm, corresponds to $\pi \rightarrow \pi^*$ transitions of the aromatic and pyridinium ring, and, at 356 nm, corresponds to $n \rightarrow \pi^*$ intraligand charge transfer band with the involvement of C=N group [31]. However, the additional bands in the higher wavelength region are observed in the complexes

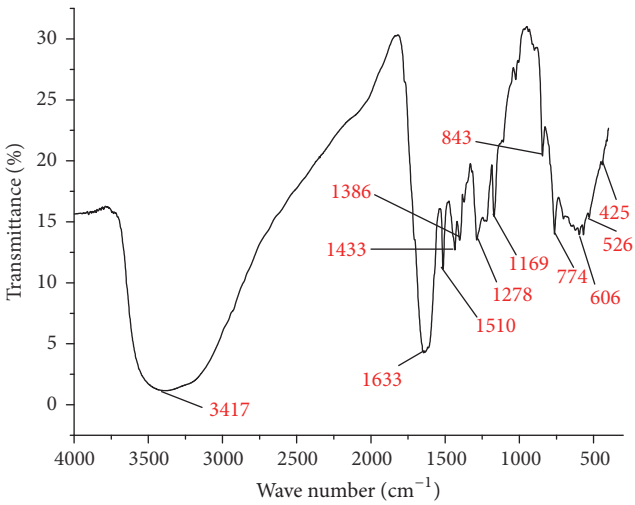

FIGURE 1: IR spectrum of cobalt complex (1a).

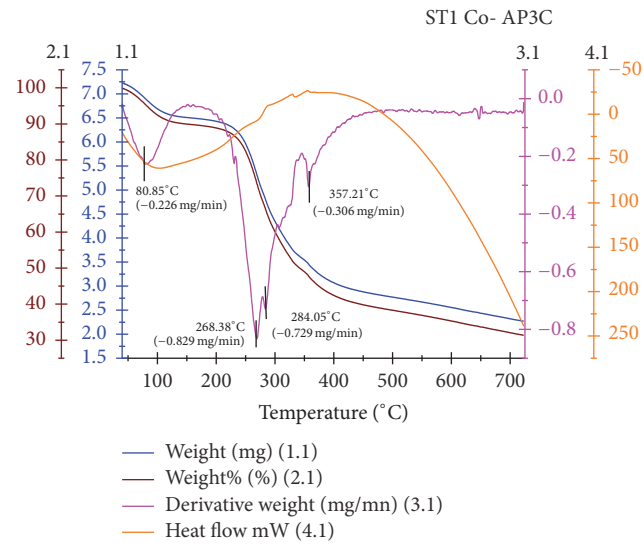

FIGURE 2: Thermogram of cobalt complex (1a).

which signify metal ligand coordination. The cobalt complex (1a) exhibits two distinct bands in high wavelength region of the spectrum at 457–488 nm and 549 nm. The former band is assignable to $^4T_{1g}(F) \rightarrow {}^4T_{1g}(P)$ and latter band indicates $^4T_{1g} \rightarrow {}^4A_{2g}$ transition, confirming its octahedral geometry [32]. The magnetic moment value (4.75 BM) further supports this geometry. The high energy bands for this complex are observed at 263 and 346–371 nm, assignable to $\pi \rightarrow \pi^*$ and $n \rightarrow \pi^*$ LMCT transitions, respectively. The electronic absorption spectrum of nickel complex (1b) displays d-d transition band at 460 nm assignable to $^1A_{1g} \rightarrow {}^1B_{1g}$ transition along with the bands in the low wavelength region at 261 and 346 nm [33, 34]. The diamagnetic nature of this complex is suggestive of the complete distortion of octahedral geometry and confirms its square planar geometry. The magnetic moment value (1.82 BM) and electronic absorption spectrum of paramagnetic copper complex (1c) exhibit absorption band in the high wavelength region at 485 nm, attributed to $^2T_{2g} \rightarrow {}^2E_g$ transition which is suggestive of tetrahedral geometry [35]. Other high energy bands for this complex are observed at 227 and 259 nm for $\pi \rightarrow \pi^*$ transition and 337 and 344 nm for $n \rightarrow \pi^*$ LMCT transition. The zinc complex (1d) displays an absorption band at 346 nm assignable to the LMCT transition, compatible with tetrahedral geometry, and this is further supported by its diamagnetic nature and absence of d-d band, due to its complete d^{10} electronic configuration.

3.4. TGA/DTA Studies. The TGA/DTA curves for the complexes were carried out within the temperature range from room temperature to 700°C with the linear heating rate of 20°C/min in the nitrogen atmosphere. Correlation of the thermal events at elevated temperatures with kinetic parameters provides useful physicochemical information of the compounds. Thermo gravimetric analysis is one such important instrumental technique to observe thermal changes with respect to increase in temperatures [36]. The computed thermal decomposition data in Table 1 are in good agreement with the suggested microanalytical data. The following findings have been achieved in our research analysis.

The thermogram of cobalt complex (1a) (Figure 2) exhibited four decomposition steps in the temperature range of 50–380°C. The first decomposition step in the temperature range of 50–110°C with % mass loss of 4.826% (0.226 mg) is assignable to the loss of two lattice water molecules from the outer sphere [37, 38]. The second and third decomposition steps with % mass loss of 25.923% (0.829 mg) and 33.837% (0.729 mg) in the temperature range of 241–273°C and 279–300°C have considered the loss of organic ligand moiety. The last decomposition step with % mass loss of 52.247% (0.306 mg) represents a complete loss of ligand from the complex in the temperature range of 338–380°C, leaving cobalt oxide as stable residue. The nickel complex (1b) exhibited thermal decomposition in two distinct steps. The first step with % mass loss of 5.6% (0.153 mg) is assignable to the loss of outer sphere lattice water molecules in the temperature range of 44–113°C. The exothermic peak with 30.86% (0.484 mg) mass loss in the temperature range of 232–403°C is attributed to loss of ligand moiety. The thermograms of other two complexes 1c and 1d are complement to the analyzed data of 1a and 1b. The first step decomposition in 1c and 1d occurred in the temperature range around 45–107°C with T_{DTG} 76.79 and 75.46°C and this again suggests the loss of two lattice water molecules. The final thermal decomposition step in all the metal complexes is noticed above 400°C, which is indicated by the formation of the horizontal TG curve. This step interprets the formation of stable metal oxide residue.

Kinetic Parameters. The thermal dehydration and decomposition of the complexes were studied by using an integral method applying a very popular Coats-Redfern method [39, 40]. The thermodynamic activation parameters of decomposition processes are essential to describe the thermal stability

Table 1: Thermal decomposition data of metal complexes.

Comp.	Step	TG range (°C)					DTA	
		$\Delta_{m\%}$ *found*	T_i	T_f	T_{DTG}	Mass loss	T_{dta}	Peak
1a	1	4.826	50	110.2	80.85	−0.226	103.68	Endo
	2	25.923	241.63	276.73	268.38	−0.829	—	—
	3	33.837	279	300	284.05	−0.729	—	—
	4	52.247	338	380	357.21	−0.306	334.9	Endo
1b	1	5.601	44	113	85.91	−0.153	105.33	Endo
	2	30.861	232	403	278.16	−0.484	382.91	Exo
1c	1	2.699	49	105	76.79	−0.100	111.23	Endo
	2	8.814	148	163	159.86	−0.395	—	—
	3	21.635	187	246	237.13	−0.310	—	—
	4	42.395	293	390	326.01	−0.244	385.92	Exo
1d	1	3.047	46	107	75.46	−0.121	115.75	Endo
	2	18.233	230	287	260.99	−0.491	339.24	Endo
	3	36.441	310	410	330.41	−0.238	365.88	Exo

as well as the nature and rates of thermal decomposition of the complexes. These parameters are evaluated graphically by plotting of data based on Coats-Redfern relation in the following form:

$$\ln\left[-\frac{\ln(1-\alpha)}{T^2}\right] = \ln\left[\frac{AR}{\beta E^*}\right] - \frac{E^*}{RT}, \quad (1)$$

where α represents the decomposition fraction at temperature T K and β denotes linear heating rate (dT/dt). E^* and A denote the activation energy and Arrhenius preexponential factor, respectively. R represents gas constant. Molding the equation for the straight line ($y = mx + c$), a linear plot of left side versus $1/T$ of Coats-Redfern equation gives a straight line, whose slope E^*/R furnishes activation energy parameter and the preexponential factor (A) can be determined from the intercept. The other thermodynamic parameters such as entropy of activation (ΔS^*), enthalpy of activation (ΔH^*), and free energy of activation (ΔG^*) have been calculated by using the following relation:

$$\Delta S^* = R\ln\left[\frac{Ah}{k_B T}\right]$$
$$\Delta H^* = E^* - RT \quad (2)$$
$$\Delta G^* = \Delta H^* - T\Delta S^*.$$

The computed data of thermodynamic activation parameters of various decomposition steps of the metal complexes are listed in Table 2. In the present work, the plot of left hand side of Coats-Redfern equation versus 1000/T in all the decomposition steps of all complexes shows a best fit for first-order reaction kinetics [41]. The high and increasing values of activation energy in the subsequent steps of all the complexes reflect high thermal stability, which may be due to covalent bond character. The entropy of activation value of first decomposition step in all the complexes is negative, which indicates nonspontaneous dehydration reaction process. Most of this value of other steps is positive and infers the dissociation character of decomposition [42]. This also attributes more ordered activated state than the reactants. The positive ΔG^* values of all the complexes justify the nonspontaneous nature of decomposition steps. The enthalpy of activation values (ΔH^*) in most of the decomposition steps is positive which reveal endothermic processes. However, this nature also depends upon the value of other thermodynamic activation parameters. The computed data of correlation coefficient (r) obtained from the graphical plot reflect a good fit of the data with linear function [43, 44].

3.5. XRPD Study. Single crystal growth of the synthesized compounds was unsuccessful, so their crystallinity was established by X-ray powder diffraction study. The ligand (HL) and complexes (1a, 1b, and 1d) were found amorphous. The crystal structure of copper complex (1c) was worked out by its well resolved crystalline peaks (Figure 3), which crystallized in a triclinic crystal system with P1 space group. The diffractogram of this complex registered 22 reflection peaks in the range of (2θ) 0 to 50° with maxima at 15.974° with corresponding d spacing value of 5.584 Å. The cell dimensions a (6.2282 Å), b (109390 Å), c (20.3388 Å), α (63.1585°), β (113.5723°), *and* γ (64.269°) are in good agreement with the refined triclinic crystal system. The unit cell volume of this compound was calculated to be 747.4131 Å^3 with FOM 31. The details of crystallographic data are summarized in Table 3. The particle size was calculated from Scherer's formula $\alpha = 0.9\lambda/\beta\cos\theta$, where λ is the wavelength, β is the full-width half maximum of the characteristic peak, and θ is the

Table 2: Kinetic and thermodynamic parameters of metal complexes.

Comp.	Step	r	A (s^{-1})	T_{max} (K)	E^* (kJ/mol)	ΔS^* (J/K·mol)	ΔH^* (kJ/mol)	ΔG^* (kJ/mol)
1a	1	−0.98495	5.62×10^6	353.85	58.36	−117.92	55.4719	97.19789
	2	−0.99209	5.06×10^{19}	541.38	229.22	126.559	224.718	156.202
	3	−0.99052	1.19×10^{36}	557.05	403.95	18.3647	399.319	389.089
	4	−0.99343	1.14×10^{22}	630.21	288.1474	170.339	282.907	175.525
1b	1	−0.99453	7.054×10^6	358.91	59.62	−40.236	56.634	71.075
	2	−0.9887	1.35×10^{13}	551.16	160.7139	35.4267	160.288	140.762
1c	1	−0.99401	4.064×10^7	349.79	63.4725	−110.3698	60.564	64.191
	2	−0.99698	10.06×10^{51}	432.86	447.68	765.803	444.080	112.594
	3	−0.99643	5.98×10^{11}	510.13	129.453	−24.716	125.2115	137.819
	4	−0.99604	6.55×10^5	599.01	93.1345	−140.1638	92.6438	176.603
1d	1	−0.99448	5.89×10^6	348.46	57.8981	−117.3976	55.00	95.908
	2	−0.99491	2.92×10^{15}	533.99	176.7582	45.523	172.318	148.00
	3	−0.99118	7.64×10^5	603.41	96.5845	−103.320	91.567	153.911

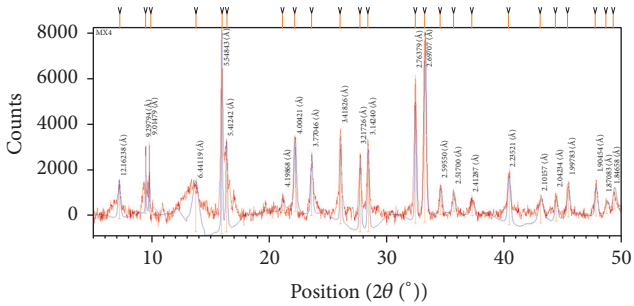

Figure 3: X-ray diffractogram of copper complex (1c).

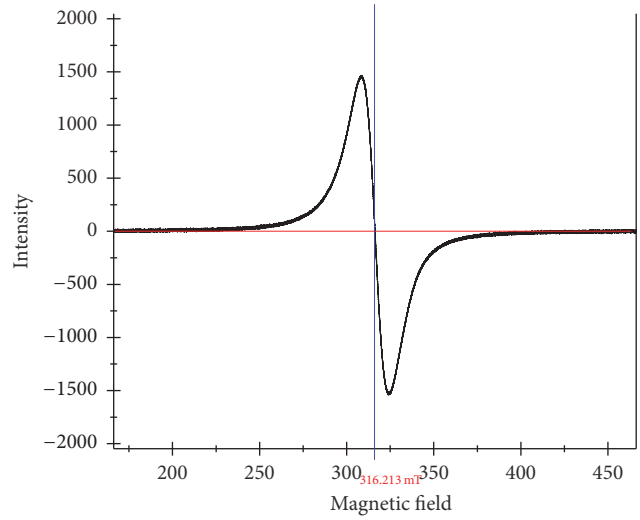

Figure 4: EPR spectrum of copper complex (1c) at room temperature.

diffraction angle of the *hkl* plane [45, 46]. The average particle size 69.34 nm suggests its nanocrystalline nature.

3.6. EPR Analysis. The solid state X-band EPR spectrum of the copper complex (1c) was recorded at room temperature under the frequency 9447.606 MHz with no marker lines used and center line at 316.213 mT. The standard lines that are used in EPR model are of Mn, which has been omitted in the graph. The EPR spectrum of complex provides useful information about the metal ion environment within the complex. The highly symmetrical EPR spectrum of copper complex (1c) (Figure 4) delivered a single isotropic signal with $g_\parallel$ value of 2.18 and $g_\perp$ value of 2.08 [47]. The absence of poorly resolved hyperfine signal may be attributed to the considerable exchange coupling interaction of the Cu^{+2} ions in the complex. The order of splitting factors $g_\parallel > g_\perp > 2.0023$ clearly indicates the localized unpaired electron in the d orbital of Cu^{+2} ion and is characteristic of axial symmetry [6, 48]. The calculated g_{av} value is 2.11 whose deviation from the free electron (2.003) is due to covalent character of the metal ligand bond. This fact is further supported by $g_\parallel$ value less than 2.3. The value of exchange coupling interaction parameter "G" = 2.25 is less than 4 and suggests considerable exchange interaction in the complex [49]. All these parameters are in support of tetrahedral geometry of copper complex (1c).

3.7. SEM Analysis. The metal coordination to ligand significantly changes the surface morphology of the complexes and this was investigated by SEM analysis. The SEM micrograph of ligand (HL) and metal complexes are shown in Figure 5 and the differences are seen in surface morphology of the metal complexes due to changes in the metal ions. The SEM micrograph of ligand demonstrates nonuniform platelet-like structure with variable lateral dimensions [50]. Moreover,

Table 3: X-ray powder diffraction data of copper complex (1c).

Peak number	2θ	θ	Sin θ	Sin$^2\theta$	$h^2 + k^2 + l^2$	hkl	d	FWHM	% int.	a in nm
1	7.2685	3.63425	0.06338	0.004017	1	0 0 1	12.16238	0.2244	16.00	61.22
2	13.7483	6.87415	0.11968	0.014323	1	0 1 0	6.44119	0.6731	21.90	20.37
3	15.9738	7.9869	0.13894	0.019304	2	1 1 0	5.54843	0.0935	100.00	146.64
4	16.3780	8.189	0.14243	0.020286	10	1 0 −3	5.41242	0.1496	42.23	91.65
5	21.1607	10.58035	0.18361	0.033712	9	1 2 2	4.19868	0.2244	6.47	61.102
6	22.2011	11.10055	0.19253	0.03706	11	1 −1 −3	4.00421	0.2244	33. 02	61.102
7	23.5966	11.7983	0.20446	0.041803	1	1 0 0	3.77046	0.1870	28.72	73.323
8	26.0686	13.0343	0.22553	0.050863	6	1 1 2	3.41826	0.1309	44.73	104.747
9	27.7288	13.8644	0.23962	0.057417	4	0 2 0	3.21726	0.1496	38.35	91.654
10	28.4032	14.2016	0.24533	0.060186	10	1 3 0	3.14240	0.1496	42.24	91.654
11	32.3941	16.19705	0.27894	0.077807	20	2 0 −4	2.76379	0.1122	70.54	122.205
12	33.2184	16.6092	0.28584	0.081704	40	2 0 −6	2.69707	0.2057	91.73	66.657
13	34.5584	17.2792	0.29702	0.088220	13	2 0 −3	2.59550	0.2244	13.44	61.103
14	35.6718	17.8359	0.30629	0.093813	2	1 −1 0	2.51700	0.2244	8.91	61.103
15	37.2666	18.6333	0.31951	0.102086	20	2 4 0	2.41287	0.3739	7.05	36.671
16	40.3520	20.176	0.34490	0.11895	80	0 4 8	2.23521	0.2617	23.89	52.394
17	43.0415	21.52075	0.36683	0.13456	9	1 −2 −2	2.10157	0.4487	11.08	30.5585
18	44.3550	22.1775	0.37747	0.14248	30	2 5 1	2.04234	0.2244	11.90	61.103
19	45.3976	22.6988	0.38588	0.14890	69	2 1 −8	1.99783	0.2244	15.90	61.103
20	47.7559	23.87795	0.40478	0.16384	25	3 4 0	1.90454	0.1870	16.97	73.324
21	48.6714	24.3357	0.41211	0.16983	58	3 0 −7	1.87083	0.2991	5.79	45.843
22	49.3094	24.6547	0.41714	0.174	18	3 3 0	1.84658	0.2736	7.79	50.116
								Average particle size		69.3474

inhomogeneous matrix with broken ice-like structure has been observed in the SEM micrograph of nickel complex (1b). The SEM micrograph of copper complex (1c) displays agglomerated morphology with small sized grains scattered in homogenous matrix and gives the appearance of coral-like structure. In the SEM micrograph of zinc complex (1d), small sized particles crumbled together to give rock-like structure with somewhat cotton-like appearance.

3.8. Molecular Modeling. The computational study of the compounds furnishes a clear idea about the three-dimensional arrangement of different atoms in the molecules. The energy optimization of the ligand (HL) and metal complexes (1a–1d) was done by Universal Force Field (UFF) technique with minimum RMS gradient 0.100, supported in ArgusLab 4.0.1 version software [51, 52]. The details of the bonding and energy parameters optimized by molecular modeling calculations of the metal complexes are depicted in Table 4. For ligand, single point energy calculation with Hamiltonian AM1 revealed final SCF energy and heat of formation, −132288.8349 and 45.0637 kcal/mol, respectively [53]. After the geometry optimization by molecular mechanics (UFF) technique, the final geometrical energy of HL has been reported to 139.2725 kcal/mols. On ESP mapped electron density surface of HL (Figure 6), red color indicates the highest electron density region which is around O-atom. The second highest electron density region is around an azomethine N-atom which is shown by mixed green and yellow colors. This is the region for stability of coordinated metal ions and supports its linkage with azomethine N-atom. It seems clear that the coordination with O-atoms is restricted due to greater electronic repulsion and field obstruction. In the nickel complex (1b), the high electron density (Figure 7) around the coordinated azomethine N-atom, indicated by red color, is in favor of its proposed geometry. Similar study and computational data of the complexes (1a to 1d) are in good support of their proposed structures.

3.9. Antibacterial Activity Study. The antibacterial efficacy of the ligand (HL) and metal complexes (1a–1d) was tested against *S. aureus, E. coli, K. pneumoniae,* and *P. vulgaris* bacteria. The antibacterial results are presented in the bar graph (Figure 8). Two different concentrations (100 and 50 mcg/mcl) of the compounds have been selected for antibacterial assay. The results suggest enhanced antibacterial activity of the ligand (HL) and metal complexes (1a–1d). The compound (1c) showed little activity against all the bacterial pathogens, compared to ligand and other metal complexes. The ligand bears activity, even greater than parent drug amoxicillin and control drug amikacin at higher concentration. This higher activity of ligand is possibly due to interference in the normal cell process of organism caused by the formation

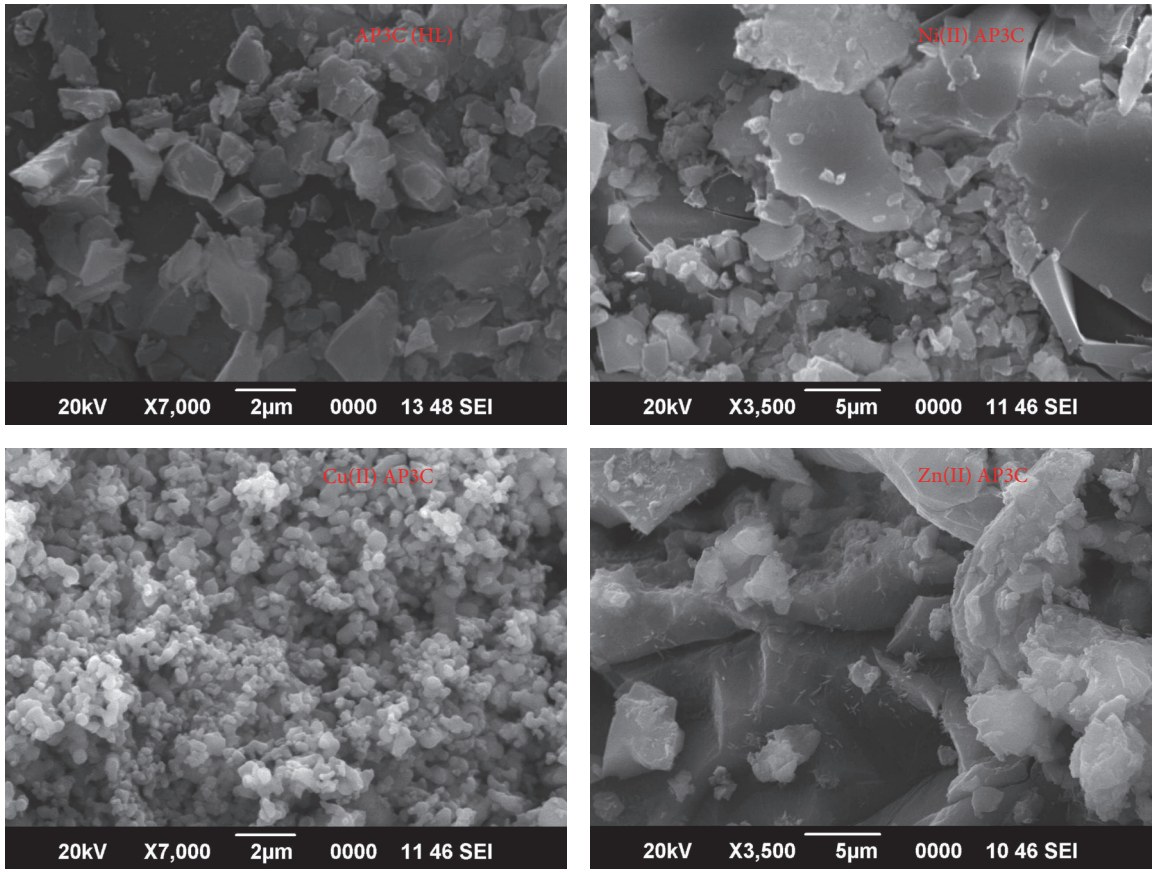

Figure 5: SEM micrographs of HL, 1b, 1c, and 1d.

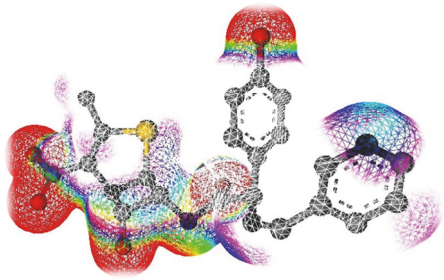

Figure 6: Electrostatic potential mapped electron density surface of HL.

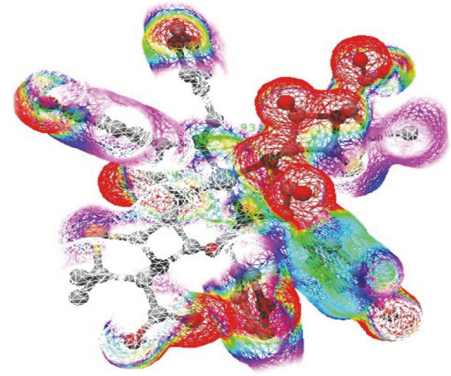

Figure 7: Electrostatic potential mapped electron density surface of nickel complex (1b).

of hydrogen bond through the azomethine group with the active center of cell constituents [54]. Further, the uncoordinated heteroatom of pyridine moiety also contributes to microbial growth inhibition. Moreover, the complexes deliver better antibacterial activity at their higher concentration. Precise observation reveals that the compounds are less active against *S. aureus* and more active against *E. coli* and *P. vulgaris* bacteria. This enhanced activity of the complexes may be attributed to chelation of Schiff base with metal ions that provide stability and more susceptibility against the bacterial pathogens [55, 56]. It has been suggested that the structural components possessing additional (C=N) bond with nitrogen and oxygen donor systems inhibit enzyme activity due to their deactivation by metal coordination. This permits their efficient permeation through the lipid layer of organisms and destroys their activity [6].

Table 4: Selected bond lengths and bond angles of metal complexes.

Complex	Atoms	Bond length (Å)	Bond energy (Kcal/mol)	Atoms	Bond angle	Bond angle energy	Final geom. energy
1a	N(3)-Co(34)	1.957	273.796	N(3)-Co(34)-N(20)	90.00	300.46	349.2538 (Kcal/mol) (0.556 au)
	N(20)-Co(34)	1.972	267.453	N(3)-Co(34)-N(35)	90.00	304.025	
	Co(34)-N(35)	1.957	273.796	N(3)-Co(34)-N(52)	90.00	300.46	
	Co(34)-N(52)	1.972	267.453	N(3)-Co(34)-O(104)	90.00	273.401	
	Co(34)-O(104)	1.964	244.913	N(3)-Co(34)-O(113)	90.00	273.401	
	Co(34)-O(113)	1.964	244.913	N(35)-Co(34)-N(20)	90.00	300.46	
				N(52)-Co(34)-N(20)	90.00	296.982	
				O(104)-Co(34)-N(20)	90.00	270.214	
				O(113)-Co(34)-N(20)	90.00	270.214	
				N(35)-Co(34)-N(52)	90.00	300.46	
				N(35)-Co(34)-N(104)	90.00	273.401	
				N(35)-Co(34)-N(113)	90.00	273.401	
				N(52)-Co(34)-O(104)	90.00	270.214	
				N(52)-Co(34)-N(113)	90.00	270.214	
1b	N(2)-Ni(33)	1.870	313.824	N(2)-Ni(33)-N(19)	90.00	344.228	324.5763 (Kcal/mol) (0.517 au)
	N(19)-Ni(33)	1.885	306.275	N(2)-Ni(33)-N(34)	90.00	348.473	
	N(34)- Ni(33)	1.870	313.824	N(2)-Ni(33)-N(51)	90.00	344.228	
	N(51)- Ni(33)	1.885	306.275	N(34)-Ni(33)-N(19)	90.00	344.228	
				N(51)-Ni(33)-N(19)	90.00	340.090	
				N(34)-Ni(33)-N(51)	90.00	344.228	
1c	N(2)-Cu(33)	2.016	181.007	N(2)-Cu(33)-N(19)	109.47	158.764	373.488 (Kcal/mol) (0.595 au)
	N(19)-Cu(33)	2.031	176.938	N(2)-Cu(33)-N(34)	109.47	160.587	
	N(34)-Cu(33)	2.016	181.007	N(2)-Cu(33)-N(51)	109.47	158.764	
	N(51)-Cu(33)	2.031	176.938	N(34)-Cu(33)-N(19)	109.47	158.764	
				N(51)-Cu(33)-N(19)	109.47	156.977	
				N(34)-Cu(33)-N(51)	109.47	158.764	
1d	N(2)-Zn(33)	1.888	164.142	N(2)-Zn(33)-N(19)	109.47	193.167	352.3697 (Kcal/mol) (0.561 au)
	N(19)- Zn(33)	1.903	160.260	N(2)-Zn(33)-N(34)	109.47	195.503	
	N(34)- Zn(33)	1.888	164.142	N(2)-Zn(33)-N(51)	109.47	193.167	
	N(51)- Zn(33)	1.903	160.260	N(34)-Zn(33)-N(19)	109.47	193.167	
				N(51)-Zn(33)-N(19)	109.47	190.879	
				N(34)-Zn(33)-N(51)	109.47	193.167	

4. Conclusion

The novel ligand (HL) and the metal complexes (1a–1d) were successfully synthesized. The ligand can complex the metal ion via N donor atoms. The electronic absorption spectral analysis in combination with ESR data revealed octahedral geometry for cobalt complex (1a), square planar geometry of nickel complex (1b), and tetrahedral geometry for both copper complex (1c) and zinc complex (1d). Several spectral data nicely support the above concerned geometry of the complexes. Furthermore, the metal complexes were screened in vitro for antibacterial assay. Based on the results of this study of synthesized compounds, it has been concluded that the ligand bears greater potency than amoxicillin and control drug amikacin. The complexes 1a, 1b, and 1d were even highly active against all the bacterial pathogens at their higher concentration; however the copper complex (1c) was less active than others. This greater activity might be due to azomethine linkage and heteroatoms present in these compounds.

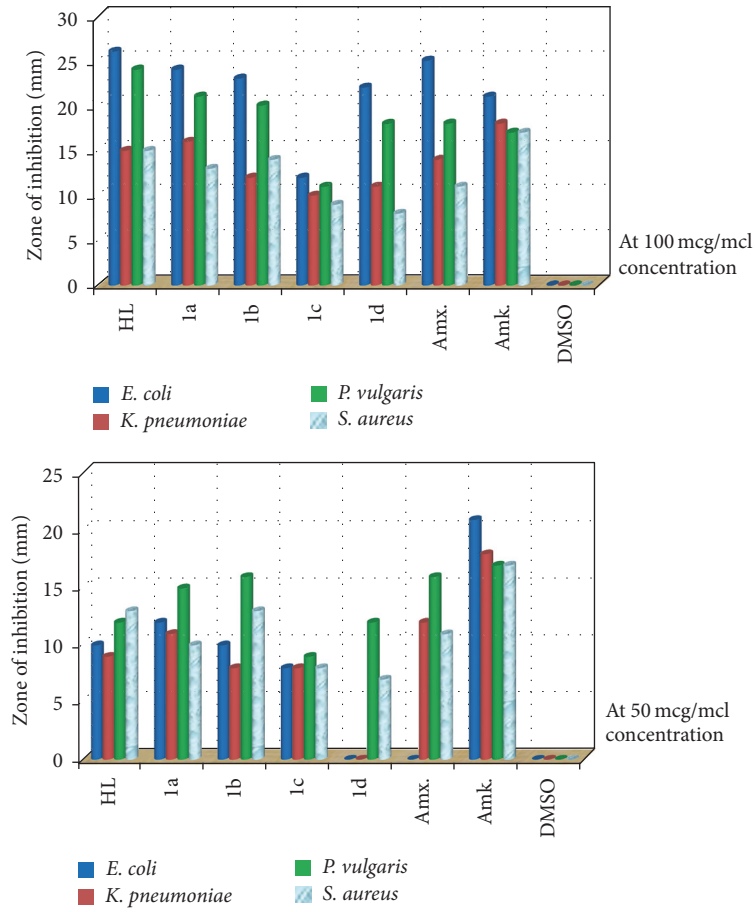

Figure 8: Bar graph of antibacterial evaluation study.

Conflicts of Interest

The authors declare that they have no conflicts of interest.

Acknowledgments

This research work was financially supported by Nepal Academy of Science and Technology (NAST) by providing fellowship, so one of the authors is highly grateful to this organization. The authors express great honor to the entire team of Solid State and Structural Unit, Indian Institute of Science, Bangalore, India, for their cooperation in recording the spectra of the compounds.

References

[1] M. Gulcan, S. Özdemir, A. Dündar, E. Ispir, and M. Kurtoğlu, "Mononuclear complexes based on pyrimidine ring azo schiff-base ligand: Synthesis, characterization, antioxidant, antibacterial, and thermal investigations," *Zeitschrift fur Anorganische und Allgemeine Chemie*, vol. 640, no. 8-9, pp. 1754–1762, 2014.

[2] M. S. Nair, D. Arish, and R. S. Joseyphus, "Synthesis, characterization, antifungal, antibacterial and DNA cleavage studies of some heterocyclic Schiff base metal complexes," *Journal of Saudi Chemical Society*, vol. 16, no. 1, pp. 83–88, 2012.

[3] W. Al Zoubi, A. A. S. Al-Hamdani, and M. Kaseem, "Synthesis and antioxidant activities of Schiff bases and their complexes: a review," *Applied Organometallic Chemistry*, vol. 30, no. 10, pp. 810–817, 2016.

[4] J. R. Anacona, N. Noriega, and J. Camus, "Synthesis, characterization and antibacterial activity of a tridentate Schiff base derived from cephalothin and sulfadiazine, and its transition metal complexes," *Spectrochimica Acta - Part A: Molecular and Biomolecular Spectroscopy*, vol. 137, pp. 16–22, 2015.

[5] R. Nair, A. Shah, S. Baluja, and S. Chanda, "Synthesis and antibacterial activity of some Schiff base complexes," *Journal of the Serbian Chemical Society*, vol. 71, no. 7, pp. 733–744, 2006.

[6] G. B. Bagihalli, P. G. Avaji, S. A. Patil, and P. S. Badami, "Synthesis, spectral characterization, in vitro antibacterial, antifungal and cytotoxic activities of Co(II), Ni(II) and Cu(II) complexes with 1,2,4-triazole Schiff bases," *European Journal of Medicinal Chemistry*, vol. 43, no. 12, pp. 2639–2649, 2008.

[7] N. Raman, A. Sakthivel, and K. Rajasekaran, "Synthesis and Spectral Characterization of Antifungal Sensitive Schiff Base Tran- sition Metal Complexes," *Mycobiology*, vol. 35, no. 3, pp. 150–153, 2007.

[8] B. S. Creaven, E. Czeglédi, M. Devereux et al., "Biological activity and coordination modes of copper(II) complexes of Schiff base-derived coumarin ligands," *Dalton Transactions*, vol. 39, pp. 10854–10865, 2010.

[9] A. Jarrahpour, D. Khalili, E. De Clercq, C. Salmi, and J. M. Brunel, "Synthesis, antibacterial, antifungal and antiviral activity evaluation of some new bis-Schiff bases of isatin and their derivatives," *Molecules*, vol. 12, pp. 1720–1730, 2007.

[10] S. K. Bharti, S. K. Patel, G. Nath, R. Tilak, and S. K. Singh, "Synthesis, characterization, DNA cleavage and in vitro antimicrobial activities of copper(II) complexes of Schiff bases containing a 2,4-disubstituted thiazole," *Transition Metal Chemistry*, 2010.

[11] M. Manjunatha, V. H. Naik, A. D. Kulkarni, and S. A. Patil, "DNA cleavage, antimicrobial, antiinflammatory anthelmintic activities, and spectroscopic studies of Co(II), Ni(II), and Cu(II) complexes of biologically potential coumarin Schiff bases," *Journal of Coordination Chemistry*, vol. 64, no. 24, pp. 4264–4275, 2011.

[12] S. Amer, N. El-Wakiel, and H. El-Ghamry, "Synthesis, spectral, antitumor and antimicrobial studies on Cu(II) complexes of purine and triazole Schiff base derivatives," *Journal of Molecular Structure*, vol. 1049, pp. 326–335, 2013.

[13] P. G. Cozzi, "Metal-Salen Schiff base complexes in catalysis: practicalaspects," *Chemical Society Reviews*, vol. 33, pp. 410–421, 2004.

[14] R. K. Singh, A. Kukrety, R. C. Saxena, G. D. Thakre, N. Atray, and S. S. Ray, "Novel Triazine Schiff Base-Based Cationic Gemini Surfactants: Synthesis and Their Evaluation as Antiwear, Antifriction, and Anticorrosive Additives in Polyol," *Industrial and Engineering Chemistry Research*, vol. 55, no. 9, pp. 2520–2526, 2016.

[15] N. Sathya, G. Raja, N. Padma Priya, and C. Jayabalakrishnan, "Ruthenium(II) complexes incorporating tridentate schiff base ligands: Synthesis, spectroscopic, redox, catalytic and biological properties," *Applied Organometallic Chemistry*, vol. 24, no. 5, pp. 366–373, 2010.

[16] V. Arun, N. Sridevi, P. P. Robinson, S. Manju, and K. K. M. Yusuff, "Ni(II) and Ru(II) Schiff base complexes as catalysts for the reduction of benzene," *Journal of Molecular Catalysis A: Chemical*, vol. 304, no. 1-2, pp. 191–198, 2009.

[17] J. L. Segura, M. J. Mancheño, and F. Zamora, "Covalent organic frameworks based on Schiff-base chemistry: synthesis, properties and potential applications," *Chemical Society Review*, 2016.

[18] J. R. Anacona, J. Calvo, and O. A. Almanza, "Synthesis, Spectroscopic, and Magnetic Studies of Mono- and Polynuclear Schiff Base Metal Complexes Containing Salicylidene-Cefotaxime Ligand," *International Journal of Inorganic Chemistry*, pp. 1–7, 2013, http://dx.doi.org/10.1155/2013/108740.

[19] I. Rama and R. Selvameena, "Synthesis, structure analysis, antibacterial and in vitro anti-cancer activity of new Schiff base and its copper complex derived from sulfamethoxazole," *Journal of Chemical Sciences*, vol. 127, no. 4, pp. 671–678, 2015.

[20] S. Jyothi, K. Sreedhar, D. Nagaraju, and S. J. Swamy, "Synthesis and spectral investigation of Co(II), Ni(II), Cu(II) and Zn(II) complexes with novel N4 Ligands," *Canadian Chemical Transactions*, vol. 3, no. 4, pp. 368–380, 2015.

[21] S. P. Jose and S. Mohan, "FT-IR and FT-RAMAN investigations of nicotinaldehyde," *Spectrochimica Acta - Part A: Molecular and Biomolecular Spectroscopy*, vol. 64, no. 1, pp. 205–209, 2006.

[22] A. K. Ghosh, M. Mitra, A. Fathima et al., "Antibacterial and catecholase activities of Co(III) and Ni(II) Schiff base complexes," *Polyhedron*, vol. 107, pp. 1–8, 2016.

[23] H. F. Abd El-Halim, M. M. Omar, G. G. Mohamed, and M. A. El-Ela Sayed, "Spectroscopic and biological activity studies on tridentate Schiff base ligands and their transition metal complexes," *European Journal of Chemistry*, vol. 2, no. 2, pp. 178–188, 2011.

[24] M. A. Pfaller, S. A. Messer, L. Boyken et al., "Evaluation of the NCCLS M44-P Disk Diffusion Method for Determining Susceptibilities of 276 Clinical Isolates of Cryptococcus neoformans to Fluconazole," *Journal of Clinical Microbiology*, vol. 42, no. 1, pp. 380–383, 2004.

[25] M. Balouiri, M. Sadiki, and S. K. Ibnsouda, "Methods for in vitro evaluating antimicrobial activity: A review," *Journal of Pharmaceutical Analysis*, vol. 6, pp. 71–79, 2016.

[26] S. M. Bell, J. N. Pham, and G. T. Fisher, "Antibiotic susceptibility testing by the CDS method," in *The prince of Wales Hospital, South Eastern Area Laboratory Services, Randwick NSW 2031*, A manual for Medical and Veterinary Laboratories, Fifth edition, 2009.

[27] S. Hazra, A. Karmakar, M. D. F. C. Guedes da Silva, L. Dlháň, R. Boča, and A. J. L. Pombeiro, "Sulfonated Schiff base dinuclear and polymeric copper(II) complexes: crystal structures, magnetic properties and catalytic application in Henry reaction," *New Journal of Chemistry*, vol. 39, pp. 3424–3434, 2015.

[28] A. Soroceanu, M. Cazacu, S. Shova et al., "Copper(II) complexes with Schiff bases containing a disiloxane unit: Synthesis, structure, bonding features and catalytic activity for aerobic oxidation of benzyl alcohol," *European Journal of Inorganic Chemistry*, no. 9, pp. 1458–1474, 2013.

[29] E. Pahonţu, D.-C. Ilieş, S. Shova et al., "Synthesis, characterization, crystal structure and antimicrobial activity of copper(II) complexes with the Schiff base derived from 2-hydroxy-4-methoxybenzaldehyde," *Molecules*, vol. 20, no. 4, pp. 5771–5792, 2015.

[30] A. M. Naglah, H. M. Awad, M. A. Bhat, M. A. Al-omar, and A. E. E. Amr, "Microwave-Assisted Synthesis and Antimicrobial Activity of Some Novel Isatin Schiff Bases Linked to Nicotinic Acid via Certain Amino Acid Bridge," *Journal of chemistry*, vol. 2015, 2015, http://dx.doi.org/10.1155/2015/364841.

[31] D. Dey, G. Kaur, A. Ranjani et al., "A trinuclear zinc-Schiff base complex: Biocatalytic activity and cytotoxicity," *European Journal of Inorganic Chemistry*, no. 21, pp. 3350–3358, 2014.

[32] O. E. Sherif and N. S. Abdel-Kader, "DFT calculations, spectroscopic studies, thermal analysis and biological activity of supramolecular Schiff base complexes," *Arabian Journal of Chemistry*, 2015.

[33] H. Amiri Rudbari, M. R. Iravani, V. Moazam et al., "Synthesis, characterization, X-ray crystal structures and antibacterial activities of Schiff base ligands derived from allylamine and their vanadium(IV), cobalt(III), nickel(II), copper(II), zinc(II) and palladium(II) complexes," *Journal of Molecular Structure*, vol. 1125, pp. 113–120, 2016.

[34] S. Kundu, A. K. Pramanik, A. S. Mondal, and T. K. Mondal, "Ni(II) and Pd(II) complexes with new N,O donor thiophene appended Schiff base ligand: Synthesis, electrochemistry, X-ray structure and DFT calculation," *Journal of Molecular Structure*, vol. 1116, pp. 1–8, 2016.

[35] S. Jana, P. Bhowmik, M. Das, P. P. Jana, K. Harms, and S. Chattopadhyay, "Synthesis and characterisation of two double EE azido and thiocyanato bridged dimeric Cu(II) complexes with tridentate Schiff bases as blocking ligands," *Polyhedron*, vol. 37, no. 1, pp. 21–26, 2012.

[36] Z. Asadi, M. Asadi, and M. R. Shorkaei, "Synthesis, characterization and DFT study of new water-soluble aluminum(III), gallium(III) and indium(III) Schiff base complexes: Effect of

metal on the binding propensity with bovine serum albumin in water," *Journal of the Iranian Chemical Society*, vol. 13, no. 3, pp. 429–442, 2016.

[37] A. S. Gaballa, S. M. Teleb, M. S. Asker, E. Yalçin, and Z. Seferoğlu, "Synthesis, spectroscopic properties, and antimicrobial activity of some new 5-phenylazo-6-aminouracil-vanadyl complexes," *Journal of Coordination Chemistry*, vol. 64, no. 24, pp. 4225–4243, 2011.

[38] H. Abu Ali, H. Fares, M. Darawsheh, E. Rappocciolo, M. Akkawi, and S. Jaber, "Synthesis, characterization and biological activity of new mixed ligand complexes of Zn(II) naproxen with nitrogen based ligands," *European Journal of Medicinal Chemistry*, vol. 89, pp. 67–76, 2014.

[39] G. G. Mohamed, M. M. Omar, and A. M. Hindy, "Metal Complexes of Schiff Bases: Preparation, Characterization, and Biological Activity," *Turkey Journal of Chemistry*, vol. 30, pp. 361–382, 2006.

[40] S. I. Al-Resayes, "Kinetics analysis for non-isothermal decomposition γ-irradiated indium acetate," *Arabian Journal of Chemistry*, vol. 3, no. 3, pp. 191–194, 2010.

[41] H. P. Ebrahimi, J. S. Hadi, Z. A. Abdulnabi, and Z. Bolandnazar, "Spectroscopic, thermal analysis and DFT computational studies of salen-type Schiff base complexes," *Spectrochim Acta A*, vol. 117, pp. 485–492, 2014.

[42] M. Montazerozohori, S. Zahedi, A. Naghiha, and M. M. Zohour, "Synthesis, characterization and thermal behavior of antibacterial and antifungal active zinc complexes of bis (3(4-dimethylaminophenyl)-allylidene-1, 2-diaminoethane," *Materials Science and Engineering C*, vol. 35, no. 1, pp. 195–204, 2014.

[43] W. H. Mahmoud, G. G. Mohamed, and M. M. I. El-dessouky, "Synthesis , Characterization and in vitro Biological Activity of Mixed Transition Metal Complexes of Lornoxicam with 1,10-phenanthroline," *International Journal of Electrochemical Science*, vol. 9, pp. 1415–1438, 2014.

[44] A. H. Kianfar, H. Farrokhpour, P. Dehghani, and H. R. Khavasi, "Experimental and theoretical spectroscopic study and structural determination of nickel(II) tridentate Schiff base complexes," *Spectrochimica Acta - Part A: Molecular and Biomolecular Spectroscopy*, vol. 150, pp. 220–229, 2015.

[45] G. Grivani, V. Tahmasebi, A. D. Khalaji, V. Eigner, and M. Dušek, "Synthesis, characterization, crystal structure, catalytic activity in oxidative bromination, and thermal study of a new oxidovanadium Schiff base complex containing O, N-bidentate Schiff base ligand," *Journal of Coordination Chemistry*, vol. 67, no. 22, pp. 3664–3677, 2014.

[46] B. B. Mahapatra, R. Mishra, and A. K. Sarangi, "Synthesis, characterisation, XRD, molecular modelling and potential antibacterial studies of Co(II), Ni(II), Cu(II), Zn(II), Cd(II) and Hg(II) complexes with bidentate azodye ligand," *Journal of Saudi Chemical Society*, 2013.

[47] O. A. El-Gammal, G. M. A. El-Reash, T. A. Yousef, and M. Mefreh, "Synthesis, spectral characterization, computational calculations and biological activity of complexes designed from NNO donor Schiff-base ligand," *Spectrochimica Acta - Part A: Molecular and Biomolecular Spectroscopy*, vol. 146, pp. 163–176, 2015.

[48] S. A. Patil, S. N. Unki, A. D. Kulkarni, V. H. Naik, U. Kamble, and P. S. Badami, "Spectroscopic, invitro antibacterial, and antifungal studies of Co(II), Ni(II), and Cu(II) complexes with 4-chloro-3-coumarinaldehyde Schiff bases," *Journal of Coordination Chemistry*, vol. 64, no. 2, pp. 323–336, 2011.

[49] A. A. Abdel Aziz, A. N. M. Salem, M. A. Sayed, and M. M. Aboaly, "Synthesis, structural characterization, thermal studies, catalytic efficiency and antimicrobial activity of some M(II) complexes with ONO tridentate Schiff base N-salicylidene-o-aminophenol (saphH 2)," *Journal of Molecular Structure*, vol. 1010, pp. 130–138, 2012.

[50] M. Shakir, A. Abbasi, M. Faraz, and A. Sherwani, "Synthesis, characterization and cytotoxicity of rare earth metal ion complexes of N,N′-bis-(2-thiophenecarboxaldimine)-3,3′-diaminobenzidene, Schiff base ligand," *Journal of Molecular Structure*, vol. 1102, pp. 108–118, 2015.

[51] V. Sharma, E. K. Arora, and S. Cardoza, "4-Hydroxy-benzoic acid (4-diethylamino-2-hydroxy-benzylidene)hydrazide: DFT, antioxidant, spectroscopic and molecular docking studies with BSA," *Luminescence*, vol. 31, no. 3, pp. 738–745, 2016.

[52] N. Kavitha and P. Anantha Lakshmi, "Synthesis, characterization and thermogravimetric analysis of Co(II), Ni(II), Cu(II) and Zn(II) complexes supported by ONNO tetradentate Schiff base ligand derived from hydrazino benzoxazine," *Journal of Saudi Chemical Society*, 2015.

[53] N. K. Chaudhary and P. Mishra, "Spectral Investigation and in Vitro Antibacterial Evaluation of NiII and CuII Complexes of Schiff Base Derived from Amoxicillin and α -Formylthiophene (α ft)," *Journal of Chemistry*, vol. 2015, Article ID 136285, 2015.

[54] R. S. Joseyphus and M. S. Nair, "Antibacterial and Antifungal Studies on Some Schiff Base Complexes of Zinc (II)," *Mycobiology*, vol. 36, no. 2, pp. 93–98, 2008.

[55] A. A. Al-Amiery, Y. K. Al-Majedy, H. H. Ibrahim, and A. A. Al-Tamimi, "Antioxidant, antimicrobial, and theoretical studies of the thiosemicarbazone derivative Schiff base 2-(2-imino-1-methylimidazolidin-4-ylidene)hydrazinecarbothioamide (IMHC)," *Organic and Medicinal Chemistry Letters*, vol. 2, no. 4, 2012.

[56] M. Jesmin, M. M. Ali, M. S. Salahuddin, M. R. Habib, and J. A. Khanam, "Antimicrobial Activity of Some Schiff Bases Derived from Benzoin, Salicylaldehyde, Aminophenol and 2,4 Dinitrophenyl Hydrazine," *Mycobiology*, vol. 36, pp. 70–73, 2008.